Periodic orbit theory beyond semiclassics: convergence, diffraction and $\hbar$ corrections

P. E. Rosenqvist

December 4, 1995

Acknowledgements

Contents

Chapter 1

Introduction

1.1 Introduction

In the beginning of the present century the discovery of the first quantum effects associated with the radiation of light from atoms, presented a serious riddle to the established community of physics. It was until then a commonly accepted fact that physics developed so far was capable of explaining *all* the phenomena of nature if one was just sufficiently detailed and patient. It was therefore natural to expect that the new quantum phenomena could be suitably explained just by hard work. By the success of the Bohr postulates and the calculation of the Rydberg constant and the energy levels of the hydrogen atom, it became clear that at least some minor modifications were needed to explain the physics going on on the atomic scale. It was first noted by Einstein [26] that the methods developed by Bohr and Sommerfeld would not be capable of describing generic systems that display chaos. Later by the failure of the Bohr-Sommerfeld model in describing the energy levels of Helium, it indeed turned out that it was necessary to introduce some drastical new concepts. This realization led in the following years to the development of the theory of quantum mechanics as we know it today.

With the development of chaos theory a new interest in the old quantum theory arose. It has been realized that dynamical systems in general display a very complicated and unpredictable behavior - *chaos*, which means that the integrable case which provided the first success of the Bohr-Sommerfeld model is rather an exception than a rule. With the work of Gutzwiller [35] the importance of classical orbits in quantum systems which has a chaotic underlying classical dynamics became evident. The Gutzwiller trace formula expresses the density of states of a quantum system as a sum over the periodic orbits of the corresponding classical system. Various resummation techniques can be applied to the Gutzwiller trace formula, yielding altogether one of the principal bodies of theoretical methods available for the analysis of quantum systems whose classical analogs are chaotic. Considerable progress has been made along these lines in the recent years, and new methods have appeared for understanding

a variety of systems in atomic, molecular and nuclear physics. Many of these results are in a sense just improvements of the Gutzwiller trace formula, having different advantages as for instance in their convergence properties. It is along this line of work the present thesis should be considered a small contribution. In the following sections we shall try to describe our search for improvements and variations on the theme of Gutzwiller.

A guide to the busy reader

The content of the following thesis might, at a first sight, seem quite overwhelming. However, because the work follows mainly three different directions, a lot of different basic material, which should not be considered as a main part of the original work, has been included. To help the reader to focus on the part of the thesis I find is due to my own work it is therefore appropriate here to sketch an outline of the following sections:

1. In section **2**, we introduce the 3-disk scattering system and describe the properties of this in order to be able to use this as an example for numerical studies throughout the following sections. This section should not provide any dramatic new information since it is based on work by Gaspard and Rice[32], and on several articles by Cvitanović [12].

2. In section **3,4**, we describe the results on flows, semiclassical quantization and cycle expansions obtained in the recent years before the start of the present work. This work should also be well known for people within the field of classical chaos and semiclassical quantization, and is only included for self consistency of the thesis.

3. The last three sections however, should finally contain my own contributions, but of course also here I have to relay on results recently obtained by others. In section **5**, we start by studying the first attempt (the quantum Fredholm determinant) to improve the convergence properties of semiclassical spectral determinants. This work is based on the articles of Cvitanović and Rosenqvist [13] and on the article by Cvitanovic, Rosenqvist, Rugh and Vattay [14]. Next we investigate the evolution operator introduced by G. Vattay [53], which has the property that it is multiplicative and therefore results in an entire spectral determinant. My work here consists in obtaining the general expression for this in the N-dimensional case, and examplify the results with a few numerical examples.

4. In section **6**, we first describe the theory of geometrical optics by Keller [38, 39], and then use his results and the work by Franz [28] to introduce new generalized diffractive periodic orbits in the Gutzwiller trace formula. This work was done together with G. Vattay and A. Wirzba and resulted in the articles [54].

5. Finaly in section **7**, we described the recent theory of G. Vattay [55] on how to calculate $\hbar$ corrections to the Gutzwiller trace formula (or the re-

lated Gutzwiller-Voros zeta function), by studying local Schrödinger problems in the neighbourhood of the classical periodic orbits of the system. It should be emphasized that we take this theory as a starting point for the further work in the section and that we do not want to steal the credit for the original idea which is solely due to G. Vattay. My contribution in this section is therefore to specialize the theory to 2-dimensional billiard systems, to develop a simple numerical code (listed in the appendix) that calculates the first $\hbar$ correction for any 2-dimensional billard system and finally to use this code for numerical studies on the 3-disk system.

6. To minimize the content of the main part of the thesis I have decided to postpone a lot of the tedious derivations to a couple of appendices. These derivations can be interesting if one would like to go through all the detailed calculations but I think that in general they would lower the readability of the main part of the work which is already bothered with a lot of tedious calculations. In the main text I have indicated which derivations one can find (at least a sketch of) in these appendices. As mentioned above we also list the FORTRAN code which has been used for calculating the $\hbar$ corrections in the 3-disk scattering system.

It is my hope that the above considerations should provide readers, who are already familiar with these topics, with a useful guide to find their way through the thesis.

Chapter 2

The laboratory

2.1 Classical Pinball

The model that we shall use for numerical studies throughout this thesis is simple, yet physical and instructive. One can use it to illustrate almost everything one needs to know about deterministic chaos: from Smale horseshoes, Cantor sets, Lyapunov exponents, symbolic dynamics, discrete symmetries, bifurcations, pruning and diffusion, all the way to transfer operators, thermodynamic formalism, and classical and quantum zeta functions.

Our classical pinball model consists of a point particle and three identical circular disks in the plane (fig. 2.1a).

The point particle is scattered elastically off the disks and moves freely between collisions. The dynamics with one or two disks is simple (there is either no or one trapped trajectory), but with three or more disks there are infinitely many trapped trajectories, forming a repeller. This repeller can be in principle observed by measurements such as irregularly fluctuating outgoing angles *vs.* impact parameter (the irregular or chaotic scattering[23]), but such measurements are difficult and very sensitive to small perturbations. Much more robust are the global averages of quantities such as the mean trapping time in the classical case or the scattering resonances in the quantum mechanical case.

2.2 Symmetries of the model

As the three disks are equidistantly spaced, the system has the C_{3v} symmetry. Applying an element (identity, rotation by $\pm 2\pi/3$, or reflection) of this symmetry group to any trajectory yields another dynamically acceptable trajectory. Symmetry operations map *nonsymmetric* orbits into different orbits of the same shape, and for a *symmetric* orbit, the symmetry operation will map the set of points making up the orbit in phase space into itself.

4
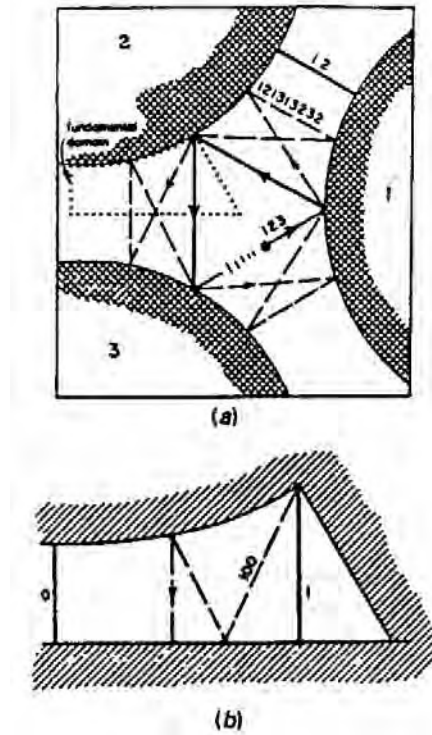
Figure 2.1: The scattering geometry for the disk radius/separation ratio a : $R = 1 : 2.5$. (a) the three disks, with $\overline{12}$, $\overline{123}$ and $\overline{121232313}$ cycles indicated. (b) the fundamental domain, *ie.* a wedge consisting of a section of a disk, two segments of symmetry axes acting as straight mirror walls, and an escape gap. The above cycles restricted to the fundamental domain are now the two fix points $\overline{0}$ and $\overline{1}$ and the $\overline{100}$ cycle.

For symmetric periodic orbits (a trajectory is periodic if it returns to the starting position and momentum in phase space) some or all symmetry operations act like a shift in time, advancing the starting point to the starting point of a symmetry related segment. In this way a symmetric periodic trajectory can be subdivided into a sequence of irreducible segments. Stability, action and traversal time is the same for all irreducible segments. The global periodic orbits can be described completely in terms of the irreducible segments, by folding the irreducible segments into periodic orbits in the *fundamental domain* [16]. The fundamental domain is a one sixth slice of the full 3-disk system, with the symmetry axes acting as reflecting mirrors, see fig. 2.1b.

Orbits related in the full space by discrete symmetries map onto a single fundamental domain orbit. The reduction to the fundamental domain desymmetrizes the dynamics and removes all global discrete symmetry induced degeneracies: rotationally symmetric global orbits have degeneracy 2, reflectionally symmetric ones have degeneracy 3, and global orbits with no symmetry are 6-fold degenerate. The time-reversal degeneracies persist in the fundamental domain as well. Some examples of such orbits are shown in fig. 2.2.
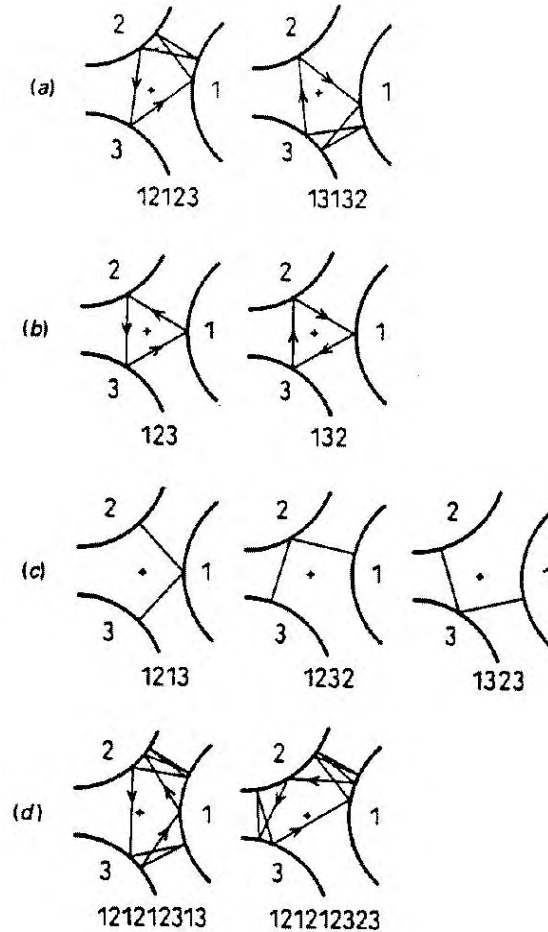
Figure 2.2: Some examples of 3-disk cycles. (a) $\overline{12123}$ and $\overline{13132}$ are mapped into each other by σ_{23}, the flip across 1 axis; this orbit has degeneracy 6 under C_{3v} symmetries. Similarly (b) $\overline{123}$ and $\overline{132}$ and (c) $\overline{1213}$, $\overline{1232}$ and $\overline{1323}$ are degenerate under C_{3v}. The orbits (d) $\overline{121212313}$ and $\overline{121212323}$ are related by time reversal but not by any C_{3v} symmetry.

2.3 Symbolic coding

The motion of a point particle is such that after a collision with one disk it either continues to another disk or it escapes to infinity. Labelling the disks 1, 2 and 3, this suggests associating with every trajectory a sequence of labels, indicating the disks with which the particle collides. The collision sequence will be finite for a scattering orbit, coming in from infinity and escaping after a finite number of collisions, and it will repeat periodically for a (trapped) periodic orbit. Arguments used in the usual horseshoe construction show that among the infinitely long sequences and the infinitely long unstable trapped orbits there is a one-to-one relationship; there exists an orbit to every (allowed) infinite sequence and every (allowed) infinite sequence labels a unique orbit.

There is one obvious restriction to the possible sequences, namely that two consecutive symbols must not be identical, since the particle cannot collide two times in succession with the same disk. In addition, there are relabeling symmetries, relating for instance the periodic orbits $\overline{12}$, $\overline{23}$, and $\overline{13}$, which are mapped into the same fundamental domain orbit. (A bar over a sequence indicates periodic repetitions; it will often be omitted when it is clear from the context that we are dealing with periodic orbits). By replacing the absolute disk labels by relative symbols, indicating only the orientation of the motion (clockwise or anticlockwise), both the symbol repetitions and the symmetry degeneracy are removed. We shall use the symbol 1 to indicate that the orientation after collision is kept, and the symbol 0 to indicate that it is reversed. Depending on the symmetry of the global orbit, periodically continued binary string labels correspond either to the full periodic orbit or to a repeating irreducible segment (examples are shown in fig. 2.1). If the disks are sufficiently far apart [1] there are no further restrictions on symbols, and all periodic binary sequences are realized as allowed periodic orbits. Table 2.1 lists some of the shortest binary symbol strings, together with the corresponding full 3-disk symbol sequences and orbit symmetries.

2.4 Counting prime cycles

In order to use the cycles of the system in our semiclassical determinants it is essential that we get all of the orbits up to a certain length. It is therefore necessary to be able to count the orbits in order not to miss any of them. For the ternary dynamics the number of periodic orbits of length n is simply $N_n^{(3)} = 3 \cdot 2^{n-1}$, since we are not allowed any consecutive bounce on the same disk. For the binary symbolic dynamics we get $N_n^{(2)} = 2^n$ since we have no pruning. Having calculated the number of periodic points, our next objective is to evaluate the number of prime cycles M_n for a dynamical system whose symbolic dynamics is built from N symbols. The problem of finding M_n is

---

[1]For ratios $R : a \geq 2.04821419\ldots$ there is no pruning of the system [49], and thus all the possible symbol sequences correspond to physically realizable periodic orbits.

$\tilde{p}$	p	$\mathbf{g}_{\tilde{p}}$
0	1 2	σ_{12}
1	1 2 3	C_3
01	12 13	σ_{23}
001	121 232 313	C_3
011	121 323	σ_{13}
0001	1212 1313	σ_{23}
0011	1212 3131 2323	C_3^2
0111	1213 2123	σ_{12}
00001	12121 23232 31313	C_3
00011	12121 32323	σ_{13}
00101	12123 21213	σ_{12}
00111	12123	e
01011	12131 23212 31323	C_3
01111	12132 13123	σ_{23}
000001	121212 131313	σ_{23}
000011	121212 313131 232323	C_3^2
000101	121213	e
000111	121213 212123	σ_{12}
001011	121232 131323	σ_{23}
001101	121231 323213	σ_{13}
001111	121231 232312 313123	C_3
010111	121312 313231 232123	C_3^2
011111	121321 323123	σ_{13}

Table 2.1: C_{3v} correspondence between the binary labeled fundamental domain prime cycles $\tilde{p}$ and the full 3-disk ternary $\{1,2,3\}$ cycles p, together with the C_{3v} transformation that maps the end point of the $\tilde{p}$ cycle into the irreducible segment of the p cycle. The degeneracy of p cycle is $m_p = 6n_{\tilde{p}}/n_p$.

classical in combinatorics (counting necklaces made out of n beads out of N different kinds) and is easily solved. There are N^n possible distinct strings of length n composed of N letters. These N^n strings include all M_d prime d-cycles whose period d equals or divides n. A prime cycle is a non-repeating symbol string: for example, $p = \overline{011} = \overline{101} = \overline{110} = \ldots 011011\ldots$ is prime, but $\overline{0101} = 010101\ldots = \overline{01}$ is not. A prime d-cycle contributes d strings to the sum of all possible strings, one for each cyclic permutation. The total number of possible periodic symbol sequences of length n is therefore related to the number of prime cycles by

$$N_n = \sum_{d|n} dM_d, \qquad\qquad (2.1)$$

where N_n equals $\mathrm{tr}\, T^n$. The number of prime cycles can be computed recursively

$$M_n = \frac{1}{n} \left(N_n - \sum_{\substack{d|n \\ d<n}} d M_d \right),$$

or by the *Möbius inversion formula*

$$M_n = n^{-1} \sum_{d|n} \mu\left(\frac{n}{d}\right) N_d. \tag{2.2}$$

where the Möbius function $\mu(1) = 1$, $\mu(n) = 0$ if n has a squared factor, and $\mu(p_1 p_2 \ldots p_k) = (-1)^k$ if all prime factors are different.

2.5 Periodic orbits

There is only one length scale in the system, the ratio of the center-to-center separation to the disk radius $R : a$. The energy is a quadratic function of momenta, $H = p^2/2m$, so motion at different energies E and E_0 is related by the scaling $p_E \to p_0 \sqrt{E/E_0}$ for momenta, $t_E \to t_0 \sqrt{E_0/E}$ for times, and

$$S(E) = L\sqrt{2mE} = S(E_0)\sqrt{E/E_0} \tag{2.3}$$

for the actions, where L is the geometrical length of the orbit. The eigenvalues of the Jacobian transverse to a periodic orbit (see below) are invariant under the above energy rescaling. These observations will be useful below in the semiclassical context where (2.3) will combine with $\hbar$ to the relevant quantum variable, the wavenumber $k = \sqrt{2mE}/\hbar$.

The motion between collisions is completely characterized by an angle φ marking the point of collision along a disk and the impact parameter $b = \tilde{b}/R$ measured in units of the radius. Because of symmetry, we can always select the disk 1 as the disk of current collision and the disk 3 as the origin of the particle. Ingoing coordinates then are (φ_{in}, b_{in}) and outgoing coordinates are $(\tilde{\varphi}_{out}, \tilde{b}_{out})$, where the ˜ indicates that these coordinates refer to the next collision disk. When working in the fundamental domain they still need to be mapped back onto disk 2. Accordingly, we have two types of collisions:

    0: the particle returns to the disk it is coming from
    1: the particle continues to the next disk.

The corresponding maps are (the angle φ is measured clockwise relative to the line connecting the centers of disks 1 and 3)

$$T_0 : \begin{cases} \varphi_{out} = -\varphi_{in} + 2\arcsin b_{in} \\ b_{out} = -b_{in} + \frac{d}{R}\sin\varphi_{out} \end{cases} \tag{2.4}$$

for reflection and

$$
T_1 : \begin{cases} \varphi_{out} = \varphi_{in} - 2\arcsin b_{in} + \varphi_{shift} \\ b_{out} = b_{in} - \frac{d}{R}\sin\varphi_{out} \end{cases}
\tag{2.5}
$$

with $\varphi_{shift} = 2\pi/3$ for the case of continuation. Each map has a fixed point, corresponding to the orbits $\overline{0}$ and $\overline{1}$. Longer periodic orbits are fixed points of sequences of maps, e.g.

$$
T_0 T_0 T_1 T_0 T_1 x_{10100} = x_{10100} \,,
\tag{2.6}
$$

(note that in our convention the maps are applied in reverse order compared to the symbolic sequence).

The Jacobian of the single collision map is given by

$$
J_i = \frac{\partial T_i(\varphi_{in}, b_{in})}{\partial(\varphi_{in}, b_{in})}
\tag{2.7}
$$

and the cycle Jacobian J_p is given by the product of Jacobians for the bounces around the cycle p. As the dynamics is phase-space volume preserving, $\det J = 1$ and the eigenvalues depend only on $tr(J)$:

$$
\Lambda_\pm = \frac{1}{2}\left(tr(J) \pm \sqrt{tr(J)^2 - 4}\right) \,.
\tag{2.8}
$$

The sign of the eigenvalue depends of the number of collisions along the cycle. For the '0' symbol there are two bounces in the fundamental domain: one with the disk and one with the reflecting wall. Since the wall can be regarded as a disk of infinite radius, the trace changes sign two times and thus the eigenvalues are positive. Symbol '1' corresponds to one bounce with the disk but two wall bounces and hence the eigenvalues of the '1'-cycle are negative. For an arbitrary fundamental domain cycle, the eigenvalue sign is given by $(-1)^{n_1}$, where n_1 is the number of '1's in the binary string corresponding to the cycle.

The exact lengths and eigenvalues of $\overline{0}$, $\overline{1}$ and $\overline{10}$ cycles follow from elementary geometrical considerations (we set the disk radius $R = 1$ throughout). For the fundamental domain $\overline{0}$ (the 2-cycle of the complete 3-disk space) and $\overline{1}$ (the 3-cycle of the complete 3-disk space) fixed points we obtain

$$
\begin{array}{lll}
\overline{0}: & L_0 = d - 2 & \Lambda_0 = (d-1) + \sqrt{(d-1)^2 - 1} \\
\overline{1}: & L_1 = d - \sqrt{3} & \Lambda_1 = -(\frac{2}{\sqrt{3}}d - 1) - \sqrt{(\frac{2}{\sqrt{3}}d - 1)^2 - 1}
\end{array} \,,
\tag{2.9}
$$

and for the $\overline{10}$-cycle we obtain

$$
\overline{10}: \quad L_{10} = \sqrt{1 + \left(2d - \sqrt{3}\right)^2} - 2, \quad tr(J_{10}) = \frac{L_{10}(L_{10}+1)(L_{10}+2)}{\sqrt{3}d/2 - 1} + 2L_{10} + 2 \quad .
$$

Λ_{10} then follows from (2.8). Longer cycles require numerical evaluation by methods such as orbit length minimization, which we describe in section (2.7). Formulas for evaluation of the cycle Jacobians we are going to study in the following section.

2.6 Cycle stability for billiards

Consider a 2-dimensional billiard with phase space coordinates (q_1, q_2, p_1, p_2). Let t_k be the instant of the k-th collision of the billiard with the billiard boundary, and $t_k^{\pm} = t_k \pm \epsilon$, ϵ positive and infinitesimal. Setting the mass and the velocity equal to 1, we impose the energy conservation by parametrizing the momentum direction by angle θ, $(q_1, q_2, \sin\theta, \cos\theta)$. Now parametrize the 2-$d$ neighborhood of a trajectory segment between $(k-1)$-th and k-th collisions by $\delta x = (\delta\theta, \delta z)$, where δz_k is the coordinate variation transverse to the k-th segment of the flow. Using $dq_i/dt = p_i$, we obtain the equations of motion for the linearized neighborhood

$$\frac{d}{dt}\delta\theta = 0, \quad \frac{d}{dt}\delta z = \delta\theta \,.$$

Let $\delta\theta_k = \delta\theta(t_k^+)$ and $\delta z_k = \delta z(t_k^+)$ be the local coordinates immediately after the k-th collision, and $\delta\theta_k^- = \delta\theta(t_k^-)$, $\delta z_k^- = \delta z(t_k^-)$ immediately before. Integrating the free flight from t_{k-1}^+ to t_k^- we obtain

$$
\begin{aligned}
\delta\theta_k^- &= \delta\theta_{k-1} \\
\delta z_k^- &= \delta z_{k-1} + \tau_k \delta\theta_{k-1} \,, \qquad \tau_k = t_k - t_{k-1} \,,
\end{aligned}
\tag{2.10}
$$

and the transverse Jacobian is given by

$$\mathbf{J}_T(x_k) = \begin{bmatrix} 1 & 0 \\ \tau_k & 1 \end{bmatrix} \,.$$

At incidence angle ϕ_k (the angle between the outgoing particle and the outgoing normal to the billiard edge), the incoming transverse variation δz_k^- projects onto an arc on the billiard boundary of length $\delta z_k^- / \cos\phi_k$. The corresponding incidence angle variation $\delta\phi_k = \delta z_k^- / R_k \cos\phi_k$, $R_k =$ local radius of curvature, increases the angular spread to

$$
\begin{aligned}
\delta\theta_k &= -\delta\theta_k^- - \frac{2}{R_k \cos\phi_k}\delta z_k^- \\
\delta z_k &= -\delta z_k^- \,,
\end{aligned}
\tag{2.11}
$$

so the Jacobian associated with the reflection is

$$\mathbf{J}_R(x_k) = -\begin{bmatrix} 1 & r_k \\ 0 & 1 \end{bmatrix} \,, \qquad r_k = \frac{2}{R_k \cos\phi_k} \,.$$

The Jacobian of a cycle p of length n_p is therefore given by

$$\mathbf{J}_p = (-1)^{n_p} \prod_{k=1}^{n_p} \left[\begin{array}{cc} 1 & r_k \\ 0 & 1 \end{array} \right] \left[\begin{array}{cc} 1 & 0 \\ \tau_k & 1 \end{array} \right] . \tag{2.12}$$

As $\det \mathbf{J} = 1$, the sign of the leading eigenvalue depends only on the trace of the determinant: $\Lambda = \frac{1}{2}(\mathrm{Tr}J \pm \sqrt{\mathrm{Tr}^2 J - 4})$, and by (2.12) the trace after n compositions of the determinants has the sign $(-1)^n$, $ie.$ the eigenvalues flip sign at each collision. This yields a convenient way of finding the correct sign of the stabilities in the fundamental domain, since a straight wall can be considered as the limit of a disk whose radius tends to infinity. A typical set of the periodic orbit data, for $d : R = 6$ and length ≤ 6, is listed in 2.2.

period	Λ_p	Action	code
1	9.898979485566E+00	4.000000000000	0
1	-1.177145519638E+01	4.267949192431	1
2	-1.240948019921E+02	8.316529485168	01
3	-1.240542557041E+03	12.321746616182	001
3	1.449545074956E+03	12.580807741032	011
4	-1.229570686196E+04	16.322276474382	0001
4	1.445997591902E+04	16.585242906081	0011
4	-1.707901900894E+04	16.849071859224	0111
5	-1.217338387051E+05	20.322330025739	00001
5	1.432820951544E+05	20.585689671758	00011
5	1.539257907420E+05	20.638238386018	00101
5	-1.704107155425E+05	20.853571517227	00111
5	-1.799019479426E+05	20.897369388186	01011
5	2.010247347433E+05	21.116994322373	01111
6	-1.205062923819E+06	24.322335435738	000001
6	1.418521622814E+06	24.585734788507	000011
6	1.525597448217E+06	24.638760250323	000101
6	-1.688624934257E+06	24.854025100071	000111
6	-1.796354939785E+06	24.902167001066	001011
6	-1.796354939785E+06	24.902167001066	001101
6	2.005733106218E+06	25.121488488111	001111
6	2.119615015369E+06	25.165628236279	010111
6	-2.366378254801E+06	25.384945785676	011111

Table 2.2: Classical periodic orbits for the three disk system at $d : R = 6$. The columns list the symbolic period, the instability Λ_p, the length or action of the orbit and the binary symbolic coding of the orbit. Note the two period 6 orbits $\overline{001011}$ and $\overline{001101}$, which have the same action and stability; they are related by time reversal symmetry but not by any discrete spatial symmetry.

2.7   Orbit length minimization method

The simplest method for determining billard cycles is given by the principle of least action, or, equivalently, by minimizing the length of an approximate orbit that visits a given sequence of disks. In contrast to the multipoint shooting method which requires variation of $2N$ phase-space points, minimization of the cycle length requires variation of only N bounce positions s_i, $i = 1, 2, \ldots, N$. In the following we shall see that this variation indeed can be accomplished by considering only a one-dimensional minimization problem.

The method works for any billard system but let us for now assume that we are working with N non-intersecting disks with radii R_i. Let the point (x_i, y_i) denote the center of the i'th disk, and $s_i^{(0)}$ be the initial guess of the i'th bouncing position, which is an angle measured with respect to some fixed point on the surface of the i'th disk. The length (or equivalently, the period or the action) of the initial approximate cycle is given by

$$L^{(0)} = \sum_{i=1}^{N} l_i^{(0)} = \sum_{i=1}^{N} [(\Delta x_i^{(0)})^2 + (\Delta y_i^{(0)})^2]^{1/2}$$

where $\Delta x_i^{(0)} \equiv x_{i+1} - x_i + R_{i+1} \cos(s_{i+1}^{(0)}) - R_i \cos(s_i^{(0)})$, $x_{N+1} \equiv x_1$, and similarly for $\Delta y_i^{(0)}$. The idea is now the following: taking the gradient of $L^{(0)}$ gives us the direction in $\mathbf{s}$ space in which the total length decreases with the highest rate. Following this direction until we reach a minimum defines a new point $\mathbf{s}^{(1)}$ which is now the next approximation to the real cycle. Iterating this procedure then finaly leads to a cycle that obeys the Fermat principle and therefore is the cycle we are interested in. In our case the gradient of the length function in the j'th approximation can be obtained directly and reads:

$$
\begin{aligned}
(\vec{\nabla} L^{(j)})_i &= \frac{\partial l_{i-1}^{(j)}}{\partial s_i^{(j)}} + \frac{\partial l_i^{(j)}}{\partial s_i^{(j)}} \\
&= R_i \left(\sin(s_i^{(j)})(\frac{\Delta x_i^{(j)}}{l_i^{(j)}} - \frac{\Delta x_{i-1}^{(j)}}{l_{i-1}^{(j)}}) - \cos(s_i^{(j)})(\frac{\Delta y_i^{(j)}}{l_i^{(j)}} - \frac{\Delta y_{i-1}^{(j)}}{l_{i-1}^{(j)}}) \right) .
\end{aligned}
$$

The minimization algorithm can now be implemented by following the recursion scheme:

1. Select an initial set of bounce positions $\vec{s}_0$.

2. Evaluate $\vec{\nabla} L \mid_{\vec{s}=\vec{s}_0}$.

3. Minimize L along the hyper line spanned by the above gradient, *ie.* minimize the function $L(\vec{s}_0 + \vec{\nabla} L \mid_{\vec{s}=\vec{s}_0} \cdot t)$ with respect to the parameter t.

4. Use the bounce points $\vec{s}_1$ so determined as the starting point for the next iteration of the algorithm, and proceed iterating items 2,3 and 4 until the desired accuracy is attained.

5. If the dynamics is pruned, check that the final minimal length orbit does not penetrate any of the disks.

One way to ensure that the algorithm has obtained the limit of the procedure is to evaluate the gradient (or the length of the gradient) at the different points $\mathbf{s}^{(0)}, \mathbf{s}^{(1)}, \mathbf{s}^{(2)}, \ldots$. In practice when the length of the gradient is zero up to accuracy of the implemented precision (quadruple precision $0 \simeq 10^{-32}$), further iteration does not alter the bouncing positions. It turns out that the algorithm converges very fast to this limit, of course depending on the initial guess and the length of the cycle. To get a good initial guess, one can construct the following $\mathbf{s}^{(0)}$: first you consider the full space itinerary $\alpha_1, \alpha_2, \ldots, \alpha_{n_p}$ that describes the sequence in which the disks are visited by the cycle. To construct $s_i^{(0)}$ we then consider the two line segments that connects the centers of the previous and following disk to the center of the current disk. Then $s_i^{(0)}$ can be set as the angle that divides the angle spanned by these two line segments in two equal parts.

The above method has been applied succesfully to the 3-disk system at three different disk-disk separations, namely with $R : a = 3$, $R : a = 6$ and $R : a = 12$, and all orbits up to topological length (in binary alphabet) 12 have been obtained. Besides this we have also [44] checked the method on the 7- and 13-disk systems where the disks have been positioned as first and second approximations to the Lorentz gas [44].

Chapter 3

Classical periodic orbit theory

3.1 Flows, evolution operators and their spectra

Functional determinants and zeta functions arise in classical and quantum mechanics because in both the dynamical evolution can be described by the action of linear evolution operators on infinite-dimensional vector spaces. The classical *evolution operator* for a d-dimensional map or a $(d + 1)$-dimensional flow is given by:

$$\mathcal{L}^t(y, x) = \delta(y - f^t(x))g^t(x) . \tag{3.1}$$

For discrete time, $f^n(x)$ is n-th iterate of the map f; for continuous flows, $f^t(x)$ is the trajectory of the initial point x. $g^t(x)$ is a weight multiplicative along the trajectory; its precise functional form depends on the dynamical average under study. For purposes of this section it suffices to take $g^t(x) = 1$, essentially the Perron-Frobenius operator case.

The global averages (escape rates, energy eigenvalues, resonances, fractal dimensions, etc.) can be extracted from the eigenvalues of the evolution operators. The eigenvalues are given by the zeros of appropriate determinants. One way to evaluate determinants is to expand them in terms of traces, *log det = tr log*, and in this way relate the spectrum of an evolution operator to its traces, *ie.* the periodic orbits of the system. Formally, the traces $\text{tr}\mathcal{L}^t$ are easily evaluated as integrals of Dirac delta functions as follows.

3.1.1 Trace formula for maps

If the evolution is given by a discrete time mapping, and all periodic points are known to have stability eigenvalues $\Lambda_k \neq 1$ strictly bounded away from unity,

the trace $\mathcal{L}^n$ is given by the sum over all periodic points x of period n:

$$\begin{aligned}
\text{tr}\mathcal{L}^n &= \int dx dy \delta(x-y)\mathcal{L}^n(y,x) \\
&= \sum_p n_p \sum_{r=1}^{\infty} \frac{\delta_{n,n_p r}}{|\det\left(\mathbf{1} - \mathbf{J}_p^r\right)|} \; ,
\end{aligned} \tag{3.2}$$

where

$$\mathbf{J}_p(x) = \prod_{j=0}^{n_p - 1} \mathbf{J}(f^j(x)), \quad J_{kl}(x) = \frac{\partial}{\partial x_l} f_k(x) \tag{3.3}$$

is the $[d \times d]$ Jacobian matrix evaluated at the periodic point x, and the product goes over all periodic points x_i belonging to a given prime cycle p. The *trace formula* is the Laplace transform of $\text{tr}\mathcal{L}^t$ which, for discrete flows, is simply the generating function

$$\text{tr}\mathcal{L}(z) = \sum_{n=1}^{\infty} z^n \text{tr}\mathcal{L}^n = \sum_{\alpha=0}^{\infty} \frac{z e^{-\nu_\alpha}}{1 - z e^{-\nu_\alpha}}$$

where $e^{-\nu_0}$, $e^{-\nu_1}$, $e^{-\nu_2}$, ... are the eigenvalues of $\mathcal{L}$. For large times $\det\left(\mathbf{1} - \mathbf{J}^{(n)}(x_i)\right) \to \Lambda_i$, where Λ_i is the product of the expanding eigenvalues of $\mathbf{J}^{(n)}(x_i)$, so the trace is dominated by

$$\begin{aligned}
\text{tr}\mathcal{L}(z) &\approx \sum_{n=1}^{\infty} z^n \sum_{x_i \in \text{Fix}(f^n)} \frac{1}{|\Lambda_i|} \\
&= \frac{z e^{-\nu_0}}{1 - z e^{-\nu_0}} + \dots \; ,
\end{aligned} \tag{3.4}$$

and diverges at the leading eigenvalue $1/z = e^{-\nu_0}$. This approximation, which in current physics literature is called the "thermodynamic" or the "f of α" formalism [36], is adequate (but far from optimal) for extraction of the leading eigenvalue of $\mathcal{L}$, and difficult to apply to extraction of the non-leading eigenvalues.

3.1.2   Trace formula for flows

For flows the eigenvalue corresponding to the eigenvector along the flow (the velocity vector) necessarily equals unity for all periodic orbits, and therefore the integral (3.2) requires a more careful treatment [17].

To evaluate the contribution of a prime periodic orbit p of period T_p, one choses a local coordinate system with a longitudinal coordinate $dx_{\parallel}$ along the direction of the flow, and d transverse coordinates $x_{\perp}$

$$\text{tr}_p\mathcal{L}^t = \int_{V_p} dx_{\perp} dx_{\parallel} \delta(x_{\perp} - f_{\perp}^t(x))\delta(x_{\parallel} - f_{\parallel}^t(x)) \; . \tag{3.5}$$

Integration is restricted to an infinitesimally thin tube V_p enveloping the cycle p.

Let $v = |\mathbf{F}(x)|$ be the velocity along the orbit, and change the longitudinal variable to $dx_\| = v d\tau$. Whenever the time t is a multiple of the cycle period T_p, the longitudinal delta function contributes a term $1/v$, canceling the corresponding factor v from the change of variables, and the integral along the trajectory yields a factor T_p:

$$
\begin{aligned}
\int_{V_p} dx_\| \delta(x_\| - f_\|^t(x)) &= \sum_{r=1}^\infty \delta(t - rT_p) \int_p d\tau \\
&= T_p \sum_{r=1}^\infty \delta(t - rT_p) \ .
\end{aligned}
\tag{3.6}
$$

Linearization of the periodic flow in a plane perpendicular to the orbit yields the same weight as for the maps:

$$
\int_{V_p} dx_\perp \delta(x_\perp - f_\perp^{-rT_p}(x)) = \frac{1}{\left|\det\left(\mathbf{1} - \mathbf{J}_p^r\right)\right|} \ ,
\tag{3.7}
$$

where $\mathbf{J}_p$ is the p-cycle $[d{\times}d]$ transverse Jacobian, and we have assumed hyperbolicity, $ie.$ that all transverse eigenvalues are bounded away from unity. A geometrical interpretation of weights such as (3.7) is that after the r-th return to a surface of section, the initial tube V_p has been stretched out along the expanding eigendirections, with the overlap with the initial volume given by $1/\left|\det\left(\mathbf{1} - \mathbf{J}_p^r\right)\right|$.

Substituting (3.6-3.7) into (3.5), we obtain an expression for $\mathrm{tr}\,\mathcal{L}^t$ as a sum over all prime cycles p and their repetitions

$$
\mathrm{tr}\mathcal{L}^t = \sum_p T_p \sum_{r=1}^\infty \frac{\delta(t - rT_p)}{\left|\det\left(\mathbf{1} - \mathbf{J}_p^r\right)\right|} \ .
$$

A Laplace transform replaces the above sum of Dirac delta functions by the $trace\ formula\ for\ classical\ flows$ [17]:

$$
\mathrm{tr}\mathcal{L}(s) = \int_0^\infty dt\, e^{st} \mathrm{tr}\mathcal{L}^t = \sum_p T_p \sum_r \frac{e^{sT_p r}}{\left|\det\left(\mathbf{1} - \mathbf{J}_p^r\right)\right|} \ .
\tag{3.8}
$$

We should caution the reader that in taking the Laplace transform we have ignored a possible $t \to 0_+$ volume term, as we do not know how to regularize the delta function kernel in this limit. In the quantum (or heat kernel) case this limit gives rise to the Weyl or Thomas-Fermi mean eigenvalue spacing. A more careful treatment might assign to such volume term some interesting role in the theory of classical resonance spectra.

The semi-classical evaluation of the quantum trace is considerably more laborious, but the final result, given in sect. 4.1, is very similar in form to the above classical trace.

3.1.3   Fredholm determinants

The problem with the classical (3.4), (3.8) and the Gutzwiller trace formulas (4.21) is that they diverge precisely where one would like to use them (we return to this in sect. 5.1.2). While in the physics literature on dynamically generated strange sets this does not prevent numerical extraction of reasonable "thermodynamic" averages, in the case of the Gutzwiller trace formula this leads to the perplexing observation that crude estimates of the radius of convergence seem to put the entire physical spectrum out of reach. This problem is cured by going from trace formulas to determinants, which turn out to have larger analyticity domains. For maps, the two are related by

$$F(z) = \det(1 - z\mathcal{L}) = \exp\left(-\sum_{n}^{\infty} \frac{z^n}{n} \mathrm{tr}\mathcal{L}^n\right)$$

For flows the classical Fredholm determinant is given by

$$F(s) = \exp\left(-\sum_{p}\sum_{r=1}^{\infty} \frac{1}{r} \frac{e^{sT_p r}}{|\det\left(\mathbf{1} - \mathbf{J}_p^r\right)|}\right) , \tag{3.9}$$

and the classical trace formula (3.8) is the logarithmic derivative of the classical Fredholm determinant

$$\mathrm{tr}\mathcal{L}(s) = -\frac{d}{ds} \log F(s) . \tag{3.10}$$

With z set to $z = e^s$, the Fredholm determinant (3.9) applies both to maps and flows. A Fredholm determinant can be rewritten as an infinite product over periodic orbits, by noting that the r sum in (3.9) is close in form to expansion of a logarithm. We cast it into such a form by expanding the Jacobian weights in terms of stability eigenvalues. For a 3-dimensional Hamiltonian flow with one expanding eigenvalue Λ, and one contracting eigenvalue $1/\Lambda$, the weight in (3.9) may be expanded as follows:

$$\frac{1}{|\det\left(\mathbf{1} - \mathbf{J}_p^r\right)|} = \frac{1}{|\Lambda|^r(1 - 1/\Lambda_p^r)^2}$$

$$= \frac{1}{|\Lambda|^r} \sum_{k=0}^{\infty} (k+1)\Lambda_p^{-kr} . \tag{3.11}$$

With this we can rewrite the Fredholm determinant exponent as

$$\sum_{r=1}^{\infty} \frac{1}{r} \frac{e^{sT_p r}}{|\det\left(\mathbf{1} - \mathbf{J}_p^r\right)|} = \sum_{k=0}^{\infty} (k+1) \log\left(1 - \frac{e^{sT_p}}{|\Lambda_p|\Lambda_p^k}\right) .$$

and represent the Fredholm determinant as a Selberg-type product [17]

$$
\begin{aligned}
F(s) &= \prod_p \prod_{k=0}^{\infty} \left(1 - t_p/\Lambda_p^k\right)^{k+1} , \\
t_p &= \frac{e^{sT_p}}{|\Lambda_p|} z^{n_p} .
\end{aligned}
\tag{3.12}
$$

z is a book-keeping variable that we will use to expand zeta functions and determinants, set to $z = 1$ in calculations. The first ($k = 0$) zeta function in the product is the Ruelle or dynamical zeta function [45]

$$
\zeta = \prod_p (1 - t_p). ,
\tag{3.13}
$$

where in general, t_p depends on the dynamical average one wishes to evaluate. The simplest example is the weight (3.12) used in computation of escape rates and correlation spectra. (3.13) also yields the leading semi–classical *quantum* resonances, if t_p is the quantum weight (4.30) associated with the cycle p.

The above heuristic manipulations are potentially dangerous, as we are dealing with infinite-dimensional vector spaces and singular integral kernels; however, the Fredholm determinants are entire functions in any dimension, provided that [48]

1. the evolution operator is *multiplicative* along the flow,
2. the symbolic dynamics is a *finite subshift*,
3. all cycle eigenvalues are *hyperbolic* (sufficiently bounded away from 1),
4. the map (or the flow) is *real analytic*, *ie.* it has a piecewise analytic continuation to a complex extension of the phase space.

The notion of Axiom A systems is a mathematical abstraction of 2 and 3. It would take us too far to give and explain the definition of the Axiom A systems (see ref. [52]). Axiom A implies, however, the existence of a Markov partition of the phase space from which 2 and 3 follow. Properties 1 and 2 enable us to represent the evolution operator as a matrix in an appropriate basis space; properties 3 and 4 enable us to bound the size of the matrix elements and control the eigenvalues.

3.2 Cycle expansions

A *cycle expansion*[19] is a series representation of a zeta function or a Fredholm determinant, expanded as a sum over *pseudo-cycles*, products of prime cycle weights t_p, ordered by increasing cycle length and instability. The products (3.13),(4.32) are really only a shorthand notation for zeta functions and determinants - for example, the zeros of the individual factors in infinite products (3.13),(4.32) are *not* the zeros of the corresponding zeta functions and determinants, and convergence of such objects is far from obvious.

3.2.1 Curvature expansions

Curvature expansions are based on the observation[19, 3, 4] that the motion in dynamical systems with finite grammar is organized around a few *fundamental* cycles; more precisely, that the cycle expansion of the dynamical zeta function (3.13) allows a regrouping of terms into dominant *fundamental* contributions t_f and decreasing *curvature* corrections c_n:

$$1/\zeta = 1 - \sum_f t_f - \sum_n c_n \, . \tag{3.14}$$

The fundamental cycles t_f have no shorter approximants; they are the "building blocks" of the dynamics in the sense that all longer orbits can be approximately pieced together from them. In piecewise linear approximations to the flow, $1/\zeta$ is given by the determinant for a finite Markov transition matrix, and all c_n vanish identically. Hence the designation "curvatures"; size of c_n is an indication how far the flow is from a piecewise linearization.

A typical curvature term in (3.14) is a difference of a long cycle $\{ab\}$ and its shadowing approximation by shorter cycles $\{a\}$ and $\{b\}$:

$$t_{ab} - t_a t_b = t_{ab}(1 - t_a t_b / t_{ab})$$

The orbits that follow the same symbolic dynamics, such as $\{ab\}$ and the "pseudo orbit" $\{a\}\{b\}$, lie close to each other, have similar weights, and for longer and longer orbits the differences are expected to fall off rapidly. For systems that satisfy Axiom A requirements, such as the 3-disk repeller, curvature expansions converge very well[18]. It is crucial that the curvature expansion is grouped (and truncated) by topologically related cycles and pseudo-cycles; truncations that ignore topology, such as inclusion of all cycles with $T_p < T_{max}$, will contain un-shadowed orbits, and exhibit a mediocre convergence compared with the curvature expansions.

3.2.2 Fredholm determinant cycle expansions

While for the dynamical zeta function cycle expansions the shadowing is easy to explain, the resulting convergence is not the best achievable; as explained above, Fredholm determinants are expected to be entire, and their cycle expansions should converge faster than exponentially. The Fredholm determinant cycle expansions are somewhat more complicated than those for the dynamical zeta functions. We expand the exponential representation (3.9) of $F(s)$ as a multinomial in prime cycle weights t_p

$$
\begin{aligned}
F_p &= 1 - \sum_{r=1}^{\infty} \frac{1}{r} \frac{t_p^r}{\left| \det \left[\mathbf{1} - \mathbf{J}_p^r \right] \right|} + \frac{1}{2}(\ldots)^2 - \ldots . \\
&= \sum_{r=1}^{\infty} C_{p^k} t_p^k \, .
\end{aligned}
$$

This yields the cycle expansion for $F(s)$:

$$F(s) = \sum_{k_1 k_2 k_3 \cdots = 0}^{\infty} \tau_{p_1^{k_1} p_2^{k_2} p_3^{k_3} \cdots}$$

$$\tau_{p_1^{k_1} p_2^{k_2} p_3^{k_3} \cdots} = \prod_{i=1}^{\infty} C_{p_i k_i} t_{p_i}^{k_i},$$

where the sum goes over all pseudo-cycles.

3.2.3 Numerical calculations with cycle expansions

In practice we do not do anything as complicated as the expansion of the pro-ceeding section. Consider the prototype of any of the determinants we are going to evaluate numerically

$$F(z, s) = \prod_p \prod_{l=0}^{\infty} (1 - t_{p,l}(s) z^{n_p}), \tag{3.15}$$

where $t_{p,l}$ is the weight associated with the p'th primitive cycle, and z is the book-keeping variable keeping track of the topological length n_p of the cycles. Now the product (3.15) can be written as an exponential like in (3.9)

$$F(z, s) = \exp\left(-\sum_p \sum_{l=0}^{\infty} \sum_{r=1}^{\infty} \frac{1}{r} (t_{p,l} z^{n_p})^r\right) \tag{3.16}$$

where we expanded the logarithm in the identity $x = \exp(\ln x)$. For most of the cases we are going to encounter the above l sum can be performed analytically so that we end up with

$$F(z, s) = \exp\left(-\sum_p \sum_{r=1}^{\infty} \frac{1}{r} c_p^r z^{n_p r}\right). \tag{3.17}$$

By gathering all terms of the same power in z we then finaly get

$$F(z, s) = \exp(-\sum_{n=1}^{\infty} \mathrm{Tr}_n z^n), \tag{3.18}$$

where Tr_n is just the total contribution, which is finite, from all the cycles to the power n of z. A cycle of topological length n_p will thus contribute to the sum by the powers of $z^{n_p}, z^{2n_p}, \ldots, z^{rn_p}, \ldots$. Adding up the contribution from all the individual cycles to the Tr_n's can then be performed by a single loop in a program. Next we expand each of the exponentials $\exp(-\mathrm{Tr}_n z^n)$ in a power series in z. Finaly, by multiplying these power series together we obtain the final power series expansion in z of the determinant. This should then be cut of at the maximal cycle length N

$$F_N(s, z) = \sum_{n=0}^{N} C_n(s) z^n \tag{3.19}$$

In the final evaluation z is set to $z = 1$, but the organization by powers of z^n is crucial to the convergence of cycle expansions.

To find the zeros of the determinant, we use the standard Newton-Raphson searching algorithm. To obtain a good starting point for this one can start by scanning the area of the complex plane under investigation. One should then search for local low values of the determinant by evaluating this on a suitable grid. Having obtained these initial guesses we apply the recursion scheme

$$ s_{i+1} \;\; = \;\; s_i - F_N(s_i, 1)/F'_N(s_i, 1), \tag{3.20} $$

to search for the zeros. To obtain the derivative of the determinant we can use exactly the same routine as to determine it. From (3.18) we can directly get the derivative

$$ F'_N(z, s) \;\; = \;\; (-\sum_{n=1}^{N} \mathrm{Tr}'_n z^n) F_N(z, s), \tag{3.21} $$

which means that in the same loop where we sum up the Tr_n's we should merely at the same time sum up also the derivatives of these. After this one just has to make one extra power series multiplication in order to obtain $F'_N(z, s)$. Of course, also here we in the end put $z = 1$.

3.2.4   Convergence of cycle expansions

It is fairly easy to establish that for Axiom A systems the trace formulas converge exponentially with the number of cycles included. As will be explained in sect. 5.1.2, the trace formulas are not absolutely convergent where you need them, and in addition, shadowing of longer orbits by nearby pseudo-orbits is not implemented, so we will not use trace formulas at all. However, it should be noted that for systems other than Axiom A, we do not know how to improve convergence by shadowing cancellations, or define determinants that are guaranteed to be entire, and it is still possible that for generic systems determinants do not converge any better than traces.

For dynamical zeta functions geometrical estimates [3] imply that for Axiom A systems the curvature expansion coefficients fall off exponentially, $C_k \approx \tilde{C}^k$, and the expansion sums up to a pole

$$ \sum_{n=0}^{\infty} C_k z^k \simeq \sum_{n=0}^{\infty} (\tilde{C} z)^k = \frac{1}{1 - \tilde{C} z}. $$

Such poles are indeed observed numerically [4]. Convergence of dynamical zeta functions cycle expansions can be accelerated by a variety of numerical methods, but both on theoretical grounds and in practice, the preferred alternative is to use Fredholm determinants instead.

3.2.5 Symmetry factorizations

Discrete symmetries of the classical dynamics play a role with which we are familiar from quantum mechanics; as they commute with the evolution operators, they can be used to decompose them and factorize the associated determinants [16]:

$$1/\zeta^{3-disk} = \prod_\alpha 1/\zeta_\alpha^{d_\alpha} \ .$$

The product is over the d_α-dimensional irreducible representations α of the symmetry group, in this case C_{3v}, with two 1-dimensional representations A_1, A_2 and a pair of 2-dimensional representations E. The factorization relates each fundamental domain orbit to the corresponding degenerate set of full space orbits as follows:

symmetry		full space		A_1	A_2	E
rotation	:	$(1 - t_{rot}^3)^2$	$=$	$(1 - t_{rot})$	$(1 - t_{rot})$	$(1 + t_{rot} + t_{rot}^2)^2$
reflection	:	$(1 - t_{ref}^2)^3$	$=$	$(1 - t_{ref})$	$(1 + t_{ref})$	$(1 - t_{ref}^2)^2$
none	:	$(1 - t_{non})^6$	$=$	$(1 - t_{non})$	$(1 - t_{non})$	$(1 - t_{non})^4$

Fundamental domain cycles up to length 5 are listed in table 2.1 in section 2.3, together with the symmetry factors that map them into the corresponding global orbit irreducible segments; these determine which of the above factorizations apply to a given cycle. Substituting the shortest cycles into the zeta functions, we obtain for the completely symmetric A_1 subspace:

$$
\begin{aligned}
1/\zeta_{A_1}(z) \ = \ & (1 - zt_0)(1 - zt_1)(1 - z^2 t_{01})(1 - z^3 t_{001})(1 - z^3 t_{011}) \\
& (1 - z^4 t_{0001})(1 - z^4 t_{0011})(1 - z^4 t_{0111})(1 - z^5 t_{00001})(1 - z^5 t_{00011}) \\
& (1 - z^5 t_{00101})(1 - z^5 t_{00111})(1 - z^5 t_{01011})(1 - z^5 t_{01111}) \dots . \quad (3.22)
\end{aligned}
$$

In the example at hand, with complete symbolic dynamics and no pruning rules, the cycle expanded zeta function is obtained by expanding the infinite product as a power series in z:

$$
\begin{aligned}
1/\zeta_{A_1}(z) \ = \ & 1 - zt_0 - zt_1 - z^2[(t_{01} - t_1 t_0)] \\
& - z^3[(t_{001} - t_{01} t_0) - (t_{011} - t_{01} t_1)] \\
& - z^4[(t_{0001} - t_0 t_{001}) + (t_{0111} - t_{011} t_1) \\
& + (t_{0011} - t_{001} t_1 - t_0 t_{011} + t_0 t_{01} t_1)] - \dots . \quad (3.23)
\end{aligned}
$$

For the A_2 subspace cycles with an odd number of 0's pick up an additional minus sign:

$$
\begin{aligned}
1/\zeta_{A_2}(z) \ = \ & 1 + zt_0 - zt_1 + z^2[(t_{01} - t_1 t_0)] \\
& - z^3[(t_{001} + t_{01} t_0) + (t_{011} - t_{01} t_1)] \\
& + z^4[(t_{0001} - t_0 t_{001}) + (t_{0111} - t_{011} t_1) \\
& + (t_{0011} - t_{001} t_1 - t_0 t_{011} + t_0 t_{01} t_1)] - \dots . \quad (3.24)
\end{aligned}
$$

The E subspace cycle expansion takes a somewhat less obvious form [16]:

$$
\begin{aligned}
1/\zeta_E &= (1 + zt_1 + z^2 t_1^2)(1 - z^2 t_0^2)(1 + zt_{100} + z^2 t_{100}^2)(1 - z^2 t_{10}^2) \\
&\quad (1 + zt_{1001} + z^2 t_{1001}^2)(1 + zt_{10000} + z^2 t_{10000}^2) \\
&\quad (1 + zt_{10101} + z^2 t_{10101}^2)(1 - z^2 t_{10011})^2 \ldots \\
&= 1 + zt_1 + z^2(t_1^2 - t_0^2) + z^3(t_{001} - t_1 t_0^2) \\
&\quad + z^4 \left[t_{0011} + (t_{001} - t_1 t_0^2)t_1 - t_{01}^2 \right] \\
&\quad + z^5 \left[t_{00001} + t_{01011} - 2t_{00111} + (t_{0011} - t_{01}^2)t_1 + (t_1^2 - t_0^2)t_{100} \right] \\
&\quad + \cdots
\end{aligned}
\tag{3.25}
$$

For orbits running on one of the symmetry lines, one has to take special care[16]. All our numerical results are obtained by determining the zeros of finite cycle length truncations of the above cycle expansions, or the corresponding ones for the Gutzwiller Voros zeta function, and related expressions for semiclassical spectral determinants which we are going to study in the following sections.

Chapter 4

Semiclassical periodic orbit quantization

4.1 The Van Vleck propagator

The Van Vleck formula is a semiclassical approximation for the usual propagator in quantum mechanics

$$G(x', t'; x, t) \quad \equiv \quad <x'|U(t', t)|x> \Theta(t) \tag{4.1}$$

where $U(t', t)$ is the unitary time evolution operator for some quantum system which might be time dependant, and $\Theta(t)$ is the unit step- or Heaviside function. The Van Vleck formula is the starting point for a number of derivations, approximations and intuitive leaps which take one from exact quantum expressions to a variety of results expressing energy eigenvalues and their correlations, wave functions and matrix elements in terms of classical periodic orbits.

The propagator

$$G(x', t'; x, t) \quad \equiv \quad <x', t'|e^{\frac{i}{\hbar}\hat{H}(t'-t)}|x, t> \tag{4.2}$$

fulfills

$$(\hat{H} - i\hbar\frac{\partial}{\partial t})G(x', t'; x, t) \quad = \quad -i\hbar\delta(t - t'). \tag{4.3}$$

To derive the semiclassical approximation to the propagator one can take as the starting point the solution to the initial value problem of quantum mechanics following the WKB procedure. This can be done since the propagator can be considered as the solution $G(x', t'; x, t)$ of the time-dependant Schrödinger equation, subject to the initial condition $G(x', t'; x, t) = \delta(x - x')$ at $t = 0$. To solve the initial value problem in the WKB approximation we start by making the following ansatz. Suppose we are given an initial wave function of the form

$$\psi(x, t) \quad = \quad A_0(x)\exp[iS_0(x)/\hbar], \tag{4.4}$$

where the initial amplitude $A_0(x)$ is assumed to be real and positive, and $S_0(x)$ is the initial action. We can then make the assumption that the wave function at a later time can again be expressed in the same WKB form i.e.

$$\psi(x, t') \quad = \quad A(x, t') \exp[iS(x, t')/\hbar]. \tag{4.5}$$

Our problem is to find the final amplitude $A(x, t')$ and action $S(x, t')$. Inserting (4.4) into the Schrödinger equation, expanding in powers of $\hbar$, and neglecting terms of order $\hbar$ and higher we get to the lowest order

$$H\left(x, \frac{\partial S(x, t')}{\partial x}; t'\right) + \frac{\partial S(x, t')}{\partial t'} \quad = \quad 0 \tag{4.6}$$

which we recognize as the time dependant Hamilton-Jacobi equation for the action S. Here the momentum dependance has been replaced by $p = \partial S/\partial x$. This result can easily be obtained for standard Hamiltonians of the form $H(x, p, t) = p^2/2m + V(x, t)$, but is actually valid for any Hamiltonian which has a classical limit. The result of the expansion to the first order in $\hbar$ is the so called amplitude transport equation which can be conveniently expressed in terms of the density ρ, defined by

$$\rho(x, t) \quad \equiv \quad |A(x, t)|^2. \tag{4.7}$$

Since ρ can be interpreted as the probability density it can be thought of as a configuration space density of *classical* particles. The amplitude transport equation then takes the shape of the usual continuity equation known from fluid mechanics and electrodynamics

$$\frac{\partial \rho(x, t)}{\partial t} + \frac{\partial}{\partial x}\left[\rho(x, t)v(x, t)\right] \quad = \quad 0, \tag{4.8}$$

where the x derivative is a divergence in more than one dimension, and where we have defined the velocity field

$$v(x, t) \quad \equiv \quad \frac{1}{m}\frac{\partial H(x, p; t)}{\partial p} \tag{4.9}$$

with $p = \partial S(x, t)/\partial x$. In the following we shall assume that $m = 1$. As we see the continuity equation is driven by the solution S of the autonomous Hamilton-Jacobi equation, and it is therefore necessary to first solve this for S. We will not solve the equations here but merely state the results. A very good derivation of the solution can be found in [40]. The solution to the Hamilton-Jacobi equation is given by

$$S(x', t') \quad = \quad S(x, t) + R(x', t'; x, t) \tag{4.10}$$

where $R(x', t'; x, t)$ is the line integral $\int(p\,dx - H\,dt)$ along a classical orbit connecting (x, t) with (x', t').

The solution of the continuity equation can be obtained in a straightforward manner by applying probability conservation. Because of the interpretation of ρ being a classical density of particles, conservation of the number of particles allows us to write

$$\rho(x', t')dx' \quad = \quad \rho(x, t)dx, \tag{4.11}$$

or, in terms of the amplitudes,

$$A(x', t') \quad = \quad A(x, t) |\det \frac{\partial x}{\partial x'}|^{1/2}, \tag{4.12}$$

where the determinant determines the volume ratio of an evolved configuration space volume element to the initial volume element. The solution to the initial value problem in WKB theory therefore takes the form

$$\psi(x', t') \quad = \quad A(x, t) |\det \frac{\partial x}{\partial x'}|^{1/2} \exp(\frac{i}{\hbar}[S(x, t) + R(x', t'; x, t)]) \tag{4.13}$$

for the case where the initial action function develops no singularities in the elapsed time. In the case where the action function goes through *caustics* one has to deal with several branches of the action function and the solution to the initial value problem correspondingly changes to be a sum over WKB terms like (4.13) - one for each branch

$$\psi(x', t') \quad = \quad \sum_b A_b(x, t) |\det \frac{\partial x}{\partial x'}|^{1/2} \exp(\frac{i}{\hbar}[S(x, t) + R_b(x', t'; x, t) - i\kappa\frac{\pi}{2}]) \tag{4.14}$$

where κ is the integer *Maslov index* absorbing the possible change of sign of the amplitude [40]

To get the semiclassical expression of the propagator we therefore just have to put in the initial value of the propagator in the WKB form. This however is not directly possible since we have $G(x, x', 0) = \delta(x - x')$ which cannot be realized in the WKB ansatz (4.4). However, by working in momentum space the initial wave function becomes completely well defined, and we can carry out the very same calculations for this wave function. After evolving the momentum wave function in time t we can then transform the solution back (by a stationary phase approximation) to configuration space and thereby finally obtain an expression for the propagator. The result of this procedure yields

$$G(x', t'; x, t) \quad = \quad \frac{1}{(2\pi i\hbar)^{f/2}} \sum_b |\frac{\partial p_b}{\partial x'}|^{1/2}$$
$$\times \quad \exp[\frac{i}{\hbar} R_b(x', t'; x, t) - i\kappa_b\frac{\pi}{2}], \tag{4.15}$$

where $p_b = p_b(x', t, t')$ is the initial momentum of the particle ending up at the p'th branch (x', p'_b) at time t' and where $i^{f/2}$ means $e^{if\pi/4}$. This is finally the Van Vleck expression of the propagator. We note that all orbits connecting x to x' in time t carry their own amplitude contributions, and that these can interfere since they are added as complex numbers.

Next we can relate the propagator to the density of states. If we start out with the special case when $\hat{H}$ is independant of time, then the propagator only depends on $t' - t$ so we can set $t = 0$ and just write $G(x, x'; t)$. In that case we have

$$G(x, x'; t) \quad = \quad \Theta(t) \sum_n e^{-iE_n t/\hbar} |n><n| \tag{4.16}$$

where the sum is over the (assumed discrete) set of energy eigenstates. Next
we can define the energy dependant Greens function

$$G(x, x'; E) \equiv \frac{1}{i\hbar} \int_{-\infty}^{\infty} dt \, e^{iEt/\hbar} G(x, x'; t) \tag{4.17}$$

Since $G(t) = 0$ for $t < 0$ the lower limit can be replaced by 0. Here E is a
complex energy like variable. The integral is guaranteed to converge only for
$\mathrm{Im}\, E > 0$, where it defines an analytic function $\tilde{G}(E)$. $\tilde{G}(E)$ is then defined for
$\mathrm{Im}\, E \geq 0$ by analytic continuation. Inserting (4.16) into (4.17) gives

$$\begin{aligned} \tilde{G}(E) &= \sum_n \frac{|n><n|}{E - E_n} \\ &= \frac{\mathbf{1}}{E - E_n} \end{aligned} \tag{4.18}$$

the resolvant operator. Finally we define $g(E)$ as the trace of $\tilde{G}(E)$,

$$\begin{aligned} g(E) &\equiv \mathrm{Tr}\, \tilde{G}(E) \\ &= \sum_n \frac{1}{E - E_n} \end{aligned} \tag{4.19}$$

which has poles at the energy eigenvalues. If we now replace the complex E by
$E + i\epsilon$, where now E is real and $\epsilon > 0$, we note that

$$\begin{aligned} \mathrm{Im}\left(\frac{1}{E + i\epsilon - E_n}\right) &= \frac{-\epsilon}{(E - E_n)^2 + \epsilon^2} \\ &\to -\pi\delta(E - E_n) \quad \text{for } \epsilon \to 0. \end{aligned} \tag{4.20}$$

Therefore we have

$$\lim_{\epsilon \to 0} \frac{-1}{\pi} \mathrm{Im}g(E + i\epsilon) = \sum_n \delta(E - E_n) \equiv n(E)$$

where $n(E)$ is the density of states.

To proceed, we can obtain a semiclassical expression for the density of states
by inserting the Van Vleck propagator into the exact quantum mechanical ex-
pression for the density of states. This calculation is not done here - we will
only state the most important steps. A very good derivation of all the necessary
steps is done in the lecture notes of Littlejohn [40].

First, when making the Fourier transform to get $G(x, x'; E)$ we make a sad-
dlepoint approximation which provides us with a simple semiclassical expression
for the energy domain propagator. We then find that the orbits that before were
parametrized by time now can be parametrized by the energy E according to
the stationary phase condition used in the saddle point approximation of the
Fourier transform. Second, by taking the trace we have to consider only the
orbits that are closed in configuration space. By also evaluating the trace by
stationary phase approximation we obtain that the orbits should also be closed
in momentum space, so that we end up considering the *periodic orbits* of the

system. The trace integral is then divided up into two parts: one integral along the periodic orbit which basically yields the *cycle period* of the periodic orbit, and $f - 1$ integrals in orthogonal directions to the cycle, which are evaluated then by stationary phase approximation. Then finally one has to work on the final expression to relate the transverse stability properties of the periodic orbit to the result of the transverse Gaussian integrations. The result for the trace is

$$\text{tr}\, G(E) = \overline{g}(E) + \frac{1}{i\hbar} \sum_p T_p \sum_r^{\infty} \frac{e^{-\frac{i}{\hbar} S_p(E) r + i\pi \frac{\kappa_p}{2} r}}{|\det\left(\mathbf{1} - \mathbf{J}_p^r\right)|^{\frac{1}{2}}} \, , \tag{4.21}$$

whereas the result for the density of states then finally reads

$$n(E) \quad = \quad \frac{1}{\pi\hbar} \sum_p T_p \sum_{r=1}^{\infty} \frac{\cos r(S_p(E)/\hbar - \kappa_p \pi/2)}{|\det(\mathbf{1} - \mathbf{J}_p^r)|^{1/2}} \tag{4.22}$$

where the sum is over the *prime* periodic orbits, $\mathbf{J}_p$ is the Jacobian containing the transverse stabilities of the surface of section or Poincare mapping and κ_p is the Maslov index associated with the orbit. A prime periodic orbit is just one single representative of the periodic manifold and all the other periodic orbits lying on top of this can be obtained by a time shift and r traversals of the orbit, where r counts the number of repetitions. Also in the formula (4.22) we have neglected the contribution from zero length orbits which gives the "averaged density of states" $\bar{n}(E)$. This is given by the Thomas-Fermi (or the first Weyl) term

$$\bar{n}(E) \quad = \quad \int \frac{d^f q \, d^f p}{(2\pi\hbar)^f} \delta(H(q,p) - E) \tag{4.23}$$

The formula (4.22) is known as the Gutzwiller trace formula, first derived by Gutzwiller [35] in 1971. Gutzwiller took as the starting point for his derivation the path integral expression for the trace of the propagator, and did not use the Van Vleck propagator directly. We find the derivation sketched above more in the spirit of modern analysis of dynamical systems in terms of periodic orbits.

4.2   The Gutzwiller-Voros zeta function

The problem with the Gutzwiller trace formula is that it diverges precisely where one would like to use it. Crude estimates of its radius of convergence lead to the observation that the entire physical spectrum may be out of reach. The problem is cured by going from the trace formula to the related spectral determinant, which can be formally written

$$\Delta(E) \quad \equiv \quad \prod_n (E - E_n), \tag{4.24}$$

which is related to the trace by

$$\text{Tr}\, G(E) \quad = \quad \frac{d}{dE} \ln \Delta(E), \tag{4.25}$$

and which has zeros at the eigenenergies. A semiclassical expression for the spectral determinant was first obtained by Voros [56] using the results of Gutzwiller. The analog of (4.25) in the semiclassical case can be derived easily for the 2-dimensional case of unstable periodic orbits by looking at the oscillatory part of the Gutzwiller trace formula. In that case the determinant in the denominator takes the form

$$\det(\mathbf{1} - \mathbf{J}_p^r) \;\; = \;\; (1 - \Lambda_p^r)(1 - \Lambda_p^{-r}) \tag{4.26}$$

because of the symplectic structure of the Jacobian. For the oscillatory part of the density of states we then have

$$
\begin{aligned}
n(E) \;\; &= \;\; \mathrm{Re} \; \frac{1}{\pi\hbar} \sum_p \sum_{r=1}^{\infty} T_p \frac{e^{i(S_p(E)/\hbar - \kappa_p \pi/2)r}}{|\Lambda_p|^{r/2}(1 - \Lambda_p^{-r})} \\
&= \;\; \mathrm{Re} \; \frac{1}{\pi\hbar} \sum_p \sum_{r=1}^{\infty} \sum_{j=0}^{\infty} T_p \left(|\Lambda_p|^{-1/2} \Lambda_p^{-j} e^{i(S_p(E)/\hbar - \kappa_p \pi/2)} \right)^r \\
&= \;\; \mathrm{Re} \; \frac{1}{\pi\hbar} \sum_p \sum_{j=0}^{\infty} T_p \frac{|\Lambda_p|^{-1/2} \Lambda_p^{-j} e^{i(S_p(E)/\hbar - \kappa_p \pi/2)}}{1 - |\Lambda_p|^{-1/2} \Lambda_p^{-j} e^{i(S_p(E)/\hbar - \kappa_p \pi/2)}} \\
&= \;\; -\frac{1}{\pi} \mathrm{Im} \sum_p \sum_{j=0}^{\infty} \frac{\partial}{\partial E} \ln \left(1 - |\Lambda_p|^{-1/2} \Lambda_p^{-j} e^{i(S_p(E)/\hbar - \kappa_p \pi/2)} \right) \\
&= \;\; -\frac{1}{\pi} \mathrm{Im} \frac{\partial}{\partial E} \ln Z(E) \tag{4.27}
\end{aligned}
$$

where $Z(E)$ is a dynamical zeta function like expression for the semiclassical spectral determinant. In the following we shall denote this determinant the *Gutzwiller-Voros* determinant or the Gutzwiller-Voros zeta function when referring to this. We see that the Gutzwiller-Voros determinant has the structure

$$
\begin{aligned}
Z(E) \;\; &= \;\; \prod_{j=0}^{\infty} \zeta_j^{-1}(E) \\
&= \;\; \exp\left(-\sum_p \sum_{r=1}^{\infty} \frac{e^{iS_p(E)r/\hbar - \kappa_p \pi/2}}{r\sqrt{|\Lambda_p|^r (1 - \Lambda_p^{-r})}} \right), \tag{4.28}
\end{aligned}
$$

where

$$\zeta_j^{-1}(E) \;\; = \;\; \prod_p (1 - t_p/\Lambda_p^j(E)), \tag{4.29}$$

and we have defined the j'th weight associated with the p'th cycle as

$$t_p(E) \;\; = \;\; z^{n_p} \frac{e^{iS_p(E)/\hbar - \kappa_p \pi/2}}{|\Lambda_p|^{1/2}}. \tag{4.30}$$

where z is a book-keeping variable that keeps track of the topological cycle length n_p, used to expand zeta functions and determinants (see sect. 3.2).

An infinite product over prime periodic orbits like the one in (4.29) is denoted a dynamical zeta function [45] by analogy to the *Riemann zeta function*

which is an infinite product over the prime integers

$$
\begin{aligned}
\zeta_R^{-1}(s) &= \left(\sum_{n=1}^{\infty} n^{-s} \right)^{-1} \\
&= \prod_p (1 - e^{-s \ln p}).
\end{aligned}
\tag{4.31}
$$

As in many applications the wave number k is a more natural choice of variable than the energy E, we shall henceforth replace E by k in all semi-classical formulas.

The Gutzwiller trace formula, apart from the quantum and Maslov phases, differs from the classical trace formula in two aspects. One is the volume term $\overline{g}(E)$ in (4.21) which is a missing from our version of the classical trace formula. While an overall pre-factor does not affect the location of zeros of the determinants, it might play a role in relations such as functional equations for zeta functions. The other difference is that the quantum kernel leads to a square root of the cycle Jacobian determinant, a reflection of the relation probability = (amplitude)^2. The $1/\sqrt{\det(1 - \mathbf{J}_p)}$ weight leads in turn to the product representation

$$
Z(k) = \prod_p \prod_{k=0}^{\infty} \left(1 - t_p / \Lambda_p^k \right) \ ,
\tag{4.32}
$$

which differs from the classical Fredholm determinant (3.12) by missing exponent $k + 1$.

Chapter 5

Convergence

5.1 Entire spectral determinants in semiclassics

Even though the divergence problem with the Gutzwiller trace formula could be partially solved by considering spectral determinants instead of trace formulas, the divergence problem is not cured in a satisfying way. This is due to the fact that the Gutzwiller-Voros zeta function has a finite radius of convergence (seen as parallel stribes), and if we look for scattering resonances in the complex k-plane we will encounter this [14] when searching for nonleading zeros. It is therefore important to get a spectral determinant which has a larger domain of analyticity or which might even be entire. As we saw in section 3.1 Such spectral- or Fredholm determinants are known in the case of maps and in the case of classical flows.

In this section we start by taking a look at the first attempts to improve the analytic properties of semiclassical spectral determinants (the Gutzwiller-Voros spectral determinant), by studying the so-called quantum Fredholm determinant introduced by Cvitanović and Rosenqvist [13]. Next we follow the work by Vattay who introduced a multiplicative operator which is capable of evolving *quasi-classical* wavefunctions and which has an *entire* related spectral determinant. Finally we derive the general N-dimensional formula of this entire determinant.

5.1.1 The quantum Fredholm determinant

While various periodic orbit formulas may be formally equivalent, in practice some are vastly preferable to others. Trace formulas, such as the thermodynamic averages in classical dynamics, and the semi-classical Gutzwiller trace formula in quantum mechanics are difficult to use for anything other than the leading eigenvalue estimates. The convergence of cycle expansions of zeta functions and Fredholm determinants depends on their analytic properties; and as we saw in section 3.1 the classical Fredholm determinants are entire functions[48]. A

formal analogy to the classical case leads us to the introduction of the *quantum Fredholm determinant* [13], which for two-dimensinal Hamiltonian flows reads

$$
\begin{aligned}
F_{qm}(E) &= \prod_p \prod_{k=0}^{\infty} \left(1 - \frac{e^{-\frac{i}{\hbar}S_p(E)+i\pi m_p/2}}{|\Lambda_p|^{1/2}\Lambda_p^k} \right)^{k+1} \\
&= \exp\left(-\sum_p \sum_{r=1}^{\infty} \frac{e^{iS_p(E)r/\hbar - \kappa_p \pi/2}}{r\sqrt{|\Lambda_p|^r}(1-\Lambda_p^{-r})^2} \right),
\end{aligned}
\tag{5.1}
$$

as an alternative to the Gutzwiller-Voros zeta function

$$
Z(E) = \prod_p \prod_{k=0}^{\infty} \left(1 - \frac{e^{-\frac{i}{\hbar}S_p(E)+i\pi m_p/2}}{|\Lambda_p|^{1/2}\Lambda_p^k} \right).
\tag{5.2}
$$

We present here the numerical evidence in support of the conjecture of ref. [13]:

For Axiom A systems the quantum Fredholm determinant has a larger domain of analyticity than the Gutzwiller-Voros zeta function.

We shall consider here only the purely hyperbolic flow of the 3-disk repeller

The conjecture we test in this section, asserts that one may replace the Gutzwiller-Voros zeta function (4.32) by the *quantum Fredholm determinant* (5.1), *ie.* the Fredholm determinant (3.12) with the *quantum* weights t_p, without disturbing the leading semi-classical eigenvalues, but improving the convergence of cycle expansions used in evaluating the spectrum.

The form of the quantum weight (4.30) suggests that the quantum evolution operator should be approximated by a classical evolution operator with a quantum weight:

$$
\mathcal{L}^t(y,x) = \delta(y - f^t(x))\sqrt{|\Lambda^t(x)|}e^{-\frac{i}{\hbar}S^t(x)+i\pi m_p(x)/2}.
$$

However, even though the Jacobians are multiplicative i.e. $\mathbf{J}_{ab} = \mathbf{J}_a \cdot \mathbf{J}_b$, the same rule does not apply to their eigenvalues so in general we have $\Lambda_{ab} \neq \Lambda_a \Lambda_b$, and the above operator is therefore not multiplicative along the trajectory, and consequently does not satisfy the assumptions required by the theorems that guarantee that a Fredholm determinant is entire [47]. Nevertheless, our numerical results support the conjecture that the $|\Lambda|^{1/2}$ weighted determinant has a larger domain of analyticity than the commonly used Gutzwiller-Voros zeta function and that some related determinant (see section 5.2) might even be entire.

5.1.2   Abscissa of absolute convergence

Consider the approximation (3.4) in the case of the Gutzwiller trace formula (4.21):

$$\operatorname{Tr} G(k) \approx \sum_p T_p \sum_r^\infty \frac{e^{-\frac{i}{\hbar} S_p(k)r + i\pi m_p r/2}}{|\Lambda_p^r|^{1/2}} \ .$$

This approximation omits the non leading $\approx 1/\Lambda_p$ terms that vanish in the $t \to \infty$ limit and do not affect the leading eigenvalues. If the phases conspire to partially cancel contributing terms, the sum diverges for a larger value of $\operatorname{Im}(k)$. The abscissa of absolute convergence in the complex k plane is obtained by maximizing the sum, $ie.$ replacing all terms by their absolute values:

$$\operatorname{tr} G(k) \approx \sum_p T_p \sum_r^\infty \frac{e^{T_p \operatorname{Im}(k)r}}{|\Lambda_p^r|^{1/2}} \ .$$

(we have for simplicity taken S_p to be the action for billiards, $S_p/\hbar = T_p k$). The value of $\operatorname{Im}(k)$ for which this sum diverges determines the abscissa of absolute convergence. We can also use determinants to accurately estimate this abscissa of absolute convergence, by replacing all cycle weights t_p in (3.12) by their absolute values.

To evaluate the abscissa of absolute convergence of the Gutzwiller-Voros zeta function we first note that inserting the identity $1 = (1 - 1/\Lambda_p^r)/(1 - 1/\Lambda_p^r)$ into the exponent of Gutzwiller-Voros zeta function (4.30), one obtains the following relation between the Gutzwiller-Voros zeta function and the quantum Fredholm determinant:

$$Z(k) = \frac{F_{qm}(k)}{F_{\frac{1}{2}}(k)} \ ,$$

where

$$F_{\frac{1}{2}}(k) = \exp\left(-\sum_p \sum_{r=1}^\infty \frac{1}{r} \frac{t_p^r}{\Lambda_p^r(1 - 1/\Lambda_p^r)^2} \right) \ . \tag{5.3}$$

The radius of convergence of $Z_{qm}(k)$ is therefore determined by the leading zeros of $F_{\frac{1}{2}}(k)$. To estimate the upper bound on $\operatorname{Im}(k)$ for the zeros of $F_{\frac{1}{2}}$, we omit all signs and phases in the weights in $F_{\frac{1}{2}}$:

$$\hat{F}_{\frac{1}{2}}(k) = \exp\left(-\sum_p \sum_{r=1}^\infty \frac{1}{r} \frac{|t_p^r|}{|\Lambda_p^r|(1 - 1/\Lambda_p^r)^2} \right) \ , \tag{5.4}$$

and compute its leading zero at $\operatorname{Re}(k) = 0$. An example is given in sect. 5.1.3.

5.1.3 Numerical results

In this section we present the evidence that the quantum Fredholm determinant is numerically as convergent as the classical Fredholm determinant, in contrast to the Gutzwiller-Voros zeta function which has a finite radius of convergence.

Following refs. [18, 24, 32, 31], we perform our numerical tests on the 3-disk repeller. The 3-disk repeller is the simplest physical realization of an Axiom A system, particularly convenient for numerical investigations. For billiards the cycle weight t_p required for evaluation of the classical escape rates and correlation spectra is given by (3.12). The action S_p is proportional to the cycle period T_p, and the Maslov index changes by $+2$ for each disk bounce, $\kappa_p = 2n_p$, so the quantum weight (4.30) is given by

$$ t_p = (-1)^{n_p} \frac{e^{-ikT_p}}{\sqrt{|\Lambda_p|}} z^{n_p} \,, \tag{5.5} $$

where $k = (\text{momentum})/2\pi$ is the wave-number, and we take velocity $= 1$, mass $= 1$.

Cycle expansion (3.19) coefficients $|C_n|$ for different determinants and zeta functions are plotted in figs. 5.1 as function of the topological cycle length n. Zeta functions exhibit exponential falloff, implying a pole in the complex plane, while both the classical and the quantum Fredholm determinants appear to exhibit a faster than exponential falloff, with no indication of a finite radius of convergence within the numerical validity of our cycle expansion truncations.

In particular, the quantum Fredholm determinant enables us to uncover more resonances than what was hitherto accessible by means of the dynamical zeta functions [31, 24, 12]. The eye is conveniently guided to the zeros by means of complex s plane contour plots, with different intervals of the absolute value of the function under investigation assigned different colours; zeros emerge as centers of elliptic neighborhoods of rapidly changing colors (see figs. 5.4). Detailed scans of the whole area of the complex s plane under investigation and searches for the zeros of classical and quantum Fredholm determinants, fig. 5.2, reveal complicated patterns of resonances, with the classical and the semi-classical resonance patterns surprisingly similar. It is known [18] that the leading semi-classical resonances are very accurate approximations to the exact quantum resonances; the semi-classical resonances further down in the s complex plane in fig. 5.2 has first recently been compared with the exact quantum values [63]. This comparison showed that the resonances of the quantum Fredholm determinant though highly convergent, unfortunately did not match the exact data. On the other hand for cycle expansions to order 6 and 7, the Gutzwiller-Voros zeta function gives remarkably good results even in this domain.

Contour plots are also helpful in comparing the domain of convergence of the Fredholm determinant to that of the Gutzwiller-Voros zeta function. As can be seen from fig. 5.4, the quantum Fredholm determinant can be continued
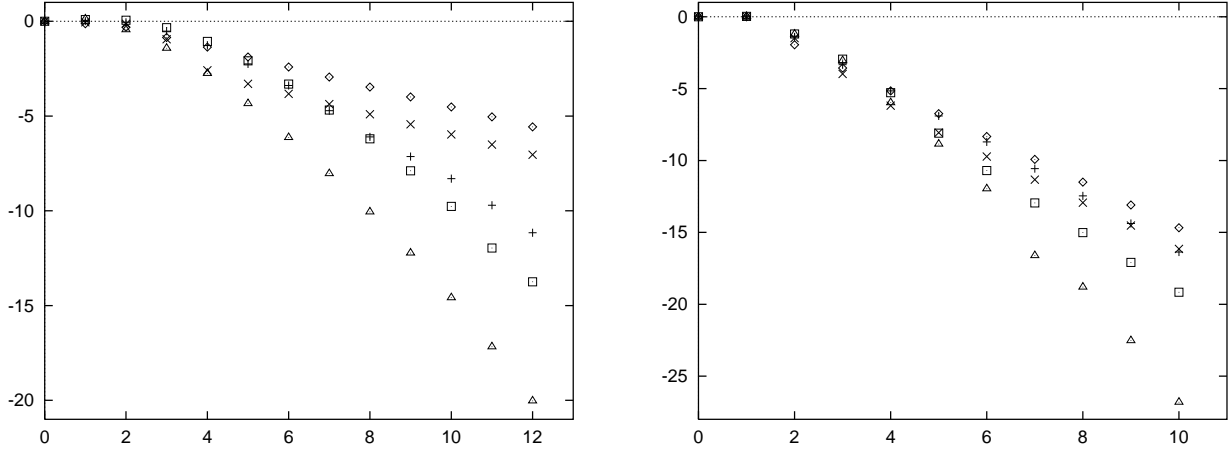
Figure 5.1: (a) $\log_{10}|C_n|$, the contribution of cycles of topological length n to the cycle expansion $\sum C_n z^n$ for 3-disk repeller. Shown are: ($\diamond$) $1/\zeta_0$, ($\times$) the Gutzwiller-Voros zeta function, ($+$) $1/\zeta_0\zeta_1^2$, and ($\square$) the quantum Fredholm determinant. Exponential falloff implies that $1/\zeta_0$ and the Gutzwiller-Voros zeta function have the same leading pole, canceled in the $1/\zeta_0\zeta_1^2$ product. For comparison, ($\triangle$) the classical Fredholm determinant coefficients are plotted as well; cycle expansions for both Fredholm determinants appear to follow the asymptotic estimate $C_n \approx \Lambda^{-n^{3/2}}$. A_1 symmetric subspace, with center spacing - disk radius ratio $R : a = 3 : 1$, evaluated at the lowest resonance, wave number $k = 7.8727 - 0.3847\,i$, maximal cycle length $n = 8$. (b) Same as (a) , but with $R : a = 6 : 1$. This illustrates possible pitfalls of numerical tests of asymptotics; the quantum Fredholm determinant appears to have the same pole as the quantum $1/\zeta_0\zeta_1^2$, but as we have no estimate on the size of pre-asymptotic oscillations in cycle expansions, it is difficult to draw reliable conclusions from such numerics. See fig. 5.5 for estimate of the quantum Fredholm determinant abscissa of absolute convergence.
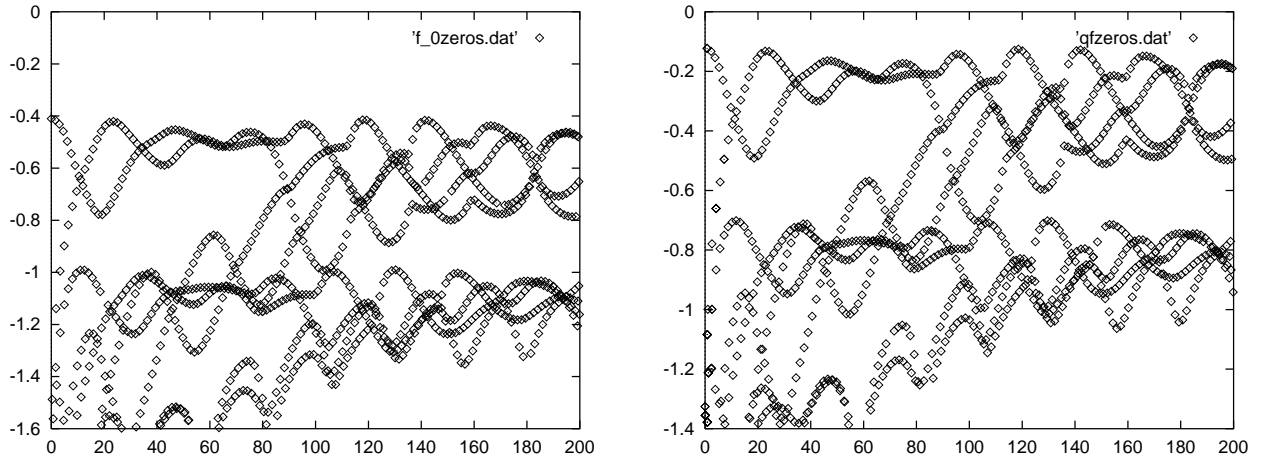
Figure 5.2: Leading resonances in the 3-disk repeller A_1 subspace, (a) for the classical Fredholm determinant, and (b) the 952 leading resonances of the quantum Fredholm determinant F_{qm}. Ratio $R : a = 6 : 0$, cycle expansions truncated at cycle length $n = 8$.

considerably farther down in the complex k plane, in contrast to the dynamical zeta function scans such as those given in ref. [31]. While the zeta functions clearly exhibit a finite radius of convergence, both the classical Fredholm determinant and the quantum Fredholm determinant behave as entire functions. We compute the abscissa of absolute convergence for the Gutzwiller-Voros zeta function by means of (5.4); for the case at hand we obtain the leading zero at $k_{ac} = 0.0 - i\,0.699110157151\ldots$. This estimate might be a bit too crude since the results of Wirzba [63] indicate that to curvature order 7 the Gutzwiller-Voros zeta function gives nice results for the resonances even down to Im$k = -1.1$, as shown in figure 5.3. Interestingly enough, the apparent border of Gutzwiller-Voros zeta function convergence in fig. 5.4 seems to coincide with Re$(s) = 0$, Im$(s) = -1.09653395\ldots$, the zero obtained from $F_{1/2}(k)$ by removing quantum phases, $t_p \to |t_p|$, but keeping the eigenvalue Λ_p sign in (5.3).

5.2 The quasi-classical approximation

In this section we follow Vattay [53] and show how the eigenvalues of the first order partial differential equation derived by the quasi-classical approximation of the Schrödinger equation in the case of an Axiom A flow, can be computed from the trace of a classical operator. The corresponding spectral determinant of the new operator is an entire function in the complex plane in contrast to the usual Gutzwiller-Voros- or quantum Fredholm determinants.

For a single particle of unit mass the Schrödinger equation in a potential U
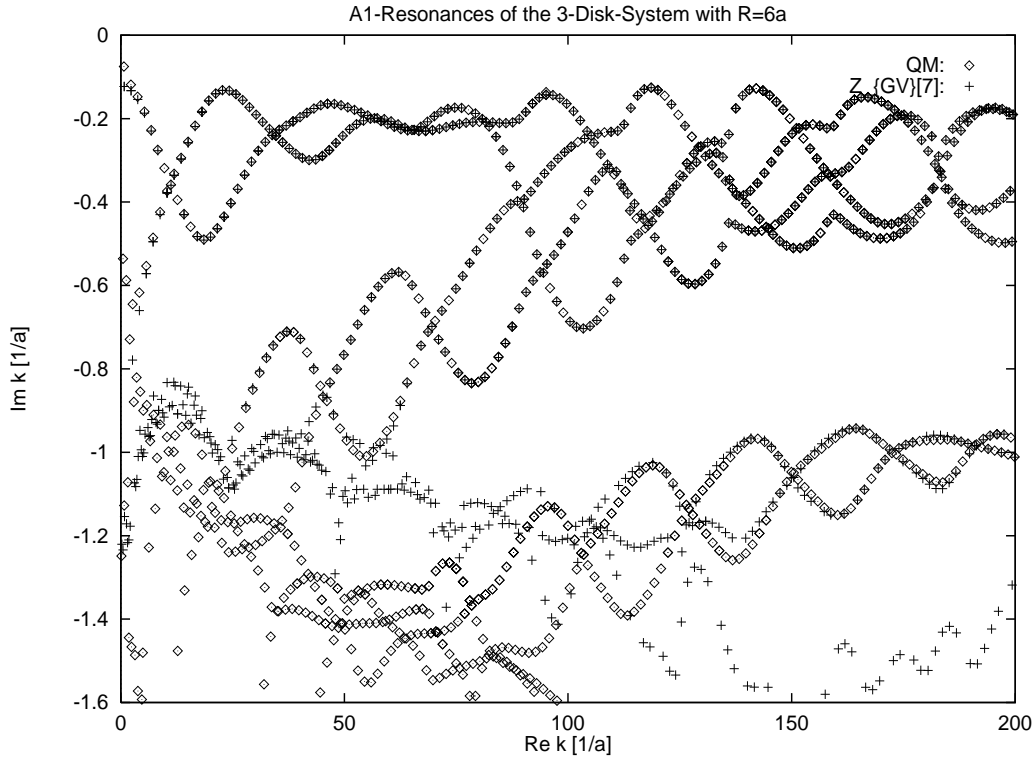
Figure 5.3: The A_1 resonances of the 3-disk system with $R : a = 6$. The exact quantum mechanical resonances calculated by A. Wirzba are denoted by a diamond. The semiclassical Gutzwiller-Voros resonances are calculated up to the 7'th order in the curvature expansion and are denoted by crosses. It should be noted that by inclusion of longer orbits in the calculation, the picture becomes much worse, as the Gutzwiller-Voros zeta function is only an asymptotic series and the cycle expansion start diverging. The data are from A. Wirzba.
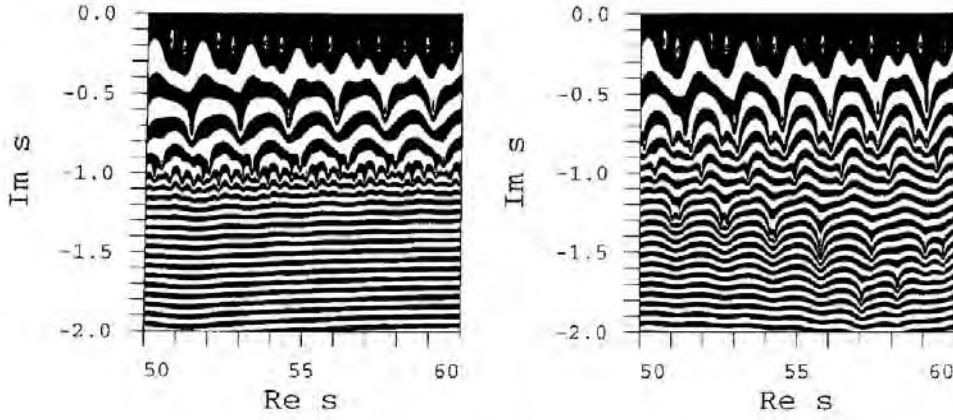
Figure 5.4: Complex s plane contour plot comparison of (a) the Gutzwiller-Voros zeta function $\log|Z_{qm}(s)|$ with (b) the quantum Fredholm determinant $\log|F_{qm}(s)|$. The border of the convergence of the Gutzwiller-Voros zeta function agrees with the location of the abscissa of absolute convergence, given by the $\hat{F}_{1/2}$ leading eigenvalue at $\text{Re}(s) = 0$, $\text{Im}(s) = -0.699110157151\ldots$. The quantum Fredholm determinant can be continued at least a factor 2 further down in the complex plane. 3-disk repeller, $R : a = 6 : 1$, A_1 subspace, maximal cycle length $n = 8$.

is

$$i\hbar \frac{\partial \psi}{\partial t} = -\frac{\hbar^2}{2}\Delta\psi + U(q)\psi, \tag{5.6}$$

where Δ is the Laplace operator and $\psi(q, t)$ is the wave function. In the limit $\hbar \to 0$ the solution of this equation is given by the quasi-classical approximation which is an asymptotic solution of the form

$$\psi(q, t) = \varphi(q, t)e^{iS(q,t)/\hbar}, \tag{5.7}$$

where the amplitude $\varphi(q, t)$ and the phase $S(q, t)$ are smooth real functions on some bounded region of the configuration space. The reason for the changed notation as compared to the WKB ansatz (4.4), is that we shall here keep the wave function as one single term of the WKB form and not as a sum of contributions from different branches as in the case of the Van Vleck propagator. This is also what lies in the notion of a quasi-classical wave function. Substituting (5.7) into the Schrödinger equation and expanding the equation to zeroth and first order in $\hbar$ we get partial differential equations for the amplitude and the phase with initial conditions $\varphi(q, 0) = \varphi_0(q)$ and $S(q, 0) = S_0(q)$ respectively. The equations are

$$\frac{\partial \varrho}{\partial t} + div\,(\varrho\nabla S) = 0, \tag{5.8}$$

$$\frac{\partial S}{\partial t} + H(q, \nabla S) = 0, \tag{5.9}$$

where $\varrho(q,t) = \varphi^2(q,t)$ and $H(q,p)$ is the Hamilton function. Equation (5.9) is the classical Hamilton-Jacobi equation. It is an autonomous first order partial differential equation whose solution corresponding to an initial $S(q,0) = S_0(q)$, can be given independently of (5.8). Equation (5.8) is the continuity equation known from e.g. fluid or electro dynamics. As we see it is not an independant equation since it is driven by the solution of (5.9).

From the theory of first order PDE's [2] we know that their solutions lead to *ordinary* differential equations. The Hamilton-Jacobi equation for instance leads to the well known Hamilton differential equations of motion

$$
\begin{aligned}
\dot{q} &= \frac{\partial H(q,p)}{\partial p}, \\
\dot{p} &= -\frac{\partial H(q,p)}{\partial q},
\end{aligned}
\tag{5.10}
$$

where the new variable

$$p = \nabla S(q,t)$$

has been introduced.

When we take the wievpoint of the PDE description we evolve the whole function $S(q,t)$ and compute its gradient at a given point q_0. This requires information about the behavior of the function $S(q,t)$ in the vicinity of q_0 and cannot be recovered from the value of $S(q_0,t)$ alone. In the ODE description however, we evolve both q and the gradient $p = \nabla S(q,t)$. At a given time we therefore do not have to compute the gradient from $S(q,t)$ since the evolution is *local* in the (q,p) space. The final solution of the partial differential equation can be constructed from the ODE description as

$$
S(q',t) = S(q,0) + \int_0^t L(q(\tau), \dot{q}(\tau)) d\tau,
\tag{5.11}
$$

where the Lagrange function is integrated along the phase space trajectory with

$$q' = q(t), q = q(0), \nabla S(q',t) = p(t), \nabla S(q,0) = p(0).$$

In general there exists only one such trajectory.

Next we consider the 'local' solution of the continuity equation (5.8). At a given starting point q_0 the momentum is given by $p_0 = \nabla S_0(q_0)$, and the amplitude of the wave function is $\varphi_0(q)$. During time t the coordinate q_0 evolves to $q(t)$ and p_0 to $p(t)$ following the full Hamiltonian flow. Using probability conservation the new amplitude can be derived as follows: First we take an infinitesimal initial d dimensional oriented volume $V(q_0)$ around q_0 in configuration space. In time t this volume evolves to the infinitesimal orientated volume $V(q(t))$ around $q(t)$ according to the full Hamiltonian flow. Applying the probability conservation the new amplitude is given by

$$
\varphi(q(t)) = \pm \left(\frac{V(q(t))}{V(q(0))} \right)^{-1/2} \varphi_0(q_0),
\tag{5.12}
$$

where the sign ± 1 reflects the ambiguity of the transformation from the density ϱ to φ. The ratio of volumes is independent of the way we specify the initial infinitesimal volume. To determine the volume ratio, we specify an initial directed parallelepiped around q_0 with edges given by d independent infinitesimal vectors $\delta\mathbf{q}_1, \delta\mathbf{q}_2, \ldots \delta\mathbf{q}_d$. In time t these vectors are transformed into $\delta\mathbf{q}'_1, \delta\mathbf{q}'_2, \ldots \delta\mathbf{q}'_d$ by the flow. We then note that the initial point (q_0, p_0) and the set of initial vectors $\delta\mathbf{q}$ is not enough to specify uniquely the image vectorsi $\delta\mathbf{q}'$. This of course is due to the fact that we have not specified the initial momenta $\delta\mathbf{p}$ of the points in the volume, and that this is evolved by the full phase flow. The initial function $S_0(q)$ however determines a set $\delta\mathbf{p}_1, \delta\mathbf{p}_2, \ldots \delta\mathbf{p}_d$ of initial momentum vectors through the second derivative matrix:

$$\delta\mathbf{p} = \mathbf{M}\delta\mathbf{q}, \quad \mathbf{M}_{ji} = \frac{\partial^2 S_0(q)}{\partial q_j \partial q_i}, \tag{5.13}$$

which we hereafter call the *curvature matrix*. The initial curvature matrix $\mathbf{M}_0$ is therefore an important initial condition, and we are able to compute the image of the volume only by specifying it. The vector $(\delta\mathbf{q}_i, \delta\mathbf{p}_i)$ is transformed by the Jacobi matrix

$$\delta\mathbf{q}'_i = \mathbf{J}_{qq}\delta\mathbf{q}_i + \mathbf{J}_{qp}\delta\mathbf{p}_i, \tag{5.14}$$
$$\delta\mathbf{p}'_i = \mathbf{J}_{pq}\delta\mathbf{q}_i + \mathbf{J}_{pp}\delta\mathbf{p}_i, \tag{5.15}$$
$$\tag{5.16}$$

where the subscripts q and p denote the corresponding $[d \times d]$ submatrices of the full $[2d \times 2d]$ Jacobian. The Jacobian is determined by the initial condition (q_0, p_0) and can be computed as a time ordered integral along the phase space trajectory

$$\mathbf{J}(q, p, t) = \mathrm{T}\exp\left\{\int_0^t d\tau \mathbf{D}^2 H(q(\tau), p(\tau))\right\}, \tag{5.17}$$

where $\mathbf{D}^2 H(q, p)$ denotes the second symplectic derivative matrix

$$\mathbf{D}^2 H = \begin{pmatrix} \frac{\partial^2 H}{\partial q_i \partial p_j} & \frac{\partial^2 H}{\partial p_i \partial p_j} \\ -\frac{\partial^2 H}{\partial q_i \partial q_j} & -\frac{\partial^2 H}{\partial q_i \partial p_j} \end{pmatrix}$$
$$\equiv \mathbf{D}^2 H$$

of the Hamiltonian and T is the time ordering operator. The derivation of equation (5.17) is sketched in appendix 9.1. The curvature matrix of the function $S(q, t)$ around $q(t)$ relates between the infinitesimal vectors as in (5.13)

$$\delta\mathbf{p}' = \mathbf{M}'\delta\mathbf{q}', \quad \mathbf{M}'_{ji} = \frac{\partial^2 S(q', t)}{\partial q_j \partial q_i}. \tag{5.18}$$

From (5.13) and (5.18), we can eliminate the vectors $\delta\mathbf{p}_i$ and $\delta\mathbf{p}'_i$ and get relations between the initial and final infinitesimal configuration vectors and

the curvature matrices

$$\delta\mathbf{q}' \quad = \quad (\mathbf{J}_{qq} + \mathbf{J}_{qp}\mathbf{M})\delta\mathbf{q}, \tag{5.19}$$
$$\mathbf{M}' \quad = \quad (\mathbf{J}_{pq} + \mathbf{J}_{pp}\mathbf{M})(\mathbf{J}_{qq} + \mathbf{J}_{qp}\mathbf{M})^{-1}. \tag{5.20}$$

From the first relation it immediately follows that the volume ratio is given by

$$\frac{V(q')}{V(q_0)} = \det(\mathbf{J}_{qq} + \mathbf{J}_{qp}\mathbf{M}). \tag{5.21}$$

The second relation is a recursion relation for $\mathbf{M}$ which can be considered as the matrix generalization of the usual rational fraction transformation. Furthermore equation (5.20) allows us to derive a differential equation for $\mathbf{M}(t)$, which yields

$$\dot{\mathbf{M}} = -\left(\frac{\partial^2 H}{\partial q \partial q} + \mathbf{M}\frac{\partial^2 H}{\partial p \partial q} + \frac{\partial^2 H}{\partial q \partial p}\mathbf{M} + \mathbf{M}\frac{\partial^2 H}{\partial p \partial p}\mathbf{M}\right), \tag{5.22}$$

The derivation of this equation is also sketched in appendix 9.1. As we see equation(5.22) is driven since the second partial derivatives of the Hamilton function should be computed along the phase space trajectory. If we solve this differential equation along the phase space trajectory the volume ratio can be written as an integral along the phase space and $\mathbf{M}(t)$ trajectory (see appendix 9.1 for the derivation):

$$\frac{V(q')}{V(q_0)} \quad = \quad \exp\left\{\int_0^t \mathrm{Tr}[\frac{\partial^2 H}{\partial p \partial q} + \frac{\partial^2 H}{\partial p \partial p}\mathbf{M}]d\tau\right\} \tag{5.23}$$

The square root of the volume ratio is then also given by an integral:

$$\left(\frac{V(q')}{V(q_0)}\right)^{-1/2} = \exp\left\{-\frac{1}{2}\int_0^t \mathrm{Tr}\left[\frac{\partial^2 H}{\partial p \partial q} + \frac{\partial^2 H}{\partial p \partial p}\mathbf{M}\right]d\tau\right\}. \tag{5.24}$$

The computation of this expression requires some care when the solution of the differential equation (5.22) is singular. Close to a singularity, where

$$\mathbf{M}(t \to t^c) = \infty,$$

we can neglect the non leading terms from (5.22) and use the solution of

$$\dot{\mathbf{M}} = -\mathbf{M}\frac{\partial^2 H}{\partial p \partial p}\mathbf{M}. \tag{5.25}$$

The second derivative matrix can be decomposed into combinations of dyads and their eigenvalues in the usual way

$$\frac{\partial^2 H}{\partial p \partial p} = \sum_{i=1}^d \lambda_i \mathbf{D}_i, \quad \mathbf{D}_i\mathbf{D}_j = \delta_{ij}\mathbf{D}_j. \tag{5.26}$$

where $\mathbf{D}_j$ is the matrix constructed by the matrix product of the j'th right and left eigenvectors of $\partial^2 H / \partial p^2$: $\mathbf{D}_j = \mathbf{e}_j^{right} \mathbf{e}_j^{left}$.

The solution close to the singularity can be a linear combination of some of these dyads corresponding to singular directions l:

$$\mathbf{M}(t) = \frac{1}{t - t^c} \sum_{l=1}^{R} \frac{1}{\lambda_l} \mathbf{D}_l, \tag{5.27}$$

where R is the number of singular directions. The time ordered integral close to the singularity is then dominated by

$$\left(\frac{V(q(t_{+0}^c))}{V(q(t_{-0}^c))} \right)^{-1/2} = \exp \left(-\frac{1}{2} \int_{t_c-0}^{t_c+0} \frac{R}{\tau - t_c} d\tau \right). \tag{5.28}$$

This integral can be computed by adding infinitesimal imaginary value $i\epsilon$ to t^c and taking the $\epsilon \to 0$ limit

$$\left(\frac{V(q(t_{+0}^c))}{V(q(t_{-0}^c))} \right)^{-1/2} = \exp(i\pi(R/2)). \tag{5.29}$$

Between two singular points the time ordered integral is positive and gives the absolute value of the volume ratio. Notice that R counts the number of rank reductions of the matrix $\mathbf{M}$ along the classical path, and it is also a function on the initial condition $\mathbf{M}_0$.

We now have the necessary ingredients to describe the time evolution of a quasi-classical wave function. The wave function at time t becomes

$$\psi(q', t) = \varphi(q', t) e^{iS(q',t)/\hbar} = \pm \left(\frac{V(q')}{V(q_0)} \right)^{-1/2} e^{i \int_0^t L d\tau / \hbar} \varphi_0(q_0) e^{iS_0(q_0)/\hbar} \tag{5.30}$$

where q_0 is the starting point of a classical trajectory with initial momentum $\nabla S_0(q_0)$ which ends up in q after time t with momentum $\nabla S(q, t)$, and the volume ratio is determined by the curvature matrix $\mathbf{M} = \partial_i \partial_j S(q, 0)$. We note again that in contrast to the solution of the initial value problem in the WKB theory (4.14), we here only get one contribution to the quasi-classical wave function at time t.

5.2.1 Time evolution

We are now in a position to express the volume ratio and the momentum by the second and first derivatives of the minimal action between q' and q. In this way we recover the usual Van Vleck propagator. However, from equation (5.30) we see that the wave amplitude φ at time t and at coordinate q' is determined

by the amplitude at $t = 0$ at coordinate q. In calculations involving the Van Vleck operator kernel this nice property is lost, and we have to compute lots of trajectories to compute the volume ratio and we have to know the whole initial wave function too. However we have a better option. We can keep track of the variables p and $\mathbf{M}$ along only one trajectory and compute (5.11) and the volume ratio (5.24). This means that the evolution takes place on the extended $(q, p, \mathbf{M})$ space. We can introduce classical density functions $\tilde{\psi}$ defined on this space. The wave function then corresponds to the special function

$$\tilde{\psi}(q, p, \mathbf{M}, t) = \psi(q, t)\delta(p - \nabla S(q, t))\delta\left(\mathbf{M} - \frac{\partial^2 S(q, t)}{\partial q_j \partial q_i}\right). \qquad (5.31)$$

The evolution of a general classical density function on the extended space according to (5.30) can be rewritten in terms of a classical transfer operator

$$\tilde{\psi}(q', p', \mathbf{M}', t) = \int dq dp d\mathbf{M} \mathcal{L}(q', p', \mathbf{M}', t \mid q, p, \mathbf{M}, 0)\tilde{\psi}(q, p, \mathbf{M}, 0), \quad (5.32)$$

with the kernel

$$e^{i\pi\nu + \int_0^t d\tau \frac{iL}{\hbar} + \frac{1}{2}\mathrm{Tr}\left\{\frac{\partial^2 H}{\partial p \partial q} + \frac{\partial^2 H}{\partial p \partial p}\mathbf{M}\right\}} \quad \times \quad \delta(q' - q^t(q, p)) \times$$
$$\delta(p' - p^t(q, p)) \quad \times \quad \delta(\mathbf{M}' - \mathbf{M}^t(q, p, \mathbf{M})), \qquad (5.33)$$

where $q^t(q, p)$, $p^t(q, p)$ and $\mathbf{M}^t(q, p, \mathbf{M})$ denote the evolution of q, p and $\mathbf{M}$ from the initial coordinates $q, p = \nabla S_0(q)$ and $\mathbf{M} = \partial_i \partial_j S_0(q)$ during the time t, and $\nu = N + R/2$. The integrals should be computed along the full trajectory, and also the number of rank reductions R and the number of orientation changes N. We note that the sign of the trace integral in the exponent has changed compared to the sign in (5.24). This arises as the integration over $p, \mathbf{M}$ and q picks up an additional volume ratio in the denominator, and the final expression should therefore be multiplied with the square root of the volume ratio in the numerator to give the right result as in (5.30). The derivation of this is shown in appendix 9.1.

We also note that the above evolution operator or kernel is *multiplicative*, since the delta functions ensure that the operator connects coordinates, which are connected by the classical dynamics, and give the correct amplitude. This operator can evolve densities, which are not of the form (5.31), and therefore we can expect that only a part of its spectrum has relevance to semiclassics.

5.3   Derivation of the trace integral

In this section we consider how the trace integration of the evolution operator introduced above, can be performed by considering the generalized rational fraction transformation (5.20) that governs the evolution of the curvature matrix. An alternative derivation of this result where we follow explicitly the

Lagrangian manifolds around the periodic orbit, is given in appendix 9.1. Here we first find explicitely the periodic $\mathbf{M}$ solutions of the map, which gives us the solution to the second order of the Hamilton Jacobi equation in the neighbourhood of a periodic orbit. Next we look at the symplectic structure of the flow which imposes the same restriction on the number of periodic $\mathbf{M}$ solutions as was previously obtained. Finally we obtain the stabilities of the $\mathbf{M}$ solutions by "differentiating" the rational fraction transformation and inserting the periodic solutions of the curvature flow.

We are interested in the trace of the evolution operator $\mathcal{L}^t$ in (9.39)

$$
\begin{aligned}
\mathrm{tr}\mathcal{L}^t &= \int dq\,dp\,d\mathbf{M}\,\delta(q - q^t)\delta(p - p^t)\delta(\mathbf{M} - \mathbf{M}^t) \\
&\times \quad \exp\left(i\pi\nu + \int_0^t d\tau \frac{iL}{\hbar} + \frac{1}{2}\mathrm{Tr}\{H_{pq} + H_{pp}\mathbf{M}\}\right).
\end{aligned}
\tag{5.34}
$$

Following the strategy in section 3.1 we introduce longitudinal $\mathbf{x}_\parallel$ and perpendicular $\mathbf{x}_\perp$ coordinates along the total $\mathbf{x} = (q, p, \mathbf{M})$ flow to evaluate the contribution from a prime periodic orbit to the trace. In the longitudinal direction we get

$$
\int d\mathbf{x}_\parallel \delta_\parallel(\mathbf{x} - \mathbf{x}^t) = T_p \sum_{r=1}^\infty \delta(t - rT_p)
\tag{5.35}
$$

where T_p is the period of the prime periodic orbit. In the perpendicular direction we get

$$
\int d\mathbf{x}_\perp \delta_\perp(\mathbf{x} - \mathbf{x}^{rT_p}) = \frac{1}{|\det(\mathbf{1} - \hat{\mathbf{J}}_p^r)|}
\tag{5.36}
$$

where $\hat{\mathbf{J}}_p$ is the transverse stability matrix, $\mathbf{u}(t + T_p) = \hat{\mathbf{J}}_p \mathbf{u}(t)$ of the entire flow. Since $\frac{\partial q^t}{\partial \mathbf{M}} = \frac{\partial p^t}{\partial \mathbf{M}} = 0$ it has the structure

$$
\det \hat{\mathbf{J}}_p = \begin{bmatrix} \mathbf{J}_{tr} & 0 \\ * & \mathbf{J_M} \end{bmatrix}
\tag{5.37}
$$

and since this is block diagonalizable the determinant splits up into a product of the usual transverse determinant and a determinant corresponding to the $\mathbf{M}$ flow

$$
\det(\mathbf{1} - \hat{\mathbf{J}}_p^r) = \det(\mathbf{1} - \mathbf{J}_p^r) \cdot \det(\mathbf{1} - \mathbf{J_M}_p^r).
\tag{5.38}
$$

We can then write the trace in a form similar to the one in [15]

$$
\mathrm{Tr}\mathcal{L}^t = \sum_p T_p \sum_{r=1}^\infty \frac{\delta(t - rT_p)e^{iS_p(E)r/\hbar}}{|\det(\mathbf{1} - \mathbf{J}_p^r)|}\Delta_{p,r},
\tag{5.39}
$$

with

$$
\Delta_{p,r} = \sum_{\mathbf{M}^{rT_p}=\mathbf{M}} \frac{e^{\frac{1}{2}\int_0^{rT_p}(H_{pq}+H_{pp}\mathbf{M})d\tau}}{|\det(\mathbf{1} - \mathbf{J_M}_p^r)|}
\tag{5.40}
$$

The related spectral (or Fredholm) determinant $F(k)$ can be obtained by observing that the Laplace transform of the trace

$$\mathrm{Tr}\mathcal{L}(k) \quad = \quad \int_{0+}^{\infty} dt\, e^{kt} \mathrm{Tr}\, \mathcal{L}^{t}, \tag{5.41}$$

is a logarithmic derivative $\mathrm{Tr}\mathcal{L}(k) = -\frac{d}{dk} \log F(k)$

$$F(k) \quad = \quad \exp\left(-\sum_{p,r} \frac{e^{i\pi\nu r + iT_p kr}}{r|\det(\mathbf{1} - \mathbf{J}_{\mathbf{M}p}^{r})|}\Delta_{p,r}\right). \tag{5.42}$$

In the following we shall refer to (5.42) as the Vattay determinant. The Vattay determinant is very similar in shape to the classical Fredholm determinant (3.9). The new thing we have to calculate is the curvature trace (9.28).

The first point in obtaining (9.28) is then to find the periodic solutions of the $\mathbf{M}$ flow, and evaluate their stabilities. Next we have to deal with the volume ratio, that is the integral

$$\exp\left(\int_0^t d\tau \frac{1}{2}\mathrm{Tr}\{H_{pq} + H_{pp}\mathbf{M}\}\right).$$

5.3.1   Finding periodic M solutions

In this section we derive a method of finding periodic solutions of the rational fraction transformation of the curvature matrix (5.20). The method is general and thus applies also to equations where the solution $\mathbf{M}$ is not required to be symmetric.

Let $\mathbf{A}, \mathbf{B}, \mathbf{C}, \mathbf{D}$ and $\mathbf{M}$ be $N \times N$ matrices. We consider the generalized rational fraction transformation map $f : \mathbf{M} \to \mathbf{M}'$ given by

$$f(\mathbf{M}) \quad = \quad (\mathbf{C} + \mathbf{DM})(\mathbf{A} + \mathbf{BM})^{-1}, \tag{5.43}$$

which we assume to be well defined. If we are looking for fixed points of the map $f(\mathbf{M}) = \mathbf{M}$ equation (5.43) results in a generalized second order equation

$$\mathbf{MBM} + \mathbf{MA} - \mathbf{DM} - \mathbf{C} = 0. \tag{5.44}$$

To solve the fixed point equation we start by taking an alternative approach to the map f. Consider the $2N \times 2N$ matrix $\mathbf{J}$ given by

$$\mathbf{J} = \begin{bmatrix} \mathbf{A} & \mathbf{B} \\ \mathbf{C} & \mathbf{D} \end{bmatrix} \tag{5.45}$$

and assume that it is diagonalizable:

$$\mathbf{\Delta} \quad = \quad \mathbf{TJT}^{-1}$$

where $\mathbf{\Delta}$ is a diagonal matrix. We note that if for instance $\mathbf{J}$ is the Jacobian of a nondegenerate Hamiltonian flow, then this diagonalization is indeed possible.

Now for any N by N matrix $\mathbf{M}$ and for any vector $\mathbf{x} \in R^N$ we can construct the $2N$ dimensional vector

$$\begin{bmatrix} \mathbf{x} \\ \mathbf{p} \end{bmatrix} = \begin{bmatrix} \mathbf{x} \\ \mathbf{Mx} \end{bmatrix}. \tag{5.46}$$

Mapping this by $\mathbf{J}$ results in

$$\begin{bmatrix} \mathbf{x}' \\ \mathbf{p}' \end{bmatrix} = \mathbf{J} \begin{bmatrix} \mathbf{x} \\ \mathbf{p} \end{bmatrix}$$

To find the fixed points of the map (5.43), we now show the following small theorem

Theorem 1 $\mathbf{M}$ *is a fixed point of the map* f *if and only if for all vectors* $\mathbf{x} \in R^N$

$$\begin{bmatrix} \mathbf{x}' \\ \mathbf{Mx}' \end{bmatrix} = \begin{bmatrix} \mathbf{A} & \mathbf{B} \\ \mathbf{C} & \mathbf{D} \end{bmatrix} \begin{bmatrix} \mathbf{x} \\ \mathbf{Mx} \end{bmatrix}. \tag{5.47}$$

Note that the curvature matrix is the same on both sides of the equality sign.

Proof

If $\mathbf{M}$ is a fixed point of the equation (5.43) we have

$$\begin{aligned} \begin{bmatrix} \mathbf{A} & \mathbf{B} \\ \mathbf{C} & \mathbf{D} \end{bmatrix} \begin{bmatrix} \mathbf{x} \\ \mathbf{Mx} \end{bmatrix} &= \begin{bmatrix} (\mathbf{A} + \mathbf{BM})\mathbf{x} \\ (\mathbf{C} + \mathbf{DM})\mathbf{x} \end{bmatrix} \\ &= \begin{bmatrix} \mathbf{x}' \\ (\mathbf{C} + \mathbf{DM})(\mathbf{A} + \mathbf{BM})^{-1}\mathbf{x}' \end{bmatrix} \\ &= \begin{bmatrix} \mathbf{x}' \\ \mathbf{Mx}' \end{bmatrix} \end{aligned} \tag{5.48}$$

so that the condition is fulfilled.

On the other hand: if the condition (5.47) is fulfilled we have

$$\begin{aligned} \mathbf{Mx}' &= \mathbf{M}(\mathbf{A} + \mathbf{BM})\mathbf{x} \\ &= (\mathbf{C} + \mathbf{DM})\mathbf{x} \end{aligned} \tag{5.49}$$

which is equivalent to

$$\mathbf{M}(\mathbf{A} + \mathbf{BM}) = (\mathbf{C} + \mathbf{DM}) \tag{5.50}$$

which gives

$$\mathbf{M} = (\mathbf{C} + \mathbf{DM})(\mathbf{A} + \mathbf{BM})^{-1} \tag{5.51}$$

implying

$$f(\mathbf{M}) \quad = \quad \mathbf{M} \quad \square \tag{5.52}$$

Now to use the theorem we can multiply by the diagonalization matrix $\mathbf{T}$ on both sides of the condition (5.47). This yields

$$\mathbf{T} \begin{bmatrix} \mathbf{x}' \\ \mathbf{M}\mathbf{x}' \end{bmatrix} \quad = \quad \mathbf{T}\mathbf{J}\mathbf{T}^{-1}\mathbf{T} \begin{bmatrix} \mathbf{x} \\ \mathbf{M}\mathbf{x} \end{bmatrix}, \tag{5.53}$$

which implies

$$\begin{bmatrix} \tilde{\mathbf{x}}' \\ \tilde{\mathbf{M}}\tilde{\mathbf{x}}' \end{bmatrix} \quad = \quad \begin{bmatrix} \tilde{\mathbf{A}} & 0 \\ 0 & \tilde{\mathbf{D}} \end{bmatrix} \begin{bmatrix} \mathbf{x} \\ \tilde{\mathbf{M}}\tilde{\mathbf{x}} \end{bmatrix}, \tag{5.54}$$

where we introduced the new coordinates

$$\begin{bmatrix} \tilde{\mathbf{x}} \\ \tilde{\mathbf{p}} \end{bmatrix} \quad = \quad \begin{bmatrix} \mathbf{T}_{qq} & \mathbf{T}_{qp} \\ \mathbf{T}_{pq} & \mathbf{T}_{pp} \end{bmatrix} \begin{bmatrix} \mathbf{x} \\ \mathbf{p} \end{bmatrix}. \tag{5.55}$$

(5.54) now shows that $\tilde{\mathbf{M}}$ is a fixed point for the map $\tilde{f}$ by the theorem. The new phase space coordinates $\tilde{\mathbf{x}}$ and $\tilde{\mathbf{p}}$ are given in terms of the old coordinates by

$$\begin{aligned} \tilde{\mathbf{x}} &= (\mathbf{T}_{qq} + \mathbf{T}_{qp}\mathbf{M})\mathbf{x}, \\ \tilde{\mathbf{p}} &= (\mathbf{T}_{pq} + \mathbf{T}_{pp}\mathbf{M})\mathbf{x}. \end{aligned} \tag{5.56}$$

Inserting this in the expression for $\tilde{\mathbf{p}} = \tilde{\mathbf{M}}\tilde{\mathbf{x}}$ we find

$$\tilde{\mathbf{M}} \quad = \quad (\mathbf{T}_{pq} + \mathbf{T}_{pp})(\mathbf{T}_{qq} + \mathbf{T}_{qp}\mathbf{M})^{-1}. \tag{5.57}$$

By the theorem we therefore have that $\mathbf{M}$ is a fixed point for f if and only if $\tilde{\mathbf{M}}$ is a fixed point of the transformed map $\tilde{f}$, which is obtained from the original map just by substituting in the new transformed tilde matrices from the transformed Jacobian. But

$$\tilde{f}(\tilde{\mathbf{M}}) \quad = \quad \tilde{\mathbf{D}}\tilde{\mathbf{M}}\tilde{\mathbf{A}}^{-1}, \tag{5.58}$$

where $\tilde{\mathbf{D}}$ and $\tilde{\mathbf{A}}$ now are diagonal so this is only a simple linear equation

$$\tilde{\mathbf{M}}_{ij} \quad = \quad \mu_{ij}\tilde{\mathbf{M}}_{ij}, \tag{5.59}$$

which can easily be solved. From the $\tilde{\mathbf{M}}$ solution we therefore finally get the $\mathbf{M}$ solution from (5.57) as

$$\mathbf{M} \quad = \quad (\tilde{\mathbf{M}}\mathbf{T}_{qp} - \mathbf{T}_{pp})^{-1}(\mathbf{T}_{pq} - \tilde{\mathbf{M}}\mathbf{T}_{qq}). \tag{5.60}$$

If we suppose that the eigenvalues of the Jacobian are non degenerate, i.e. $\mu_{ij} \neq 1$, we therefore only have the trivial solution for $\tilde{\mathbf{M}}$:

$$\tilde{\mathbf{M}} \quad = \quad \mathbf{0} \tag{5.61}$$

which finally gives the $\mathbf{M}$ solution

$$\mathbf{M} \quad = \quad -\mathbf{T}_{pp}^{-1}\mathbf{T}_{pq} \tag{5.62}$$

A couple of examples of the solution of second order matrix equations by use of (5.62) are given in appendix 9.1.

5.3.2 Symplectic matrices

By the above procedure we get $K_{2N,N} = (2N)!/N!^2$ periodic solutions of the rational fraction transformation, which are too many since the matrix **M** should fulfill certain conditions imposed by the intrinsic nature of the Hamiltonian flow. In this section we show which restrictions the symplectic structure of the Jacobian imposes on the curvature matrix.

Let ω be the *symplectic* $[2N \times 2N]$ bilinear invariant

$$\omega = \begin{bmatrix} \mathbf{0} & \mathbf{1} \\ -\mathbf{1} & \mathbf{0} \end{bmatrix}. \tag{5.63}$$

A matrix **A** is said to be symplectic if

$$\mathbf{A}^t \omega \mathbf{A} = \omega. \tag{5.64}$$

Writing **A** as four block matrices

$$\mathbf{A} = \begin{bmatrix} a_{11} & a_{12} \\ a_{21} & a_{22} \end{bmatrix}, \tag{5.65}$$

the condition (5.64) immediately implies the following rules for the individual block matrices in order that the total matrix should be symplectic

$$a_{11}^t a_{21} = a_{21}^t a_{11}, \quad \text{and} \quad a_{12}^t a_{22} = a_{22}^t a_{12}, \tag{5.66}$$

$$a_{11}^t a_{22} - a_{21}^t a_{12} = a_{12}^t a_{21} - a_{22}^t a_{11} = 1. \tag{5.67}$$

Further more we get from (5.64) that

$$\mathbf{A}^{-1} = -\omega \mathbf{A}^t \omega, \tag{5.68}$$

since $\omega^{-1} = -\omega$, which implies

$$a_{21} a_{22}^t = a_{22} a_{21}^t \ , \text{ and } a_{11} a_{12}^t = a_{12} a_{11}^t. \tag{5.69}$$

5.3.3 The general M solution

In section 5.3.1 we saw that the general solution of the fixed point equation for the curvature matrix was given by

$$\mathbf{M} \quad = \quad (\tilde{\mathbf{M}} \mathbf{T}_{qp} - \mathbf{T}_{pp})^{-1} (\mathbf{T}_{pq} - \tilde{\mathbf{M}} \mathbf{T}_{qq}).$$

If $\mathbf{J}$ is a symplectic matrix and the diagonalizing matrix $\mathbf{T}$ is also a symplectic matrix, then the diagonalization $\boldsymbol{\Delta}$ of $\mathbf{J}$ is also symplectic. Writing the diagonalized Jacobian as

$$\mathbf{TJT}^{-1} \;\; = \;\; \left[\begin{array}{cc} \boldsymbol{\Delta}_A & \boldsymbol{\Delta}_B \\ \boldsymbol{\Delta}_C & \boldsymbol{\Delta}_D \end{array} \right],$$

this however implies that

$$\boldsymbol{\Delta}_A = \boldsymbol{\Delta}_D^{-1}, \tag{5.70}$$

so that the eigenvalues belonging to each other must be placed in the same order in the diagonal of $\boldsymbol{\Delta}_A$ and $\boldsymbol{\Delta}_D$ respectively. Assuming that we are dealing with Hamiltonian hyperbolic systems the linear fixed point equation (5.58) for $\tilde{\mathbf{M}}$ then becomes

$$\tilde{m}_{ij} = \lambda_i^2 \tilde{m}_{ij}, \tag{5.71}$$

where $\lambda_i \neq 1$ and hence the equation has only the solution

$$\tilde{\mathbf{M}} = \mathbf{0}. \tag{5.72}$$

This means that the solution in the original coordinate system will have the form

$$\mathbf{M} \;\; = \;\; -\mathbf{T}_{pp}^{-1} \mathbf{T}_{pq}, \tag{5.73}$$

which follows from (5.60). From the results in (5.69) we obtain

$$\begin{aligned} \mathbf{M}(\mathbf{M}^{-1})^t \;\; &= \;\; \mathbf{T}_{pp}^{-1} \mathbf{T}_{pq} ((\mathbf{T}_{pp}^{-1} \mathbf{T}_{pq})^{-1})^t \\ &= \;\; \mathbf{T}_{pp}^{-1} \mathbf{T}_{pq} \mathbf{T}_{pp}^t (\mathbf{T}_{pq}^{-1})^t \\ &= \;\; \mathbf{T}_{pp}^{-1} \mathbf{T}_{pp} \mathbf{T}_{pq}^t (\mathbf{T}_{pq}^{-1})^t \\ &= \;\; \mathbf{1}, \end{aligned} \tag{5.74}$$

so that

$$\begin{aligned} \mathbf{M} \;\; &= \;\; -\mathbf{T}_{pp}^{-1} \mathbf{T}_{pq} \\ &= \;\; \mathbf{M}^t, \end{aligned} \tag{5.75}$$

and hence the curvature matrix is symmetric as a consequence of the symplectic structure. This implies that $(\mathbf{q}, \mathbf{Mq})$ does in fact span a Lagrangian manifold as it should since $\mathbf{M}$ is the symmetric second derivative matrix of the phase function $S(x,t)$ (see appendix 9.1).

The next question is how many symmetric $\mathbf{M}$ solutions are there? To get the answer we have to study the diagonalization matrix $\mathbf{T}$. We know that $\mathbf{T}^{-1}$ have to contain the eigenvectors of $\mathbf{J}$ but it seems that we are free to permute them as we want as well as we have the possibility to scale the individual

eigenvectors arbitrarily. As we shall see now the symplectic structure puts quite a restriction on this liberty. A permutation of the columns of $\mathbf{T}^{-1}$ can be performed by multiplication from the right by a permutation matrix $\mathbf{P}_\tau(\mathbf{a})$ that permutes the columns following the permutation τ and at the same time multiply the columns by the weighting vector $\mathbf{a} = (a_1, a_2, \ldots, a_{2N})$. Such a permutation matrix can be defined by

$$[\mathbf{P}_\tau(\mathbf{a})]_{ij} \quad = \quad \delta_{\tau(j),i} a_j. \tag{5.76}$$

For instance

$$\begin{bmatrix} 1 & a & 7 & e \\ 2 & b & 9 & f \\ 3 & c & 1 & g \\ 4 & d & 3 & h \end{bmatrix} \begin{bmatrix} 0 & 0 & a_3 & 0 \\ a_1 & 0 & 0 & 0 \\ 0 & a_2 & 0 & 0 \\ 0 & 0 & 0 & a_4 \end{bmatrix} = \begin{bmatrix} a_1 a & a_2 7 & a_3 1 & a_4 e \\ a_1 b & a_2 9 & a_3 2 & a_4 f \\ a_1 c & a_2 1 & a_3 3 & a_4 g \\ a_1 d & a_2 3 & a_3 4 & a_4 h \end{bmatrix}.$$

Similarly the rows can be permuted by multiplication from the left with permutation matrices. From the definition of $\mathbf{P}_\tau(\mathbf{a})$ it follows immediately that

$$\mathbf{P}_\tau^{-1}(\mathbf{a}) \quad = \quad \mathbf{P}_\tau^t(\mathbf{a}^{-1}), \tag{5.77}$$

where $\mathbf{a}^{-1}$ means $(a_1^{-1}, a_2^{-1}, \ldots, a_N^{-1})$, and superscript t denotes the transposed matrix. The symplectic condition for a permutation matrix can be written

$$\mathbf{P}_\tau^t(\mathbf{a})\omega \quad = \quad \omega \mathbf{P}_\tau^{-1}(\mathbf{a}), \tag{5.78}$$

and using the relation (5.77) and writing the permutation matrix as the usual four block matrices we get

$$\begin{bmatrix} -\mathbf{P}_{21}^t(\mathbf{a}) & \mathbf{P}_{11}^t(\mathbf{a}) \\ -\mathbf{P}_{22}^t(\mathbf{a}) & \mathbf{P}_{12}^t(\mathbf{a}) \end{bmatrix} = \begin{bmatrix} \mathbf{P}_{12}^t(\mathbf{a}^{-1}) & \mathbf{P}_{22}^t(\mathbf{a}^{-1}) \\ -\mathbf{P}_{11}^t(\mathbf{a}^{-1}) & -\mathbf{P}_{21}^t(\mathbf{a}^{-1}) \end{bmatrix},$$

so that the condition for a permutation matrix to be symplectic is

$$-\mathbf{P}_{21}(\mathbf{a}) = \mathbf{P}_{12}(\mathbf{a}^{-1}), \tag{5.79}$$

and

$$\mathbf{P}_{11}(\mathbf{a}) = \mathbf{P}_{22}(\mathbf{a}^{-1}). \tag{5.80}$$

Since the columns in $\mathbf{T}^{-1}$ *must* contain the eigenvectors of the Jacobian, we see that the Jacobian can only be diagonalized by symplectic rotations if they are of the form

$$\tilde{\mathbf{T}} \quad = \quad \mathbf{PT}, \tag{5.81}$$

where $\mathbf{T}$ is a symplectic matrix that diagonalizes $\mathbf{J}$, and $\mathbf{P}$ is a symplectic permutation matrix.

Now what is the significance of the local block matrices in $\mathbf{P}$? The blocks in the diagonal $\mathbf{P}_{11}$ and $\mathbf{P}_{22}$ simply permutes the local rows of $\mathbf{T}_{qq}, \mathbf{T}_{qp}$ and $\mathbf{T}_{pq}, \mathbf{T}_{pp}$ respectively. As we can write

$$\tilde{\mathbf{M}} = -(\mathbf{p}\mathbf{T}_{pp})^{-1}\mathbf{p}\mathbf{T}_{pq} = \mathbf{M},$$

we see that such a *local* permutation $\mathbf{p}$ does not change the $\mathbf{M}$ solution. However, the elements different from zero in $\mathbf{P}_{21}$ exchange rows in $\mathbf{T}_{pp}$ and $\mathbf{T}_{pq}$ with upper rows in $\mathbf{T}$ and hence change the $\mathbf{M}$ solution. Each row in $\mathbf{P}_{21}$ say, has then essentially two possible states: either it is a pure zero row, or it contains a '1'. The exact position of the '1' is not important since this can be shifted by a local permutation and thus does not alter the $\mathbf{M}$ solution. Since $\mathbf{P}_{21}$ has N rows each having two possible states there must be 2^N different solutions to the $\mathbf{M}$ fix point equation, which can be obtained from symplectic diagonalizations of the Jacobian.

By studying the symplectic structure we have thus found that there are 2^N symmetric periodic solutions to (5.20). A couple of examples where the solution formula (5.62) and the above considerations is applied to a symplectic matrix are given in appendix 9.1.

5.3.4   Stabilities of the periodic curvature solutions

Let us for now suppose that we have found the periodic solutions of the rational fraction transformation map f,

$$f(\mathbf{M}) = (\mathbf{C} + \mathbf{D}\mathbf{M})(\mathbf{A} + \mathbf{B}\mathbf{M})^{-1}, \tag{5.82}$$

i.e. the periodic curvature matrix solutions. We now would like to find the stabilities of the periodic solutions by using (5.82). This can be accomplished by variation of the map

$$f(\mathbf{M} + \delta\mathbf{M}) = f(\mathbf{M}) + Df(\delta\mathbf{M}) + \mathcal{O}(\|\delta\mathbf{M}^2\|), \tag{5.83}$$

where the so called *Frechet derivative* Df is just a linear map. For an alternative approach to the stability calculation see appendix 9.1. To simplify notation we introduce the two functions

$$N(\mathbf{M}) = \mathbf{C} + \mathbf{D}\mathbf{M},$$
$$D(\mathbf{M}) = \mathbf{A} + \mathbf{B}\mathbf{M}, \tag{5.84}$$

where N stands for the numerator, and D for the denominator. To obtain the Frechet derivative of the rational fraction transformation we proceed in the way of usual differentiation

$$\begin{aligned} f(\mathbf{M} + \delta\mathbf{M}) - f(\mathbf{M}) &= N(\mathbf{M} + \delta\mathbf{M})D^{-1}(\mathbf{M} + \delta\mathbf{M}) - N(\mathbf{M})D^{-1}(\mathbf{M}) \\ &= (N(\mathbf{M} + \delta\mathbf{M}) - N(\mathbf{M}))D^{-1}(\mathbf{M} + \delta\mathbf{M}) \\ &+ N(\mathbf{M})(D^{-1}(\mathbf{M} + \delta\mathbf{M}) - D^{-1}(\mathbf{M})), \tag{5.85} \end{aligned}$$

where in the last equation we have just subtracted and added the same term $N(\mathbf{M})D^{-1}(\mathbf{M} + \delta\mathbf{M})$.

If we now consider the first term, we obtain in the limit $\delta\mathbf{M} \to \mathbf{0}$ directly

$$1.term \quad = \quad \mathbf{D}\delta\mathbf{M}N^{-1}(\mathbf{M}). \tag{5.86}$$

For the denominator part in the second term we write

$$
\begin{aligned}
D^{-1}(\mathbf{M} + \delta\mathbf{M}) - D^{-1}(\mathbf{M}) \quad &= \quad D^{-1}(\mathbf{M} + \delta\mathbf{M})\{\mathbf{1} - \\
&\qquad [D(\mathbf{M} + \delta\mathbf{M}) - D(\mathbf{M}) + D(\mathbf{M})]D^{-1}(\mathbf{M})\} \\
&= \quad D^{-1}(\mathbf{M} + \delta\mathbf{M})\left[D(\mathbf{M} + \delta\mathbf{M}) - D(\mathbf{M})\right]D^{-1}(\mathbf{M}).
\end{aligned}
$$

In the limit $\delta\mathbf{M} \to \mathbf{0}$ this becomes

$$2.term \quad = \quad -D^{-1}(\mathbf{M})\mathbf{B}\delta\mathbf{M}D^{-1}(\mathbf{M}). \tag{5.87}$$

Gathering both terms we can write

$$f(\mathbf{M} + \delta\mathbf{M}) - f(\mathbf{M}) \quad = \quad \left(\mathbf{D} - N(\mathbf{M})D^{-1}(\mathbf{M})\mathbf{B}\right)\delta\mathbf{M}D^{-1}(\mathbf{M}) + \mathcal{O}(\|\delta\mathbf{M}^2\|),$$
$$\tag{5.88}$$

so that the general expression for the derivative is

$$Df(\delta\mathbf{M}) \quad = \quad (\mathbf{D} - N(\mathbf{M})D^{-1}(\mathbf{M})\mathbf{B})\delta\mathbf{M}D^{-1}(\mathbf{M}). \tag{5.89}$$

Since the stabilities are robust to change of coordinates i.e. the fix point x for the map f has the same stability as the transformed fix point $g(x)$ of the map $\tilde{f} = g \odot f \odot g^{-1}$, we can calculate the stabilities in the basis where we have diagonalized the Jacobian matrix.

In the case where $\mathbf{M}$ is a fixed point of the map we get

$$
\begin{aligned}
Df(\delta\mathbf{M}) \quad &= \quad (\mathbf{D} - \mathbf{MB})\delta\mathbf{M}D^{-1}(\mathbf{M}) \\
&= \quad (\mathbf{D} - \mathbf{MB})\delta\mathbf{M}(\mathbf{A} + \mathbf{BM})^{-1}. \tag{5.90}
\end{aligned}
$$

And in the case where we have diagonalized $\mathbf{J}$ we therefore simply get

$$
\begin{aligned}
Df(\delta\mathbf{M}) \quad &= \quad \mathbf{D}\delta\mathbf{M}\mathbf{A}^{-1} \\
&= \quad [\Lambda_i\Lambda_j\delta\mathbf{M}_{ij}],
\end{aligned}
$$
$$\tag{5.91}$$

where $\mathbf{A}$ and $\mathbf{D}$ are diagonal. We note (5.91) is a *symmetric* matrix if the variation $\delta\mathbf{M}$ is itself symmetric. The eigenvariations can now be found from the equation

$$Df(\delta\mathbf{M}) \quad = \quad \tilde{\Lambda}\delta\mathbf{M}, \tag{5.92}$$

and for symmetric variations $\delta\mathbf{M}$ the $N(N + 1)/2$ eigenvalues are read off as

$$\tilde{\Lambda}_i \quad = \quad \Lambda_i\Lambda_j, \quad i = 1, \ldots N \quad j = i, \ldots, N \tag{5.93}$$

since the matrices $\mathbf{A}$ and $\mathbf{D}$ are diagonal and fulfills $\mathbf{A}^{-1} = \mathbf{D}$ according to (5.70). The eigenvalues are thus given in terms of the original cycle stabilities.

The volume ratio

The only thing we miss in obtaining the general result for $\text{Tr}\mathcal{L}$, is then to find the volume ratio (5.21)

$$\frac{V(q')}{V(q_0)} \;=\; \det(\mathbf{J}_{qq} + \mathbf{J}_{qp}\mathbf{M}). \tag{5.94}$$

To determine this, we note that for a given $\mathbf{M}$ (the periodic solutions) the matrix

$$\mathbf{j_M} \;=\; \mathbf{J}_{qq} + \mathbf{J}_{qp}\mathbf{M}, \tag{5.95}$$

is the *configuration space Jacobian*, which governs the evolution of the projection of the total phase space flow on configuration space. The configuration space flow of course depends on the momentum also and to see that (5.95) is the right expression, we can look at the map given by the full phase space Jacobian

$$\left[\begin{array}{c} \mathbf{x}' \\ \mathbf{M}'\mathbf{x}' \end{array}\right] \;=\; \left[\begin{array}{cc} \mathbf{J}_{qq} & \mathbf{J}_{qp} \\ \mathbf{J}_{pq} & \mathbf{J}_{pp} \end{array}\right] \left[\begin{array}{c} \mathbf{x} \\ \mathbf{M}\mathbf{x} \end{array}\right], \tag{5.96}$$

which tells us that local variations in configuration space $\delta\mathbf{q}$ maps into

$$\delta\mathbf{q}' \;=\; (\mathbf{J}_{qq} + \mathbf{J}_{qp}\mathbf{M})\delta\mathbf{q}. \tag{5.97}$$

The volume ratio (5.94) is therefore given by the product of the N eigenvalues λ_i of $\mathbf{j_M}$. To find these eigenvalues let us first assume that we have found the corresponding eigenvectors $\mathbf{e}_1, \ldots, \mathbf{e}_N$. Then by constructing the full phase space vector $(\mathbf{e}_i, \mathbf{M}\mathbf{e}_i)$, and mapping this by the full phase space Jacobian $\mathbf{J}$ we obtain

$$\mathbf{J}\left[\begin{array}{c} \mathbf{e}_i \\ \mathbf{M}\mathbf{e}_i \end{array}\right] \;=\; \left[\begin{array}{c} (\mathbf{J}_{qq} + \mathbf{J}_{qp}\mathbf{M})\mathbf{e}_i \\ (\mathbf{J}_{pq} + \mathbf{J}_{pp}\mathbf{M})\mathbf{e}_i \end{array}\right],$$
$$\;=\; \left[\begin{array}{c} (\mathbf{J}_{qq} + \mathbf{J}_{qp}\mathbf{M})\mathbf{e}_i \\ (\mathbf{J}_{pq} + \mathbf{J}_{pp}\mathbf{M})(\mathbf{J}_{qq} + \mathbf{J}_{qp}\mathbf{M})^{-1}\mathbf{e}_i' \end{array}\right] \tag{5.98}$$

but since $\mathbf{e}_i$ was assumed to be an eigenvector of $\mathbf{j_M}$ corresponding to the *periodic* curvature solution $\mathbf{M}$ we just get

$$\mathbf{J}\left[\begin{array}{c} \mathbf{e}_i \\ \mathbf{M}\mathbf{e}_i \end{array}\right] \;=\; \lambda_i \left[\begin{array}{c} \mathbf{e}_i \\ \mathbf{M}\mathbf{e}_i \end{array}\right], \tag{5.99}$$

which implies that λ_i must be the same as one of the full phase space eigenvalues ie. $\lambda_i = \Lambda_j$ for some j. Conversely it is easy to show (see appendix 9.1) that if we can write a full phase space eigenvector as $\mathbf{e} = (\delta\mathbf{q}, \tilde{\mathbf{M}}\delta\mathbf{q})$ for some $\tilde{\mathbf{M}}$, then this $\tilde{\mathbf{M}}$ will be a periodic solution of the curvature map (5.20). For each periodic $\mathbf{M}$ solution we therefore have N configuration space eigenvalues which are just given by the eigenvalues of the full phase space eigenvectors corresponding to the periodic solution $\mathbf{M}$ (see appendix 9.1). The volume ratio (5.94) is therefore just the product of the cycle stabilities corresponding to the given $\mathbf{M}$ solution.

These can be identified by noting that for a given $\mathbf{M}$ solution, the manifold spanned by $(\delta\mathbf{q}, \mathbf{M}\delta\mathbf{q})$ corresponds to a definite subset of the $2N$ phase space eigenvectors spanning the same (Lagrangian) manifold. For a detailled study of this correspondance we refer to appendix 9.1. The volume ratio after r repetitions of the cycle can now be written as

$$\frac{V(q^{rT_p})}{V(q)} = \prod_{i=1}^{N} |\Lambda_i^{-r}| \tag{5.100}$$

We are thus finally in a position where we can state the general result for the curvature trace (9.28). This reads

$$\Delta_{p,r} = \int d\mathbf{M} e^{\int_0^{rT_p} d\tau \frac{1}{2} \text{Tr}(H_{pq} + H_{pp}\mathbf{M})} \delta(\mathbf{M} - \mathbf{M}^{rT_p}(\mathbf{M}))$$

$$= \sum_{l=1}^{2^N} \prod_{i_l=1}^{N} |\Lambda_{i_l}|^{-r/2} \prod_{j=i_l}^{N} |1 - \Lambda_j^r \Lambda_{i_l}^r|^{-1}, \tag{5.101}$$

where l labels the periodic $\mathbf{M}$ solutions. From this result we are now also able to evaluate the Vattay determinant (5.42) in any number of dimensions.

In the simple 2-dimensional case the above formula reduce to

$$\Delta_{p,r} = \int d\mathbf{M} e^{\int_0^{rT_p} d\tau \frac{1}{2} \text{Tr}\mathbf{M}} \delta(\mathbf{M} - \mathbf{M}^{rT_p}(\mathbf{M}))$$

$$= \sum_{l=1}^{2} \prod_{i_l=1}^{1} |\Lambda_{i_l}|^{-r/2} \prod_{j=1}^{1} |1 - \Lambda_j^r \Lambda_{i_l}^r|^{-1}$$

$$= \frac{|\Lambda_p^r|^{1/2}}{|1 - \Lambda_p^{-2r}|} + \frac{|\Lambda_p^r|^{-1/2}}{|1 - \Lambda_p^{2r}|}$$

$$= \frac{|\Lambda_p^r|^{1/2}}{1 - \Lambda_p^{-2r}} + \frac{|\Lambda_p^r|^{-5/2}}{1 - \Lambda_p^{-2r}}, \tag{5.102}$$

which is the result obtained in [15].

5.4 Validity of the entire determinant

To examplify the validity of the new determinant we can try to do the same calculation as we did with the quantum Fredholm determinant in section 5.1.3. Evaluating the coefficients of the cycle expansion of the Vattay determinant at the leading zero $0.75831\ldots - i0.12282\ldots$ in the case of the 3-disk scatterer with $R : a = 6$ we get the results shown in figure 5.5. As we see the coefficients of the Vattay determinant displays a super exponential decay indicating that indeed there is no pole present. In the case of the quantum Fredholm determinant we see that the initial super exponential decay turns over in an exponential decay implying the presence of a pole.

The new spectral determinant has also recently been subject to a large number of investigations due to A. Wirzba [65]. This was due to the following observation: the Gutzwiller-Voros zeta function is an asymptotic series that
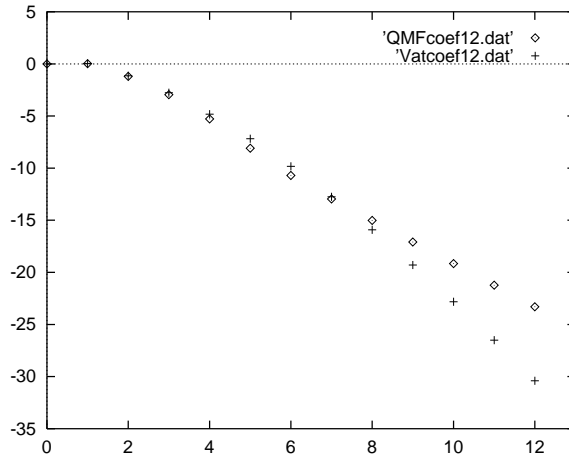
Figure 5.5: The logarithm (base 10) of the absolute value of the expansion coefficients C_n of the quantum Fredholm determinant ($\diamond$) and the Vattay determinant ($+$) versus cycle length n. The coefficients are evaluated at the leading zero $0.75831\ldots - i0.12282\ldots$ of the 3-disk system at $R : a = 6$.

mimics the behaviour of the quantum resonances up to a certain curvature order and then diverges. At curvature order 7 the leading as well as the subleading resonances are very well approximated as we saw in figure 5.3, but by inclusion of more periodic orbits the series diverges and the subleading resonances disappear. For the Vattay determinant the situation is much different. At curvature order 7 the leading resonances are found with high precision but in the domain of the subleading resonances a very complicated pattern of resonances occur, that does not resemble the correct resonances at all. However, if one continues and include more periodic orbits in the curvature expansion it turns out that at curvature order 12 (see figure 5.6) the resonance system breaks up into two different parts: the first part now also approximates the subleading resonances with good precision and the second part has nothing to do with the exact quantum resonances at all. These "fake" quantum resonances are presumably due to the fact that the Vattay evolution operator is not constructed specifically for quantum densities but is capable of evolving classical densities as well. We should therefore only expect a part of the resonance spectrum to be related to quantum mechanics. By inclusion of still more periodic orbits in the expansion we expect that the leading as well as the subleading resonances will stay put, since the spectral determinant should be an entire function in the complex plane.

Another problem occurs when one considers the "fake" resonances. Here it is hoped that these resonances can be filtered away by following the technique of Ref. [14]. The main idea here is that one can formally rewrite the Gutzwiller-Voros determinant as [15]

$$Z(k) \quad = \quad \frac{F_+\left(\frac{1}{2}, k\right) F_-\left(\frac{7}{2}, k\right)}{F_-\left(\frac{3}{2}, k\right) F_+\left(\frac{5}{2}, k\right)} \tag{5.103}$$
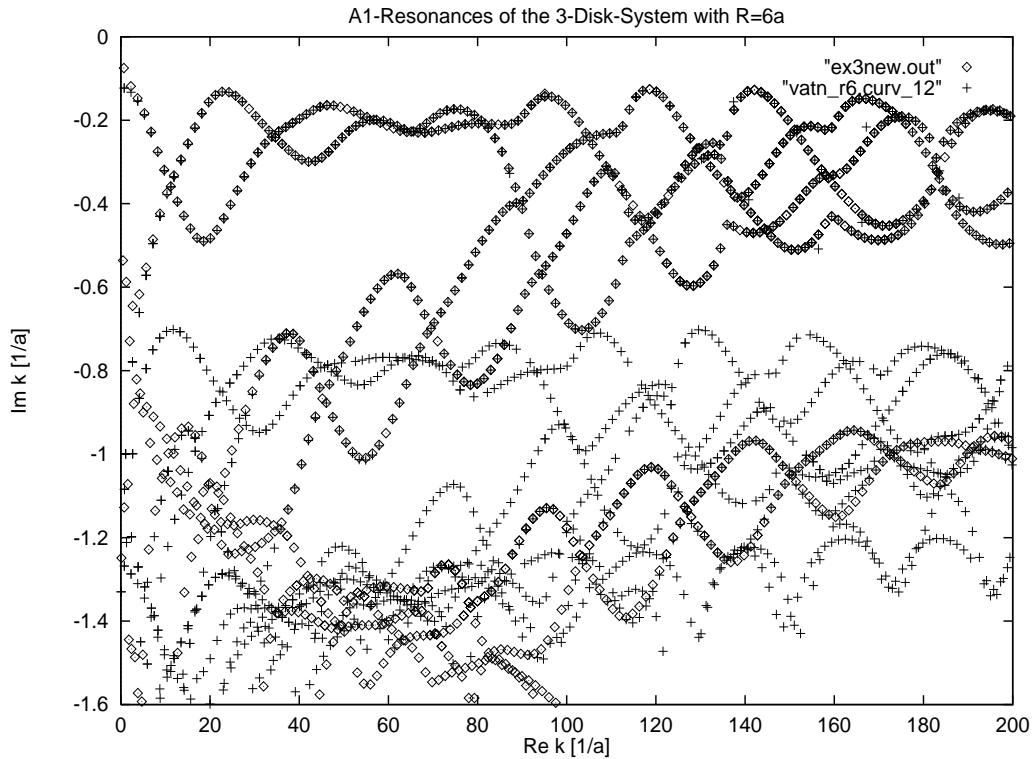
Figure 5.6: Scattering resonances of the A_1 representation of the $R : a = 6$ 3-disk system. The exact quantum resonances are denoted by diamonds, and the Vattay determinant resonances by crosses. In the cycle expansion of the Vattay determinant periodic orbits up to topological length 12 were used. The leading part of the spectrum is very well matched by the Vattay determinant. For the nonleading part of the spectrum the Vattay determinant also has the right quantum mechanical resonances, but furthermore yields a lot of unphysical resonances. It should be noted that the nonleading part of the spectrum is first obtained at curvature order 12 of the Vattay determinant. The data are from A. Wirzba.

where

$$F_\sigma(\beta, k) = \exp\left(-\sum_{p,r} \frac{\sigma_p^r}{r|\Lambda_p^r|} \frac{e^{rkT_p}}{(1-\Lambda_p^{-r})^2} \Delta_{p,r}(\beta)\right) \tag{5.104}$$

with $\sigma_p = \Lambda_p/|\Lambda_p|$ for F_-, and $\sigma_p = 1$ for F_+, and where only the first term in $\Delta_{p,r}$

$$\Delta_{p,r}(\beta) = \frac{|\Lambda_p^r|^{-\beta+1}}{1-\Lambda_p^{-2r}} + \frac{|\Lambda_p^r|^{\beta-3}}{1-\Lambda_p^{-2r}} \tag{5.105}$$

is included. The Gutzwiller-Voros zeta function is thus written as a ratio of entire functions [15], and the fake zeros of $F_+(\frac{1}{2}, k)$ should be cancelled by the zeros of $F_-(\frac{3}{2}, k)$. By numerical studies it turns out that the "fake" quantum resonances of $F_+(\frac{1}{2}, k)$ almost coincide (up to a few digits) with the zeros of $F_-(\frac{3}{2}, k)$, so that it is possible to extract the final approximation to the true quantum spectrum. The remaining problem is to find out why the cancellation of the fake zeros is not exact, which it should be as the determinants in the ratio should be entire. This might have to do with the interpretation of how a formal expansion like (5.103) should be carried out. Also numerical studies on the total scattering phase shift [65] indicates that the Gutzwiller-Voros zeta function is preferable to any other determinants or just the quantum zeta function. These problems are therefore still open. For the reader interested in following the discussion and developments on these subjects we refer to [65].

5.5   Conclusion

In this section we have followed the work on improving the convergence properties of the Gutzwiller-Voros zeta function by introducing new evolution operators that yield a larger domain of analyticity and at the same time still gives the correct semiclassical resonances. First we studied the "quantum Fredholm" determinant which was (historically) our first candidate for this. This determinant has convergence properties that are superior to the Gutzwiller-Voros zeta function, but unfortunately it does not give the correct nonleading resonances. Next we followed the work of Vattay and studied an evolution operator which is multiplicative and therefore gives an entire spectral determinant. We derived the general N-dimensional expression for this determinant in terms of the cycle stabilities, and made a few numerical 3-disk investigations on our result. In contrast to the Gutzwiller-Voros zeta function which is only an asymptotic series, the Vattay determinant converges to the right resonances by inclusion of still more and more orbits. It has however, certain disadvantages as well: first, to get the quantum resonances with large negative imaginary part one has to include many more periodic orbits in the calculation of the determinant than in the Gutzwiller-Voros zeta function case. In the Gutzwiller-Voros zeta function case on the other hand, inclusion of longer orbits makes the determinant diverge and destroys all the previously obtained lowlying resonances. Second, the Vattay determinant has resonances that are not at all related to the physical

problem, - a problem which one does not encounter in the Gutzwiller-Voros zeta function. One can hope that it will be possible to filter out these fake resonances by the technique used in [14].

Chapter 6

Diffraction

6.1 The Geometrical theory of diffraction

The geometrical theory of optics has eversince its emergence been a very useful tool in describing the evolution of waves in terms of rays. Starting in 1959 Keller strongly improved this theory by extending it to include diffraction effects. In a series of papers [38] he introduced and developed the geometrical theory of diffraction describing the well known wave phenomena ranging from diffraction around smooth objects to diffraction on vertices and edges. He tested the theory on several examples and observed an excelent agreement with experiments and theoretical results obtained by direct wave mechanics.

In this section we first start by a brief review of the ordinary theory of geometrical optics whereafter we describe Kellers construction of the geometrical theory of diffraction.

In geometrical optics the aim is to describe the electromagnetic field under the assumption that the field propagates along *rays*. The rays are determined by the *principle of least action* or the Fermat principle which states that among all trajectories between two points A and B, only the paths of least travel time should give a contribution to the resulting field.

In the ordinary theory of geometrical optics a field value is associated with each ray. The field is composed of a phase function $\phi(s)$ and an amplitude $A(s)$ which are both functions of the distance s along the ray. The phase is just a linear function of the distance: $\phi(s) = \phi_0 + s$, which follows from the optical law $d\phi/ds = 1$. The initial phase ϕ_0 is the phase at the point from which the distance s is measured. The amplitude is determined by conservation of energy along the ray. For a tube of rays the energy flux is the same through every cross section of the tube. If the amplitude and cross section area at some point in the tube is given by A_0 and $d\sigma_0$ and by A and $d\sigma$ at some later point, then the principle of conservation of energy states that $A_0^2 d\sigma_0 = A^2 d\sigma$ and hence the amplitude is given by $A = A_0\sqrt{d\sigma_0/d\sigma}$. To calculate the field at some point P we just follow all the rays that emerge from the source Q (or sources) and

impinges at the final point under investigation. The resulting field $u(P)$ is then the sum of the contributions from the different paths p:

$$u(P) = \sum_p A_p e^{ik(s+\phi_0)} \tag{6.1}$$

where $k = \omega/c$ is the wavenumber, ω is the angular frequency of the field and c is its propagation speed. At this point we have only described the evolution of a scalar field, but for a vector field the description is completely analogous. For simplicity we shall here continue to treat scalar fields.

The next step is to calculate the area ratio $d\sigma_0/d\sigma$. To do this, consider figure 6.1. Since $d\sigma_0$ and $d\sigma$ are just the areas cut out by the tube at the
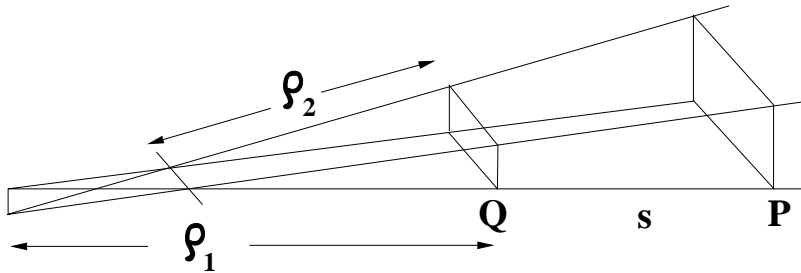
Figure 6.1: A tube of rays emerging from Q and impinging at P. The principal radii of curvature are indicated as ρ_1 and ρ_2.

wavefronts $\phi = \phi_0$ and $\phi = \phi_0 + s$, and since the rays are just straight lines we obtain by simple geometry

$$\frac{d\sigma_0}{d\sigma} = \frac{\rho_1 \rho_2}{(\rho_1 + s)(\rho_2 + s)} \tag{6.2}$$

and hence the field contribution from a single ray at the point P is just

$$u(P) = A_0 \left(\frac{\rho_1 \rho_2}{(\rho_1 + s)(\rho_2 + s)} \right)^{1/2} e^{ik(\phi_0 + s)} \tag{6.3}$$

In two dimensions the result would be the same except for the first factor in both nominator and denominator. This specific result holds only for free propagation, but can easily be generalised to include specular reflections from smooth surfaces by introducing an effective traveled distance. The above results contain the essence of the ordinary theory of geometrical optics.

Next we shall use the above ideas to describe diffraction from the exterior of a smooth convex body. Besides the straight line rays from the usual geometrical optics theory we then need additional diffraction rays. These are introduced by an extention of Fermat's principle stating that the diffracted rays connecting

two points Q and P are those curves which have stationary length among all the topologically different curves joining Q and P. From this principle it follows, that in a homogeneous medium the rays will be straight lines for the free flight and that they will follow the geodesics on the surface of the obstacles on which they diffract. An example of such a ray is shown on figure 6.1. From the usual
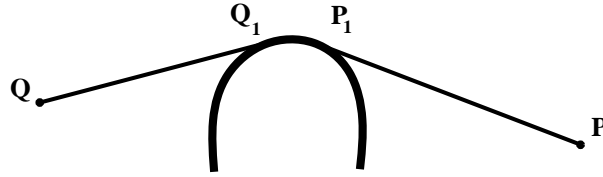
Figure 6.2: A diffracted ray from a point Q to P. The points Q_1 and P_1 are the points where the straight line ray hits the obstacle tangentially and creates the diffracted ray, and where the diffracted ray leaves the obstacle by acting like a source for a new straight line trajectory. The ray is seen to be the shortest among all the continuous curves joining Q and P by passing over the obstacle.

geometrical optics described above we can easily get the field value at the point where the ray impinges. We now *assume* that the field on the diffracted (or surface) ray at the point Q_1 is proportional to the incident field

$$A_d(Q_1) \quad = \quad D(Q_1)A_i(Q_1) \tag{6.4}$$

where we have defined the *diffraction coefficient* $D(Q_1)$, which we assume depends only on the nature of the field, the local properties of the obstacle at Q_1 and the wavenumber k. In cases where boundary conditions requires that the field be identically zero at the surface of the obstacle (as for instance hard wall potentials in quantum mechanics) the result is the same except that the diffracted field u_d must be interpreted as a measure of the typical size of the field in the vicinity of the surface. The diffraction constant is determined by comparison to the exact field solution for some simple geometry. We postpone this calculation till section 6.3.

Next step is to get the variation of the field along the surface ray. If we let t denote the distance traveled along the surface of the obstacle then the previous considerations yields for the phase: $\phi_d(t) = \phi_i(Q_1) + t$. To determine the amplitude as function of t we apply the principle of energy conservation along a narrow strip of geodesics on the surface of the obstacle containing the surface ray (see figure 6.1).

We denote the width of the strip $d\sigma(t)$ and the energy flux through a cross
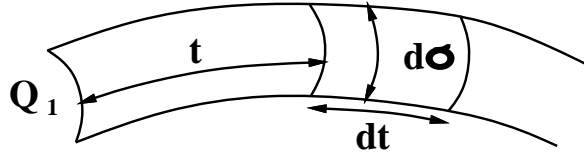
Figure 6.3: A strip of diffracted rays moving along the geodesics of the surface of the obstacle.

section of the strip is then proportional to $A_d^2(t)d\sigma(t)$. At a slightly later time the energy flux through the cross section $d\sigma(t+dt)$ will be smaller because diffracted rays have been shed out in the meantime. We assume that the radiated energy is proportional to dt, $d\sigma(t)$ and to the square of the amplitude $A_d(t)^2$. The energy conservation requires

$$A_d^2(t+dt)d\sigma(t+dt) - A_d^2(t)d\sigma(t) = -2\alpha(t)A_d^2(t)d\sigma(t)dt \tag{6.5}$$

where we have introduced the proportionality constant $2\alpha(t)$ relating the energy flux to the radiated energy. As in the case of the diffraction coefficient we expect that $\alpha(t)$ depends of the local properties of the obstacle and of the nature of the field. The determination of $\alpha(t)$ takes place in the same way as that of D, and will also be postponed untill section 6.3. (6.5) yields a differential equation for the time dependance of the amplitude

$$\frac{d}{dt}(A_d^2(t)d\sigma) = -2\alpha(t)A_d^2 d\sigma \tag{6.6}$$

which immediately yields

$$A_d(t) = A_d(0)\left(\frac{d\sigma_0}{d\sigma}\right)^{1/2}\exp\left(-\int_0^t \alpha(\tau)d\tau\right). \tag{6.7}$$

Here $d\sigma_0/d\sigma$ is the ratio with which the geodesics spread out over the surface of the obstacle. If for instance the geodesics are parallel, this ratio would simply be unity - a case we shall encounter in the 2-dimensional description where the width of the strip is constant equal zero. The diffracted field on the surface of the obstacle at distance t from Q_1 thus reads

$$u_d(t) = D(Q_1)A_i(Q_1)\left(\frac{d\sigma_0}{d\sigma}\right)^{1/2}\exp\left(ik(\phi_i(Q_1)+t) - \int_0^t \alpha(\tau)d\tau\right) \tag{6.8}$$

From (6.8) we get the field at the point P_1. To get the field at P we should make use of the usual geometrical optics propagation. However this is not directly

applicable because at P_1 the field acts like a source implying that one of the principal radii of curvature is zero. We make use of a limiting procedure where we determine the field at P as function of the field at a variable point x on the line connecting P_1 with P. Letting x tend to P_1 we then obtain the field at P by demanding this to be constant during this procedure. As x tends to P_1 we have the following scenario: ρ_2 tends to zero, ρ_1 tends to some finite value, ϕ_0 tends to $\phi_d(P_1)$ and s tends to the distance from P_1 to P while $u(P)$ remains constant. It then follows from (6.3) that A_0 must tend to infinity in such a way that $A_0\sqrt{\rho_2}$ converges to a finite limit. Denoting this limit $A'_d(P_1)$ we can write the field at P

$$u_d(P) \quad = \quad A'_d(P_1)\left(\frac{\rho_1}{s(\rho_1+s)}\right)^{1/2}\exp(ik(\phi_d(P_1)+s)) \tag{6.9}$$

We assume now that $A'_d(P_1)$ is proportional to the diffracted field at P_1 so that $A'_d(P_1) = D(P_1)u_d(P_1)$ and that the diffraction constant $D(P_1)$ is *the same* function of the local properties of the obstacle and of the field as the diffraction constant at Q. This assumption is based on the reciprocity principle which states that a source at Q produces the same field at P as a source located at P would produce in Q. We can now write the field at P as

$$
\begin{aligned}
u_d(P) \quad = \quad & A_i(Q_1)D(P_1)D(Q_1)\left(\frac{d\sigma(Q_1)}{d\sigma(P_1)}\right)^{1/2}\left(\frac{\rho_1}{s(\rho_1+s)}\right)^{1/2} \\
\times \quad & \exp\left(ik(\phi_i(Q_1)+t+s)-\int_0^t\alpha(\tau)d\tau\right) \tag{6.10}
\end{aligned}
$$

In the derivation we have excluded fields which are required by boundary conditions to vanish on the surface of the obstacle. This is due to the fact that we have considered the amplitude function on the surface A_d. However, since the surface of the obstacle is a caustic for the diffracted field it follows that the field is much stronger in a surface layer some few wavelengths thick than it is at points further away from the surface. Therefore the discussion still holds if we interpret A_d as a measure of the field amplitude in this layer. The field within the caustic layer will have a certain profile variation with the distance along the direction of a surface normal. The amplitude at any point of the profile (except where this has a zero) can serve as a measure of the field amplitude in the caustic layer. In general it turns out to be practical at this point to expand the field in a basis of *modes* each with its own profile. Each mode will also be characterized by its own amplitude A_{dm} and its own diffraction constant $D_m(Q_1)$. According to the principle of superposition the total field must be the sum over contributions from each mode

$$
\begin{aligned}
u_d(P) \quad = \quad & A_i(Q_1)\left(\frac{d\sigma(Q_1)}{d\sigma(P_1)}\right)^{1/2}\left(\frac{\rho_1}{s(\rho_1+s)}\right)^{1/2} \tag{6.11} \\
\times \quad & \sum_m D_m(P_1)D_m(Q_1)\exp\left(ik(\phi_i(Q_1)+t+s)-\int_0^t\alpha_m(\tau)d\tau\right)
\end{aligned}
$$

Equation (6.12) yields the final expression for the field contribution associated with a single diffracted ray. The total field at P will then be the sum over all

rays, both usual geometric and diffracted, passing through P

$$u(P) = u_g(P) + u_d(P). \tag{6.12}$$

Expression (6.12) is the general result of the geometrical theory of diffraction, with the diffraction coefficients D_m and the decay constants α_m to be determined for the explicit problem under investigation. In the next section we shall see how this can be done for the 2-dimensional 1-disk problem.

6.2   The 1-disk Keller propagator

In this section we will construct a semiclassical expression for the energy domain quantum propagator in the simple 2-dimensional 1-disk scattering system using Keller's geometrical theory of diffraction together with the usual geometrical optics. Having done this, the next step will be to determine the diffraction coefficients $D(Q_1)$ and the proportionality constant α. This we will do by comparing the semiclassical expression to the semiclassical expansion of the quantum mechanical *exact 1-disk propagator*.

We consider a disk of radius a centered at the origin of a polar coordinate system (r, θ). Assuming that the disk represents an infinite potential implies that the wave function should vanish at the surface of the disk. The Greens function or propagator of the system therefore fulfills

$$(\Delta + k^2)G(\vec{r}, \vec{r}'; k) = \delta(\vec{r} - \vec{r}') \tag{6.13}$$

with Dirichlet boundary conditions on the surface of the disk. At $\vec{r}$ we place a wave or ray source and then try to determine the field at the receiver located at $\vec{r}'$. The geometry of the system is shown in figure 6.2. Since the operator in equation (6.13) is self adjoint we must furthermore have that the propagator is symmetric in its arguments [34]

$$G(\vec{r}, \vec{r}') = G(\vec{r}', \vec{r}) \tag{6.14}$$

We consider the case where the point of the observer is in the lit region of the source since this also covers the case where the observer is in the shadow region relative to the source. To obtain the field at the points of tangential incidence we use the 2-dimensional version of (6.3). If R is the distance from the source to this point we obtain

$$G_i = \frac{i}{4}\left(\frac{2}{k\pi R}\right)^{1/2} e^{ikR - i\pi/4} \tag{6.15}$$

where we have chosen the constant in front so that G_i represents the short-wave limit of the field from a source of unit strength i.e. a source for which $-iH_0^{(1)}(kR)/4$ is the exact solution.

From (6.4) it follows that the diffraction constant $D(Q_1)$ is dimensionless and therefore if it depends on the wavenumber k it must do so in a dimensionless combination ka where a has the dimension of length. We shall let a be the local
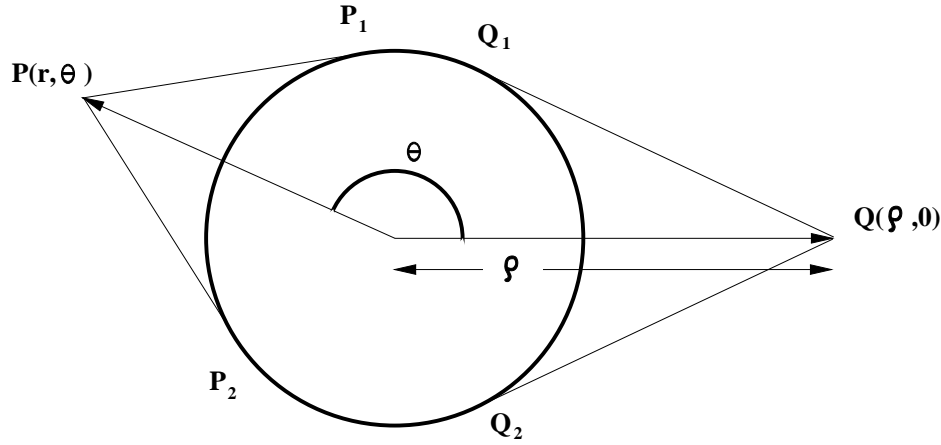
Figure 6.4: The geometry of the disk and the source. The two families of rays going from the source Q to the receiver P are shown.

radius of curvature at the point where the ray impinges. One might expect that a detailed description of $D(Q_1)$ would include all kinds of derivatives of the surface, but we shall assume from now that to the leading order $D(Q_1)$ only depends on the local properties of the obstacle through this combination. The decay exponent α which has the dimension 1/length we shall also assume depends only on k and on the local radius of curvature even though small correction terms might depend on other geometrical properties of the surface. Under these assumptions it should be possible to determine the leading terms in D_m and α_m from the field diffracted by any simple shape.

The geodesics on the surface of the circle are simply arcs of the circle implying that the ratio $d\sigma(Q_1)/d\sigma(t)$ is unity since the tube of rays cannot spread into the direction orthogonal to the plane. Further more because the wavefronts on the surface of the cylinder are simply points the radius of curvature ρ_1 is infinite so that $(\rho_1/(\rho_1+s))^{1/2}$ obtains its limitting value $s^{1/2}$ in the expression (6.12). Also, since the radius of curvature is constant, the diffraction coefficients and the decay exponent will be constants. Using (6.15) for the incident field and for the field leaving the disk and hitting the receiver we obtain by applying the above considerations

$$
\begin{aligned}
G_d(\vec{r},\vec{r}') &= (8\pi k)^{-1}[(r^2-a^2)(r'^2-a^2)]^{-1/4}\exp\{ik[(r'^2-a^2)^{1/2}+(r^2-a^2)^{1/2}] \\
&+ \frac{i\pi}{2}\}\sum_m D_m^2 e^{(ik-\alpha_m)t}
\end{aligned}
\tag{6.16}
$$

Equation (6.16) gives the value of the field at P associated with any ray from Q that creeps along the surface of the cylinder a distance t. As we see there are two families of rays. The first family follows the straight line QP_1 winds around the disc a number of times and then follows the straight line Q_1P. The second family follows the path $QP_2(windings)Q_2P$. For the first family t takes the values $t_n = t_0 + 2n\pi a$ where $t_0 = a(2\pi+\theta) - a\cos^{-1}(a/r) - a\cos^{-1}(a/r')$ and θ is the angle between the source and the observer. In case of the existence of more

than one obstacle of course one or both of the families might be nonexisting. Inserting these values of t_n, the expression (6.16) becomes a geometrical series and we obtain for the first family

$$
\begin{aligned}
G_d^{(1)}(r,\theta) &= (8\pi k)^{-1}(r^2-a^2)^{-1/4}(r'^2-a^2)^{-1/4} \\
&\times \exp\{ik([r'^2-a^2]^{1/2}+[r^2-a^2]^{1/2}+\frac{i\pi}{2}\} \\
&\times \sum_m D_m^2 e^{(ik-\alpha_m)t_0}[1-\exp\{2\pi(ika-a\alpha_m)\}]^{-1}.
\end{aligned}
\tag{6.17}
$$

For the second family everything is the same except that $(2\pi+\theta)$ is replaced by $2\pi-\theta$ and adding the contributions from both families we get

$$
\begin{aligned}
G_d(r,\theta) &= (8\pi k)^{-1}(r^2-a^2)^{-1/4}(r'^2-a^2)^{-1/4} \\
&\times \exp\{ik([r'^2-a^2]^{1/2}+[r^2-a^2]^{1/2}+\frac{i\pi}{2}\} \\
&\times \sum_m D_m^2 \frac{\exp\{(ika-a\alpha_m)(2\pi+\theta)\}+\exp\{(ika-a\alpha_m)(2\pi-\theta)\}}{1-\exp\{2\pi(ika-a\alpha_m)\}} \\
&\times \exp\{-(ika-a\alpha_m)[\cos^{-1}(a/r)+\cos^{-1}(a/r')]\}
\end{aligned}
\tag{6.18}
$$

Equation (6.18) is the final Keller expression for the field at P caused by the source at Q in the frame of the geometrical theory of diffraction. As we see the reciprocity condition (6.14) is automatically fulfilled as it should, and we note that the Greens function has the structure

$$
G_d = G_{free}G_{diff}G_{free}.
\tag{6.19}
$$

What is left to be done is to compare this expression to the expansion of the exact solution of the propagator of the problem for large ka to determine the coefficients D_m and α_m. An expression for such an expansion we shall obtain in the following section.

6.3 The exact 1-disk propagator

In the following derivations we shall mainly follow the work of Franz [28] and the excellent rewiev notes by A. Wirzba [63]. As above we assume that the disk is centered at the origin in the two-dimensional plane, and we introduce the usual polar coordinate system (r,θ). The stationary 1-disk problem therefore corresponds to the Helmholtz equation in 2 dimensions

$$
\left(\frac{\partial^2}{\partial r^2}+\frac{1}{r}\frac{\partial}{\partial r}+\frac{1}{r^2}\frac{\partial^2}{\partial\theta^2}+k^2\right)u(r,\theta) = 0
\tag{6.20}
$$

(with $k = \sqrt{2mE}/\hbar$). Since we are interested in scattering off a hard wall we impose the Dirichlet boundary condition $u(r,\theta)|_{r=a} = 0$. The free energy-domain Greens function of the problem is given by [28]

$$
G_0(k|\vec{r}'-\vec{r}|) = -\frac{i}{4}H_0^{(1)}(k|\vec{r}'-\vec{r}|)
\tag{6.21}
$$

$$= -\frac{i}{4} \sum_{m=-\infty}^{+\infty} e^{im\theta} H_m^{(1)}(kr') J_m(kr) \quad \text{for } r' > r, \qquad (6.22)$$

where θ is the angle between $\vec{r}'$ and $\vec{r}$.

As the 1-disk scattering problem is separable the full propagator can be simply constructed by splitting J_m in the free propagator expression in an incoming and outgoing Hankel function and imposing the boundary conditions

$$J_m(kr) = \frac{1}{2}(H_m^{(1)}(kr) + H_m^{(2)}(kr))$$

where the asymptotically outgoing Hankel function $H_m^{(1)}(kr)$ obtains a scattering phase from the boundary condition $G = 0$ on the surface

$$H_m^{(2)}(ka) + S_{mm}H_m^{(1)}(ka) = 0 \Rightarrow$$

$$S_{mm} = -\frac{H_m^{(2)}(ka)}{H_m^{(1)}(ka)} \quad \text{Dirichlet b.c.} \quad (6.23)$$

We can therefore write the 1-disk Greens function as

$$G(k\vec{r}', k\vec{r}) = -\frac{i}{8} \sum_{m=-\infty}^{+\infty} e^{im\theta} H_m^{(1)}(kr') \left(H_m^{(2)}(kr) + S_{mm}H_m^{(1)}(kr) \right) (6.24)$$

where the scattering matrix $S_{mm'} = \delta_{mm'} S_{mm}$ contains the boundary condition. As for $kr \gg 1$ the number of contributing terms in the sum in (6.24) becomes bigger and bigger the result is only useful for small values of kr. Our aim is to find a numerical useful result also for large values of kr. Such an expression can be obtained by following the work of Franz [28] and use the Watson resummation method [58] which leads to an asymptotic expansion of the field. The idea here is to write the sum (6.24) as a contour integral in the complex plane and obtain the individual terms as the residues of a suitable function. More explicitly we have

$$\sum_{m=-\infty}^{+\infty} f(m) = \oint_C d\nu \frac{f(\nu)}{e^{i2\pi\nu} - 1} = \oint_C d\nu \frac{e^{-i\pi\nu} f(\nu)}{2i \sin(\nu\pi)} , \qquad (6.25)$$

where the path C encircles counterclock-wise the real ν-axis. This resummation is valid in case $f(\nu)$ is holomorphic in the strip D which covers the real ν-axis, i.e. $\delta D = C$.

Using the Watson resummation the 1-disk propagator yields

$$G(k\vec{r}', \vec{r}) = -\frac{i}{8} \oint_C d\nu \frac{e^{i\nu(\theta-\pi)}}{2i \sin(\nu\pi)} H_\nu^{(1)}(kr') \left(H_\nu^{(2)}(kr) + S_{\nu,\nu} H_\nu^{(1)}(kr) \right)$$

$$(6.26)$$

The contour C can be transformed to a path above the real ν-axis

$$-\frac{i}{8} \oint_C d\nu \chi_\nu = -\frac{i}{8} \int_{+\infty+i\epsilon}^{-\infty+i\epsilon} d\nu \chi_\nu - \frac{i}{8} \int_{-\infty-i\epsilon}^{+\infty-i\epsilon} d\nu \chi_\nu$$

$$= +\frac{i}{8} \int_{-\infty+i\epsilon}^{+\infty+i\epsilon} d\nu \chi_\nu - \frac{i}{8} \int_{-\infty+i\epsilon}^{+\infty+i\epsilon} d\nu \chi_{-\nu} \qquad (6.27)$$

where the integration variable ν has been changed to $-\nu$ in the last term. Using the rules $H_{-\nu}^{(1)}(kr) = \exp(i\nu\pi)H_\nu^{(1)}(kr)$ and $H_{-\nu}^{(2)}(kr) = \exp(-i\nu\pi)H_\nu^{(2)}(kr)$ for the Hankel functions we find the following form of the one-disk Greens function

$$G(k\vec{r}', k\vec{r}) = -\frac{i}{8} \int_{-\infty+i\epsilon}^{+\infty+i\epsilon} d\nu \frac{\cos(\nu(\theta-\pi))}{2i\sin(\nu\pi)} H_\nu^{(1)}(kr') \left(H_\nu^{(2)}(kr) + S_{\nu\nu} H_\nu^{(1)}(kr) \right).$$

(6.28)

We now have the following three possible situations: (a) $\vec{r}$ lies in the "shadow region" of $\vec{r}'$ with respect to the disk; (b) $\vec{r}$ lies in the lit region, and (c) $\vec{r}$ lies on the boundary of the lit and the shadow region. We will exclude the latter case since in the two- and three-disk cases which we are mostly interested in there are no grazing contributions for the corresponding diffractional rays. This case has to be handled with different methods than the ones presented here. Further more the situation (a) is a special case of case (b) since they will both have diffractional terms whereas in case (b) there will also be a direct and a reflected ray. We shall therefore in the following deal only with case (b) i.e. the lit region. This case also corresponds to the semiclassical derivation above using the Keller construction. The creeping angles can be immediately obtained as

$$\alpha_n^{(-)} = 2\pi - \theta - \arccos\frac{a}{r'} - \arccos\frac{a}{r} + 2\pi n$$

(6.29)

$$\alpha_n^{(+)} = 2\pi + \theta - \arccos\frac{a}{r'} - \arccos\frac{a}{r} + 2\pi n$$

(6.30)

and are positive for any $n = 0, 1, 2, \ldots$. As in the Keller construction the index n parameterizes the fact that the creeping ray can wind around the disk n times before leaving it. The prefactor in (6.28) can be written as

$$\frac{\cos(\nu(\theta-\pi))}{i\sin(\nu\pi)} = -\frac{e^{i\nu(2\pi+\theta)}}{1-e^{i2\nu\pi}} - \frac{e^{i\nu(2\pi-\theta)}}{1-e^{i2\nu\pi}} - e^{i\nu\theta}.$$

(6.31)

Note that the last term does not contain any poles on the real axis any longer, as we shall see this term will contribute only to the direct and reflected ray contributions in the semiclassical approximation. We can therefore write

$$G(k\vec{r}, k\vec{r}') = G_{\text{geo}}(k\vec{r}, k\vec{r}') + G_{\text{creep}}(k\vec{r}, k\vec{r}')$$

(6.32)

with

$$G_{\text{geo}}(k\vec{r}, k\vec{r}') = -\frac{i}{8} \int_{-\infty+i\epsilon}^{+\infty+i\epsilon} d\nu\, e^{i\nu\theta} \left(H_\nu^{(1)}(kr')H_\nu^{(2)}(kr) - H_\nu^{(1)}(kr')\frac{H_\nu^{(2)}(ka)}{H_\nu^{(1)}(ka)}H_\nu^{(1)}(kr) \right)$$

(6.33)

$$G_{\text{creep}}(k\vec{r}, k\vec{r}') = -\frac{i}{8} \int_{-\infty+i\epsilon}^{+\infty+i\epsilon} d\nu\, \frac{e^{i\nu(2\pi+\theta)} + e^{i\nu(2\pi-\theta)}}{1-e^{i2\nu\pi}} H_\nu^{(1)}(kr')$$

$$\times \frac{H_\nu^{(2)}(kr)\, H_\nu^{(1)}(ka) - H_\nu^{(2)}(ka)H_\nu^{(1)}(kr)}{H_\nu^{(1)}(ka)},$$

(6.34)

where we have splitted up the Greens function in a pure geometrical term corresponding to the ordinary geometrical theory of diffraction and into a pure

diffractional or creeping term corresponding to the new introduced diffractional rays propagating on the surface of the obstacle. The semiclassical evaluation of these two contributions will be quite different. In the following we shall investigate the two cases in some detail.

6.3.1   The geometrical contribution

In this paragraph we shall account for the geometrical part of the semiclassical expression of the propagator. The expression for the geometrical part reads

$$G_{\text{geo}}(k\vec{r}, k\vec{r}') = -\frac{i}{8} \int_{-\infty+i\epsilon}^{+\infty+i\epsilon} d\nu \, e^{i\nu\theta} \left(H_\nu^{(1)}(kr') H_\nu^{(2)}(kr) - H_\nu^{(1)}(kr') \frac{H_\nu^{(2)}(ka)}{H_\nu^{(1)}(ka)} H_\nu^{(1)}(kr) \right)$$

As we see the expression does not contain the Watson denominator so we are free to deform the integration path across the real axis. However the integral cannot be substituted by a residua sum because there is no damping term ensuring that the integrant vanishes at infinity. Before evaluating the integral we note that we can split up the expression further into the first part which is independant of a and which therefore can only contain information about the direct geometrical contribution, and into the second term which then turns out to contain the reflection contribution. The semiclassical evaluation of the summands will now consist in first inserting the Debye approximation for the Hankel functions

$$H_\nu^{(1)}(kr) \sim \sqrt{\frac{2}{\pi \sqrt{(kr)^2 - \nu^2}}} \exp\left(i\sqrt{(kr)^2 - \nu^2} - i\nu \arccos \frac{\nu}{kr} - i\frac{\pi}{4} \right)$$

$$(6.35)$$

$$H_\nu^{(2)}(kr) \sim \sqrt{\frac{2}{\pi \sqrt{(kr)^2 - \nu^2}}} \exp\left(-i\sqrt{(kr)^2 + \nu^2} - i\nu \arccos \frac{\nu}{kr} + i\frac{\pi}{4} \right)$$

$$(6.36)$$

which is valid for $(kr)^2 > \nu^2 \gg 1$. Second we shall evaluate the resulting integrals via the saddlepoint approximation where the saddles are located on the real ν axis. The result of this procedure yields (see appendix 9.2 for details)

$$G_{\text{geo}}(k\vec{r}, k\vec{r}') \simeq -\frac{i}{4} \sqrt{\frac{2}{\pi}} \frac{e^{iL_{\text{direct1}} - i\pi/4}}{\sqrt{kL_{\text{direct1}}}} + \frac{i}{4} \sqrt{\frac{2}{\pi}} \frac{e^{ikL_{\text{refl}} - i\pi/4}}{\sqrt{kR_{\text{eff}}}}$$

$$(6.37)$$

where $L_{\text{direct1}} = \sqrt{(kr')^2 - \nu_{S1}^2} - \sqrt{(kr)^2 - \nu_{S1}^2} = |\vec{r}' - \vec{r}|$ is the geometrical distance between $\vec{r}'$ and $\vec{r}$, and where

$$L_{\text{refl}} = d' + d \tag{6.38}$$

$$R_{\text{eff}} = d' + d + \frac{2dd'}{\sqrt{a^2 - b^2}}$$

$$= d' + d + \frac{2dd'}{a \cos \varphi} \tag{6.39}$$

with

$$
\begin{aligned}
d' &\equiv \sqrt{r'^2 - b^2} - \sqrt{a^2 - b^2} \\
d &\equiv \sqrt{r^2 - b^2} - \sqrt{a^2 - b^2} \\
b &\equiv a|\sin\varphi| \ ,
\end{aligned}
$$

where φ is the angle of incidence measured with repect to the normal at the point of reflection. The parameter b thus becomes the usual impact parameter known from scattering theory.

Note that the result (9.61) is exactly what we get if we insert the semiclassical Debye approximation in the expression (6.21) for the free propagator, as it also should in the semiclassical limit $kr \gg 1$.

Modulo a sign change (which takes into account the Dirichlet boundary condition at the disk) the reflection contribution of the semiclassical propagator (9.63) has the same structure as the semiclassical direct piece (9.61), the only difference being that the length L_{direct1} is replaced by L_{refl} in the exponent and by R_{eff} in the denominator. The quantity L_{refl} is just the length of the reflected ray between $\vec{r}'$ and $\vec{r}$, whereas R_{eff} is the effective radius which determines the strength of a corresponding ray bundle. It takes into account that a ray bundle which starts at $\vec{r}'$ spreads not only according to the passed distance $L_{\text{refl.}}$, but gets a further spreading by the reflection on the concave surface of the disk. If we compare the effective radius to what we get when we use the formula for the development of the Sinai Bunimovich curvatures in a single bounce

$$
\begin{aligned}
\Lambda &= l_0 \prod_{i=1}^{n_{bounce}} (1 + l_i \kappa_i^+) \\
&= l_0 \left(1 + l_1 \left(\frac{1}{l_0} + \frac{2}{a\cos\varphi} \right) \right) \\
&= l_0 + l_1 + \frac{2 l_0 l_1}{a\cos\varphi} \\
&= R_{\text{eff}}
\end{aligned}
\tag{6.40}
$$

where κ_i^+ is the curvature right after the i'th bounce

$$
\kappa_i^+ = \kappa_i^- + \frac{2}{a\cos\varphi_i} \quad , \quad \kappa_i^- = \frac{\kappa_{i-1}^+}{l_i \kappa_{i-1}^+ + 1}.
\tag{6.41}
$$

The effective radius is then nothing else than the usual stabilities which we can obtain from the Jacobian of the flow 2.12.

6.3.2 The diffraction case

Let us now turn to the evaluation of the creeping terms (6.34). The creeping terms still contains the denominator $(1 - e^{i2\nu\pi})$ and the integration path can therefore not be deformed on the real axis. However, since the creeping angles are all positive they lead to an exponential damping $\exp(i\nu\alpha_n^\pm)$ in the semiclassical limit and the path can be deformed in the upper half plane and the

integral replaced by a convergent sum of the residua i.e. the zeros of the Hankel function $H_\nu^{(1)}(ka)$. The creeping parts of the 1-disk Greens function therefore becomes

$$G_{\text{creep}}(k\vec{r}, k\vec{r'}) = -\frac{1}{8i} \sum_{l=1}^{\infty} 2\pi i H_{\nu_l}^{(1)}(kr') \frac{e^{i\nu_l(2\pi+\theta)} + e^{i\nu_l(2\pi-\theta)}}{1 - e^{i\nu_l 2\pi}} \frac{H_{\nu_l}^{(2)}(ka)}{\frac{\partial}{\partial\nu} H_\nu^{(1)}(ka)|_{\nu=\nu_l}} H_{\nu_l}^{(1)}(kr)$$

$$(6.42)$$

where ν_l (with $l = 1, 2, 3, ...$) labels the zeros of the Hankel functions, $H_\nu^{(1)}(ka)$, in the upper complex ν-plane. Expression (6.42) is still exact. The semiclassical approximation is to evaluate the Hankel functions $H_\nu^{(1)}(ka)$ and $H_\nu^{(2)}(ka)$ under the Airy approximation (which is valid for $ka \gg 1$)

$$H_\nu^{(1)}(ka) \sim \frac{2}{\pi} e^{-i\frac{\pi}{3}} \left(\frac{6}{ka}\right)^{\frac{1}{3}} A(q^{(1)}) \qquad \text{and} \qquad H_\nu^{(2)}(ka) \sim \frac{2}{\pi} e^{+i\frac{\pi}{3}} \left(\frac{6}{ka}\right)^{\frac{1}{3}} A(q^{(2)})$$

with (see ref.[28])

$$q^{(1)} \equiv e^{-i\frac{\pi}{3}} \left(\frac{6}{ka}\right)^{\frac{1}{3}} (\nu - ka) \qquad \text{and} \qquad q^{(2)} \equiv e^{+i\frac{\pi}{3}} \left(\frac{6}{ka}\right)^{\frac{1}{3}} (\nu - ka).$$

Thus

$$\nu_l \quad \sim \quad ka + q_l \left(\frac{1}{6}ka\right)^{\frac{1}{3}} e^{i\frac{\pi}{3}} := ka(1 + i\alpha_l/k) \tag{6.43}$$

and

$$\nu_l \quad \simeq \quad ka \quad \text{for } ka \gg 1 \tag{6.44}$$

where the q_ℓ's are the zeros of the Airy integral $A(q) = \int_0^\infty dt \cos(qt - t^3)$, approximately given by $q_l \approx \frac{1}{2}(6)^{\frac{1}{3}}(3\pi\{l-\frac{1}{4}\})^{\frac{2}{3}}$. The coefficients α_l are damping coefficients introduced in the Keller derivation above (6.5)

$$\alpha_l = q_l e^{-i\pi/6} \left(\frac{k}{6a^2}\right)^{\frac{1}{3}}, \qquad l = 1, 2, 3, \ldots. \tag{6.45}$$

This approximation is justified since there are two competing saddles in the integral representation of $H_\nu^{(1)}(ka)$ in the case $H_\nu^{(1)}(ka) = 0$ which is the condition for the poles. After inserting the Airy approximations into (6.42) and using

$$A(q_l^{(2)}) = \frac{\pi}{6} \frac{e^{-i\pi/6}}{A'(q_l^{(1)})} \tag{6.46}$$

which follows from the Wronskian of Airy integrals[1],

$$A(z)A'(ze^{\pm i2\pi/3}) - A'(z)A(ze^{\pm i2\pi/3}) = -\frac{\pi}{6}e^{\mp i\pi/6} , \tag{6.47}$$

the energy-domain creeping propagator becomes

$$G_{\text{creep}}(k\vec{r}, k\vec{r'}) \sim \sum_{l=1}^{\infty} \frac{1}{4i} H_{\nu_l}^{(1)}(kr') D_l \frac{e^{i\nu_l(2\pi+\theta)} + e^{i\nu_l(2\pi-\theta)}}{1 - e^{i\nu_l 2\pi}} D_l \frac{1}{4i} H_{\nu_l}^{(1)}(kr) ,$$

$$(6.48)$$

with

$$D_l = 2^{\frac{1}{3}} 3^{-\frac{2}{3}} \pi e^{i5\pi/12} \frac{(ka)^{\frac{1}{6}}}{A'(q_l^{(1)})} \; . \tag{6.49}$$

Finally we replace the remaining Hankel functions, $H_{\nu_l}^{(1)}(kr')$ and $H_{\nu_l}^{(1)}(kr)$, by their Debye approximation (6.35), a step which is justified, since we work under the condition that $|\vec{r}'| > |\vec{r}| \gg a \approx |\nu_l/k|$. The Debye approximation for the Hankel functions reads

$$H_{\nu_l}^{(1)}(kr) \sim \left(\frac{2}{\pi\sqrt{(kr)^2 - \nu_l^2}} \right)^{\frac{1}{2}} e^{i\sqrt{(kr)^2 - \nu_l^2} - i\nu_l \arccos(\nu_l/kr) - i\pi/4} \; . \tag{6.50}$$

We would of course like if we could substitute the disk radius a for the ratio ν_l/k since we would then obtain the creeping ray interpretation of *all* the l-mode contributions. In order to check if this is a valid approximation we write the zeros of the Hankel functions in the Airy approximation as

$$\nu_l = ka(1 + i\alpha_l/k) := ka + \delta\nu_l = ka \left(1 + \mathcal{O}(\hbar^{\frac{2}{3}}) \right) \tag{6.51}$$

Inserting this into the Debye approximation and expanding to the second order in $\delta\nu_l$ we obtain

$$\begin{aligned}
\sqrt{k^2 r^2 - \nu_l^2} - \nu_l \arccos(\nu_l/kr) &= k\sqrt{r^2 - a^2} - ka \arccos(a/r) - \delta\nu_l \arccos(a/r) \\
&\quad + \frac{1}{2} \frac{(\delta\nu_l)^2}{k\sqrt{r^2 - a^2}} + \mathcal{O}(\delta\nu_l^3) \\
&= k\sqrt{r^2 - a^2} - \nu_l \arccos(a/r) + \frac{1}{2} \frac{(\delta\nu_l)^2}{k\sqrt{r^2 - a^2}} + \mathcal{O}(\delta\nu_l^3) \\
&= k\sqrt{r^2 - a^2} - \nu_l \arccos(a/r) + \mathcal{O}(\hbar^{\frac{1}{3}}) \\
&= \frac{1}{\hbar} \left(p\sqrt{r^2 - a^2} - \hbar\nu_l \arccos(a/r) + \mathcal{O}(\hbar^{\frac{4}{3}}) \right) \tag{6.52}
\end{aligned}$$

for the exponent, where we have used the relation $p = \hbar k$. In this calculation the linear terms arising from the square root and from the arc cosine cancels exactly allowing us to obtain the creeping interpretation of the geometrical contents of the expression. For the prefactor a similar calculation gives

$$\begin{aligned}
\frac{1}{(k^2 r^2 - \nu_l^2)^{\frac{1}{4}}} &= \frac{1}{(k\sqrt{r^2 - a^2})^{\frac{1}{2}}} + \frac{1}{2} \frac{ka\delta\nu_l}{(k\sqrt{r^2 - a^2})^{\frac{5}{2}}} + \mathcal{O}\left(\frac{(\delta\nu_l)^2}{(k\sqrt{r^2 - a^2})^{\frac{5}{2}}} \right) \\
&= \frac{1}{(k\sqrt{r^2 - a^2})^{\frac{1}{2}}} \left(1 + \frac{1}{2} \frac{ka\, \delta\nu_l}{(k^2(r^2 - a^2))} + \mathcal{O}(\hbar^{\frac{4}{3}}) \right) \\
&= \frac{1}{(k\sqrt{r^2 - a^2})^{\frac{1}{2}}} \left(1 + \mathcal{O}(\hbar^{\frac{2}{3}}) \right) \tag{6.53}
\end{aligned}$$

Note, it is not justified to throw away the $\delta\nu_l \arccos(a/r)$ term in the exponent, since this term scales as $\mathcal{O}(\hbar^{-\frac{1}{3}})$. The $\mathcal{O}(\hbar^{\frac{2}{3}})$ correction of the prefactor can

however be safely neglected, since it is a $\mathcal{O}(\hbar)$ correction to the above mentioned term in the exponent.

Inserting these expansions into (6.48) we get modulo $\mathcal{O}(\hbar^{\frac{2}{3}})$ corrections in the semiclassical limit

$$
\begin{aligned}
G_{\text{creep}}(k\vec{r}, k\vec{r}') \quad \sim \quad & \frac{1}{4i}\left(\frac{2}{\pi k\sqrt{r'^2 - a^2}}\right)^{\frac{1}{2}} e^{ik\sqrt{r'^2 - a^2} - i\pi/4} \\
& \times \sum_{l=1}^{\infty} D_l \frac{e^{i\nu_l\{2\pi + \theta - \arccos(a/r') - \arccos(a/r)\}} + e^{i\nu_l\{2\pi - \theta - \arccos(a/r') - \arccos(a/r)\}}}{1 - e^{i\nu_l 2\pi}} D_l \\
& \times \frac{1}{4i}\left(\frac{2}{\pi k\sqrt{r^2 - a^2}}\right)^{\frac{1}{2}} e^{ik\sqrt{r^2 - a^2} - i\pi/4}
\end{aligned}
$$

(6.54)

Comparing this expression to (6.18) we see that they coincide and thus that the diffraction coefficients D_l in (6.54) are to be identified with the original introduced diffraction coefficients D_m in (6.4). By using the Airy approximation of the ν_l's (6.43) we also note that the phase factors $e^{i\nu_l\theta_{diff}}$ contains a damping term of the form $\exp(-\theta_{diff}q_l(\frac{1}{6}ka)^{1/3}\sin(\pi/3))$, even when k is real. This is the damping exponential of the creeping path. This concludes our semiclassical evaluation of the 1-disk Greens function.

It should at this point be noted that the derivation above is not valid for rays that are almost grazing (tangent) or for rays that are scattered in a very forward direction. This is due to that in the illuminated region the Debye approximation fails if $(ka - l_r) \le (ka)^{1/3}$, where l_r is the angular momentum of the reflected ray. In the shadow region the residuum resumation fails if the creeping angle becomes very small i.e. of order $\alpha \le (ka)^{1/3}$. The region in between the illuminated and the shadow region is called the *penumbra* and if one wants to evaluate the Greens function here one should consider the *penumbra corrections* as introduced by Smilansky et. al [43] and which are different from the creeping contributions discussed above. In the examples we are going to study which are basically the three-disk scattering system, the periodic orbits are composed by segments that are either purely geometric or purely creeping since the ray wind around the disk by at least $\pi/3$. We shall therefore not consider these contributions further.

6.3.3   Fields diffracted by edges

As a further development of the geometrical theory of diffraction in two dimensions we here consider the field diffracted by the sharp edge or vertex of two semi infinite straight lines meeting with an angle $(2 - n)\pi$, where $0 \le n \le 2$ is a real number [54, 39]. We proceed in quite the same fashion as in the case of diffraction by a smooth object and start by introducing the usual polar coordinate system (ρ, θ) with the vertex of the wedge centered at the origin of the coordinate system. We let α and θ be the angles of the incident and diffracted

rays measured with respect to the direction normal to the wedge on the side
where the rays come from (see figure 6.5).
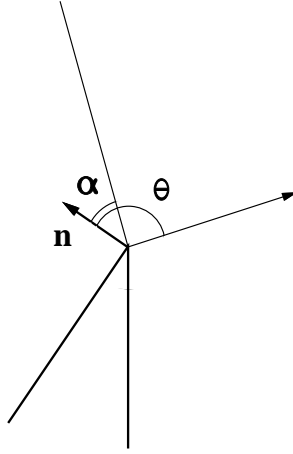
Figure 6.5: The geometry of the incident and diffracted rays, and the wedge.

First of all the free propagation is still done by the usual geometrical optics
so that the field is described by rays that are straight lines (in a homogeneous
medium) and the field at distance R from a source of unit strength is given
by (6.15). To find the amplitude $A(r)$ we consider the tube enclosed by two
neighbouring rays. The cross-sectional area of this tube is proportional to r and
the flux through it is proportional to rA^2. As a consequence of flux conservation
we therefore find that $A(r)$ must be proportional to $r^{-1/2}$. As in the case of
diffraction by a smooth object we also assume that the diffracted amplitude is
proportional to the incident amplitude and we can therefore write

$$u_d = Du_i r^{-1/2} e^{ikr} \qquad (6.55)$$

where u_i denotes the incident field, and D is the diffraction constant. As in
the case of the 1-disk system we can, because of the simple structure of the
problem, obtain an exact solution for the Greens function also in this case.
This is done in detail in ref.[67, 68]. Here we merely state the result of this
asymptotic expansion which reads

$$u_d \simeq \frac{e^{ikr}}{\sqrt{kr}}$$
$$\times \frac{\sin(\pi/n)}{n}[(\cos(\pi/n) - \cos((\theta - \alpha)/n)^{-1} - (\cos(\pi/n) - \cos((\theta + \alpha + \pi)/n)^{-1}]$$

Comparison to equation (6.55) now yields

$$D = \frac{\sin(\pi/n)}{n}[(\cos(\pi/n) - \cos((\theta - \alpha)/n)^{-1} - (\cos(\pi/n) - \cos((\theta + \alpha + \pi)/n)^{-1}]$$

which is the expression for the diffraction constant in case of edge diffraction.

6.4   The general Keller propagator

We next adress the problem of getting the complete Greens function in the general case. Here there might be many different obstacles and therefore many different trajectories leading from the source to the receiver. For each such ray ξ the contribution to the Green's function is the product of the Green's functions and diffraction coefficients along the ray:

$$
\begin{aligned}
G_\xi(q_\mathcal{A}, q_\mathcal{B}, E) \quad = \quad & \prod_{i=1}^{n_\xi} G_i(q_\mathcal{A}, q_{\mathcal{A}'}, E) \sum_{l=1}^{\infty} D_{l,\mathcal{A}'} G_l^D(q_{\mathcal{A}'}, q_{\mathcal{B}'}, E) \\
& \times D_{l,\mathcal{B}'} G(q_{\mathcal{B}'}, q_\mathcal{B}, E).
\end{aligned}
\tag{6.56}
$$

where n_ξ is the number of segments of the path and the Greens functions are either the Van Vleck, the creeping or the edge diffraction propagators. To get the complete Greens function $G(q, q', E)$ of the system we should then finaly sum up the contributions of the form (6.56) for *all* the paths that connects q with q' at energy E

$$
G(q, q', E) \quad = \quad \sum_{\xi:q \to q'} G_\xi(q, q')
\tag{6.57}
$$

where ξ labels the paths connecting q with q' at energy E.

6.4.1   Connection to the trace formula

To incorporate diffraction effects into the trace formula, one should compute the trace of the Green's function derived above. As in the case of the Gutzwiller trace formula – derived from a pure geometrical approximation of the Green's function – the trace receives the leading contributions from tubes encircling the closed curves, which now can have diffractional arcs too. In the case of ordinary geometrical orbits the trace can be evaluated in terms of a saddlepoint approximation which transforms the integral to a sum over paths that are not just closed but are in fact periodic. This is due to the fact that the saddle point condition is equivalent to identifying initial and final momentum. In the case of creeping orbits, the situation is not that straightforward since we are dealing with hard wall potentials that does not allow for variation of the path on the inside of the boundary of the obstacle. This means that we can only approach the saddle point from one side which inhibits the usual saddle point approximation. At this point it is therefore not clear how to proceed with the usual scheme to obtain the trace. Since the aim of all our efforts is not directly to get the trace but to obtain a quantization condition i.e. a condition for a complex k value to be a resonance of the system we shall here take another approach to this problem than the usual direct trace integration. We simply determine the exact quantum mechanical resonance condition for a simple example (the two-disk scattering system) and then make the usual cycle expansion ansatz for the spectral determinant related to the scattering problem. By comparison of the exact resonance condition and the cycle expansion we then can obtain a

rule relating the ingredients of the semiclassical propagator including diffraction terms to the weigths of the periodic orbits used in the cycle expansion. That this procedure is valid and really gives an approximation to the exact quantum mechanical resonances, were recently shown by A. Wirzba and M. Henseler [66]. In a remarkable work they investigate the two-dimensional scattering of a point particle from n non-overlapping fixed disks and study the connection between the spectral properties of the quantum mechanical scattering matrix and its semi-classical equivalent based on the Gutzwiller-Voros zeta function. They rewrite the determinant of the scattering matrix in such a way that it separates into a product over n determinants of 1-disk scattering matrices (representing the incoherent part of the scattering from the n-disk system) and the ratio of two mutually complex conjugate determinants of the genuinely multi-disk scattering kernel $\mathbf{M}$, which represents the coherent part of the scattering

$$\det \mathbf{S}^{(n)}(k) = \left\{ \prod_{j=1}^{n} \det \mathbf{S}^{(1)}(ka_j) \right\} \frac{\det \mathbf{M}(k^*)^{\dagger}}{\det \mathbf{M}(k)} \qquad (6.58)$$

where a_j are the radii of the n disks. Further more they show that in the semiclassical limit, the $\mathbf{M}$ determinants will approach the Gutzwiller-Voros spectral determinants *with the inclusion of diffractional periodic orbits*. In the following we shall sketch how this relation can be obtained just for the $\mathbf{M}$ determinant which is sufficient to obtain the scattering resonances i.e. the poles of the scattering matrix $\mathbf{S}$.

6.4.2 The exact poles of the scattering matrix

As a specific example we choose the two disk scattering system which has only a single geometric periodic orbit. We shall here mainly follow A. Wirzba [60, 61] and Gaspard and Rice [32]. In [32] it was found that the Scattering matrix $\mathbf{S}$ had the following structure

$$\mathbf{S} = \mathbf{1} - i\mathbf{C}\mathbf{M}^{-1}\mathbf{D} \qquad (6.59)$$

The exact quantum mechanical resonances are found as the pole of the scattering matrix which then becomes the wave numbers where the characteristic determinant $\det \mathbf{M}(k)$ vanishes

$$\det \mathbf{M}(k) = 0. \qquad (6.60)$$

The matrix $\mathbf{M}$ can be constructed according to the methods in ref.[32], and for the A_1 symmetry (which corresponds to regarding the fundamental domaine as the system in it self) it has the following structure

$$\mathbf{M} = \mathbf{1} + \mathbf{A}$$
$$\mathbf{A}_{mm'} = \frac{1}{2} \frac{J_m(ka)}{H_{m'}^{(1)}(ka)} \left((-1)^{m'} H_{m-m'}^{(1)}(kR) + H_{m+m'}^{(1)}(kr) \right). \qquad (6.61)$$

Here R is the seperation of the centers of the two disks wheras a is the radius of the disks. Since $\mathbf{M}(k)$ has the structure $\mathbf{M}(k) = \mathbf{1} + \mathbf{A}(k)$, it is natural to

expand the determinant in the characteristic equation (6.60) as

$$
\begin{aligned}
\det \mathbf{M} &= \exp(\operatorname{Tr}\ln(\mathbf{1} + \mathbf{A})) \\
&= 1 + \operatorname{Tr}\mathbf{A} - \frac{1}{2}[\operatorname{Tr}\mathbf{A}^2 - (\operatorname{Tr}\mathbf{A})^2] + \dots
\end{aligned}
\tag{6.62}
$$

This procedure is mathematically valid since the matrix $\mathbf{A}$ is *trace class* [66]. We now make the ansatz that (6.62) should be semiclassicaly represented by some Gutzwiller-Voros like spectral determinant

$$
\tilde{Z}(z,k) = \prod_p \prod_{l=0}^{\infty} (1 - t_{p_l}(k)z^{n_p})
\tag{6.63}
$$

where the prime periodic orbits should now allow also for diffractive periodic orbits. In (6.63) z is as usual just a book keeping parameter keeping track of the topological order n_p of the cycles. In the end after expanding the determinant in powers of z it will finally be put equal to 1. To get the ansatz into a shape where it is comparable to (6.62) we rewrite it as

$$
\begin{aligned}
\tilde{Z}(z,k) &= \exp\left(\sum_p \sum_{l=0}^{\infty} \ln(1 - t_{p_l}(k)z^{n_p}) \right) \\
&= \exp\left(-\sum_p \sum_{l=0}^{\infty} \sum_{m=1}^{\infty} \frac{(t_{p_l}(k)z^{n_p})^m}{m} \right) \\
&\equiv \exp(-\sum_{n=1}^{\infty} \operatorname{Tr}_n z^n)
\end{aligned}
\tag{6.64}
$$

where we have gathered all terms of power z^n in the terms Tr_n. Expanding the exponential this finally yields

$$
\tilde{Z}(z,k) = 1 - \operatorname{Tr}_1 z - \frac{1}{2}(\operatorname{Tr}_2 - \operatorname{Tr}_1^2)z^2 + \dots
\tag{6.65}
$$

As we see this has exactly the same structure as (6.62) due to the expansion of an exp(log) in both cases. It is therefore natural to make the transition from exact quantum mechanics to semiclassics at this point since this yields a shortcut compared to the trace evaluation of the creeping Greens function.

To proceed we then have to first get $\mathbf{A}$ and evaluate its trace and then compare this to our semiclassical ingredients from the geometrical and creeping propagators.

For the A_1 subspace the matrix $\mathbf{A}$ is [60]

$$
\mathbf{A}_{m,m'} = \frac{1}{2} \frac{J_m(ka)}{H_{m'}^{(1)}(ka)} \left((-1)^{m'} H_{m-m'}^{(1)}(kR) + H_{m+m'}^{(1)}(kR) \right)
\tag{6.66}
$$

which gives the trace

$$
\operatorname{Tr}\mathbf{A} = \frac{1}{2} \sum_{m=-\infty}^{+\infty} \frac{J_m(ka)}{H_m^{(1)}(ka)} \left((-1)^{m'} H_0^{(1)}(kR) + H_{2m}^{(1)}(kR) \right).
\tag{6.67}
$$

Using the Watson transformation (6.25) we can transform the sum to a complex contour integral

$$\mathrm{Tr}\mathbf{A} = \frac{1}{4i}\oint_C d\nu \frac{1}{\sin(\pi\nu)}\frac{J_\nu(ka)}{H_\nu^{(1)}(ka)}\left(H_0^{(1)}(kR) + \exp(-i\nu\pi)H_{-2\nu}^{(1)}(kR)\right),$$

where we used $H_{-2m}^{(1)}(kr) = H_{2m}^{(1)}(kr)$. As in the case of the one disk propagator we can transform the contour path C to run in the upper half plane by substituting $-\nu$ for ν in the second part of the contour integral

$$\frac{1}{4i}\oint_C d\nu\ldots = \frac{1}{4i}\int_{+\infty+i\epsilon}^{-\infty+i\epsilon} d\nu\ldots\frac{1}{4i}\int_{-\infty-i\epsilon}^{+\infty-i\epsilon} d\nu\ldots. \tag{6.68}$$

After some rewriting where we use for instance [1]

$$H_{-\nu}^{(1)}(kr) = \exp(i\nu\pi)H_\nu^{(1)}(kr)$$

and

$$J_{-\nu}(kr) = \frac{1}{2}\left(\exp(i\nu\pi)H_\nu^{(1)}(kr) + \exp(-i\nu\pi)H_\nu^{(1)}(kr)\right) \tag{6.69}$$

the trace reads

$$\mathrm{Tr}\mathbf{A} = \frac{1}{4}\int_{-\infty+i\epsilon}^{+\infty+i\epsilon} d\nu \frac{H_\nu^{(2)}(ka)}{H_\nu^{(1)}(ka)}\left(\exp(-i\nu\pi)H_0^{(1)}(kR) + \exp(-2i\nu\pi)H_{-2\nu}^{(1)}(kR)\right)$$

$$-\frac{1}{2i}\int_{-\infty+i\epsilon}^{+\infty+i\epsilon} d\nu \frac{H_\nu^{(2)}(ka)}{H_\nu^{(1)}(ka)}\left(\frac{1}{\sin(\nu\pi)}H_0^{(1)}(kR) + \frac{\exp(-i\nu\pi)}{\sin(\nu\pi)}H_{-2\nu}^{(1)}(kR)\right)$$

As in the case of the 1-disk propagator we can here split the trace into a geometrical and a creeping contribution, where the latter is the one that still contains the Watson denominator $\sin(\nu\pi)$. Under the semiclassical assumption that $ka >> 1$ we can therefore evaluate the integral by using the same procedure as in the case of the 1-disk Greens function. The geometrical part of the trace yields [61]

$$\mathrm{Tr}\mathbf{A}_{geo} \simeq \frac{1}{2}\sqrt{\frac{a}{2R}}\left(1 + \frac{1}{\sqrt{1-2a/R}}\right)\exp(ik(R-2a)) \tag{6.70}$$

Truncating the cumulant expansion (6.62) to the first order in $\mathbf{A}$ we therefore get the condition for resonances using only geometrical input

$$1 - \frac{1}{2}\sqrt{\frac{a}{2R}}\left(1 + \frac{1}{\sqrt{1-2a/R}}\right)\exp(ik(R-2a)) = 0 \tag{6.71}$$

This should be compared to the first order truncation of the cycle expansion of the semiclassical expression for the spectral determinant i.e. the Gutzwiller-Voros determinant

$$\Delta_G(k) = \prod_{l=0}^\infty\left(1 - \frac{e^{ikT_0}z}{\Lambda_0^{(1+4l)/2}}\right)$$

$$\simeq 1 - \frac{e^{ikT_0}}{\sqrt{\Lambda_0}(1-\Lambda_0^{-2})} \tag{6.72}$$

where the fact that the stability is squared comes from the symmetry reduction since we are dealing with a boundary orbit. From the analytic expression for Λ_0

$$\Lambda_0 \quad = \quad \frac{R - a + \sqrt{R^2 - 2Ra}}{a} \tag{6.73}$$

it can indeed be shown that (see appendix 9.2):

$$\frac{1}{2}\sqrt{\frac{a}{2R}}\left(1 + \frac{1}{\sqrt{1 - 2a/R}}\right) \quad = \quad \frac{1}{\sqrt{\Lambda_0}(1 - \Lambda_0^{-2})} \tag{6.74}$$

so that the stability factor as well as the phase of the semiclassical expansion of the geometrical part are in comlete agreement with the ordinary semiclassical Gutzwiller-Voros expression of the spectral determinant.

The semiclassical evaluation of the creeping part of Tr$\mathbf{A}$ takes place in exactly the same fashion as in the 1-disk propagator. There are two fundamental creeping paths corresponding to the two kR-dependant Hankel functions $H_0^{(1)}(kR)$ and $H_{-2\nu}^{(1)}(kR)$. Following [60, 28] we can therefore immediately write down the contributions

$$\begin{aligned}
\text{Tr}\mathbf{A}_{creepa} &\simeq -\sqrt{\frac{a}{2R}}\frac{\exp(i\pi/12)}{(ka)^{1/6}}\exp(ikR)\sum_{l=1}^{\infty}C_l\frac{\exp(i\nu_l\pi)}{1 - \exp(2i\nu_l\pi)} \\
&= \frac{1}{4i}\sqrt{\frac{2}{\pi kR}}e^{ikR - i\pi/4}\sum_{l=1}^{\infty}D_l^2\frac{e^{i\nu_l\pi}}{1 - \exp(i\nu_l 2\pi)}
\end{aligned} \tag{6.75}$$

where we used the expression (6.49) for D_l in order to make the expression resemble the creeping propagator (6.54), and where

$$C_l \quad = \quad \frac{1}{3}\frac{\pi^{3/2}}{6^{1/3}}\frac{1}{A'(q_l)^2} \tag{6.76}$$

whith $A'(q_l)$ denoting the derivative of the Airy integral at q_l. In the expression (6.75) we recognize the exact form of the creeping propagator for the '0' shaped orbit in the fundamental domain.

The b trace yields similarly

$$\begin{aligned}
\text{Tr}\mathbf{A}_{creepb} &\simeq -\sqrt{\frac{a}{2R}}\frac{\exp(i\pi/12)}{(ka)^{1/6}}\sum_{l=1}^{\infty}C_l\left(\frac{k^2R^2}{k^2R^2 - 4\nu_l^2}\right)^{1/4} \\
&\times \exp\left(i\sqrt{k^2R^2 - 4\nu_l^2}\frac{\exp[i\nu_l(\pi + 2\arcsin(2\nu_l/kR))]}{1 - \exp(2i\nu_l\pi)}\right) \\
&= \frac{1}{4i}\sum_{l=1}^{\infty}\left(\frac{2}{\pi k\sqrt{R^2 - 4\nu_l^2}}\right)^{1/2}e^{ik\sqrt{R^2 - 4\nu_l^2} - i\pi/4}D_l^2\frac{e^{i\nu_l(2\pi - 2\cos^{-1}(2\nu_l/kR))}}{1 - e^{i\nu_l 2\pi}} \\
&\simeq \frac{1}{4i}\left(\frac{2}{\pi k\sqrt{R^2 - 4a^2}}\right)^{1/2}e^{ik\sqrt{R^2 - 4a^2} - i\pi/4}\sum_{l=1}^{\infty}D_l^2\frac{e^{i\nu_l(2\pi - 2\cos^{-1}(2a/R))}}{1 - e^{i\nu_l 2\pi}}
\end{aligned}$$

where we used the approximation

$$\nu_l \quad \simeq \quad ka \tag{6.77}$$

which is valid for large values of ka. In both cases the sum runs over the zeros ν_l of the Hankel function $H_\nu^{(1)}(ka)$ in the upper half plane. In the last expression we recognize the contribution to the Greens function from the periodic ∞ shaped orbit in the fundamental domaine.

By comparison to the cumulant expansion it then becomes clear how to get the resonance condition at least to the first order: to get the trace of $\mathbf{A}$, we simply take the contributions to the Greens function from all the periodic orbits of topological length 1 including the *diffractive* orbits. For the higher orders in z terms like $(\mathrm{Tr}\mathbf{A})^2$ gives combinations of shorter orbits whereas $\mathrm{Tr}\mathbf{A}^n$ terms will contain higher order periodic creeping orbits. That this is so for the two disk system is quite obvious because of the simple geometry. For a general N-disk system the proof is not quite that simple but for low orders in z it can be checked by direct computation of the traces. In the three disk system the relation between low order periodic creeping orbits and the trace of $\mathbf{A}$ has been performed by A. Wirzba [60, 61].

Even though it is not necessary for finding the resonances we can now also get the semiclassical approximation of the trace by using the relation

$$\mathrm{Tr}G(E) \quad = \quad \frac{d}{dE}\ln\Delta(E) \tag{6.78}$$

Here the diffraction as well as the creeping segments will give extra contributions compared to the usual geometrical time contribution, but since these contributions are of the order $(ka)^{-2/3}$ we can neglect these since we have already done this in our approximation of ν_l. The diffraction contribution to the trace therefore reads in this approximation

$$\mathrm{Tr}G_D(E) \quad = \quad \sum_{cycles} \frac{T(E)}{i\hbar} \prod_{i=1}^n D(q_i)G(q_i, q_{i+1}, E) \tag{6.79}$$

where $T(E)$ is the time period of the cycle (without repeats) and $G(q_i, q_{i+1}, E)$ is alternatingly the free propagator and the creeping propagator.

6.4.3 Cycle expansion of the diffraction spectral determinant

To apply the diffraction spectral determinant we here discuss how to use the well known cycle expansion [18] to calculate this. Using the ansatz (6.63) the total spectral determinant can be written

$$\Delta(k) \quad = \quad \Delta_G(k)\Delta_D(k) \tag{6.80}$$

where we have split the formal product into the usual Gutzwiller Voros spectral determinant representing the purely geometrical input and the diffractive

spectral determinant representing the new information obtained from the geo-
metrical theory of diffraction. The product is only formal, since the eigenener-
gies are not given by the zeros of $\Delta_G(E)$ or $\Delta_D(E)$ individually, but have to
be calculated from a curvature expansion of the *combined* determinant $\Delta(E)$
itself.

The diffraction part of the spectral determinant is

$$\Delta_D(E) = \exp\left(-\sum_{p,r=1}^{\infty} \frac{1}{r} \prod_{i=1}^{n_p} [D(q_i^p)G(q_i^p, q_{i+1}^p, E)]^r \right), \tag{6.81}$$

where the summation goes over closed primitive (non-repeating) cycles p and
the repetition number r. The product of Green's functions should be evaluated
for q_i^p belonging to the primitive cycle p. After summation over r, the spectral
determinant can be written as

$$\Delta_D(E) = \prod_p (1 - t_p) \tag{6.82}$$

with

$$t_p = \prod_{i=1}^{n_p} D(q_i^p)G(q_i^p, q_{i+1}^p, E), \tag{6.83}$$

where q_i^p belongs to the primitive cycle p. Here the mode numbers l of the
diffraction constants and the corresponding summations have been surpressed
for notational simplicity; they can be easily restored as e.g. in the final expres-
sion (6.92).

We can conclude that the diffractional part $\Delta_D(E)$ of the spectral determi-
nant shares some nice features of the periodic orbit expansion of the dynamical
zeta functions[18], and it can be expanded as

$$\Delta_D(E) = 1 - \sum_p t_p + \sum_{p,p'} t_p t_{p'} - \cdots. \tag{6.84}$$

Now if we restrict ourselves to include only the $l = 1$ mode then the weight
(6.83) has the following property which helps in radically reducing the number
of relevant contributions in the expansion: If two different cycles p and p' have
at least one common piece in their diffraction arcs, then the two cycles can be
composed to one longer cycle $p+p'$ and the weight corresponding to this longer
cycle is the product of the weights of the short cycles

$$t_{p+p'} = t_p \cdot t_{p'}. \tag{6.85}$$

As a consequence, the product of primitive cycles, which have at least one common piece in their diffraction arcs, can be reduced in such a way that the composite cycles are exactly canceled in the curvature expansion

$$\prod_p (1 - t_p) = 1 - \sum_b t_b, \tag{6.86}$$

where t_b are *basic* primitive orbits which can not be composed from shorter primitive orbits. To see that this nice composition rule does not hold if we include the higher l modes as well, we can consider the two shortest pure creeping orbits and their composition in the two-disk system. These two orbits are then the 0- and the ∞ shaped orbits. If we consider the two orbits in the fundamental domain, they will have the following schematic form

$$
\begin{aligned}
t_0 &= \frac{e^{ikR}}{\sqrt{R}} \sum_l C_l e^{i\nu_l \pi} \\
t_\infty &= \frac{e^{ik\sqrt{R^2-4a^2}}}{\sqrt{(R^2-4a^2)^{1/2}}} \sum_l C_l e^{i\nu_l \pi + i\nu_l 2\theta}
\end{aligned}
\tag{6.87}
$$

where θ is the little extra angle the ray has to creep in the case of the ∞ shaped orbit as compared to the 0 shaped orbit. The above weights are only given modulus an for this purpose unimportant overall factor. The composition of the two orbits can be constructed by first following the 0- and then the ∞ shaped orbit. The weight for the composed orbit therefore reads

$$
\begin{aligned}
t_{0\infty} &= \frac{e^{ikR}}{\sqrt{R}} \sum_l C_l e^{i\nu_l \pi + i\nu_l \theta} \frac{e^{ik\sqrt{R^2-4a^2}}}{\sqrt{(R^2-4a^2)^{1/2}}} \sum_{l'} C'_l e^{i\nu'_l \pi + i\nu'_l \theta} \\
&= const \times \sum_{ll'} C_l C_{l'} e^{i(\nu_l+\nu_{l'})\pi + i(\nu_l+\nu_{l'})\theta}
\end{aligned}
\tag{6.88}
$$

If the composition rule were to hold when including all the l modes we would expect that the expression (6.88) should be the product of the two individual terms in (6.87). By taking the product

$$t_0 t_\infty = const \times \sum_{ll'} e^{i(\nu_l+\nu_{l'})\pi + i2\nu_{l'}\theta} \tag{6.89}$$

we see that this is not the case in general. This is due to that in the composed orbit the overlapping creeping segments are not identical to any of the original creeping segments, since the orbit shifts from "0"-creeping to "∞"-creeping each time the ray creeps around the disk. Of course the composition rule would still hold if the creeping segments were identically the same, as it is the case for repetitions of a creeping orbit: $t_{2a} = t_a^2$.

6.5 Numerical results

In this section we try to demonstrate the significance of the diffraction corrections to the trace formula. As working examples we have chosen our usual

favorite systems: the two- and three-disk scattering systems. In order to be able to use only the basic primitive orbits and the composition rule for these, we have restricted the calculations to the $l =$ mode only. As the real part of the damping coefficient α_l goes like $\alpha_l(k) = const \times \operatorname{Re} k^{1/3}(l - \frac{1}{4})^{2/3}$, and since the diffraction coefficients C_l is a decreasing function of l, we assume that the calculation will give the leading behaviour of the full spectral determinant.

6.5.1   Results for the two-disk system

To demonstrate the importance of the diffraction effects to the spectra, we have calculated the A_1 resonances of the scattering system of two equally sized hard circular disks with disk separation $R = 6a$, where a is the radius of one disk. In this system there is only one geometrical periodic cycle along the line connecting the centers of the disks. Its stability $\Lambda_p = 9.8989794$ and action $S_p = kL_p = k \cdot 4a$, yield the geometrical part of the spectral determinant[16, 61]

$$\Delta_G(k) = \prod_{j=0}^{\infty} \left(1 + \frac{e^{ikL_p}}{\Lambda_p^{(1+4j)/2}} \right), \tag{6.90}$$

where $k = \sqrt{2mE}/\hbar$ and $2m = \hbar = 1$, and leads to the following predictions for the semiclassical A_1 resonances

$$k_{n,j}^{\text{res}} = \left(\pi(2n - 1) - i\frac{1 + 4j}{2} \ln \Lambda_p \right) / L_p \tag{6.91}$$

with $n = 1, 2, 3, \cdots$. Note in the above expressions $(1 + 4j)/2$ replaces the usual weight $(1 + 2j)/2$, since the geometrical orbit in the two-disk problem lies on the boundary of the fundamental domain.

Fig. 6.6 shows the first four new basic cycles in the fundamental domain[16]. We computed the geometrical data of the first ten orbits and used them to construct the creeping and geometrical Green's functions. If the ray connecting q and q' is reflected once or more from the curved hard walls before hitting tangentially one of the surfaces, we can keep track of the change in the amplitude by the help of the Sinai-Bunimovich curvatures (6.41). The effective radius R_b^{eff}, the length of the geometrical arc L_b^G and the length of the diffraction part L_b^D of the first ten orbits with creeping sections are listed in Table 6.1.

The diffraction part of the spectral determinant is finally given by

$$\begin{aligned} \Delta_D(k) \quad &= \quad 1 - \sum_{b,l}(-1)^{m_b} C_l \frac{a^{1/3}e^{i\pi/12}e^{ik(L_b^G + L_b^D) - \alpha_l L_b^D}}{k^{1/6}\sqrt{R_b^{\text{eff}}}} \\ &\quad \times \frac{1}{1 - e^{2\pi(ik - \alpha_l)a}}, \end{aligned} \tag{6.92}$$

where $C_l = \pi^{3/2}3^{-4/3}2^{-5/6}/Ai'(x_l)^2$, and $Ai'(x_l)$ is the derivative of the Airy function evaluated at it's l'th zero x_l. We computed the spectra by truncating

m_b	L_b^G/a	R_b^{eff}/a	L_b^D/a
0	5.656854249492	5.656854249424	3.821266472498
0	6.000000000000	6.000000000000	3.141592653589
1	9.832159566199	58.16784043380	3.476488812029
1	9.797958971132	58.78775382679	3.544308495170
2	13.81654759452	578.1406653460	3.507404058891
2	13.81309379078	579.7434283719	3.514253447057
3	17.81499162871	5729.649817456	3.510488616089
3	17.81464272590	5732.235502463	3.511180541615
4	21.81483475355	56728.70010470	3.510799703655
4	21.81479950722	56732.26871144	3.510869602322

Table 6.1: The first ten basic cycles t_b which include creeping sections in the fundamental region of two-disk problem (with disk separation $R = 6a$). The cycles are labeled by the number m_b of geometrical reflections from one of the disks. The length of the geometrical arc L_b^G, the effective radius R_b^{eff} and the length of the diffraction segment L_b^D are listed in units of the disk radius a.

the product $\Delta_G(k)\Delta_D(k)$ at maximal cycle length 5 and using only the $l = 1$ term in the now restored summation over the creeping mode number. The exact quantum mechanical resonances were computed following ref.[60].

The leading semiclassical resonances are given equally well with and without creeping modifications. In fig. 6.7 we can see that the new formula describes the resonances of the two disk system with a few-percent error, while the computation based on the geometrical cycle alone, (6.90), gives completely false results for the next-to-leading resonances (see (6.91)).

6.5.2 Results for the 3-disk scattering system

In order to apply the geometrical theory of diffraction to the calculation of semiclassical resonances, we also have to account for the diffraction (creeping) orbits of the system. To give an overview of the work to be done, we start by counting the number of periodic creeping orbits to be evaluated. Because of the symmetry of the system we can assume that the creeping orbit always starts tangentially from the (half-) disk in the fundamental domain which we label disk number 1 see fig. 6.8. Considering first an orbit with no geometrical bounces we see that it has two different disks to go to, and for each each disk two different sides to creep in. This makes a total of four diffraction orbits of topological length 1. When these are folded back into the fundamental domain we see that two of them are self retracing. The two other orbits are tracing the same orbit, but in opposite directions. If we consider paths of the particle with m bounces, we see that there will be $2^{n+1} = 2^{m+2}$ periodic creeping orbits of topological order n, as for each one of the m bounces the particle can choose between two disks. Thus the number of periodic creeping orbits grows exponentially fast with
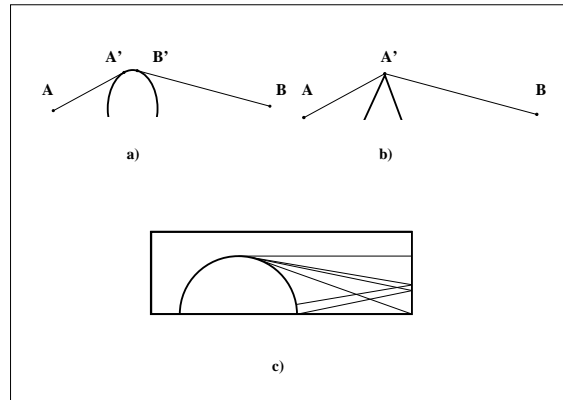
Figure 6.6: The simplest classes $\mathcal{D}_{100}$ (a) and $\mathcal{D}_{001}$ (b) of curves in two dimensions. In the window (c): the first four basic orbits in the fundamental domain of the two-disk system.
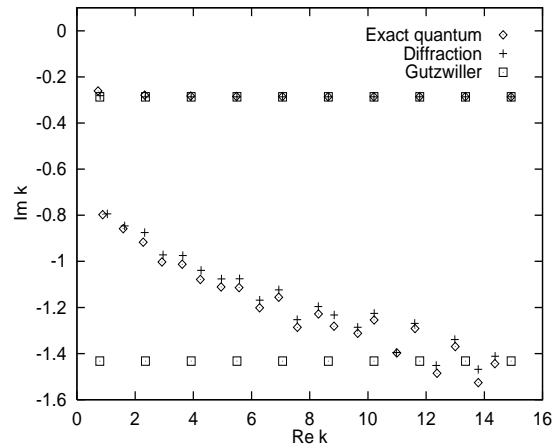
Figure 6.7: Resonances for the $A1$ subspace of the two-disk system (with disk separation $R = 6a$) in the complex k plane in units of the disk radius a. The diamonds label the exact quantum mechanical resonances, which are the poles of the scattering matrix. The crosses are their semiclassical approximations including the diffraction terms derived in this paper. The boxes refer to the ordinary Gutzwiller semiclassical approximation, with $(j = 0, 1)$, where the diffraction effects are not included.

the topological length, n, of the orbit. It is quite astonishing however, as we will see later, how few of these orbits are in fact needed to get a good description of the scattering resonances (including the ones with large imaginary parts). The creeping orbits can be described completely by their itinerary $1\alpha_1\alpha_2\ldots\alpha_n$ where the α_i's are taken from the alphabet $\{1, 2, 3\}$ and where we do not allow the repeats $\ldots 11 \ldots$, $\ldots 22 \ldots$ and $\ldots 33 \ldots$. This description contains a double degeneracy due to the fact that the orbit has the choice to creep around the final disk clockwise or anti-clockwise. For instance, '123' can represent two different orbits which start from disk 1 in the fundamental domain, then hit disk number 2 and finally creep around the final disk (3) clockwise or anti-clockwise.

The restriction that the creeping periodic orbits should start and end tangentially on one of the disks simplifies the search procedure for them considerably: whereas in the case of geometrical n-bounce cycles one had to minimize a function of n bouncing parameters, we here only have one parameter in play, namely the angle where the creeping orbit leaves the initial disk. Suppose now that we want a specific creeping orbit described by a series of disk bounces plus the specification of the final creeping domain as above. We then scan through all the angles that leave the first disk in the fundamental domain. This gives us an interval of angles where the first wanted disk is being hit. We then scan this interval for bounces on the next disk in the itinerary and so on. Finally we scan the last obtained interval to find the angle under which the ray creeps into the wanted side of the final disk. Having obtained the creeping cycles we can calculate the effective radius by using the usual Jacobian (2.12) for the stabilities. In table 6.2 we list the data for the first few creeping cycles.

To evaluate the results of the diffraction extended Gutzwiller-Voros spectral determinant, we compare the resonances determined by this, to the resonances determined just from geometrical orbits and to the exact quantum resonances.

The data are displayed in fig. 6.9. As one can see the Gutzwiller Voros determinant accounts reasonably well for the leading order of resonances, whereas it fails for the next series. In fig. 6.9, however, we can see that – when a few periodic creeping orbits are introduced – the results are *qualitatively different*, and represent much better the trend of the exact quantum resonance data. For instance, one can make a one-to-one identification of the quantum and semiclassical resonances, which is not possible in the purely geometrical theory, since in that approximation even the number of resonances is wrong.

The series of subleading resonances also approximately defines the lower boundary of the region in which the diffractional spectral determinant still has a high accuracy and good convergence properties. This can also be seen from fig. 6.9 since for small Re k and large negative Im k we have a relatively larger deviation between the exact and creeping resonances.
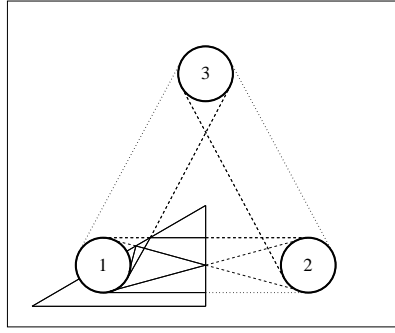
Figure 6.8: The full 3-disk system with a copy of the fundamental domain. Representatives of the creeping orbits of topological length 1 are displayed in full space as well as in the fundamental one.
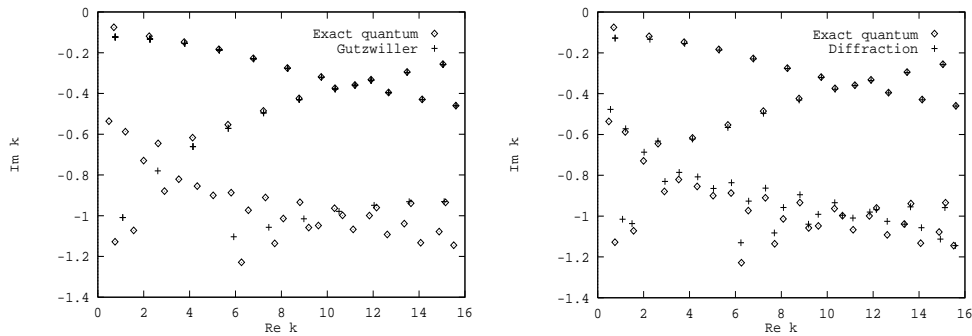
Figure 6.9: (Left) The exact quantum mechanical resonances (diamonds) and the pure geometrical Gutzwiller Voros resonances (crosses) in units of $1/a$ in the complex k plane. The resonances belong to the one-dimensional A_1 representation of the 3-disk system with $R{:}a = 6$. In the semiclassical calculation cycles up to topological length 4 have been used. The leading resonances close to the real axis are described well by the Gutzwiller Voros resonances whereas the subleading semiclassical resonances clearly deviate from the exact quantum resonances. (Right) The exact quantum mechanical (diamonds) and the semiclassical (crosses) A_1 resonances of the $R{:}a = 6$ three-disk system. The resonances are calculated by including diffractional creeping orbits up to order 4 in the geometrical theory of diffraction. As in the two disk case an improvement of the approximation is clearly visible, especially for the second row of the leading resonances as well as for the subleading diffractional ones. In the latter case the qualitative trend is clearly reproduced. As discussed above, the accuracy of the semiclassical resonances becomes worse in the region where Re k is small and Im k is large.

p_c	R_b^{eff}/a	L_b^G/a	L_b^D/a
12	6.000000	6.000000	4.188790
12	5.656854	5.656854	3.821266
13	6.000000	6.000000	2.094395
13	5.656854	5.656854	3.821266
121	58.167840	9.832159	4.523686
121	58.787753	9.797958	3.544308
131	58.167840	9.832159	2.429291
131	58.787753	9.797958	3.544308
123	66.352162	10.120809	4.384819
123	73.492203	10.147842	3.478142
132	84.855171	10.120809	2.678761
132	73.492203	10.147842	3.478142

Table 6.2: Creeping cycle data for the 3-disk system with $R : a = 6$. The first column indicates the itinerary of the orbit, second column the effective radius of the orbit calculated by means of the Sinai-Bunimovich curvatures and finaly the third and fourth columns shows the length of the free flight and the creeping sections respectively.

6.5.3 Corrections to the Airy approximation

In our calculation of the diffractive Greens function G_{creep} we used the Airy approximation (6.43) for the Hankel functions and its zeros. This approximation is only the leading term in a polynomial series of corrections to the zeros. In reference [28] and especially in Franz and Galle [29] one can find correction terms to order $\mathcal{O}((ka)^{-5/3})$ to the standard Airy approximation of the zeros ν_l of the Hankel function $H_\nu^{(1)}(ka)$ in the complex plane. These corrections read
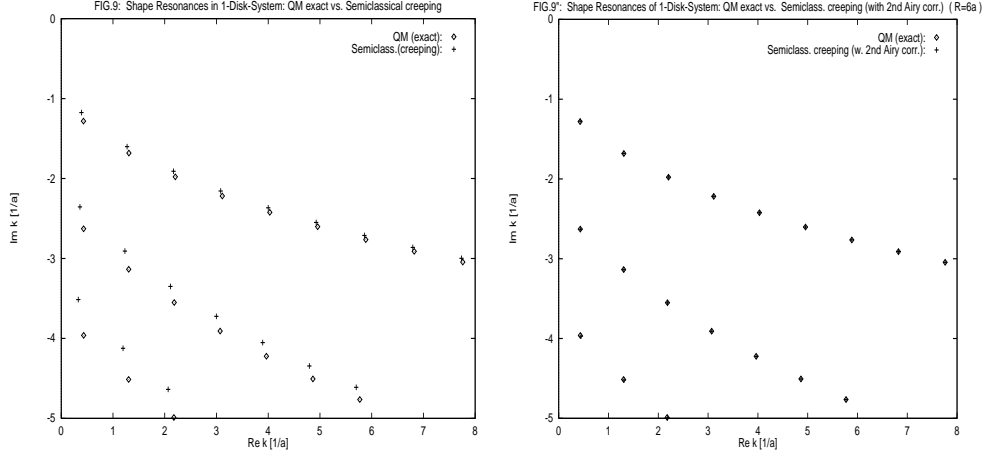
Figure 6.10: (Left) The exact quantum-mechanical resonances for the 1-disk scattering system (given by the zeros of $H_m^{(1)}(ka)$) are plotted as diamonds, the diffractional semiclassical resonances which are given by the zeros of the creeping determinant $\Delta_{1-disk}(k) = \prod_{l=1}^{\infty}(1 - e^{i\nu_l 2\pi a})$ are plotted as crosses. In this calculation only the standard Airy approximation is used. Note that the creeping terms to this order systematically underestimate the magnitude of the imaginary part of the exact resonances. We also see that the semiclassical data becomes better with increasing real part of the wave number k, and with decreasing $|\text{Im}k|$, as they should as semiclassical approximations. (Right) The same as above figure except that the semiclassical resonances now include the two first terms up to order $\mathcal{O}((ka)^{-1})$ in the Airy corrections. We see that the approximation is almost perfect, especially for the leading row of resonances. The inclusion of the 3rd Airy correction (terms of order $\mathcal{O}((ka)^{-5/3})$) does not change the plot further. The data are from A. Wirzba.

$$
\begin{aligned}
\nu_l \;=\;& ka + e^{i\pi/3}(ka)^{1/3}s_l \\
& -e^{-i\pi/3}(ka)^{-1/3}\frac{s_l^2}{30} \\
& -\frac{(ka)^{-1}}{70}\left(1 - \frac{s_l^3}{5}\right) \qquad\qquad\qquad (6.93) \\
& +e^{i\pi/3}\frac{(ka)^{-5/3}}{3150}\left(29s_l - \frac{281s_l^4}{180}\right) \\
& +\dots, \qquad\qquad\qquad\qquad\qquad\qquad (6.94)
\end{aligned}
$$

where $s_l = 6^{-1/3}x_l$, and x_l is the l'th zero of the Airy integral $Ai(x) = \int_0^{\infty} dt \cos(xt - t^3)$. The standard Airy approximation only contains the first two terms in the above series and therefore is only of order $\mathcal{O}((ka)^{1/3})$. Wirzba [64] has studied the influence of these corrections in the simple case of the 1- and 2-disk scattering systems. As can be seen from figure 6.10, it turns out that the corrections improve the pure creeping results considerably. For the 2-disk scatterer a similar improvement of the resonances are observed by inclusion of the next terms in the Airy approximation.

As seen from the numerical results it would be very nice if one could incorporate the Airy corrections into our expression for the creeping propagator. This however is not so straightforward in the general case as in the 1-disk situation. The reason is that it is not sufficient to include the Airy corrections in the decay exponents α_l, since one should also include the changes in ν_l in the Debye approximation, which makes the previous so clear geometrical interpretation of the ingredients of the propagator more ambiguous. The improvements in the results are though quite dramatic, so it seems worthwile to try to find the analog in the Keller construction. However, this still remains to be done.

6.6 Discussion

In this chapter we have derived a method to obtain a semiclassical approximation to the quantum propagator including certain diffraction effects such as diffraction along smooth surfaces as well as diffraction from vertices. The method is based on the geometrical theory of diffraction introduced by Keller. We have shown how the introduced periodic creeping orbits inflict on the Gutzwiller trace formula and we have constructed a scheme on how to incorporate the diffraction effects in the semiclassical spectral determinant for quantum systems. By numerical computations we have furthermore shown that by inclusion of the diffraction effects the semiclassical resonances of simple scattering systems changes dramatically and describes very well the exact quantum resonances. As the description is semiclassical we use the Van Vleck propagator for the free flight sections and our semiclassical approximation to the creeping propagator for the creeping sections. The errors of the resonances entering by this approach are therefore mainly originated in three sources:

1. To be able to keep our calculation in terms of basic primitive cycles we used only the $l = 1$ mode in the semiclassical approximation to the creeping propagator. This approximation is justified when the real part of ka is of order of, or larger than 1, since the exponential damping term $\alpha_l(k)$ goes like

$$\alpha_l(k) \quad \simeq \quad const \times \mathrm{Re}\ (ka)^{1/3}(l - \frac{1}{4})^{2/3} \qquad (6.95)$$

and the relative error thus introduced is less than 1 percent for $ka \leq 2$. This error is therefore not sufficient to explain our deviations from the exact resonances.

2. In our semiclassical evaluation of the creeping propagator we use the Airy approximation. As it was demonstrated by the calculations of A. Wirzba, the polynomial terms in the Airy corrections can give sizeable corrections to the calculated resonances. In the simpler 1-disk[29] and 2-disk[64] problems the contributions resulting from the higher polynomial terms in the Airy expansion of the creeping propagator move the subleading semiclassical resonances on top of their corresponding exact quantum analogs to

figure accuracy. In the three-disk case the corresponding calculation is plagued by the exponentially proliferating number of periodic orbits, but the hope is of course that the corresponding Airy correction terms could improve the subleading semiclassical resonances as well.

3. Even the cumulant expansion of the exact quantum mechanical scattering determinant is for large negative Im k very delicate as the single terms entering the cumulant expansion become individually large[64]. As the periodic orbit expansion is just the semiclassical approximation to the cumulant expansion [61], it cannot be expected that the periodic orbit expansion works better than this. In fact, as the individual contributions of the periodic orbits become larger with increasing negative Im k, the individual errors from the semiclassical expansion are also increasing such that the total error can become sizable.

It would be natural to expect that the exponential proliferation of periodic orbits in the case of the 3-disk system, might destroy the validity of the semiclassical description completely. We conclude that this seems not to be the case. As we have demonstrated, one only need the basic representatives of the creeping families to change the picture of the scattering resonances drastically, in the direction of the exact quantum resonances.

Chapter 7

$\hbar$ corrections

7.1 $\hbar$ corrections to the Gutzwiller trace formula

The Gutzwiller trace formula (4.21) is the most compact formulation of the semiclassical quantization of multidimensional systems. In recent years it has been demonstrated[35] on many classically chaotic systems that it is indeed a very good approximation.

As mentioned the starting point of the Gutzwiller derivation of the trace formula can be taken in the Feynman path integral form[27, 50] of the propagator. But, calculations with path integrals are difficult in general. It is often easier to find the numerical solution of the underlying Schrödinger equation. The most convenient asymptotic method to evaluate the path integral is the saddle point approximation. The leading Gaussian approximation is easy to perform and gives very good results, as we saw in the two previous sections.

There are many attempts to improve the semiclassical approximation within the framework of the Gaussian approximation in order to get accurate energies and resonances. But the Gaussian approximation has its inherent limitation and one should go beyond it to improve the accuracy. Recently, Gaspard and Alonso [33] computed corrections of the Gutzwiller trace formula and showed that the resonances of the two and three disk scattering systems[32, 61] can be improved considerably. They have used the usual Feynman graph technique of the perturbation theory and computed large number of graphs to get the corrections. In general the conventional graph calculus is very cumbersome. In this chapter we shall describe an alternative approach to the calculation of $\hbar$ corrections, using ordinary differential equations.

The basic idea is the following. Suppose you have a time independant bound system and are looking for the energy eigenvalues of the Hamilton operator. An eigenfunction ψ_n, fulfills the time independant Schrödinger equation

$$\hat{H}\psi_n = E_n\psi_n. \tag{7.1}$$

Now if you consider a periodic orbit of the corresponding classical system, then

93

you can expand the potential in the Hamiltonian around this orbit and try
to solve the Schrödinger problem with appropriate boundary conditions in the
neighbourhood of this orbit. This will in general give a complete eigenspectrum
with coresponding eigenfunctions. However, since the local problem contains
the full problem as a special case, the original spectrum will be contained in the
local spectrum. If you now follow the same procedure for all the periodic orbits
in the system, and if the set of periodic orbits are sufficiently proliferating then
the union of restrictions prescribed by all the periodic orbits will finally lead
to the spectrum we were originally looking for. Now the ℏ correction scheme
enters in the solution of the local Schrödinger problem. If we make the usual
ansatz that the local wave function is given by

$$\psi_p \quad = \quad \varphi_p e^{iS_p/\hbar}, \tag{7.2}$$

then by inserting this expression into the local Schrödinger equation and ex-
panding in orders of ℏ, we end up with the Hamilton-Jacobi equation for the
(local) action S_p and with an evolution equation for the amplitude φ. In this
last equation one usually neglects the $\hbar^2$ term and is then led to the classi-
cal continuity equation for the amplitude, which gives the usual semiclassical
result as we saw in section 4.1. Here we instead expand the amplitude in a
perturbation series in ℏ, and keep the $\hbar^2$ term in the equation for the purpose
of connecting different orders in ℏ in the expansion. This results in an iterative
scheme where the coefficients in the ℏ expansion of the amplitude can be de-
termined successively. Finally the ℏ corrected amplitude function can then be
connected to the spectral determinants of the local problem, and by multiplying
these together, we finally end up with an ℏ corrected spectral determinant for
the full problem.

The above considerations are of course in no sense rigorous but they give
the main idea of the strategy we are going to follow in this chapter. It should
be emphasised that the theory sketched in the following sections is *still not in
complete mathematical rigour*. We take this theory as *the starting point*, and
concentrate in this thesis on applications of the theory to billiard systems.

The strategy of this chapter is therefore the following: first we describe the
method developed in [55] and obtain differential equations for computing ℏ cor-
rections to the Gutzwiller trace formula. We then specialize to billiard systems
and develop an algorithm to compute the corrections which using geometrical
information about periodic orbits, such as their lengths, stabilities, bouncing
angles etc. Finaly we carry out several numerical computations on the two-
and three-disk scattering systems and compare the results to the exact quan-
tum results and to the work by Gaspard et al. [33] to show that our theory
gives equivalent results.

7.2   Path integrals and partial differential equations

In this section we show how the path integral expression for the propagator
can be connected to a set of partial differential equations in the case where

one uses the saddlepoint approximation to restrict the path integral to tubes around classical paths, or paths that has a minimal action.

The path integral representation of the propagator is

$$G(q, q', t) = \int \mathcal{D}q'' e^{\frac{i}{\hbar}S(q,q',t|q'')}, \tag{7.3}$$

where $\int \mathcal{D}q''$ represents the functional integral measure for all the paths connecting q with q' in time t, and $S(q, q', t|q'')$ is the classical action between q and q' computed along a given path q''. We are interested in the path integral expression for the trace which reads

$$\text{Tr}G(t) = \int dq G(q, q, t) = \int \mathcal{D}q'' e^{\frac{i}{\hbar}S(t|q'')}, \tag{7.4}$$

where $\int \mathcal{D}q''$ now represents the functional integration for closed paths. In the saddle point approximation the leading contribution to the path integral is coming from the neighbourhood of paths for which the classical action is stationary. This condition singles out the classical periodic trajectories from the infinite variety of possible paths;

$$\text{Tr}G(t) = \sum_p \int \mathcal{D}q_p \exp\left(\frac{i}{\hbar}S_p(q_p, t)\right), \tag{7.5}$$

where $\sum_p$ denotes the summation for the classical primitive periodic orbits and $\int \mathcal{D}q_p$ denotes a functional integral in the neighborhood of periodic orbits, where we Taylor expand the classical action around the periodic orbit $x_p(t)$

$$S_p(x, t) = \sum_{\mathbf{n}}^{\infty} s_{\mathbf{n}}(t)(x - x_p(t))^{\mathbf{n}}/\mathbf{n}!. \tag{7.6}$$

The symbol $\mathbf{n} = (n_1, n_2, ..., n_d)$ denotes the multi index in d dimensions, $\mathbf{n}! = \prod_{i=1}^{d} n_i!$ the multi factorial and $(q_p - x_p(t))^{\mathbf{n}} = \prod_{i=1}^{d}(q_{p,i} - x_{p,i}(t))^{n_i}$, respectively.

Since the saddle points are taken in the configuration space, only spatially distinct periodic orbits, the so called primitive periodic orbits, appear in the summation. If we continue the standard textbook calculation scheme, we should truncate the Taylor expansion in the exponent at the quadratic order term while treating the higher order terms as corrections. Then we can compute the path integrals with the help of Gaussian integrals. In this way one can derive Gutzwiller's trace formula. Corrections to the Gaussian approximation can be found by expanding the action to higher orders, expanding the exponential and performing the Gaussian cumulant integrals.

Here we do not follow the textbook approach. Instead we observe that the terms in (7.5) are similar to the original path integral expression of the

trace (7.4). The only difference is that each term has to be computed in the neighborhood of a periodic orbit and that the classical actions are given in power series form.

We now consider the *local* Schrödinger equation,

$$\hat{H}_p \psi_p(x,t) \ = \ i\hbar \frac{\partial \psi_p(x,t)}{\partial t} \tag{7.7}$$

which leads to the *local* path sum

$$\int \mathcal{D}q_p e^{i/\hbar \sum_{\mathbf{n}} S_{\mathbf{n}}(x_p(t),t)q_p^{\mathbf{n}}/\mathbf{n}!} \ = \ \mathrm{Tr} G_p(q_p, q_p', t). \tag{7.8}$$

The saddle point expansion of the full trace in terms of local traces then becomes

$$\mathrm{Tr} G(x,x',t) = \mathrm{Tr} G_W(x,x',t) + \sum_p \mathrm{Tr} G_p(q_p, q_p', t), \tag{7.9}$$

where $G_W(x,x',t)$ denotes formally the Green function expanded around zero length (non moving) periodic orbits, known as the Weyl term[6]. Each Green function can be seperately Fourier transformed and we get in the energy domain:

$$\mathrm{Tr} G(x,x',E) = g_0(E) + \sum_p \mathrm{Tr} G_p(q_p, q_p', E). \tag{7.10}$$

Notice, that in contrast to the derivation of section 4.1 we do not need here to take further saddle points in time, since we are dealing with exact time and energy domain Green functions.

The local spectral determinant $\Delta_p(E)$ for the local operators is defined as

$$\mathrm{Tr} G_p(q_p, q_p', E) = \frac{d}{dE} \log \Delta_p(E). \tag{7.11}$$

Using (7.10) we can express the full spectral determinant as a product over the sub-determinants

$$\Delta(E) \ = \ e^{W(E)} \prod_p \Delta_p(E), \tag{7.12}$$

where $W(E) = \int^E g_0(E')dE'$ is the term coming from the Weyl expansion.

In general, there are many different types of closed periodic orbits which can contribute to the product (7.12). The spectral determinant of the zero length orbits gives a smooth contribution, which is the counterpart of the Weyl or Thomas-Fermi terms. From now on we neglect these terms since they do not change the location of the zeroes of the spectral determinant. Also, the periodic orbits in the complexified phase space of the Hamiltonian system can contribute[8], as well as the diffraction cycles introduced in section 6.1. In the following we concentrate only on the usual classical periodic orbits.

We should mention that here we do not investigate the general validity of the saddle point approximation. However, it is important to note that the power series expansion of the action is an asymptotic expansion, where contributions from different orbits overlap and this causes some overcounting in the formula (7.5). Therefore in computations the number of periodic orbits included in the sum should depend on the order of truncation of the power series. In the semiclassical or Gaussian approximation the criterion proposed by Berry and Keating [7] can be used. We hope, that a similar condition can be derived for the situation discussed here.

Local spectra of the Schrödinger equation

To compute the local spectral determinants $\Delta_p(E)$ we have to solve the local Schrödinger problem (7.7) in the neighborhood of a classical periodic orbit, and all variables should be indexed with a p. For simplicity we shall drop this index in the rest of this section.

The local Schrödinger equation

$$i\hbar\partial_t\psi = -\frac{\hbar^2}{2m}\Delta\psi + U\psi \tag{7.13}$$

can be constructed by expanding the Hamilton operator in the neighbourhood of the periodic orbit and imposing appropriate boundary conditions in the direction orthogonal to the velocity direction of the orbit. The boundary conditions are

$$\max_{|\mu|=R}|A(s,\vec{\mu})| \quad \to \quad 0, \quad \text{for} \quad R \to \infty \tag{7.14}$$

$$A(s+L,\vec{\mu}) = e^{i\kappa}A(s,\vec{\mu}) \tag{7.15}$$

where A is the amplitude of the wave function, s measures the length along the periodic orbit and $\vec{\mu}$ is a small vector orthogonal to the direction of the flow. With the conditions (7.15) the local Schrödinger equation (7.7) becomes a precisely formulated boundary value problem. This idea is described in detail and with all the mathematical rigour in [5].

The equation is most conveniently solved by rewriting it with the usual ansatz

$$\psi = \varphi e^{iS/\hbar}, \tag{7.16}$$

where we have not yet imposed any restrictions on the functions $\varphi(x,t)$ and $S(x,t)$. Inserting these equations into the Schrödinger equation (7.13) yields

$$\begin{aligned}
-\varphi\partial_t S + i\hbar\partial_t\varphi &= -\frac{\hbar^2}{2}(\Delta\varphi + 2i/\hbar\nabla\varphi\nabla S \\
&+ i/\hbar\varphi\Delta S - 1/\hbar^2\varphi(\nabla S)^2) + U\varphi.
\end{aligned} \tag{7.17}$$

Here we have many possibilities to group the terms since we have not made any restriction for S and φ yet. Our main concern is to separate the classical and the quantum time evolution. Therefore, we require the phase to fulfill the Hamilton-Jacobi equation

$$\partial_t S + \frac{1}{2}(\nabla S)^2 + U = 0. \tag{7.18}$$

which yields the *classical* action solution. As we see the Hamilton-Jacobi equation is an autonomous equation which can be solved by just using the knowledge of the behaviour of the potential in the neighbourhood of the periodic orbit. We note that the potential only occurs in this equation. Having found the solution $S(x,t)$ to the Hamilton-Jacobi equation, the amplitude (which we now allow to be complex) fulfills

$$\partial_t \varphi + \nabla\varphi\nabla S + \frac{1}{2}\varphi\Delta S - \frac{i\hbar}{2}\Delta\varphi = 0. \tag{7.19}$$

It is *this* partial differential equation that corresponds to the local path sum (7.8). It is driven by the solution of the Hamilton-Jacobi equation and should be solved in the neighborhood of a periodic orbit with the action expanded like in (7.6).

If the local Schrödinger equation around the periodic orbit has an eigenenergy E the corresponding eigenfunction fulfills

$$\psi_p(t + T_p) = e^{-iET_p/\hbar}\psi_p(t). \tag{7.20}$$

For a general energy value E, the eigenfunctions of the local Hamiltonian $\psi_p^l(t)$ fulfill

$$\psi_p^l(t + T_p) = e^{-iET_p/\hbar}\lambda_p^l(E)\psi_p^l(t). \tag{7.21}$$

where $\lambda_p^l(E) = \exp(i(E - E_l)T_p/\hbar)$. If the eigenvalues $\lambda_p^l(E)$ are known, the local functional determinant (7.12) can be formally written as

$$\Delta_p(E) = \prod_l(1 - \lambda_p^l(E)), \tag{7.22}$$

since $\Delta_p(E) = 0$ yields the eigenenergies of the local Schrödinger problem. We can insert the ansatz (7.16) and reformulate (7.21) as

$$e^{\frac{i}{\hbar}S(t+T_p)}\varphi_p^l(t + T_p) = e^{-iET_p/\hbar}\lambda_p^l(E)e^{\frac{i}{\hbar}S(t)}\varphi_p^l(t). \tag{7.23}$$

The phase change is given by the action integral for one period $S(t+T_p)-S(t) = \int_0^{T_p} L(t)dt$. Using this and the identity for the reduced action $S_p(E)$ of the periodic orbit

$$S_p(E) = \oint pdq = \int_0^{T_p} L(t)dt + ET_p, \tag{7.24}$$

we get

$$e^{\frac{i}{\hbar}S_p(E)}\varphi_p^l(t + T_p) = \lambda_p^l(E)\varphi_p^l(t). \tag{7.25}$$

Introducing the eigenequation for the amplitude

$$\varphi_p^l(t + T_p) = R_p^l(E)\varphi_p^l(t), \tag{7.26}$$

the local spectral determinant can be expressed as

$$\Delta_p(E) = \prod_l (1 - R_p^l(E)e^{\frac{i}{\hbar}S_p(E)}). \tag{7.27}$$

To get the full spectral determinant we therefore have to solve the equation (7.26) in order to get the local eigenvalues. As we shall see this equation can be easily solved on an analytic basis.

We can also reexpress the quantum Gutzwiller-Voros spectral determinant in terms of the local eigenvalues. This reads

$$\Delta(E) = \prod_p \prod_l (1 - R_p^l(E)e^{\frac{i}{\hbar}S_p(E)}). \tag{7.28}$$

The trace formula can be recovered from (7.11):

$$
\begin{aligned}
\text{Tr}G(E) &= \frac{1}{i\hbar}\sum_p \sum_l \frac{R_p^l(E)e^{\frac{i}{\hbar}S_p(E)}}{1 - R_p^l(E)e^{\frac{i}{\hbar}S_p(E)}} \\
&\times \left(T_p(E) - i\hbar\frac{d\log R_p^l(E)}{dE}\right).
\end{aligned} \tag{7.29}
$$

To keep an overview over the work that is to be done, it seems appropriate at this point to emphasize an outline over the steps we are going to persue in the following:

1. First of all we have to solve the local Hamilton Jacobi equation (7.18), in order to be able to drive the amplitude transport equation. This is done by expanding the phase function in a Taylor series, inserting this into the Hamilton-Jacobi equation, and solve the resulting ordinary differential equations.

2. Next we should solve the amplitude transport equation (7.19). This is basically done by using the same strategy as with the phase function, i.e. by expanding the amplitude in a Taylor series around the periodic orbit and solving the ordinary differential equations obtained after insertion into the amplitude equation. However, the $i\hbar\Delta$ term in (7.19) suggest us to expand the Taylor coefficients in a polynomial series in $\hbar$. Having done

this, we then solve the amplitude equation in two steps: first we solve the *autonomous set* of *semiclassical* equations where we set $\hbar = 0$. Next we can solve the equation recursively to any desired order in $\hbar$ by inserting the previously obtained solutions and keeping the term $i\hbar\Delta$, that connect different orders in $\hbar$.

3. Now we can concentrate on our main point, namely to solve equation (7.26). By also expanding the local eigenvalues R_l in a powerseries in $\hbar$ and inserting this in the eigenvalue equation (7.26), we can, by comparing terms of same order in $\hbar$, solve for the R_l coefficients in the expansion of the eigenvalues. This again defines an iterative scheeme, where we can get the $\hbar$ corrections to the eigenvalues by successively inserting the previous found solutions of the eigenvalue equation to lower orders in $\hbar$.

4. Having found the $\hbar$ corrections of the local eigenvalue problem, we can now get an $\hbar$ corrected local spectral determinant for each periodic orbit, by using (7.27). Multiplying these together we finally end up with an $\hbar$ corrected spectral determinant according to (7.28), or we can get an $\hbar$ corrected trace formula from (7.29).

Solving the equations (7.18-7.19) and (7.26) can be done by a variety of numerical methods. The analytic perturbation method we develop here, can be easily applied also in numerical calculations.

7.3   Analytic eigenbasis

To get the local eigenvalues we have to solve the Hamilton-Jacobi- and the amplitude equations (7.18) (7.19) in order to follow the evolution of a wavepacket around the periodic orbit. In this section we show how the Hamilton-Jacobi equation and the amplitude equation can be solved by changing them into *ordinary* differential equations. For simplicity we shall keep the derivation in one dimension but as we shall demonstrate later the equations are easily obtained in higher dimensions as well.

The Hamilton-Jacobi equation

In the saddlepoint approximation of the trace (7.8) we expressed the phase function S in a powerseries form to get a sum over the local traces. In the neighborhood of a classical periodic orbit we can therefore look for the solution of the Hamilton-Jacobi equation in a power series form. Let $x_p(t)$ denote a classical periodic orbit with period T_p. Let us expand the phase around the time dependent trajectory as in (7.6). To derive ordinary differential equations for the expansion coefficients we expand also the potential around the periodic

orbit

$$U(x) = \sum_{\mathbf{n}}^{\infty} u_{\mathbf{n}}(t)(x - x_p(t))^{\mathbf{n}}/\mathbf{n}!, \tag{7.30}$$

where $u_{\mathbf{n}}$ are rank n tensors in general. If we put these two expressions into the Hamilton-Jacobi equation we get in the one-dimensional case

$$\dot{s}_n - s_{n+1}\dot{q} + \frac{1}{2}\sum_{l=0}^{n}\frac{n!}{(n-l)!l!}s_{n-l+1}s_{l+1} + u_n = 0 \tag{7.31}$$

which represents a hierarchy of equations. In the multidimensional case we get similar expressions for the entries of the s matrices. In the Hamilton-Jacobi equation it is common to interpret the gradient of the phase function as the momentum. If the s_1 vector is choosen to be the momentum of the classical orbit

$$p = \dot{q} = s_1, \tag{7.32}$$

the equations are simpler and their meanings are obvious. The first equation in the hierarchy corresponds to the classical action along the path:

$$\dot{s}_0 = \frac{p^2}{2} - u_0 = L(t), \tag{7.33}$$

where $L(t)$ is the Lagrange function evaluated on the periodic orbit. The second is the Newton equation

$$\dot{p} = -u_1, \tag{7.34}$$

since u_1 is the force along the trajectory. The $d \times d$ matrix s_2 is familiar from the wave packet theory and describes the shape of a Gaussian wave packet[37]

$$\dot{s}_2 = -s_2^2 - u_2. \tag{7.35}$$

We earlier encountered this equation in (5.22) where we studied the time evolution of the curvature matrix $\mathbf{M}$. Equation (7.35) is simply the one dimensional version of this evolution equation for the curvature matrix, which in this case is just the Sinai Bunimovic curvature. We therefore also know that $\mathrm{Tr}s_2$ describes the expansion of infinitesimal volume elements evolving along the classical orbit. The next equation

$$\dot{s}_3 = -3s_2s_3 - u_3, \tag{7.36}$$

and the rest of the equations are linear equations for s_n. These are pure classical equations describing the analytic structure of the action around the periodic orbits p.

Since the phase change along the periodic orbit is just given by the action integral (7.24), the gradient of $S(x,t)$ entering in the amplitude equation (7.19) must be a periodic function along the periodic orbit. Therefore, the $s_n, n > 0$ matrices are also periodic yielding the boundary conditions $s_n(t) = s_n(t + T_p)$ where T_p is the period of the orbit. The term $s_0(t)$ given by the action integral $s_0(t) = \int_0^t L(t)dt$ is then not periodic whereas for instance the momentum $s_1(t)$ along the periodic orbit varies periodically with time. The most complicated equation we have to solve is (7.35). In general it has more than one periodic solution. In case of unstable periodic orbits the solution of the equation (7.35) converges to a single stable solution starting from almost all initial conditions. A simple example of this can be obtained by considering the periodic orbit '0' of the 3-disk system. This has the Jacobian:

$$\mathbf{J}_0 \quad = \quad \begin{bmatrix} 1 & 4 \\ 2 & 9 \end{bmatrix}. \tag{7.37}$$

The rational fraction transformation (5.20) in this case yields

$$f(s_2) \quad = \quad \frac{2 + 9s_2}{1 + 4s_2} \tag{7.38}$$

and starting from almost any point this converges after a few iterations to the stable solution $s_2 = f(s_2) = 2.22474487\ldots$. The rest of the solutions are unstable. The wave packet described by the stable solution is decaying in time, while the rest of the solutions describe wave packets with increasing amplitudes. These solutions are non-physical, since they describe local wave functions with exponentially increasing norms. We have to exclude these solutions. In case of stable periodic orbits we also have only one solution of (7.35) for which the local wave function is decaying and we have to choose this solution. The higher order $(n > 2)$ equations are linear in s_n and their unique periodic solutions can be found order by order.

The evolution of the amplitude

After solving locally the Hamilton-Jacobi equation we can look for the local solution of the amplitude equation. In a similar way as with the phase function, we can expand the amplitude around the classical path in power series. This analytic basis is appropriate for classical Perron-Frobenius operators since it is very easy to diagonalize the evolution operator on this basis[47]. Inserting the expansion

$$\varphi_p(x, t) = \sum_{\mathbf{n}}^{\infty} \varphi_{\mathbf{n}}(t)(x - x_p(t))^{\mathbf{n}}/\mathbf{n}! \tag{7.39}$$

into the equation (7.19) yields in one dimension the following equations for the coefficients

$$\dot{\varphi}_n - \varphi_{n+1}\dot{q} \quad + \quad \sum_{l=0}^{n} \frac{n!}{(n-l)!l!} \left(\varphi_{n-l+1}s_{l+1} + \frac{1}{2}\varphi_{n-l}s_{l+2} \right)$$

$$-\frac{i\hbar}{2}\varphi_{n+2} \;=\; 0. \tag{7.40}$$

Note that the term $i\hbar/2\varphi_{n+2}$ connects different orders in $\hbar$.

In the multidimensional case we get similar equations for the expansion coefficient matrices. Using eq. (7.32) one can slightly reduce these equations:

$$
\begin{aligned}
\dot{\varphi}_0 &= -\frac{s_2}{2}\varphi_0 + \frac{i\hbar}{2}\varphi_2 \\
\dot{\varphi}_1 &= -\frac{3s_2}{2}\varphi_1 - \frac{s_3}{2}\varphi_0 + \frac{i\hbar}{2}\varphi_3 \\
\dot{\varphi}_2 &= -\frac{5s_2}{2}\varphi_2 - 2s_3\varphi_1 - \frac{s_4}{2}\varphi_0 + \frac{i\hbar}{2}\varphi_4
\end{aligned} \tag{7.41}
$$

and so on. These equations are linear and have the general form

$$\dot{\varphi}_n = -\frac{(2n+1)s_2}{2}\varphi_{n\ldots} + \frac{i\hbar}{2}\varphi_{n+2}. \tag{7.42}$$

In the semiclassical limit where we can set $\hbar = 0$, we see that the hierachy of equations take the form

$$\dot{\varphi} \;=\; \mathbf{T}\varphi \tag{7.43}$$

where $\mathbf{T}$ is a lower triangular matrix. This means that the solutions φ^l can be found successively by setting all $\varphi_i^l = 0$ for $i < l$. In the case of higher dimensions this still holds but the indexation is more tedious, since the equations are matrix equations in higher dimensions. However the structure of the hierachy of equations remain the same in any number of dimensions.

7.4 Stationary solutions

The set of equations (7.31),(7.40) and (7.26) define the full set of equations we have to solve. Furthermore we know, that we are seeking the stationary solutions of the Schrödinger equation. The stationarity condition implies that the phase of the wave function fulfills the condition

$$\frac{\partial S(x,t)}{\partial t} = -E, \tag{7.44}$$

and the amplitude has no *explicit* time dependence

$$\frac{\partial \varphi(x,t)}{\partial t} = 0. \tag{7.45}$$

These equations give us additional equations for the expansion coefficients, which have the form

$$
\begin{aligned}
\dot{s}_0(t) - \dot{q}(t)s_1(t) &= -E, \tag{7.46} \\
\dot{s}_n(t) - \dot{q}(t)s_{n+1}(t) &= 0 \quad \text{for } n > 0, \tag{7.47} \\
\dot{\varphi}_n(t) - \dot{q}(t)\varphi_{n+1}(t) &= 0 \quad \text{for } n \geq 0, \tag{7.48}
\end{aligned}
$$

in the one-dimensional case. In the multidimensional case the coefficient matrices fulfill similar equations. These equations can help us to reduce the number of equations that we have to solve, since some of the higher order expansion coefficients can be expressed by the time derivatives of the lower order coefficients. In one dimension all the higher coefficients can be directly computed from the time derivatives of the zero order terms. In two dimensions the number of s_n and φ_n matrix elements is $n + 1$. For example we need the $4 = 3 + 1$ coefficients $S_{x^3}, S_{x^2 y}, S_{xy^2}, S_{y^3}$ in the Taylor expansion of the phase function to the $n = 3$'rd order. The number of the additional equations derived above is n. Therefore, on each level we need to solve 1 new equation. In three dimensions we get n entirely new equations for the phase and the amplitude on each level. In section 7.7 we show how the reduction of the equations can be carried out.

7.5   ℏ expansion in the analytic base

As we saw in (7.40) the amplitude equation expanded in the analytical basis yields a coupling between different orders of $\hbar$. Since $\hbar$ is a small parameter we can develop a perturbation series for the amplitudes

$$\varphi^l(t) = \sum_{m=0}^{\infty} \left(\frac{i\hbar}{2} \right)^m \varphi^{l(m)}(t) \tag{7.49}$$

which we can then insert into the equation (7.40 -7.42). This results in a tower of coupled equations. In this section we discuss the semiclassical or zeroth order in $\hbar$ of these equations whereas the coupling to higher orders in $\hbar$ which yields the $\hbar$ corrections, will be discussed in the next section. The zeroth order or semiclassical equations form an autonomous system

$$\dot{\varphi}_n^{(0)} - \varphi_{n+1}^{(0)} \dot{q} \; + \; \sum_{l=0}^{n} \frac{n!}{(n-l)!l!} \left(\varphi_{n-l+1}^{(0)} s_{l+1} + \frac{1}{2} \varphi_{n-l}^{(0)} s_{l+2} \right)$$
$$= \; 0. \tag{7.50}$$

For example, the first three equations have the form

$$\dot{\varphi}_0^{(0)} \;\; = \;\; -\frac{s_2}{2} \varphi_0^{(0)},$$
$$\dot{\varphi}_1^{(0)} \;\; = \;\; -\frac{3s_2}{2} \varphi_1^{(0)} - \frac{s_3}{2} \varphi_0^{(0)}, \tag{7.51}$$
$$\dot{\varphi}_2^{(0)} \;\; = \;\; -\frac{5s_2}{2} \varphi_2^{(0)} - 2s_3 \varphi_1^{(0)} - \frac{s_4}{2} \varphi_0^{(0)}.$$

The important feature of these equations is that they are linear and have the general form

$$\dot{\varphi}_n^{(0)} = -\frac{(2n+1)s_2}{2} \varphi_n^{(0)} + ..., \tag{7.52}$$

and so on. We note that this hierachy of equations has the same structure as (7.43) and can therefore be solved in the same fashion, i.e. by successively putting the low order $n < l$ equal to zero in order to get the l'th eigen function.

Now the eigenvalue $R_l(E)$ which it is our main task to obtain, can also be expanded in powers of $i\hbar/2$:

$$R_l(E) = \exp\left\{\sum_{m=0}^{\infty}\left(\frac{i\hbar}{2}\right)^m C_l^{(m)}\right\}. \tag{7.53}$$

Expanding the exponential yields

$$R_l(E) = \exp(C_l^{(0)})\left(1 + \frac{i\hbar}{2}C_l^{(1)}\left(\frac{i\hbar}{2}\right)^2\left(\frac{1}{2}(C_l^{(1)})^2 + C_l^{(2)}\right) + ...\right) \tag{7.54}$$

The eigenvalue equation (7.26) in $\hbar$ expanded form now reads

$$\sum_{m=0}^{\infty}\left(\frac{i\hbar}{2}\right)^m \varphi^{l(m)}(t+T_p) =$$

$$\exp\left\{\sum_{m=0}^{\infty}\left(\frac{i\hbar}{2}\right)^m C_l^{(m)}\right\} \cdot \sum_{m=0}^{\infty}\left(\frac{i\hbar}{2}\right)^m \varphi^{l(m)}(t). \tag{7.55}$$

Expanding the eigenvalue like in (7.54) and collecting the terms of the same order in $\hbar$ yield a set of eigenequations

$$\begin{aligned}
\varphi^{l(0)}(t+T_p) &= \exp(C_l^{(0)})\varphi^{l(0)}(t), \\
\varphi^{l(1)}(t+T_p) &= \exp(C_l^{(0)})[\varphi^{l(1)}(t) + C_l^{(1)}\varphi^{l(0)}(t)], \\
\varphi^{l(2)}(t+T_p) &= \exp(C_l^{(0)})[\varphi^{l(2)}(t) + C_l^{(1)}\varphi^{l(1)}(t) \\
&\quad + (C_l^{(2)} + \frac{1}{2}(C_l^{(2)})^2)\varphi^{l(0)}(t)],
\end{aligned} \tag{7.56}$$

and so on. These equations are the conditions selecting the eigenvectors and eigenvalues and they hold for all t. Without loss of generality we can also assume that $\varphi^{l(0)}(0) = 1$ and $\varphi^{l(m)}(0) = 0$ for $m > 0$. By adding these assumptions we can simplify the equations (7.56):

$$\begin{aligned}
\varphi^{l(0)}(T_p) &= \exp(C_l^{(0)}), \\
\varphi^{l(1)}(T_p) &= \exp(C_l^{(0)})C_l^{(1)}, \\
\varphi^{l(2)}(T_p) &= \exp(C_l^{(0)})(C_l^{(2)} + \frac{1}{2}(C_l^{(2)})^2).
\end{aligned} \tag{7.57}$$

Now by solving the first of these equations (7.51) we get

$$\varphi_0^{0(0)}(t) = \varphi_0^{0(0)}(0)\exp\left(-\int_0^t \frac{1}{2}s_2(t)dt\right). \tag{7.58}$$

By using (7.57) we can read off the zeroth eigenvalue

$$C_0^{(0)} = -\int_0^{T_p} \frac{1}{2}s_2(t)dt. \tag{7.59}$$

The s_2 in general goes through $1/t$ type singularities. If this happens the integral should be carried out by principal value integration, as we saw in section ??.

The rest of the equations do not play a role in yielding the first eigenvalue. The solution $\varphi_0^{0(0)}(t)$ can be inserted into the next equation (7.51). Since equation (7.51) is a linear one driven by $\varphi_0^{0(0)}(t)$ its particular solution fulfills the condition (7.56). The rest of the equations can be solved the same way and we get the eigenamplitudes $\varphi_n^{0(0)}$. The rest of the semiclassical eigenvalues $R_l(E)$, $l > 0$ can be recovered by setting $\varphi_n^{l(0)} = 0$ for $n < l$ since the system of equations has the upper triangular structure as we saw in the previous section. Then the l-th semiclassical eigenvalue is given by

$$C_l^{(0)} = -\frac{2l+1}{2} \int_0^{T_p} s_2(t)dt. \tag{7.60}$$

The semiclassical eigenvalues are connected with the stability properties of the periodic orbits. For example the first ($l = 0$) eigenvalue is related to the product of the expanding eigenvalues[53]

$$\exp(C_0^{(0)}) = \frac{e^{i\mu_p\pi}}{|\prod_i \Lambda_i|^{1/2}} \tag{7.61}$$

and in the general l case we obtain

$$\exp(C_l^{(0)}) \quad = \quad \frac{e^{i\mu_p\pi}}{|\prod_i \Lambda_i|^{1/2}(\prod_i \Lambda_i)^l} \tag{7.62}$$

where Λ_i denotes the expanding ($\Lambda_i > 1$) eigenvalues of the linear stability or Jacobi matrix of the periodic orbit and ν_p is the Maslov index of the periodic orbit. The Maslov phase comes from the singularities of $s_2(t)$ (see ref.[53].) The product

$$\begin{aligned}
\Delta(E) \quad &= \quad \prod_p \prod_l (1 - \exp(iS_p/\hbar + C_l^{(0)})) \\
&= \quad \prod_p \prod_{l=0}^{\infty} (1 - \frac{\exp(iS_p/\hbar + i\mu_p\pi)}{|\prod_i \Lambda_i|^{1/2}(\prod_i \Lambda_i)^l})
\end{aligned}$$

$$\tag{7.63}$$

in this approximation is the previously obtained Gutzwiller-Voros zeta function.

7.6   The $\hbar$ correction equations

By following the strategy outlined in section (7.2) we have now finished the semiclassical part where we put $\hbar = 0$ in all the equations. As we have demonstrated we end up (not surprisingly) with the usual Gutzwiller Voros results.

After the calculation of the local semiclassical eigenvalues and eigenvectors we can now concentrate on the main item: to find $\hbar$ corrections to the semiclassical eigenvalues. As mentioned in section (7.2) we can use the semiclassical results to find the first $\hbar$ correction by inserting them in the next level of approximation.

The differential equations connecting the $m + 1$-th order amplitudes with the m-th order amplitudes are

$$\dot{\varphi}_n^{(m+1)} - \varphi_{n+1}^{(m+1)}\dot{q} \;+$$

$$\sum_{l=0}^{n} \frac{n!}{(n-l)!l!} \left(\varphi_{n-l+1}^{(m+1)}s_{l+1} + \frac{1}{2}\varphi_{n-l}^{(m+1)}s_{l+2} \right) - \varphi_{n+2}^{(m)} \;=\; 0. \tag{7.64}$$

which we get from the original amplitude equations (7.19), or (7.40) which still contains the $\hbar$ term. Again, using (7.32) we can reduce these equations

$$\begin{aligned}
\dot{\varphi}_0^{(m+1)} &= -\frac{s_2}{2}\varphi_0^{(m+1)} + \varphi_2^{(m)}, \\
\dot{\varphi}_1^{(m+1)} &= -\frac{3s_2}{2}\varphi_1^{(m+1)} - \frac{s_3}{2}\varphi_0^{(m+1)} + \varphi_3^{(m)}, \\
\dot{\varphi}_2^{(m+1)} &= -\frac{5s_2}{2}\varphi_2^{(m+1)} - 2s_3\varphi_1^{(m+1)} - \frac{s_4}{2}\varphi_0^{(m+1)} + \varphi_4^{(m)},
\end{aligned} \tag{7.65}$$

and so on. These equations are linear and have the general form

$$\dot{\varphi}_n^{(m+1)} = -\frac{(2n+1)s_2}{2}\varphi_n^{(m+1)} + ... + \varphi_{n+2}^{(m)}. \tag{7.66}$$

Inserting the eigenamplitudes $\varphi_n^{l(m)}(t)$ we get linear driven equations for the next order of the amplitudes. The solutions of these equations, which satisfy the conditions of type (7.56), yield the corrections $C_l^{(m)}$ of the semiclassical eigenvalues $C_l^{(0)}$.

In the following we just want to calculate the first $\hbar$ correction $C_l^{(1)}$ to the eigenvalues R_l. To do this we have to proceed in the following way

1. First we observe from (7.57) that $C_l^{(1)}$ can be obtained if we can find $\varphi^{l(1)}(t)$. More precisely, it suffices to find $\varphi_0^{l(1)}(t)$ since all the expansion coefficients in $\varphi^{l(1)}$ decays with the same ratio during one period. This means that we just have to solve equation (7.65) with $m = 0$.

2. From equation (7.65) we see that this implies that we need $\varphi_2^{l(0)}$, that is, the zeroth order in $\hbar$ or semiclassical solution of the l'th eigenfunction to the second order in the powerseries expansion. To get this, we then have to solve the equations (7.51 - 7.52) successively for the l'th eigenfunction.

3. Finaly we see from equation (7.52) that the above item 2. requires that we solve the Hamilton-Jacobi equation (7.18) up to fourth order to provide us with s_1, s_2, s_3 and s_4.

In the following we shall refer to the above list as the *prescription* to obtain
the first order $\hbar$ correction to the local eigenvalues. Of course, to get the first
$\hbar$ correction, one should start from the last item and finally end up with

$$C_l^{(1)} \quad = \quad \frac{\varphi^{l(1)}(T_p)}{\exp(C_l^{(0)})}. \tag{7.67}$$

The higher order $\hbar$ corrections can be found in a similar fashion by observing
which ingredients are needed in equation (7.57) to provide us with $C_l^{(2)}$ and so
on.

As a consequence of the above hierarchy of equations one has to solve, it
is increasingly difficult to get corrections to the eigenvalues corresponding to
large l. It is more convenient to reorganize the quantum Selberg product as a
product of quantum inverse zeta functions

$$\Delta(E) = \prod_l \zeta_l^{-1}(E) \tag{7.68}$$

where the quantum zeta functions are defined by

$$\zeta_l^{-1}(E) = \prod_p \left(1 - \exp(iS_p(E)/\hbar + \sum_m (i\hbar/2)^m C_l^{p(m)}(E))\right). \tag{7.69}$$

These zeta functions are the quantum generalizations of the Ruelle zeta functions[45,
3]. The leading resonances and the eigenenergies can be computed from the ze-
roes of the $l = 0$ quantum zeta function. The curvature expansion explained in
section (3.1) can also be applied using the new quantum mechanical weights

$$t_p = \exp\left(iS_p(E)/\hbar + \sum_m (i\hbar/2)^m C_0^{p(m)}(E)\right). \tag{7.70}$$

In the next section we show how the method can be applied to obtain the
first $\hbar$ correction $C_l^{(1)}$ in the case of two-dimensional billards.

7.7   Billards

To apply the theory on billiard systems we first have to discuss some special
features of these systems. In billiards the potential is not an analytic function:
the Dirichlet boundary condition for the wave function on a hard wall implies
that the wave function should vanish on the wall. Our approach here is basically
to trace a wave packet along the classical trajectory in the configuration space.
When the packet hits the wall, the incoming wave function at time t is given
by the packet right before the collision, evaluated on the wall

$$\psi_{in}(x(s), y(s), t) = \varphi(x(s), y(s), t_{-0})e^{iS((x(s), y(s), t_{-0})/\hbar}, \tag{7.71}$$

where $(x(s), y(s))$ is some analytic parametrization of the wall around the classical point of reflection. The outgoing wave function is the wave function right after the collision

$$\psi_{out}(x(s), y(s), t) = \varphi(x(s), y(s), t_{+0})e^{iS((x(s),y(s),t_{+0})/\hbar}. \tag{7.72}$$

The sum of the incoming and the outgoing wave functions should vanish on the hard wall due to the Dirichlet condition. This implies that the incoming and the outgoing amplitude and the phase are related by

$$\varphi(x(s), y(s), t_{-0}) = \varphi(x(s), y(s), t_{+0}) \tag{7.73}$$
$$S(x(s), y(s), t_{-0}) = S(x(s), y(s), t_{+0}) + i\pi. \tag{7.74}$$

These relations mean that the power series with respect to s of these functions are equal on both sides of the collision modulo the π phase shift. This phase shift can be interpreted as the Maslov phase coming from the hard wall.

The stationarity conditions for billards

In this paragraph we derive the stationarity conditions (7.44) and (7.45) for the special case two-dimensional of billards. We start by introducing the notation

$$\Delta x^n = (x - q_x(t))^n$$
$$\Delta y^m = (y - q_y(t))^m \tag{7.75}$$

where $(q_x(t), q_y(t))$ denotes the classical trajectory of the particle. We can then expand the phase function $S(x, y, t)$ as

$$\begin{aligned} S(x, y, t) &= S_0 + S_x \Delta x + S_y \Delta y \\ &+ \frac{1}{2}(S_{x^2}\Delta x^2 + 2S_{xy}\Delta x \Delta y + S_{y^2}\Delta y^2) \\ &+ \dots \end{aligned} \tag{7.76}$$

By choosing the right hand orientated coordinate system so that the x axis is directed along the particle trajectory we can already simplify the equations considerably since we then have

$$S_x = \dot{q}_x = 1$$
$$S_y = \dot{q}_y = 0 \tag{7.77}$$

because the gradient of the phase function is just equal to the momentum which we have set to be of unit size. From the general stationarity conditions (7.44) and (7.45) we then get

$$\begin{aligned} \frac{\partial S}{\partial t} &= \dot{S}_0 - \dot{q}_x S_x - \dot{q}_y S_y \\ &+ (\dot{S}_x - S_{x^2}\dot{q}_x - S_{xy}\dot{q}_y)\Delta x \\ &+ (\dot{S}_y - S_{xy}\dot{q}_x - S_{y^2}\dot{q}_y)\Delta y \\ &+ \dots \\ &= -E. \end{aligned} \tag{7.78}$$

From this we get by using (7.77) the relations

$$\begin{aligned}
\dot{S}_0 - \dot{q}_x S_x &= -E \\
\dot{S}_x - S_{x^2}\dot{q}_x &= 0 \\
\dot{S}_y - S_{xy}\dot{q}_x &= 0
\end{aligned} \tag{7.79}$$

where the last two relations can also be written

$$\begin{aligned}
S_{x^2} &= 0 \\
S_{xy} &= \frac{\dot{S}_y}{S_x}
\end{aligned} \tag{7.80}$$

since $\dot{S}_x = 0$ and $S_x = \dot{q}_x$. In general we get to order $\Delta x^n \Delta y^m$ where $n+m > 0$:

$$\begin{aligned}
\frac{\partial S}{\partial t}\Big|_{\Delta x^n \Delta y^m} &= \frac{1}{(n+m)!}\Big[\binom{n+m}{n}\dot{S}_{x^n y^m} - \dot{q}_y(m+1)\binom{n+m+1}{n}S_{x^n y^{m+1}} \\
&\quad - \dot{q}_x(n+1)\binom{n+m+1}{m}S_{x^{n+1}y^m}\Big] \\
&= 0
\end{aligned} \tag{7.81}$$

which by use of (7.77) gives the stationarity conditions

$$S_{x^{n+1}y^m} = \frac{\dot{S}_{x^n y^m}}{S_x}. \tag{7.82}$$

For the amplitude everything works in exactly the same fashion and we get

$$\varphi_{x^{n+1}y^m} = \frac{\dot{\varphi}_{x^n y^m}}{S_x}. \tag{7.83}$$

for all orders $n + m \geq 0$.

The Hamilton-Jacobi equation for billards

In order to solve the Hamilton-Jacobi equation along the periodic orbit we shall in the following first investigate how the phases change in the case of a bounce on the hard walls. Here we keep the calculation in two dimensions but the generalization to higher dimensions follows the same strategy. We start by expanding the phase function S around the periodic orbit in the neighbourhood of the bouncing point. The expansion must be to the fourth order since we need this in order to solve equation (7.52) according to the 3'rd item in the prescription. The expansion then reads:

$$\begin{aligned}
S(x, y; t) &= S_0 + S_x x + S_y y \\
&\quad + \frac{1}{2!}(S_{xx}x^2 + 2S_{xy}xy + S_{yy}y^2) \\
&\quad + \frac{1}{3!}(S_{xxx}x^3 + 3S_{xxy}x^2 y + 3S_{xyy}xy^2 + S_{yyy}y^3) \\
&\quad + \frac{1}{4!}(S_{xxxx}x^4 + 4S_{xxxy}x^3 y + 6S_{xxyy}x^2 y^2 + 4S_{xyyy}xy^3 + S_{yyyy}y^4) \\
&\quad + \dots
\end{aligned} \tag{7.84}$$

Here x and y are shorthand notations for the previously introduced notation $x = \Delta x = (x - q_x(t))$ and $y = \Delta y = (y - q_y(t))$, i.e. the deviations from the periodic orbit at time t in a right hand orientated coordinate systems with x-axis in to the momentum direction. According to the stationarity conditions (7.82) some of these terms are zero so we get:

$$
\begin{aligned}
S(x, y; t) \;=\;& S_0 + S_x x \\
+\;& \frac{1}{2!} S_{yy} y^2 \\
+\;& \frac{1}{3!}(3 S_{xyy} x y^2 + S_{yyy} y^3) \\
+\;& \frac{1}{4!}(6 S_{xxyy} x^2 y^2 + 4 S_{xyyy} x y^3 + S_{yyyy} y^4).
\end{aligned}
\tag{7.85}
$$

We should of course work with two such expansions, one corresponding to the incomming wave packet, which we shall denote S^-, and an expansion S^+ corresponding to the outgoing wave. Consequently we also have two different coordinate representations (x^{in}, y^{in}) and (x^{out}, y^{out}) each of wich are right hand orientated and with the x-axis in the momentum direction. It is in these coordinates that S^- and S^+ should be expanded. The two expansions S^- and S^+ should then coincide locally on the wall at the bouncing point. In the general case the wall is determined locally by the set of points $\{(x, y) | x(y) = C_2 y^2 / 2! + C_3 y^3 / 3! + C_4 y^4 / 4!\}$. where (x, y) now denotes a local intermediate coordinate system with y-axis tangent to the wall at the bouncing point. The geometry of the entire construction is shown in figure 7.1. It is in
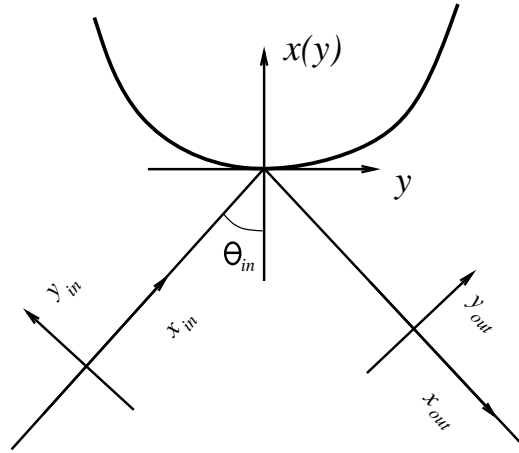
Figure 7.1: The coordinate systems introduced.

the local intermediate coordinates that we shall make the incoming and outging phase function coincide.

The incoming and outgoing coordinate systems are given by the set of transformation equations:

$$
\begin{aligned}
x^{in} &= \cos\theta x + \sin\theta y \\
y^{in} &= \sin\theta x - \cos\theta y
\end{aligned}
\tag{7.86}
$$

and

$$
\begin{aligned}
x^{out} &= -\cos\theta x + \sin\theta y \\
y^{out} &= \sin\theta x + \cos\theta y.
\end{aligned}
\tag{7.87}
$$

As mentioned, the transformations are chosen in order to get $S_x = p$ both before and after the bounce, and so that all the coordiante systems are right hand orientated. Taking each of the terms in (7.86) and expanding them in terms of the intermediate $(x(y), y)$ yields

$$
\begin{aligned}
x^{in} &= \sin\theta y + \cos\theta[C_2 y^2/2! + C_3 y^3/3! + C_4 y^4/4! + \ldots] \\
y^{in} &= -\cos\theta y + \sin\theta[C_2 y^2/2! + C_3 y^3/3! + C_4 y^4/4! + \ldots].
\end{aligned}
$$

Now, by expanding S^- and S^+ in the *intermediate* coordinate system, and by comparing terms of same order in y we can get the equations that describes the discontinuous change of the expansion coefficients at the bouncing point. To the second order in y we get:

$$
S_x \cos\theta \frac{C_2}{2} + \frac{1}{2!} S^-_{yy} \cos^2\theta = -S_x \cos\theta \frac{C_2}{2} + \frac{1}{2!} S^+_{yy} \cos^2\theta
\tag{7.88}
$$

which just yields the usual formula (6.41) for the Sinai-Bunimovich curvature:

$$
S^+_{yy} = S^-_{yy} + \frac{2C_2}{\cos\theta}.
\tag{7.89}
$$

To the third order in y we get :

$$
\begin{aligned}
S^+_{yyy} =\ & -S^-_{yyy} + \frac{2C_3 S_x}{\cos^2\theta} \\
& - \frac{3\sin\theta}{\cos^2\theta} C_2 (S^-_{yy} + S^+_{yy}) \\
& + \frac{3\sin\theta}{\cos\theta} (S^-_{xyy} - S^+_{xyy}),
\end{aligned}
\tag{7.90}
$$

and finally we get to the fourth order of y:

$$
\begin{aligned}
S^+_{yyyy} =\ & S^-_{yyyy} \\
& - 4\frac{\sin\theta}{\cos\theta}(S^-_{xyyy} + S^+_{xyyy}) \\
& + 6\frac{\sin^2\theta}{\cos^2\theta}(S^-_{xxyy} - S^+_{xxyy}) \\
& + 6\frac{\sin\theta}{\cos^2\theta}C_2(S^-_{yyy} - S^+_{yyy}) \\
& + 12(\frac{1}{2\cos\theta} - \frac{\sin^2\theta}{\cos^3\theta})C_2(S^-_{xyy} + S^+_{xyy}) \\
& + 3\frac{\sin^2\theta}{\cos^4\theta}C_2^2(S^-_{yy} - S^+_{yy}) \\
& - 4\frac{\sin\theta}{\cos^3\theta}C_3(S^-_{yy} + S^+_{yy}) \\
& + \frac{2C_4}{\cos^3\theta}.
\end{aligned}
\tag{7.91}
$$

As we see, the result of the discontinuous bounce evolution is still not a closed expression. In addition we should also obtain the bouncing rules for the mixed derivatives. This is accomplished by applying the stationarity conditions (7.82). For instance we have

$$S_{xyy} = \frac{\dot{S}_{yy}}{S_x} = -\frac{S_{yy}^2}{S_x},$$

which gives us

$$S_{xyy}^+ = -\frac{(S_{yy}^- + \frac{2C_2}{\cos\theta})^2}{S_x}, \tag{7.92}$$

and similarly we get

$$S_{xyyy} = \frac{\dot{S}_{yyy}}{S_x} = -\frac{3 S_{yy} S_{yyy}}{S_x},$$

and

$$S_{xxyy} = \frac{\dot{S}_{xyy}}{S_x} = \frac{\ddot{S}_{yy}}{S_x^2} = -\frac{\dot{S}_{yy}^2}{S_x^2} = \frac{2 S_{yy}^3}{S_x^2}.$$

This concludes our derivation of the discontinuous evolution of the coefficients $S_{x^n y^m}$, at the bouncing points.

To derive the continuous time evolution we have to solve the Hamilton-Jacobi equations (7.18). Since we can find the mixed coefficients by the stationarity conditions (7.82), we only have to solve for the S_{y^n} coefficients. Inserting the expansion (7.86) into the Hamilton-Jacobi equations (7.18) the equations for these becomes

$$\dot{S}_{yy} + S_{yy}^2 = 0$$
$$\dot{S}_{yyy} + 3 S_{yy} S_{yyy} = 0$$
$$\dot{S}_{yyyy} + 4 S_{yyyyy} S_{yy} + 3 S_{yyy}^2 + 3 S_{xyy}^2 = 0. \tag{7.93}$$

since there is no potential present except for the hard walls. By integration these equations immediately yield

$$S_{yy}(t) = \frac{1}{t + t_0}$$
$$S_{yyy}(t) = \frac{A}{(t + t_0)^3} \tag{7.94}$$
$$S_{yyyy}(t) = -\frac{3}{(t + t_0)^3} + \frac{B}{(t + t_0)^4} + \frac{3 A^2}{(t + t_0)^5}$$

where the constants are to be determined from the initial values of the coefficients of the phase function. We now have the necessary ingredients for solving the Hamilton-Jacobi equation to the 4'th order: between the bounces we use the continuous time evolution (7.95), and on the bouncing points we use the derived bouncing relations (7.89),(7.90) and (7.91) to follow evolution of the phase function.

The amplitude evolution for billards

Next we need to solve the amplitude equations. As before, we start by looking at the amplitude and how its expansion coefficients change when the wave goes through a bounce. This is done by using exactly the same procedure as outlined above. For simplicity we start by only looking at the 0'th order $l = 0$ eigenfunction. We first expand the amplitude in the same fashion as we expanded the action. According to the second item in the *prescription* we only need the expansion to second order:

$$\varphi(x, y) \quad = \quad \varphi_0 + \varphi_x x + \varphi_y y + \frac{1}{2!}(\varphi_{xx} x^2 + 2\varphi_{xy} xy + \varphi_{yy} y^2) + \ldots$$

Here again we actually have two expansions φ^- and φ^+ corresponding to the incomming and the outgoing wavepacket. By comparing the different powers of y in the intermediate coordinate system we get:

$$\varphi_0^+ \quad = \quad \varphi_0^- \tag{7.95}$$
$$\varphi_x^+ \sin\theta + \varphi_y^+ \cos\theta \quad = \quad \varphi_x^- \sin\theta - \varphi_y^- \cos\theta \tag{7.96}$$

for the zeroth and first order, and

$$\varphi_x^- \cos\theta \frac{C_2}{2} + \varphi_y^- \sin\theta \frac{C_2}{2} \quad + \quad \varphi_{xx}^- \sin^2\theta \frac{1}{2} - \sin\theta\cos\theta\varphi_{xy}^- + \frac{1}{2}\varphi_{yy}^- \cos^2\theta =$$
$$-\varphi_x^+ \cos\theta \frac{C_2}{2} + \varphi_y^+ \sin\theta \frac{C_2}{2} \quad + \quad \varphi_{xx}^+ \sin^2\theta \frac{1}{2} + \sin\theta\cos\theta\varphi_{xy}^+ + \frac{1}{2}\varphi_{yy}^+ \cos^2\theta$$

for the second order in y. This gives the set of bounce equations:

$$\varphi_0^+ \quad = \quad \varphi_0^-$$
$$\varphi_y^+ \quad = \quad -\varphi_y^- + \tan\theta(\varphi_x^- - \varphi_x^+) \tag{7.97}$$

and

$$\varphi_{yy}^+ \quad = \quad \varphi_{yy}^- - 2\tan\theta(\varphi_{xy}^- + \varphi_{xy}^+) + \tan^2\theta(\varphi_{xx}^- - \varphi_{xx}^+)$$
$$+ \quad C_2 \frac{\sin\theta}{\cos^2\theta}(\varphi_y^- - \varphi_y^+) + \frac{C_2}{\cos\theta}(\varphi_x^- + \varphi_x^+). \tag{7.98}$$

To reduce these equations further we have to make use of the stationarity equations for the amplitude (7.83). The ones we need are given by

$$\dot{\varphi}_0 - \varphi_x S_x \quad = \quad 0,$$
$$\dot{\varphi}_x - \varphi_{xx} S_x \quad = \quad 0,$$
$$\dot{\varphi}_y - \varphi_{xy} S_x \quad = \quad 0.$$
$$\tag{7.99}$$

These equations together with the semiclassical amplitude equations (7.51 - 7.52) for the φ_{y^n}'s yield the reductions. In the two-dimensional case the semiclassical amplitude equations becomes

$$\dot{\varphi}_0 + \frac{1}{2}S_{yy}\varphi_0 \quad = \quad 0$$

$$\dot{\varphi}_y + \frac{3}{2}S_{yy}\varphi_y + \frac{1}{2}S_{yyy}\varphi_0 \;\; = \;\; 0 \tag{7.100}$$

$$\dot{\varphi}_{yy} + \frac{5}{2}S_{yy}\varphi_{yy} + S_{yyx}\varphi_x \;\; +$$

$$2S_{yyy}\varphi_y + \frac{1}{2}(S_{xxyy} + S_{yyyy})\varphi_0 \;\; = \;\; 0$$

Using these equations and the above stationarity conditions we get

$$\varphi_x^{+/-} \;\; = \;\; \frac{\dot{\varphi}_0^{+/-}}{p} = \frac{-S_{yy}^{+/-}\varphi_0^{+/-}}{2p}.$$

By using this reduction and the previously obtained expressions for the S_y's we can derive the explicit bouncing relations:

$$\varphi_0^+ \;\; = \;\; \varphi_0^-, \tag{7.101}$$

$$\varphi_y^+ \;\; = \;\; -\varphi_y^- + \frac{C_2 \sin\theta}{\cos^2\theta}\varphi_0. \tag{7.102}$$

Similarly we have

$$\varphi_{xx} \;\; = \;\; \dot{\varphi}_x = -\frac{1}{2}\frac{d}{dt}S_{yy}\varphi_0 = \frac{3}{4}S_{yy}^2\varphi_0, \tag{7.103}$$

and

$$\varphi_{xy} \;\; = \;\; \dot{\varphi}_y = -\frac{1}{2}(3S_{yy}\varphi_y + S_{yyy}\varphi_0). \tag{7.104}$$

Introducing these relations in (7.97) we get

$$\begin{aligned}
\varphi_{yy}^+ \;\; = \;\; & \varphi_{yy}^- \\
& + \;\; \tan\theta[3(S_{yy}^-\varphi_y^- + S_{yy}^+\varphi_y^+) + (S_{yyy}^- + S_{yyy}^+)\varphi_0] \\
& + \;\; \tan^2\theta\frac{3}{4}[(S_{yy}^-)^2 - (S_{yy}^+)^2] \\
& + \;\; C_2\frac{\sin\theta}{\cos^2\theta}(\varphi_y^- - \varphi_y^+) \\
& - \;\; \frac{C_2}{2\cos\theta}(S_{yy}^- + S_{yy}^+)\varphi_0,
\end{aligned} \tag{7.105}$$

which ends our set of bouncing rules for the amplitude coefficients up to second order.

To find the continuous time evolution of the amplitudes we can use the solution of the Hamilton-Jacobi equation to drive the differential equations (7.101) for the amplitudes. From the first equation in (7.101) and the initial condition $\varphi_0(0) = 1$ we get

$$\varphi_0(t) \;\; = \;\; \frac{Et_0^{1/2}}{(t + t_0)^{1/2}}. \tag{7.106}$$

Substituting this solution into the next equation yields

$$\varphi_y(t) \;\; = \;\; \frac{E}{(t + t_0)^{3/2}}\left[C + \frac{\frac{1}{2}At_0^{1/2}}{(t + t_0)}\right], \tag{7.107}$$

and finally after yet another substitution and a tedious calculation we get

$$\varphi_{yy}(t) \quad = \quad \frac{E}{(t+t_0)^{5/2}}\left[D + \frac{2AC + \frac{1}{2}Bt_0^{1/2}}{(t+t_0)} + \frac{\frac{5}{4}A^2 t_0^{1/2}}{(t+t_0)^2}\right]. \qquad (7.108)$$

In the last calculation we have made use of the stationarity conditions for S_{xyy} and S_{xxyy} in equation (7.101). Again the constants C, D and E are to be determined from the initial conditions of the amplitude coefficients and the previously determined constants from the phase functions. This concludes our derivation of the evolution equations for the $l = 0$ amplitude coefficients.

The general l'th order amplitude equations for billards

Next we shall obtain the analogous amplitude evolution equations for general l'th order eigenfunction. The l'th order eigenfunction of course obeys the same amplitude evolution equations as the $l = 0$ eigenfunction. However, if we just start with some arbitrary function and iterate the amplitude evolution equations, we will in general end up just with the $l = 0$ eigenfunction since this is given by the leading eigenvalue of the evolution operator. This is completely analogous to iterating a matrix $\mathbf{A}$ on a final dimensional vector $\mathbf{x}$. This analogy also holds for the subleading eigenfunctions: if we subtract the leading eigenvector from $\mathbf{x}$ and iterate with $\mathbf{A}$ we will generate the next-to-leading eigenvector etc. In our evolution operator (the amplitude equations) this subtraction of the leading eigenfunction is quite straightforward. In the semiclassical hierarchy of equations (7.51-7.52) we can simply get the $l = 1$ eigenfunction by first setting $\varphi_0^{(0)} = 0$, and then iterating. This is because of the triangular structure of the system of equations. If we keep the $\varphi_0^{(0)}$ term we cannot get anything but the $l = 0$ eigenfunction, but by removing this part we get the next eigenfunction. To get the l'th eigenfunction one should therefore set all the coefficients $\varphi_0^{(0)}, \ldots, \varphi_{l-1}^{(0)}$ equal to zero and then iterate the evolution operator on some initial wavefunction. By using these considerations we can also characterize the l'th order eigenfunction by being the one for which all the first $l - 1$ expansion coefficients are identical zero, and which has $\varphi_l^{(0)} \neq 0$.

In two dimensions the situation is completely the same, except that we have two indeces on our expansion coefficients $\varphi_{x^n y^m}$. We also should keep in mind that all the $\varphi_{x^n y^m}$ can be obtained from pure φ_{y^m} coefficients by using the stationarity conditions (7.83). Thus it is sufficient to consider only the φ_{y^m} coefficients. The specific continuous time evolution of the amplitude coefficients of the l'th order eigenfunction can therefore be derived from the original semiclassical equation (7.50)

$$\varphi_t + (S_x\varphi_x + S_y\varphi_y) + \frac{1}{2}(S_{xx} + S_{yy})\varphi \quad = \quad 0 \qquad (7.109)$$

by taking the $\frac{\partial^l}{\partial y^l}$ derivative and using that we can set $\varphi_{y^k x^m} = 0$ for $k < l$. Also using the stationarity equations

$$\dot{\varphi}_{y^k x^m} \quad = \quad \varphi_{y^k x^{m+1}}$$

we get

$$
\dot{\varphi}_{y^l} = -(l + \frac{1}{2}) S_{y^2} \varphi_{y^l}
$$

$$
\dot{\varphi}_{y^{l+1}} = -(l + \frac{3}{2}) S_{y^2} \varphi_{y^{l+1}} - \frac{1}{2}(l+1)^2 S_{y^3} \varphi_{y^l}
$$

$$
\dot{\varphi}_{y^{l+2}} = -(l + \frac{5}{2}) S_{y^2} \varphi_{y^{l+2}} - \frac{1}{2}(l+1)^2 S_{y^3} \varphi_{y^{l+1}}
$$

$$
- \frac{(l+2)(l+1)}{2}(\frac{l}{3} + \frac{1}{2}) S_{y^4} \varphi_{y^l}
$$

$$
- \frac{(l+2)(l+1)}{4} S_{x^2 y^2} \varphi_{y^l}
$$

$$
- \frac{(l+2)(l+1)}{2} S_{xy^2} \varphi_{xy^l} \tag{7.110}
$$

for the semiclassical equations. The solutions to these equations are easily obtained

$$
\varphi_{y^l}(t) = E \left(\frac{t_0}{t + t_0} \right)^{l+1/2}
$$

$$
\varphi_{y^{l+1}}(t) = \frac{E}{(t + t_0)^{l+3/2}} \left[C + \frac{A}{2}(l+1)^2 t_0^{l+1/2} \frac{1}{t + t_0} \right]
$$

$$
\varphi_{y^{l+2}}(t) = \frac{E}{(t + t_0)^{l+5/2}} \{ D + \frac{1}{t + t_0}[\frac{(l+2)^2}{2} AC
$$

$$
+ \; Bt_0^{l+1/2} \frac{(l+2)(l+1)}{2}(\frac{l}{3} + \frac{1}{2})]
$$

$$
+ \; \frac{1}{2(t + t_0)^2} A^2 t_0^{l+1/2}[\frac{(l+2)^2(l+1)^2}{4}
$$

$$
+ \; \frac{3}{2}(l+2)(l+1)(\frac{l}{3} + \frac{1}{2})]\} \tag{7.111}
$$

Next we should derive the semiclassical bouncing equations for the amplitudes. The nonvanishing terms in φ^l are

$$
\varphi^l = \frac{y^l}{l!}[\varphi_{y^l} + \frac{1}{l+1}\varphi_{y^{l+1}} y + \frac{1}{(l+1)(l+2)}\varphi_{y^{l+2}} y^2
$$

$$
+ \; \varphi_{xy^l} x + \frac{1}{2}\varphi_{x^2 y^l} x^2 + \frac{1}{l+1}\varphi_{y^{l+1} x} yx], \tag{7.112}
$$

where we note the factor $\frac{y^l}{l!}$ in front of the expression. As usual we now expand the incoming and outgoing amplitude in the intermediate coordinate system and set

$$
\varphi_{in} = \varphi_{out} \tag{7.113}
$$

on the bouncing point on the wall. Because of the above factor $\frac{y^l}{l!}$ we can now write the bouncing condition

$$
\varphi_{y^l}^+ + \frac{1}{l+1}\varphi_{y^{l+1}}^+ y_{out} + \ldots = \left(\frac{y_{in}}{y_{out}} \right)^l \times [\varphi_{y^l}^- + \frac{1}{l+1}\varphi_{y^{l+1}}^- y_{in} + \ldots]
$$

Since to get the first correction where we only need $\varphi_2^{l(0)}$ according to second item in the recipe, we only have to compare terms up to the second order in y (on the wall). We therefore expand the fraction factor to second order in y. Using the coordinate transformations (7.86-7.87) this reads

$$
\begin{aligned}
\left(\frac{y_{in}}{y_{out}}\right)^l &= (-1)^l \left(\frac{1 - ay - by^2}{1 + ay + by^2}\right)^l \\
&= (-1)^l (1 - 2lay + 2l(la^2 - b)y^2 + \mathcal{O}(y^3)) \qquad (7.114)
\end{aligned}
$$

where

$$
a = \frac{C_2}{2}\tan\theta, \quad b = \frac{C_3}{6}\tan\theta
$$

The detailed equations (7.114) then become

$$
\begin{aligned}
\varphi_{y^l}^+ + y(\varphi_{y^l x}^+ \sin\theta + \frac{\varphi_{y^{l+1}}^+}{l+1}\cos\theta) \quad &+ \\
y^2(-\varphi_{xy^l}^+ \cos\theta\frac{C_2}{2} + \frac{\varphi_{y^{l+1}}^+}{l+1}\sin\theta\frac{C_2}{2} \quad &+ \\
\frac{1}{2}\sin^2\theta\varphi_{y^l x^2}^+ + \sin\theta\cos\theta\frac{\varphi_{xy^{l+1}}^+}{l+1} \quad &+ \\
\frac{\varphi_{y^{l+2}}^+ \cos^2\theta}{(l+1)(l+2)}) &= (-1)^l[1 - l\tan\theta C_2 y + 2l(l\frac{C_2^2\tan^2\theta}{4} - \frac{C_3}{6}\tan\theta)y^2] \\
&\times [\varphi_{y^l}^- + y(\varphi_{y^l x}^- \sin\theta - \frac{\varphi_{y^{l+1}}^-}{l+1}\cos\theta) \\
&+ y^2(\varphi_{xy^l}^- \cos\theta\frac{C_2}{2} + \frac{\varphi_{y^{l+1}}^-}{l+1}\sin\theta\frac{C_2}{2} \\
&+ \frac{1}{2}\sin^2\theta\varphi_{y^l x^2}^- - \sin\theta\cos\theta\frac{\varphi_{xy^{l+1}}^-}{l+1} \\
&+ \frac{\varphi_{y^{l+2}}^- \cos^2\theta}{(l+1)(l+2)})].
\end{aligned}
$$

This gives the equations

$$
\varphi_{y^l}^+ = (-1)^l \varphi_{y^l}^-, \qquad (7.115)
$$

$$
\varphi_{y^{l+1}}^+ = (-1)^{l+1}(\varphi_{y^{l+1}}^- - C_2(l+1)^2\frac{\tan\theta}{\cos\theta}\varphi_{y^l}^-), \qquad (7.116)
$$

to the zeroth and first order in y, and

$$
\begin{aligned}
\varphi_{y^{l+2}}^+ &= (-1)^l \varphi_{y^{l+2}}^- \\
&+ ((-1)^l \varphi_{xy^l}^- + \varphi_{xy^l}^+)\frac{C_2(l+1)(l+2)}{2\cos\theta}
\end{aligned}
$$

$$+ \quad ((-1)^l \varphi^-_{y^{l+1}} - \varphi^+_{y^{l+1}}) \frac{\sin\theta\, C_2(l+2)}{2\cos^2\theta}$$

$$+ \quad ((-1)^l \varphi^-_{y^l x^2} - \varphi^+_{y^l x^2}) \frac{(l+1)(l+2)\tan^2\theta}{2}$$

$$- \quad ((-1)^l \varphi^-_{xy^{l+1}} + \varphi^+_{xy^{l+1}})(l+2)\tan\theta$$

$$- \quad (-1)^l ((\varphi^-_{y^l x}\sin\theta - \frac{\varphi^-_{y^{l+1}}}{(l+1)}\cos\theta) \frac{l\tan\theta\, C_2(l+1)(l+2)}{\cos^2\theta}$$

$$+ \quad (-1)^l (\frac{lC_2^2\tan^2\theta}{4} - \frac{C_3\tan\theta}{6}) \varphi^-_{y^l} \frac{2l(l+1)(l+2)}{\cos^2\theta}, \qquad (7.117)$$

to the second order in y.

The last equation can of course again be simplified by using the stationarity conditions for the mixed derivatives, which yields a formula similar to (7.105). This ends our derivation of the discontinuous evolution of the l'th order amplitude coefficients at the bouncing points.

The first $\hbar$ correction for billards

To get the first $\hbar$ correction $C_l^{(1)}$ to the local eigenvalues R_l we use (7.57) and get

$$C_l^{(1)} \quad = \quad \frac{\varphi^{l(1)}(T_p)}{\exp(C_l^{(0)})}, \qquad (7.118)$$

To get the time dependance of the full function $\varphi^{l(1)}$ we have to solve the amplitude equation to first order in $\hbar$ and to order x^l in the one-dimensional case. Since we shall later need the result for 2-dimensional billard systems we here show how the calculation goes in this case . This also illustrates how the stationarity conditions (7.82,7.83) are applied in general. In two dimensions we therefore have to solve the amplitude equation up to order $x^m y^n$ where $m + n = l$. From the stationarity conditions (7.83) we get

$$\dot{\varphi}_{x^m y^n} \quad = \quad S_x \varphi_{x^{m+1} y^n} \qquad (7.119)$$

which can the be used to reduce all the mixed amplitude coefficients to time derivatives of pure φ_{y^n} coefficients. It is therefore sufficient to look at the equation of order y^l. Now the original amplitude equation reads

$$\partial_t \varphi + \nabla\varphi\nabla S + \frac{1}{2}\varphi\Delta S - \frac{i\hbar}{2}\Delta\varphi = 0. \qquad (7.120)$$

We now should find out which ingredients are needed in this equation to get the first order in $\hbar$ and the order y^l. Since we are dealing with the l'th solution we can put all the amplitude coefficients $\varphi_{x^n y^m} = 0$ for $m < l$, because of the triangular structure of the hierarchy of equations. This simplifies the situation considerably. Next we can select our coordinate system so that the x-axis is

directed along the momentum direction. This means that the zeroth order of the gradient of the phase function will take the form

$$
\begin{aligned}
\nabla S &= \vec{p} \\
&= (1,0),
\end{aligned} \tag{7.121}
$$

where $\vec{p}$ is the momentum set to $|\vec{p}| = 1$.

Expandig the amplitude in a power series around the periodic orbit like in (??) we get the following necessary ingredients

$$
\begin{aligned}
\dot{\varphi}^l &= \frac{y^l}{l!}(\dot{\varphi}_{y^l} - \dot{x}_{cl}\varphi_{y^l x} + \dots) \\
\nabla \varphi^l &= (\varphi_{y^l x}y^l/l! + \dots, \varphi_{y^{l+1}}y^l/l! + \varphi_{y^l}y^{l-1}l/l! + \dots) \\
\Delta \varphi^l &= \frac{y^l}{l!}(\varphi_{y^l x^2} + \varphi_{y^{l+2}}) + \dots,
\end{aligned} \tag{7.122}
$$

and for the phase function we get similarly

$$
\begin{aligned}
\nabla S &= (S_x + S_{xy} + \dots, S_y + S_{y^2}y + \dots) \\
\Delta S &= S_{x^2} + S_{y^2} + \dots \\
&= S_{y^2} + \dots,
\end{aligned} \tag{7.123}
$$

where we in the last equation used that $S_{x^2} = 0$ since by the stationarity conditions this is proportional to the time derivative of S_x which is zero since S_x is the constant momentum p_x . The differential equation for the l'th amplitude function now reads

$$
\dot{\varphi}_{y^l}^{(1)} - \dot{x}_{cl}\varphi_{y^l x}^{(1)} + \varphi_{y^l x}^{(1)}S_x + S_y\varphi_{y^{l+1}}^{(1)} + lS_{y^2}\varphi_{y^l}^{(1)} = \varphi_{y^l x^2}^{(0)} + \varphi_{y^{l+2}}^{(0)} \tag{7.124}
$$

to the first order in $\hbar$. This implies

$$
\dot{\varphi}_{y^l}^{(1)} + \left(l + \frac{1}{2}\right)S_{y^2}\varphi_{y^l}^{(1)} = \varphi_{y^l x^2}^{(0)} + \varphi_{y^{l+2}}^{(0)} \tag{7.125}
$$

to the zeroth order in $\hbar$ we get analogously

$$
\dot{\varphi}_{y^l}^{(0)} + \left(l + \frac{1}{2}\right)S_{y^2}\varphi_{y^l}^{(0)} = 0 \tag{7.126}
$$

The last equation immediately yields

$$
\begin{aligned}
\varphi_{y^l}^{(0)}(t) &= \exp\left(-\frac{2l+1}{2}\int_0^t S_{y^2}dt'\right) \\
&= \exp(C_l^{(0)})
\end{aligned}
$$

which is the two-dimensional equivalent to the result (7.60). We can therefore write the solution of equation (7.125) as

$$
\varphi_{y^l}^{(1)}(t) = \exp\left(-\frac{2l+1}{2}\int_0^t S_{y^2}dt'\right)\int_0^t (\varphi_{y^l x^2}^{(0)} + \varphi_{y^{l+2}}^{(0)})\exp\left(\frac{2l+1}{2}\int_0^t S_{y^2}dt'\right)
$$

$$
\tag{7.127}
$$

and the first correction finally reads

$$C_l^{(1)} = \int_0^{T_p} \frac{(\varphi_{y^l x^2}^{(0)} + \varphi_{y^{l+2}}^{(0)})}{\varphi_{y^l}^{(0)}} dt \tag{7.128}$$

This concludes the derivation of the first order $\hbar$ correction term in the case of two dimensional billiards. To implement this integration one should determine the phase and amplitude coefficients for each individual periodic orbit. This we shall do in section (7.7).

7.7.1 A numerical algorithm to calculate the first $\hbar$ correction

The above derivations now allow us to follow an initial wave along the periodic orbit. Each such iteration changes the initial amplitude coefficients and will for almost all initial conditions converge to the leading eigenfunction of the evolution operator. To get the action coefficients and the leading amplitude function we can therefore just select a set of initial S and φ coefficients and iterate the evolution equations derived above while properly normalizing the amplitudes after each iteration.

Now the iteration sequence goes as follows: choose initial (random) values of the derivative constants of the action function. From these you calculate the initial values of t_0, A and B:

$$t_0 = 1/S_{yy}(0)$$
$$A = S_{yyy}(0)t_0^3$$
$$B = S_{yyyy}(0)t_0^4 + 3t_0 - \frac{3A^2}{t_0}$$

Then you evolve the S_{y^n}'s to the first bouncing point is reached. Here one makes use of the derived bouncing relations to establish the $S_{y^n}(t_i^+)$ values. These are then used to calculate the new constants t_0, A and B. In this way one can by a few iterations around the periodic orbit obtain the action function corresponding to the local Schrödinger problem. Actually the calculation can be speeded up a bit since we can calculate the S_{yy} term directly from the solution of the rational fraction transformation of the curvature matrix $\mathbf{M}$ which were derived in section 5.3.1. In the two dimensional case this can be demonstrated very easily: First we have to find the Jacobian of the periodic orbit which we also need to in the case of the usual Gutzwiller-Voros zeta function. To find $\mathbf{M}$ we need in general to work on the symplectic matrix $\mathbf{T}$ that diagonalizes $\mathbf{J}$. We know that $\mathbf{T}^{-1}$ must contain the eigenvectors of $\mathbf{J}$ so that we can write

$$\mathbf{T}^{-1} = \begin{bmatrix} u_1 & s_1 \\ u_2 & s_2 \end{bmatrix} \tag{7.129}$$

where $\mathbf{u}$ is the unstable and $\mathbf{s}$ is the stable eigenvector. Then $\mathbf{T}$ is given by

$$\mathbf{T} = \frac{1}{\det \mathbf{T}^{-1}} \begin{bmatrix} s_2 & -s_1 \\ -u_2 & u_1 \end{bmatrix} \tag{7.130}$$

and from the solution formula (5.62) for **M** we obtain

$$
\begin{aligned}
\mathbf{M} &= -\mathbf{T}_{pp}\mathbf{T}_{pq}^{-1} \\
&= u_2/u_1 \quad \text{or} \quad s_2/s_1
\end{aligned}
\tag{7.131}
$$

where the last solution corresponds to interchanging the rows of **T**. Here in the two dimensional case the **M** solutions are then just the slopes of the invariant manifolds at the periodic orbit (see fig. refmanifolds in appendix 9.1). To get an explicit expression for **M** (which in this case is actually just the Sinai Bunimovic curvature κ) in terms of the ingredients of the Jacobian and the stability, we note that the eigendirections can also be represented in the form

$$
\begin{aligned}
\tilde{\mathbf{u}} &= \left[\begin{array}{c} 1 \\ \kappa_u \end{array}\right] \\
\tilde{\mathbf{s}} &= \left[\begin{array}{c} 1 \\ \kappa_s \end{array}\right]
\end{aligned}
$$

and we then have

$$
\mathbf{J}\tilde{\mathbf{u}} = \Lambda\tilde{\mathbf{u}}
$$

which then gives

$$
\kappa_u = (\Lambda - J_{11})/J_{12}
\tag{7.132}
$$

and similarly for the stable direction. For the '0' orbit of the $R:a = 6.0$ 3-disk system the exact calculation yields $\kappa_u = 2.224744871\ldots$, whereas the numerical algorithm sketched above gives $\kappa_u = 2.224744871\ldots$ after 25 iterations. This is of course the same result (7.38) as we obtained in section (7.3) by iterating the rational fraction transformation for the Sinai Bunimovic curvature. In higher dimensions the **M** solution formula (5.62) of course provides this first step as well.

The evolution of the amplitudes take place in exactly the same fashion. The equations for the constants are here:

$$
\begin{aligned}
E &= a(0) \equiv 1 \\
C &= \frac{t_0^{3/2}}{E}\varphi_y(0) - \frac{A}{2t^{1/2}} \\
D &= \frac{t_0^{5/2}}{E}\varphi_{yy}(0) - \frac{2AC + \frac{Bt_0^{1/2}}{2}}{t_0} - \frac{5A^2}{4t_0^{3/2}}
\end{aligned}
\tag{7.133}
$$

where the $a(0)$ constant is fixed by normalization after each iteration.

When these calculations are done we have just to calculate the correction $C_l^{(1)}$ by means of the integral (7.128). A program that performs this calculation is listed in appendix 9.3.

Putting the results of the constants t_0, A, B, C, D and E into the expression (7.128) for the first order $\hbar$ correction we get

$$
\begin{aligned}
C_l^{(1)} &= \int_0^{T_p} \frac{\varphi_{y^{l+2}} + \varphi_{y^l x^2}}{\varphi_{y^l}} dt \\
&= \int_0^{T_p} dt \frac{1}{(t+t_0)^2} \left[\frac{D}{t_0^{l+1/2}} + (l+\frac{1}{2})(l+\frac{3}{2}) \right] \\
&+ \frac{1}{(t+t_0)^3} \left[\frac{(l+2)^2}{2} \frac{AC}{t_0^{(l+1/2)}} + B \frac{(l+1)(l+2)}{2}(\frac{l}{3} + +\frac{1}{2}) \right] \\
&+ \frac{1}{(t+t_0)^4} \frac{A^2}{2} \left\{ \frac{(l+1)^2(l+2)^2}{4} + \frac{(l+1)(l+2)}{2}(\frac{l}{3} + +\frac{1}{2})3 \right\}
\end{aligned}
$$

(7.134)

which finally gives

$$
\begin{aligned}
C_l^{(1)} &= \left[(l+\frac{1}{2})(l+\frac{3}{2}) + \frac{D}{t_0^{(l+1/2)}} \right] \frac{t}{t_0(t+t_0)} \\
&+ \left[(l+2)^2(\frac{AC}{4})/ \left(t_0(l+\frac{1}{2}) \right) + (l+2)(l+1)(l+\frac{3}{2})B/12 \right] \\
&\times \frac{t(t+2t_0)}{(t_0(t+t_0))^2} \\
&+ (l+1)(l+2) \left[(l^2+3l+2)\frac{1}{2} + l + \frac{3}{2} \right] \frac{A^2}{12} \\
&\times (\frac{1}{t_0^3} - \frac{1}{(t+t_0)^3})
\end{aligned}
$$

(7.135)

7.8 Application to the 3-disk system

To test our method outlined above we here investigate how it works on the three disk scattering system. Taking as starting point the $\hbar$ corrected spectral determinant (7.68)

$$
\Delta(E) = \prod_l \zeta_l^{-1}(E) \tag{7.136}
$$

we can study either the entire determinant or the individual quantum zetafunctions

$$
\zeta_l^{-1}(E) = \prod_p \left(1 - \exp(iS_p(E)/\hbar + \sum_m (i\hbar/2)^m C_l^{p(m)}(E)) \right). \tag{7.137}
$$

where we can get the leading resonances from the $l = 0$ zeta function.

For the 3-disk system our calculation involved the 226 shortest periodic orbits of the system including all cycles up to topological length 10. We computed the corrections to these orbits in the fundmental domain, since our method

makes it possible to utilize the symmetry reduction of Cvitanović and Eck-
hardt [16]. The results can be compared to the exact quantum resonances as
well as to the pure semiclassical calculation based on the usual Gutzwiller Voros
determinant. We have studied the leading scattering resonances in the region
$0 \leq \mathrm{Re}k \leq 200$ and $-0.5 \leq \mathrm{Im}k \leq 0$, in the complex k-plane, by using the
Gutzwiller-Voros zeta function and also by just using the leading quantum zeta
function $\zeta^{-1}(k)$ with and without the $\hbar$ corrections. The latter has been done
for comparison reasons with Ref. [33].

We start by considering the shortest periodic orbit in the 3-disk system,
which is the one bouncing back and forth between the same two disks. The
situation is here similar to that in the confocal hyperbola problem, where the
first correction term to the Gutzwiller trace formula has been computed numer-
ically [59]. The geometry of the orbit in these problems is so simple that we
can calculate the first correction term directly. The result of this calculation
yields

$$C_0^{0(1)} \quad = \quad \frac{1}{p} \left(C_2 - \frac{3}{8} C_2 \frac{2 + LC_4/3C_2^2}{2 + C_2 L} \right), \tag{7.138}$$

where C_2 and C_4 denotes the expansion coefficients of the wall at the bouncing
point and where L is the length of the periodic orbit. This result can be
compared with the findings of ref.[33] for the two disk system and with those of
ref.[59] for the confocal hyperbolae. In case of the two disk scattering system
$C_2 = 1/a$ and $C_4 = 3/a^3$, where a is the radius of the disk. In this case we get

$$C_0^{(1)} = \frac{5}{8ap}, \tag{7.139}$$

which coincides withe the result of Ref.[33] derived via Feynman graph tech-
nique. In the case of the two disc scattering system our results will therefore
be identical to the results of Ref [33]. In the case of the confocal hyperbolae we
have $C_4 = -6C_2^2/L$, and the correction is

$$C_0^{(1)} = \frac{C_2}{p}, \tag{7.140}$$

which was numerically confirmed in ref.[59].

Next we study the $\hbar$ corrections to the genuine 3-disk orbits. First we
can try to compare our $\hbar$ corrections $C_0^{(1)}$ to the fullspace calculation of Ref
[33]. Here we do not use the symmetry reduction, but find the first correction
to all the 25 shortest orbits of topological length up to 9 in the full 3-disk
domain. The calculation can then be compared directly with the results in [33].
Our results are listed in table (7.1). We see that the two calculations which
takes quite different approaches gives the same results except for a few of the
orbits. On the base of the results in table 7.1 Gaspard et al. also calculates
the first few resonances of the 3-disk system using the full space dynamical

Orbit	deg.	$C_{0,GA}^{(1)}$	$C_{0,VR}^{(1)}$
12	3	0.62500	0.62500
123	2	1.68647	1.68647
1213	3	2.03980	2.03979
12123	6	2.45127	2.45127
121323	3	3.11233	3.11383
121213	6	2.68951	2.68951
1212123	6	3.07848	3.07846
1212313	6	3.24027	3.24026
1213123	6	3.74224	3.70424
12121213	6	3.31483	3.31483
12121313	3	3.34018	3.34017
12121323	6	3.75662	3.75662
12123123	6	4.13736	4.13736
12123213	6	3.93185	3.93185
12132123	3	4.24438	4.24438
121212123	6	3.70350	3.70349
121212313	6	3.86777	3.86776
121212323	6	3.86777	3.86776
121213123	6	4.35071	4.35071
121213213	6	4.35071	4.35071
121231323	6	4.46254	4.46254
121231213	6	4.49403	4.49403
121232123	6	4.49403	4.49403
121232313	2	4.06479	4.06478
121321323	6	4.80313	4.80312

Table 7.1: The first order $\hbar$ correction for the first 25 orbits in the full 3-disk scattering system. First two columns show the symbolic representation of the periodic orbit and its symmetry degeneracy. Next two columns show the $\hbar$ correction obtained by Gaspard and Alonso, and the $\hbar$ correction obtained by our method, respectively.

quantum zeta function and periodic orbits up to topological length 8 and 9. We tried to compare the analogue fundamental domain calculation to these results using only the first five periodic orbits (all up to topological length 3) in the fundamental domain as input in the dynamical $l = 0$ quantum zeta function. The results are displayed in figure 7.2 together with the resonances from [33].
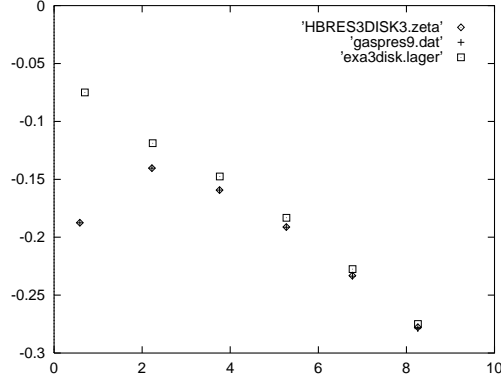
Figure 7.2: The first 6 A_1 resonances in the $R : a = 6.0$ 3-disk scattering system. The squares denotes the exact data from A. Wirzba, crosses denotes the full space calculation to curvature order 9 of Gaspard and Alonso and finally diamonds denotes our fundamental domain calculation using the shortest 5 periodic orbits as input. The last two calculations are both corrected to the first order in $\hbar$.

Next we can compare our results for the leading A_1 resonances to the exact data which are provided by A. Wirzba. First we note that at curvature order 7 the $\hbar$ corrected as well as the usual Gutzwiller-Voros zeta function resonances does not change in the leading digits by inclusion of more periodic orbits, and that they are located basically on top of the exact resonances. In the following calculations we therefore keep the truncation of the cycle expansions at topological order 7. The leading part of the resonance spectrum is depicted in figure 7.3 As it can be seen it is not difficult to identify the exact resonances with the corresponding semiclassical Gutzwiller-Voros and $\hbar$ corrected resonances. From this correspondance we can compare the pure semiclassical results to the $\hbar$ corrected calculation. We do this by plotting the deviation in real and imaginary k from the corresponding exact resonance as a function of for instance Rek. A plot like this is shown in figure 7.4 The $\hbar$ corrected resonances are seen to be clearly better than the ordinary Gutzwiller-Voros resonances. Even more instructive it might be to look at a plot of the relative error of the resonances, that is the ratio $|\text{Re}k_\hbar - \text{Re}k_{exact}|/|\text{Re}k_{GV} - \text{Re}k_{exact}|$ as function of Rek or Imk and the analogous plots for the imaginary part. Such two plots are shown in figures 7.6 and 7.7 By comparing the two figures one can see that in general the $\hbar$ corrected resonances are much better than the semiclassical resonances except for a very few resonances in the area Re$k \geq 100$ and for Im$k \leq -0.4$. For instance the 8 resonances where the relative deviation is larger than or of order 1, are all located far down in the complex plane. By inclusion of the $l = 1$
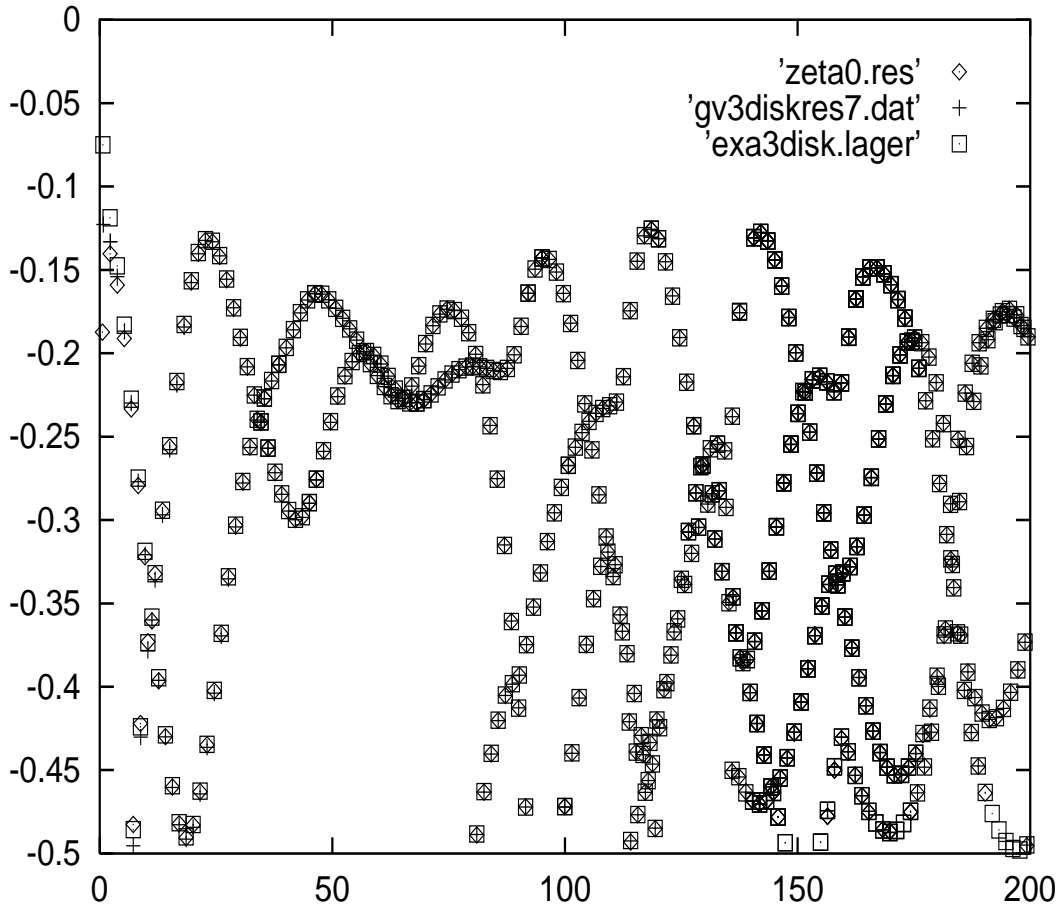
Figure 7.3: The leading part of the A_1 resonance spectrum of the $R : a = 6.0$ 3-disk scattering system. The exact spectrum is from A. Wirzba and is denoted with dotted squares. The Gutzwiller-Voros zeta function resonances are denoted with a '+' and the $\hbar$ corrected resonances from the $l = 0$ quantum zeta function with a $\diamond$.
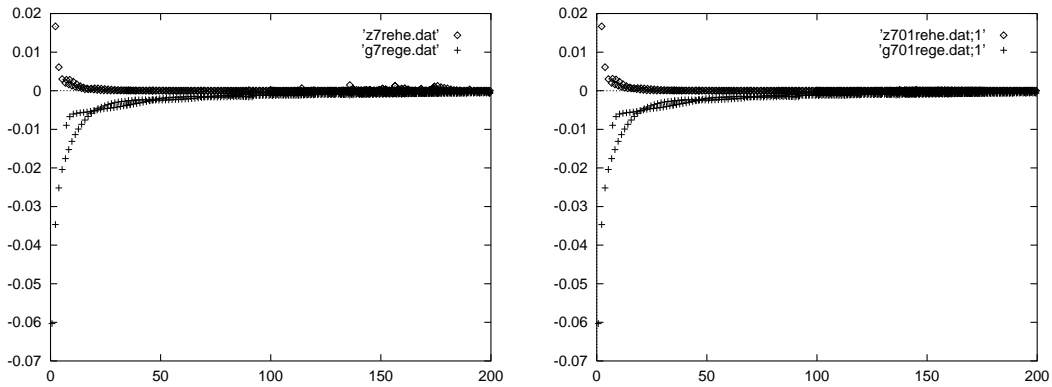
Figure 7.4: The deviation in real part of the Gutzwiller Voros resonances and the $\hbar$ corrected $l = 0$ and $l = 0, 1$ quantum zeta resonances ($\diamond$) from the exact quantum resonances. The exact data are from A. Wirzba. By inclusion of $l = 2, 3$ the picture does not change in a visible way.
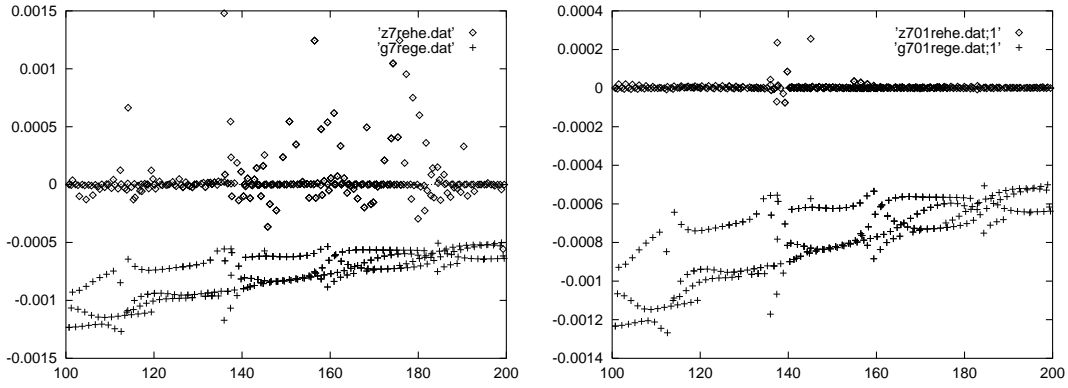
Figure 7.5: The same as above except the different Re k domain.
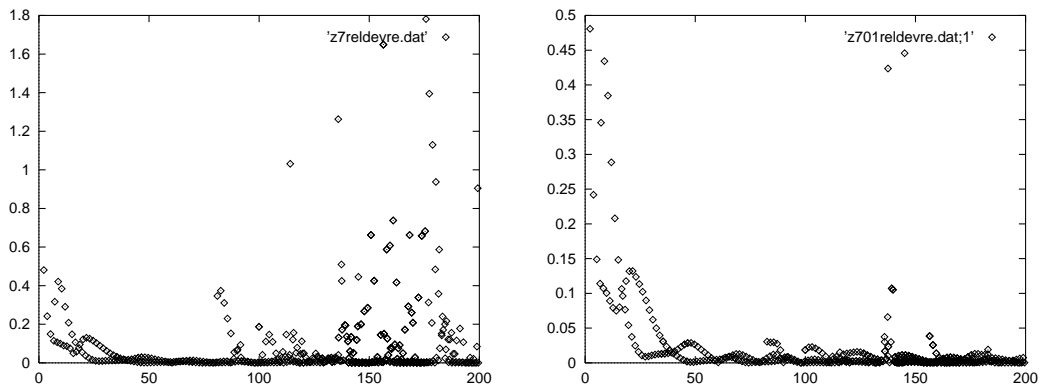
Figure 7.6: Relative deviation in real part of k as function of Re k. The first picture compares the Gutzwiller-Voros zeta function resonances to the $l = 0$ dynamical quantum zeta resonances with the first $\hbar$ correction included. In the right side picture both $l = 0, 1$ are included with the first $\hbar$ correction. Note the different scales on the y-axis.
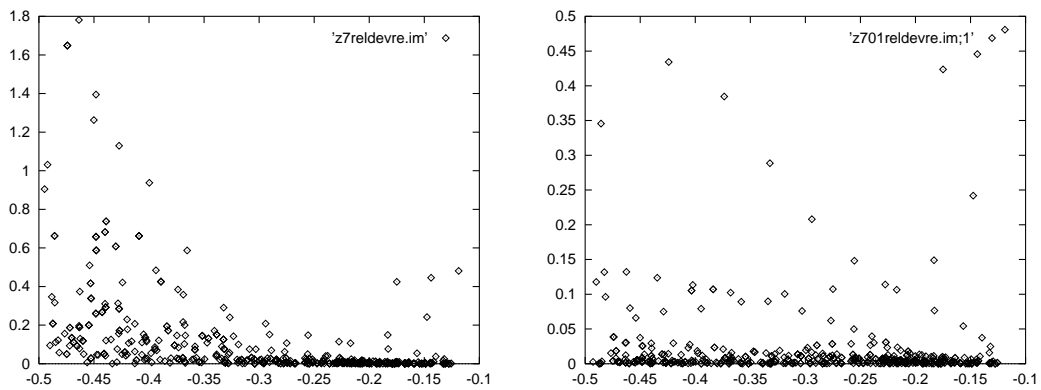
Figure 7.7: Relative deviation in real part of k as function of Imk. The same calculations as in the previous figure are compared. Again one should note the different scales in the y-axis.

corrected quantum zeta function as well the picture improves further: whereas for the first quantum zeta most of the resonances improved by a factor 2 in real part of k, we obtain by inclusion of the next corrected zeta function an improvement of a factor 20 for most of the resonances. By inclusion of further zeta functions this picture does not change considerably at least not by inclusion of the first four $l = 0, 1, 2, 3$ quantum zeta functions.

The leading part of the A_1 resonance spectrum is therefore in general improved by a factor 2-20, in the real part of k, by inclusion of the first $\hbar$ correction in the first few zeta functions of the Gutzwiller-Voros product.

Making the analogue plots for the deviation in imaginary part results in figures 7.8 and 7.10 Here we see basically the same tendency as for the real
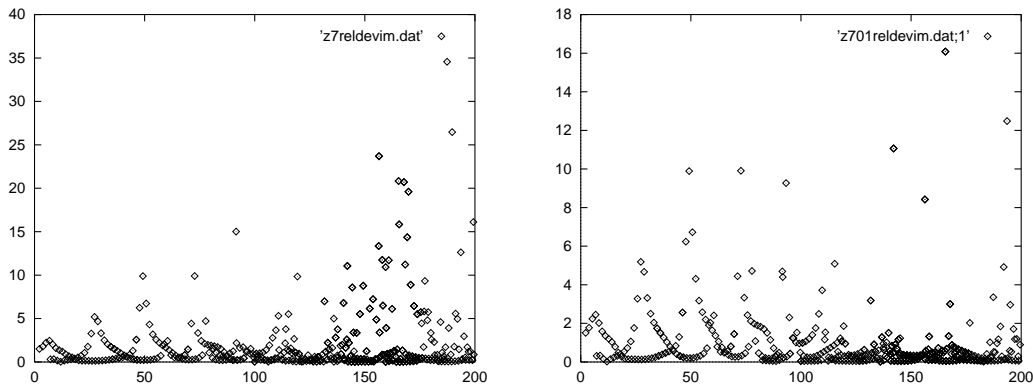
Figure 7.8: Relative deviation in imaginary part of k as function of Rek. The first picture compares the Gutzwiller-Voros zeta function resonances to the $l = 0$ dynamical quantum zeta resonances with the first $\hbar$ correction included. In the right side picture both $l = 0, 1$ are included with the first $\hbar$ correction. Note the different scales on the y-axis.
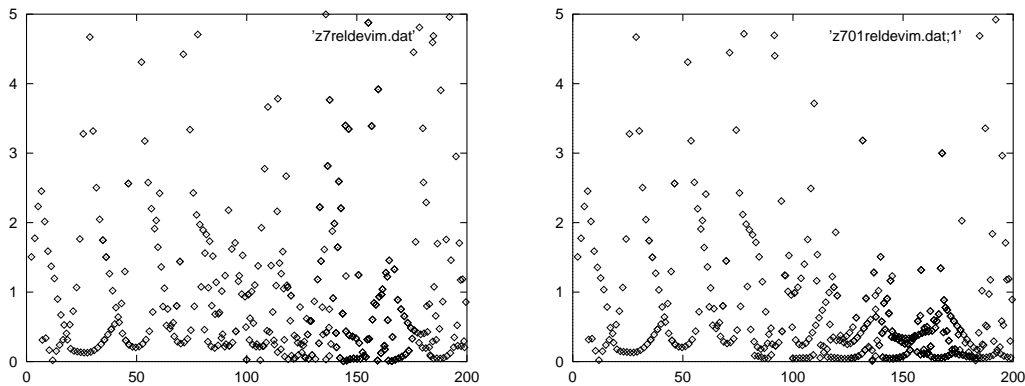
Figure 7.9: A blow-up of the previous picture reveals that approximately only half of the resonances are improved in the imaginary part.

part except that approximately only half of the resonances are improved in imaginary part by the inclusion of the $\hbar$ correction. The picture is thus not
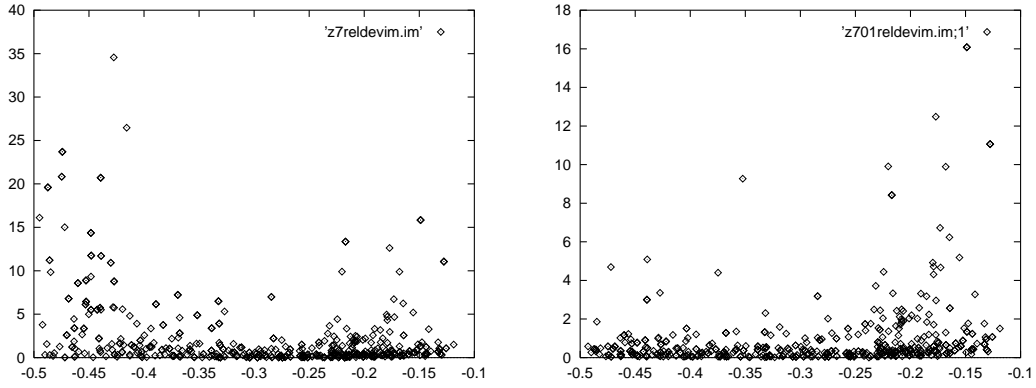
Figure 7.10: Relative deviation in imaginary part of k as function of Imk.

as clear as for the real part: most of the $\hbar$ corrected resonances are as good as, or even better than their semiclassical counterparts but for some resonances the situation is completely opposite. The reason for this is at least partially explained by Gaspard who observed that the *first order* $\hbar$ correction entering in the Gutzwiller-Voros zeta function has the same phase as the stability whereas the second order $\hbar$ correction has an additional $e^{i\pi/2}$ phase. Consequently the first order $\hbar$ correction improves the real part of the resonance whereas we have to go to second order in the $\hbar$ expansion to also improve the imaginary part of the resonances. So even though we also observe an improvement for half of the resonances by inclusion of only the first order $\hbar$ correction, the above explanation might account for the other resonances. This could of course be investigated by using the procedure outlined in this section to obtain also the second order $\hbar$ correction to the local eigenvalues. However, also in the case of the imaginary deviation we see a considerable improvement when going from the pure $\hbar$ corrected quantum zeta function to the product of the first few $\hbar$ corrected zeta functions. This can clearly be seen from the figures 7.8 and 7.10 by noting the different scale on the y-axis.

Generally we note, that the relative error of the corrected calculation versus the error of the semiclassical calculation decreases with the real part of the wavenumber and increases with the magnitude of the imaginary part of the wavenumber. By inclusion of still more corrected zeta functions in the Gutzwiller-Voros product we at first see a nice improvement. We do not expect this to continue when including still further corrected zeta functions in the product. This is because the $\hbar$ expansion is only an asymptotic series: From (7.135) we see that the first order correction $C_l^{(1)}$ is at most a fourth order polynomial in l. This can easily be checked by computing $C_l^{(1)}$ for $l = 1, 2, 3, \ldots, l_{max}$ and fit the result by a polynomial. For the $\overline{0}$ orbit of the 3-disk system such a fit (by Mathematica) for $l = 1, 2, \ldots, 10$, yields

$$C_l^{\overline{0}(1)} \;=\; 0.625 + 1.4375l - 0.3125l^2 - 0.625l^3 - 3.32179 \times 10^{-13}l^4$$

which has been numerically confirmed by A. Wirzba in [?] For the $\overline{1}$ orbit a

similar calculation yields

$$
\begin{aligned}
C_l^{\overline{1}(1)} &= 1.68647 + 3.90756l + 0.593969l^2 - 0.728335l^3 + 0.0327606l^4 \\
&+ 3.97459842815806 \times 10^{-14}l^5
\end{aligned}
$$

For large l the numerical value of $C_l^{(1)}$ therefore diverges and the first order corrected Gutzwiller-Voros product will therefore also diverge.

7.9 Conclusions

In this chapter we have described a new method developed by G. Vattay to evaluate corrections to the leading saddle point approximation of the Feynman path integral [55]. The method reduces the problem to a set of ordinary differential equations which have to be solved at certain boundary conditions. In all orders the product structure of the functional determinant $\Delta(E)$ is maintained. One can introduce the quantum zeta functions. The corrections to the leading zeta function is easier to calculate than a general $l > 0$ term and it is very practical to use it for extended computations. Taking the theory as a starting point we found analytically the necessary ingredients for calculating the first $\hbar$ correction term in the case of a general 2-dimensional billard system. We obtained this formalism for a general l value, in order to be able to correct several of the quantum zeta functions $\zeta_l^{-1}(k)$. A simple numerical calculation scheme for the method has been evolved for the special case of two dimensional billiard systems. The calculation scheme which works for general values of l, was implemented in a FORTRAN program. The program only uses simple geometrical information from the periodic orbits namely the lengths of their flight sections, their transverse stabilities and the local derivatives of the walls at the bouncing points. The program is therefore immediately applicable to any two-dimensional billiard system. The program has been tested on the 3-disk scattering system and the results compared to the exact as well as the pure semiclassical calculations. The comparison shows a clear improvement in real part of k of the predicted resonances by including the first correction term. By inclusion of further corrected quantum zeta functions in the Gutzwiller-Voros product the calculation improves considerably for both the real and imaginary part of the resonances. The imaginary part of our estimates however, does not improve as dramatically as the real parts, and only approximately half of the resonances are directly improved in the imaginary part by inclusion of the first $\hbar$ correction. We expect that inclusion of the second order $\hbar$ correction will result in a general improvement of the imaginary part of the resonances as well.

Chapter 8

Perspectives

In this thesis we have adressed three main points concerning the general purpose of improving the semiclassical rules of quantization in hyperbolic Hamiltonian systems that classicaly display chaos.

<u>First</u> we investigated the quasiclassical propagator introduced by Vattay [53] and derived the spectral determinant for this in the general N dimensional case. As a byproduct of this we obtained an explicit solution formula to the Hamilton-Jacobi equation to the second order in the case of a periodic orbit by solving the fixpoint equation of the generalized rational fraction transformation that governs the evolution of the second derivative or curvature matrix of the phase function. By numerical calculation we showed that the determinant indeed seems to be an entire function since the expansion coefficients in the cycle expansion of the determinant exhibits a super exponential decay towards 0, indicating that the determinant has no poles. By considering the numerical studies of A. Wirzba, which are based on the periodic orbits obtained by our numerical routines, we concluded that to obtain the lowlying resonances of the $R : a = 6.0$ 3-disk system one has to expand the determinant to 12'th order in the cycle expansion. This means that one here has to do more work than is necessary when using the Gutzwiller-Voros spectral determinant. The advantage on the other hand, is that in contrast to the Gutzwiller-Voros spectral determinant the Vattay determinant is not just an asymptotic series. The resonances thus obtained will therefore stay put by inclusion of still more periodic orbits. The price we have to pay for this is then the work of obtaining more periodic orbits and to calculate the stabilities of the periodic solutions of the curvature matrix flow.

<u>Second</u> we introduced the geometrical theory of diffraction develloped by Keller, and showed how the semiclassical expression of the propagator can be condisderably improved by introducing generalized minimal action rays or creeping orbits that has no physical classical limit but still fulfills the generalized Fermat principle. In this theory the semiclassical propagator is then extended from the usual Van Vleck propagator to also include a summation over diffractive or creeping orbits that connects q with q' in time t. As a fur-

ther development of the Keller procedure we showed how diffraction from edges can also be described by this theory. By making the usual cycle expansion of a generalized spectral determinant that allows diffractive periodic orbits, and by comparing this to the exact quantum mechanical cumulant expansion for the simple 2-disk scattering system, we obtained a rule relating the ingredients of the diffractive propagator to the cycle expansion of the diffraction spectral determinant. By analyzing the order of approximation, we could derive an expression for the trace of the k domain Greens function in the case of diffractive periodic orbits by using the relation

$$\mathrm{Tr}G(k) \quad = \quad -\frac{d}{dk}\ln\Delta(k). \tag{8.1}$$

By numerical investigation of the scattering resonances of our 2- and 3-disk systems and by comparison to the exact results, we showed that the semiclassical calculation including diffraction effects deviated clearly from the usual Gutzwiller-Voros results and that the correct quantum results were at least qualitatively obtained. For instance families of resonances that were not at all present in the pure geometrical calculation could be uniquely identified by resonances resulting from the diffractive spectral determinant. These new resonances however, showed a systematical deviation from the exact results. We expect that this is due to the cutoff in the Airy corrections since the numerical studies by A. Wirzba indicates a tremendous improvement of the resonances when including the higher order Airy corrections in the simple case of the 1-disk scatterer.

Our expression of the semiclassical creeping propagator still has short commings, which are open to improvements:

- The creeping expression for $G(x, x', t)$ is only valid if x' does not lie in the penumbra region i.e. x' should either be in the illuminated region or in the shadow region. So our propagator can not deal with the socalled penumbra correction introduced recently by Smilansky et al. as it stands.

- In the cycle expansion of the diffraction spectral determinant the exact cancellation of the curvature terms is only correct for the $l = 1$ modes. For higher modes one has to keep track of the full set of curvature terms, since the propagator is only multiplicative for the $l = 1$ mode.

- In the diffractive part of the propagator we make use of the Airy approximation of the Hankel function and their zeros. By numerical studies A. Wirzba [63] showed that the results of the calculations using our propagator highly improves when taking the polynomial corrections to this approximation into account. At this point however, there does not seem to be any simple way to include these corrections into the expression of the propagator and at the same time keep the nice multiplicative structure even for the $l = 1$ mode.

<u>Third</u> we introduced the method of obtaining $\hbar$ corrections to the Gutzwiller trace formula by using ordinary differential equations as developed by Vattay

et. al. in [55]. Taking this theory as the *starting point* we showed how it could be specialized to the case of two dimensional billard systems and we develloped a simple algorithm that gives the contribution associated with each periodic orbit, to the first order $\hbar$ correction to the dynamical quantum zeta functions $\zeta_l^{-1}(k)$. By applying our solution to the Hamilton-Jacobi equation obtained in the section on entire spectral determinants, we could slightly speed up this calculation. The method however, works nicely even without this result.

By calculating numerically the $\hbar$ corrections to all the periodic orbits with topological length less than 9 in the full 3-disk system, we showed that our results are almost equivalent to the $\hbar$ corrections obtained by Gaspar and Alonso, using the Gaussian corrections to the saddlepoint approximation. At this point it is still not clear where the origin of the small deviations in this comparison lies. In the special case of the 2-disk system the agreement is exact though.

As a further study, we calculated the first $\hbar$ correction to the $l = 0, 1, 2, 3$ quantum zeta functions in the A_1 representation, for all the orbits up to topological legth 10 in the fundamental domain of the $R : a = 6.0$ 3-disk system. The resonances of the corrected quantum zeta functions were compared to the pure semiclassical and the exact quantum resonances by including more and more corrected zeta functions in the Gutzwiller-Voros product. Generally we observed that the relative error of the corrected calculation versus the error of the semiclassical calculation decreases with the real part of the wavenumber and increases with the magnitude of the imaginary part of the wavenumber. By comparing first the $l = 0$ and next the $l = 0, 1$ product of corrected quantum zeta functions to the Gutzwiller-Voros determinant we found a good improvement of almost all the resonances of approximately a factor 2 respectively 20 in the real part of the wave number. By inclusion of further corrected quantum zeta functions in the Gutzwiller-Voros product the calculation did not improve dramatically. The imaginary part of our estimates however, does not improve as much as the real parts, and only approximately half of the resonances are directly improved in the imaginary part by inclusion of the first $\hbar$ correction. We expect that inclusion of the second order $\hbar$ correction will result in a general improvement of the imaginary part of the resonances as well.

Bibliography

[1] M. Abramowitz and I. Stegun, *Handbook of Mathematical Functions* (Dover, New York, 1964)

[2] V.I. Arnold, *Geometrical Methods in the Theory of Ordinary Differential Equations* (Springer, New York 1983)

[3] R. Artuso, E. Aurell and P. Cvitanović, *Nonlinearity* **3**, 325 (1990).

[4] R. Artuso, E. Aurell and P. Cvitanović, *Nonlinearity* **3**, 361 (1990).

[5] V. M. Babić and V. S. Buldyrev, *Short Wavelength Diffrac tion Theory*, Springer Series on Wave Phenomena, Springer-Verlag (1990)

[6] R. B. Balian and C. Bloch, Ann. Phys. (New York) **60**, 81 (1970);ibid. **63**, 592 (1971); M.V. Berry, M.V., C.J. Howls, C.J. Proceedings of the Royal Society of London. **447**, 1931 (1994)

[7] M. V. Berry and J. P. Keating, J. Phys. **A23**, 4839 (1990)

[8] M. V. Berry and K. E. Mount, Rep. Prog. Phys. **35**, 315 (1972)

[9] V. A. Buslaev, Sov. Phys.-Dokl. **10**, 17-9 (1965)

[10] F. Christiansen, P. Cvitanović and H.H. Rugh, *J. Phys* **A 23**, L713 (1990).

[11] F. Christiansen, G. Paladin and H.H. Rugh, *Phys. Rev. Lett.* **65**, 2087 (1990).

[12] P. Cvitanović, B. Eckhardt, P.E. Rosenqvist, G. Russberg and P. Scherer, "Pinball Scattering", in G. Casati and B. Chirikov, eds., *Quantum Chaos*, (Cambridge University Press, Cambridge 1994).

[13] P. Cvitanović and P.E. Rosenqvist, "A new determinant for quantum chaos", in G.F. Dell'Antonio, S. Fantoni and V.R. Manfredi, eds., *From Classical to Quantum Chaos, Soc. Italiana di Fisica Conf. Proceed.* **41**, 57 (Ed. Compositori, Bologna 1993).

[14] P. Cvitanović, P.E. Rosenqvist, H.H. Rugh, and G. Vattay, *A Fredholm determinant for semi-classical quantization, CHAOS* **3**, 619 (1993).

[15] P. Cvitanović and G. Vattay, *Entire Fredholm determinants for evaluation of semi-classical and thermodynamical spectra, Phys. Rev. Lett.* **71**, 4138 (1993).

[16] P. Cvitanović and B. Eckhardt, *Symmetry decomposition of chaotic dynamics, Nonlinearity* **6**, 277 (1993).

[17] P. Cvitanović and B. Eckhardt, *J. Phys.* **A 24**, L237 (1991).

[18] P. Cvitanović and B. Eckhardt, *Phys. Rev. Lett.* **63**, 823 (1989).

[19] P. Cvitanović, *Phys. Rev. Lett.* **61**, 2729 (1988).

[20] P. Cvitanović, *Physica* **D 51**, 138 (1991).

[21] P. Cvitanović, N.J. Balmforth, G.R. Ierley, E.A. Spiegel and G. Vattay, "Periodic orbit expansions for smooth flow fast dynamos", *Proc. of the "Noise in Astrophysics" workshop*, Gainsville, Florida 1993, to appear.

[22] P. Cvitanović, ed., *Periodic Orbit Theory - theme issue, CHAOS* **2**, 1-158 (1992).

[23] B. Eckhardt, *Physica* **D 33**, 89 (1988)

[24] B. Eckhardt and G. Russberg, *Phys. Rev.* **E 47**, 1578 (1993).

[25] H.M. Edwards, *Riemann's Zeta Function* (Academic, New York 1974)

[26] A. Einstein, *Verhand. Deut. Phys. Ges.*, **19**, 82, (1917)

[27] R. P. Feynman, Rev. Mod. Phys. **20**, 367 (1948), R. P. Feynman and A. R. Hibbs, Quantum Mechanics and Path Integrals, McGraw-Hill, New York (1965)

[28] W. Franz, *Theorie der Beugung Elektromagnetischer Wellen*, Springer Verlag, Berlin (1957); Z. Naturforschung **9a**, 705 (1954)

[29] W. Franz and R. Galle, *Z. Naturforschung* **10a**, 374 (1955)

[30] D. Fried, *Ann. Scient. Éc. Norm. Sup.* **19**, 491 (1986).

[31] P. Gaspard and D. Alonso Ramirez, *Phys. Rev.* **A 45**, 8383 (1992).

[32] P. Gaspard and S. A. Rice, J. Chem. Phys. **90**, 2225, 2242, 2255 (1989); **91**, E3279 (1989)

[33] P. Gaspard and D. Alonso, Phys. Rev. **A47**, R3468 (1993); D. Alonso and P. Gaspard, Chaos **3**, 601 (1993)

[34] M. D. Greenberg, *Application of Greens Functions in Science and Engeneering*, Prentice-Hall, Inc. Englewood Cliffs, New Jersey, (1971)

[35] M. C. Gutzwiller, J. Math. Phys. **12**, 343 (1971); *Chaos in Classical and Quantum Mechanics* (Springer-Verlag, New York, 1990)

[36] T.C. Halsey, M.H. Jensen, L.P. Kadanoff, I. Procaccia and B.I. Shraiman, *Phys. Rev.* **A107**, 1141 (1986).

[37] E. J. Heller, J. Chem. Phys. **62**, 1544 (1975); **64**, 63 (1976); W. Eastes and R. Marcus, J. Chem. Phys. **61**, 4301 (1974); W. H. Miller, J. Chem. Phys. **63**, 996 (1975)

[38] Joseph B. Keller and Herbert B. Keller *Journal of the Optical Society of America* **40**, number 1, p. 48, 1950; Bertram R. Levy and Joseph B. Keller *Communications on Pure and Applied Mathematics* Vol. XII, 159-209, (1959)

[39] Joseph B. Keller *Journal of the Optical Society of America* **52**, number 2, p. 116, 1962;

[40] R. G. Littlejohn, *J. Stat. Phys.*, **68** No. 1-2, 7, 1992; Lecture notes (Berkely 1990)

[41] V. P. Maslov and M. V. Fjedoriuk, *Semiclassical Approximation in Quantum Mechanics*, Dordrecht-Reidel (1981)

[42] E. Ott, *Chaos in Dynamicla Systems*, Cambridge University Press, 1993

[43] H. Primack, H. Schanz, U. Smilansky and I. Ussishkin, *The Rôle of Diffraction in the Quantization of Dispersing Billards* , Preprint August 1995.

[44] P. E. Rosenqvist, Master thesis, Niels Bohr Institute, Copenhagen 1992

[45] D. Ruelle, *Statistical Mechanics, Thermodynamic Formalism* (Addison-Wesley, Reading, MA, 1978)

[46] D. Ruelle, *Inventiones math.* **34**, 231 (1976).

[47] H. H. Rugh, Nonlinearity **5**, 1237 (1992); H. H. Rugh, *Thesis*, Copenhagen University (1992); G. Vattay, *Thesis*, Eötvös University Budapest (1992); P. Cvitanović, P. E. Rosenqvist, G. Vattay and H. H. Rugh, CHAOS **3** (4), 619 (1993)

[48] H.H. Rugh, *Nonlinearity* **5**, 1237 (1992).

[49] K. T. Hansen, *Symbolic Dynamics in Chaotic Systems*, University of Oslo, (September 1993); Nonlinearity **6**, No. 5, 753, 771, (1993)

[50] L. S. Schulman, *Techniques and Applications of Path Integration*, (Wiley-Interscience Publication, 1981)

[51] A. Selberg, J. Indian Math. Soc. **20**, 47 (1956)

[52] S. Smale, *Bull. Am. Math. Soc.* **73**, 747 (1967).

[53] G. Vattay, " An Entire Spectral Determinant for Semiclassical Quantization", Progress of Theoretical Physics, Supplement No. 116, p. 251, (1994)

[54] G. Vattay, A. Wirzba and P.E. Rosenqvist, *Periodic Orbit Theory of Diffraction*, *Phys. Rev. Lett.* **73**, 2304 (1994). G.Vattay, A. Wirzba, P. Rosenqvist, *Inclusion of Diffraction Effects in the Gutzwiller Trace Formula*, in Dynamical Systems and Chaos Vol. 2. p. 463, proceedings of ICDC Tokyo 23-27 May 1994, (World Scientific, Singapore 1995); P. E. Rosenqvist, G. Vattay and A. Wirzba, *Application of the diffraction trace formula to the three disk scattering system*, J. Stat. Phys. to appear (1995)

[55] G. Vattay and P. Rosenqvist, Periodic Orbit Theory of Quantum Mechanics, Phys. Rev. Lett. acc. to appear (1995); Differential equations to compute hbar corrections (http://xyz.lanl.gov) (1994)

[56] A. Voros, *J. Phys.* **A 21**, 685 (1988).

[57] A. Voros, Prog. Theor. Phys. Suppl. **116**,17 (1994); M. Saraceno and A. Voros, to appear in Physica D.

[58] G. N. Watson, Proc. R. Soc. London **A95**, 83 (1918)

[59] N. Whelan, *Phys. Rev. E.*, **51**, No. 4, 3778, 1995

[60] A. Wirzba, *Validity of the Semiclassical Periodic Orbit Approximation in the 2-and 3-Disk Problems*, CHAOS **2**, (1992), 77-83.

[61] A. Wirzba, *Test of the Periodic Orbit Approximation in n-Disk Systems*, Nucl. Phys. **A560**, (1993), 136-150.

[62] A. Wirzba *Hyperbolic scattering, periodic orbits and diffraction*, in preparation.

[63] A. Wirzba, privat communication.

[64] A. Wirzba, in preparation.

[65] For more details on these topics, see the "non-papers" of Andreas Wirzba on: http://crunch.ikp.physik.th-darmstadt.de/ wirzba/

[66] A. Wirzba and M Henseler, *The missing link between the quantum mechanical and semi-classical determination of scattering resonance poles*, to appear. For preview see http://crunch.ikp.physik.th-darmstadt.de/ wirzba/

[67] A. Sommerfeld *Optics*, New York, Academic Press, Inc., (1954)

[68] W. Pauli, *Physical Review* **54**, 924, 1938

Chapter 9

Appendices

9.1 Derivations and examples of chapter 5

The Jacobian as an integral

Equation (5.17) can be obtained by integrating the time derivative of the Jacobian, which can be obtained as follows

$$
\begin{aligned}
q(t + \delta t) &= q(t) + q\delta t \\
&= q(t) + \frac{\partial H}{\partial p}\delta t & (9.1) \\
p(t + \delta t) &= p(t) + p\delta t \\
&= p(t) - \frac{\partial H}{\partial q}\delta t & (9.2)
\end{aligned}
$$

which gives

$$
\begin{aligned}
\mathbf{J}(t + \delta t) &= \begin{pmatrix} \mathbf{1} + \frac{\partial^2 H}{\partial q_i \partial p_j}\delta t & \frac{\partial^2 H}{\partial p_i \partial p_j}\delta t \\ -\frac{\partial^2 H}{\partial q_i \partial q_j}\delta t & \mathbf{1} - \frac{\partial^2 H}{\partial q_i \partial p_j}\delta t \end{pmatrix} \\
&= \mathbf{1} + \mathbf{J}(t)\delta t. & (9.3)
\end{aligned}
$$

From the last expression we can read of the time derivative of the Jacobian

$$
\begin{aligned}
\mathbf{J}(t) &= \begin{pmatrix} \frac{\partial^2 H}{\partial q_i \partial p_j} & \frac{\partial^2 H}{\partial p_i \partial p_j} \\ -\frac{\partial^2 H}{\partial q_i \partial q_j} & -\frac{\partial^2 H}{\partial q_i \partial p_j} \end{pmatrix} \\
&\equiv \mathbf{D}^2 H
\end{aligned}
$$

The differential equation for the M flow

The differential equation that drives the **M** flow can be derived in the following way. If we substitute the elements of the infinitesimal Jacobi matrix (9.3). For

infinitesimal time we have

$$
\begin{aligned}
\Delta \mathbf{M} &= \mathbf{M}' - \mathbf{M} \\
&= (\mathbf{J}_{pq} + \mathbf{J}_{pp}\mathbf{M})(\mathbf{J}_{qq} + \mathbf{J}_{qp}\mathbf{M})^{-1} - \mathbf{M} \\
&= ((\mathbf{J}_{pq} + \mathbf{J}_{pp}\mathbf{M}) - \mathbf{M}(\mathbf{J}_{qq} + \mathbf{J}_{qp}\mathbf{M}))(\mathbf{J}_{qq} + \mathbf{J}_{qp}\mathbf{M})^{-1} \qquad (9.4)
\end{aligned}
$$

which gives

$$
\begin{aligned}
\Delta \mathbf{M}(\mathbf{J}_{qq} + \mathbf{J}_{qp}\mathbf{M}) &= (\mathbf{J}_{pq} + \mathbf{J}_{pp}\mathbf{M}) - \mathbf{M}(\mathbf{J}_{qq} + \mathbf{J}_{qp}\mathbf{M}) \\
&= -(\frac{\partial^2 H}{\partial q \partial q} + \frac{\partial^2 H}{\partial q \partial p}\mathbf{M}) - \mathbf{M}(\frac{\partial^2 H}{\partial p \partial q} + \frac{\partial^2 H}{\partial p \partial p}\mathbf{M}) \quad (9.5)
\end{aligned}
$$

And since in the limit $\delta t \to 0$ we have $\mathbf{J}_{qq} \to \mathbf{1}$ and $\mathbf{J}_{qp} \to \mathbf{0}$ we get

$$
\mathbf{M} = -\left(\frac{\partial^2 H}{\partial q \partial q} + \mathbf{M}\frac{\partial^2 H}{\partial p \partial q} + \frac{\partial^2 H}{\partial q \partial p}\mathbf{M} + \mathbf{M}\frac{\partial^2 H}{\partial p \partial p}\mathbf{M} \right), \qquad (9.6)
$$

The volume ratio as an integral

The expression for the volume ratio (5.24) can be derived by splitting the ratio into a product over ratios of infinitesimal time evolution:

$$
\begin{aligned}
\frac{V(q')}{V(q_0)} &= \prod_{t=0}^{\tau} \frac{V_{t+dt}}{V_t} \\
&= \prod_{t=0}^{\tau} \det(\mathbf{J}_{qq} + \mathbf{J}_{qp}\mathbf{M}^t) \\
&= \prod_{t=0}^{\tau} \det(\mathbf{1} + \left(\frac{\partial^2 H}{\partial q \partial p} + \frac{\partial^2 H}{\partial p \partial p}\mathbf{M}^t \right)\delta t) \\
&= \exp\{ \int_0^t [\frac{\partial^2 H}{\partial p \partial q} + \frac{\partial^2 H}{\partial p \partial p}\mathbf{M}] d\tau \} \qquad (9.7)
\end{aligned}
$$

Evolution of the quasi-classical wave function

If we only consider the delta functions in the kernel (9.39) and the initial wave function the calculation goes as follows. First we integrate out $\mathbf{M}$ and p in the evolved wave function:

$$
\begin{aligned}
\tilde{\psi}(q, p, \mathbf{M}, t) &= \int dq\, dp\, d\mathbf{M}\, \delta(q' - q^t(q,p))\delta(p' - p^t(q,p))\delta(\mathbf{M}' - \mathbf{M}^t(q,p,\mathbf{M})) \\
&\times \delta(p - \nabla S(q,0))\delta(\mathbf{M} - \frac{\partial^2 S(q,0)}{\partial q^2})\psi(q,0) \\
&= \int dq\, dp\, \delta(q' - q^t(q,p))\delta(p' - p^t(q,p))\delta(\mathbf{M}' - \mathbf{M}^t(q,p,\partial^2 S(q,0)/\partial q^2)) \\
&\times \delta(p - \nabla S(q,0))\psi(q,0) \\
&= \int dq\, \delta(q' - q^t(q,\nabla S(q,0)))\delta(p' - p^t(q,\nabla S(q,0))) \\
&\times \delta(\mathbf{M}' - \mathbf{M}^t(q,\nabla S(q,0),\partial^2 S(q,0)/\partial q^2))\psi(q,0)
\end{aligned}
$$

Then when we finaly do the q integral we obtain the evolved wave function in the same form as the initial one, divided with the determinant of the Jacobian of the configuration space evolution which is just the volume ratio

$$\tilde{\psi}(q, p, \mathbf{M}, t) \quad = \quad \frac{1}{|\det\left(\frac{\partial q^t}{\partial q}\right)|} \delta(p' - \nabla S(q', t)) \delta(\mathbf{M}' - \frac{\partial^2 S(q', t)}{\partial q' \partial q'}) \psi(q^{-t}(q'), 0).$$

(9.8)

In order to get the right volume ratio in front of the old wave function we therefore have to multiply this expression with $\sqrt{|\det\left(\frac{\partial q^t}{\partial q}\right)|}$, which is just equal to the term $(V(q')/V(q))^{1/2}$ in (5.24), and hence gives the change of the sign in the trace integral in the exponent.

9.1.1 Alternative derivation of the curvature trace

In this section we shall derive the general result of the curvature integration in an arbitrary number of dimensions. The derivation of the result will follow a different approach than the on in section 5.3. Here we consider the general evolution of Lagrangian manifolds corresponding to the periodic solutions of the curvature flow.

Lagrangian manifolds

The definition of a Lagrangian manifold involves the symplectic form denoted ω, which is an antisymmetric, bilinear operator acting on vectors in phase space. If we let $\delta \mathbf{z}_1 = (\delta \mathbf{q}_1, \delta \mathbf{p}_1)$ and $\delta \mathbf{z}_2 = (\delta \mathbf{q}_2, \delta \mathbf{p}_2)$ be two small displacements in phase space, then the action of the symplectic form on them is defined by

$$\omega(\delta \mathbf{z}_1, \delta \mathbf{z}_2) \quad = \quad \delta \mathbf{p}_1 \cdot \delta \mathbf{q}_2 - \delta \mathbf{p}_2 \cdot \delta \mathbf{q}_1 \tag{9.9}$$

or, in matrix form

$$\omega(\delta \mathbf{z}_1, \delta \mathbf{z}_2) \quad = \quad \delta \mathbf{z}_1 \cdot \omega \cdot \delta \mathbf{z}_2 \tag{9.10}$$

where ω is the unit symplectic matrix,

$$\omega \quad = \quad \begin{bmatrix} \mathbf{0} & \mathbf{1} \\ -\mathbf{1} & \mathbf{0} \end{bmatrix}. \tag{9.11}$$

The matrix ω is antisymmetric and orthogonal, so $\omega^t = \omega^{-1} = -\omega$. Note that only two vectors are involved in the definition of the symplectic form no matter how many dimensions in the phase space. The symplectic form is invariant under canonical transformations, in the sense that the value of the right hand side of equation (9.9) is independant of the canonical coordinates used to compute it.

We now define a Lagrangian manifold as an f-dimensional surface L in the $2f$ dimensional phasespace such that at all points $(\mathbf{x}, \mathbf{p})$ on L and for all vectors $\delta\mathbf{z}_1, \delta\mathbf{z}_2$ tangent to L at $(\mathbf{x}, \mathbf{p})$, we have

$$\omega(\delta\mathbf{z}_1, \delta\mathbf{z}_2) \quad = \quad 0. \tag{9.12}$$

As an example we can investigate under which conditions a surface of the form

$$L \quad = \quad \{(\mathbf{x}, \mathbf{p}) | \mathbf{p} = \mathbf{M}\mathbf{x}\} \tag{9.13}$$

is lagrangian. Inserting the condition (9.13) into the definition of the symplectic form yields

$$(\mathbf{M}\delta\mathbf{q}_1) \cdot \delta\mathbf{q}_2 - (\mathbf{M}\delta\mathbf{q}_2) \cdot \delta\mathbf{q}_1 \quad = \quad 0 \tag{9.14}$$

which implies

$$\mathbf{M}_{ij} \quad = \quad \mathbf{M}_{ji} \tag{9.15}$$

i.e. that that matrix $\mathbf{M}$ should be symmetric. This is going to be an important restriction in the following sections.

As we menchioned before the symplectic form is conserved by canonical transformations. As a special case this implies that the symplectic form is conserved by a Hamiltonian flow since this can be considered as a canonical transformation. This means that Lagrangian manifolds evolve into Lagrangian manifolds in Hamiltonian flows, - an important fact that we shall also use in our following considerations.

The curvature integral

We consider integrals of the type

$$\mathrm{I}(q', p', \mathbf{M}') \quad = \quad \int dq\, dp\, d\mathbf{M}\, f(q, p, \mathbf{M}; t)\delta(q' - q^t)\delta(p' - p^t)\delta(\mathbf{M}' - \mathbf{M}^t) \tag{9.16}$$

where the super script t indicates the variabel evolved in time t . Doing the q integral gives a sum over certain q values who has the possibility to end up at the correct final q' if they are provided the correct initial momentum. The p integration rules out all except one of the initial q values since the phase space flow gives unique solutions to the Hamilton equations. In this way we get a unique point (q, p) defined in phase space namely the initial condition that leads to (q', p') in time t.

Once this point is specified the flow defines a (parametrized) flow on the curvature subspace $g_{q,p(q)} : \mathbf{M} \to \mathbf{M}'$. The map works in the following way: given (q_0, p_0) and $\mathbf{M}_0$ we have defined a little fraction of a Lagrangian manifold

$$L \quad = \quad \{(q, p) | p(\delta q) = p_0 + \mathbf{M}_0 \delta q\}$$

where we assume that $\delta q = q - q_0$ is very small. That the manifold is really Lagrangian is ensured by the fact that $\mathbf{M}$ is symmetric since it is the second

derivative of the action function $\mathbf{M} = \partial^2 S / \partial q_i \partial q_j$. This manifold can then be uniquely evolved in time t according to Hamilton Jacoby equations and from the new manifold generated in this way we can obtain $\mathbf{M}' = \mathbf{M}^t(q_0, p_0)$ as a function of the original curvature. $\mathbf{M}'$ then specifies the tangent manifold at the point (q', p') by the relation

$$\delta p' = \mathbf{M}' \delta \mathbf{q}'. \tag{9.17}$$

Example

As an example of the time evolution of the curvature matrix, we consider the free flight part of an N dimensional billard. Here we have

$$x(t) = x(0) + \mathbf{M}_0 x(0) t \tag{9.18}$$

and

$$p(t) = p(0) \tag{9.19}$$

so that we can write

$$\begin{aligned} p(t) &= \mathbf{M}_0 x_0 \\ &= \mathbf{M}_0 (\mathbf{1} + \mathbf{M}_0 t)^{-1} x(t) \end{aligned} \tag{9.20}$$

which gives

$$p(t) = \mathbf{M}_0 (\mathbf{1} + \mathbf{M}_0 t)^{-1} x(t) \tag{9.21}$$

and hence we see that the curvature matrix is a sort of generalized Sinai-Bunimowich curvature.

We are interested in the trace of the evolution operator $\mathcal{L}^t$ in (9.16)

$$\begin{aligned} \mathrm{tr}\mathcal{L}^t &= \int dq\, dp\, d\mathbf{M}\, \delta(q - q^t)\delta(p - p^t)\delta(\mathbf{M} - \mathbf{M}^t) \\ &\times\ e^{\frac{1}{2}\int_0^{T_p}(H_{pq} + H_{pp}\mathbf{M})d\tau} \end{aligned} \tag{9.22}$$

Following the strategy in section 3.1 we introduce longitudinal $\mathbf{x}_\parallel$ and perpendicular $\mathbf{x}_\perp$ coordinates along the total $\mathbf{x} = (q, p, \mathbf{M})$ flow to evaluate the contribution from a prime periodic orbit to the trace. In the longitudinal direction we get

$$\int d\mathbf{x}_\parallel \delta_\parallel(\mathbf{x} - \mathbf{x}^t) = T_p \sum_{r=1}^{\infty} \delta(t - rT_p) \tag{9.23}$$

where T_p is the period of the prime periodic orbit. In the perpendicular direction we get

$$\int d\mathbf{x}_\perp \delta_\perp(\mathbf{x} - \mathbf{x}^{rT_p}) = \frac{1}{|\det(\mathbf{1} - \hat{\mathbf{J}}_p^r)|} \tag{9.24}$$

where $\hat{\mathbf{J}}_p$ is the transverse stability matrix, $\mathbf{u}(t + T_p) = \hat{\mathbf{J}}_p \mathbf{u}(t)$ of the entire flow. Since $\frac{\partial q^t}{\partial \mathbf{M}} = \frac{\partial p^t}{\partial \mathbf{M}} = 0$ it has the structure

$$\det \hat{\mathbf{J}}_p = \begin{bmatrix} \mathbf{J}_{tr} & 0 \\ * & \mathbf{J_M} \end{bmatrix} \tag{9.25}$$

and since this is block diagonalizable the determinant splits up into a product of the usual transverse determinant and a determinant corresponding to the $\mathbf{M}$ flow

$$\det(\mathbf{1} - \hat{\mathbf{J}}_p^r) = \det(\mathbf{1} - \mathbf{J}_p^r) \cdot \det(\mathbf{1} - \mathbf{J_M}_p^r). \tag{9.26}$$

We can then write the trace in a form similar to the one in [15]

$$\mathrm{Tr}\,\mathcal{L}^t = \sum_p T_p \sum_{r=1}^{\infty} \frac{\delta(t - rT_p)}{|\det(\mathbf{1} - \mathbf{J}_p^r)|} \Delta_{p,r}, \tag{9.27}$$

with

$$\Delta_{p,r} = \sum_{\mathbf{M}^{rT_p} = \mathbf{M}} \frac{e^{\frac{1}{2} \int_0^{rT_p} (H_{pq} + H_{pp}\mathbf{M}) d\tau}}{|\det(\mathbf{1} - \mathbf{J_M}_p^r)|} \tag{9.28}$$

The first point in obtaining (9.28) is then to find the periodic solutions of the $\mathbf{M}$ flow. To do this we note that the invariant manifolds W^s and W^u of the periodic orbit locally defines linear subspaces E^s and E^u which are tangent to the invariant manifolds at the periodic orbit [42] Let us say that $E^s = \mathrm{span}\{\mathbf{s}_1, \mathbf{s}_2, \ldots \mathbf{s}_N\}$ and $E^u = \mathrm{span}\{\mathbf{u}_1, \mathbf{u}_2, \ldots \mathbf{u}_N\}$. Now let us look at the mixed subspace $L = \mathrm{span}\{\mathbf{e}_1, \mathbf{e}_2, \ldots \mathbf{e}_N\}$ where the $\mathbf{e}_i$'s are taken from the union $\{\mathbf{s}_1, \mathbf{s}_2, \ldots \mathbf{s}_N, \mathbf{u}_1, \mathbf{u}_2, \ldots \mathbf{u}_N\}$. This space has the right dimension for being a Lagrangian manifold, and taking the symplectic form on two of the eigenvectors and evolving the flow for one period of the orbit we get

$$\begin{aligned} \omega(f^t(\delta \mathbf{e}_i), f^t(\delta \mathbf{e}_j)) &= \lambda_i \lambda_j \omega(\delta \mathbf{e}_i, \delta \mathbf{e}_j) \\ &= \omega(\delta \mathbf{e}_i, \delta \mathbf{e}_j) \end{aligned} \tag{9.29}$$

where the last equation follows since the symplectic form is conserved by the flow. From this it follows that the symplectic form actually vanishes on any set of eigenvectors where the product $\lambda_i \lambda_j$ is different from unity. This implies that a mixed subspace choosen in this way is actually a Lagrangian manifold. If we now let the flow evolve such a manifold for one period, we get for points on the Lagrangian manifold close to the periodic point

$$\begin{aligned} \mathcal{F}^t(x^* + \delta a_1 \mathbf{e}_1 + \ldots + \delta a_N \mathbf{e}_N) &= x^* + \mathbf{J}_p(\delta a_1 \mathbf{e}_1 + \ldots + \delta a_N \mathbf{e}_N) \\ &= x^* + \Lambda_1 \delta a_1 \mathbf{e}_1 + \ldots + \Lambda_N \delta a_N \mathbf{e}_N \\ &\in x^* + L \end{aligned} \tag{9.30}$$

so that an N-dimensional superposition of the linear subspaces is also locally invariant and hence leads to a periodic solution of the curvature flow.

If we are only looking at Hamiltonian flows where the eigenvalues of the Jacobian are non degenerate, we see that for every eigenvector of the Jacobian the symplectic form on all other eigenvectors except the one with eigenvalue Λ^{-1} must vanish due to the above argument. However, the symplectic form on an eigenvector with eigenvalue Λ and its adjoint with eigenvalue Λ^{-1} does not vanish. To see this we can consider the simple case where the phase space is 4-dimensional. Let us denote the four eigenvectors $\delta\mathbf{e}_1,\ldots,\delta\mathbf{e}_4$ with corresponding eigenvalues $\Lambda_1,\Lambda_2,\Lambda_1^{-1},\Lambda_2^{-1}$. We can now choose a vector $\mathbf{x}$ so

$$\omega(\delta\mathbf{e}_1,\mathbf{x}) \;\neq\; 0 \tag{9.31}$$

Expanding $\mathbf{x}$ on the four eigenvectors and applying the linearity of ω then yields

$$\omega(\delta\mathbf{e}_1,\delta\mathbf{e}_3) \;\neq\; 0 \tag{9.32}$$

since all the other terms vanish due to the above argument. This means that in the non degenrate case where one can uniquely define the adjoint vector corresponding to an eigenvector by virtue of having the inverse eigenvalue, such two adjoint vectors can never lie in the same Lagrangian manifold. In this case the number of Lagrangian manifolds that are periodic solutions to our extended flow can therefore easily be counted. A given Lagrangian manifold is expanded by N eigenvectors of the Jacobian which each can be either an unstable or the adjoint stable eigenvector. This gives 2^N different possibilities and hence there are 2^N periodic solutions of the curvature flow.

By the above considerations we have now found all the periodic solutions of the curvature flow as the 2^N possible null-manifolds spanned by the eigenvectors of the Jacobian. The task is therefore now to find the eigenvalues of $\mathbf{J_M}$ as a function of the usual cycle stabilities.

2-dimensional flows

In the case of a 2-dimesional Hamiltonian flow reduced to a 2-dimensional Poincare section return map one can use the rational fraction transformation technique of the Sinai Bunimovich curvature to get the variation of $\mathbf{M}$ as illustrated in [15]. Since this procedure is restricted to two dimensions we will here show a procedure to get the $\mathbf{M}$ stabilities which can be generalised to higher dimensions. The idea is simply the following. Suppose that we have already found the periodic solutions of the $\mathbf{M}$ flow. Then we make a small variation $\delta\mathbf{M}$ of the periodic solution $\mathbf{M}_0$. This gives us a new manifold according to (9.17). Using the *usual* Jacobian we then evolve as many points on this new manifold as it takes to span it (N) for a period of time T_p and then from the evolved points we construct the linearization of the evolved manifold. From this manifold we then get the evolved curvature matrix $\mathbf{M}^t$ which is of the form

$$(\mathbf{M}_0 + \delta\mathbf{M})^t \;=\; \mathbf{M}_0 + \mathbf{J_M}\delta\mathbf{M} + \mathcal{O}(\delta\mathbf{M}^2) \tag{9.33}$$

where now $\mathbf{J_M}$ should be expressed in terms of the cycle stabilities.

To see how this works we first consider a simple two-dimensional example where the result is known [15]. In two dimensions we can reduce the problem to a 2-dimensional Poincaré surface of section mapping which will then have an unstable $\mathbf{u} = (u_1, u_2)$ direction of stability Λ and a stable direction $\mathbf{s} = (s_1, s_2)$ of stability Λ^{-1}. If the system is hyperbolic we have $\Lambda > 1$. In the usual Cartesian coordinates the full Jacobian can be found by the set of equations

$$\mathbf{Ju} = \Lambda \mathbf{u}$$
$$\mathbf{Js} = \Lambda^{-1} \mathbf{s}$$

This gives the Jacobian

$$\mathbf{J} = (s_1 u_2 - s_2 u_1)^{-1} \begin{pmatrix} -(\Lambda u_1 s_2 - \frac{s_1 u_2}{\Lambda}) & (\Lambda - \frac{1}{\Lambda})u_1 s_1 \\ -(\Lambda - \frac{1}{\Lambda})u_2 s_2 & (\Lambda u_2 s_1 - \frac{s_2 u_1}{\Lambda}) \end{pmatrix}$$

The linearized stable and unstable manifolds which are both simply lines on the Poincare section see fig 9.1 are characterized by their slopes $m_s = s_2/s_1$
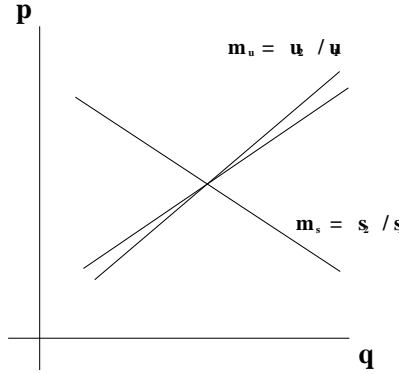
Figure 9.1: The stable and unstable manifolds in the Poincare section. A variation of the unstable manifold is shown.

and $m_u = u_2/u_1$. We now make a small variation δm_s of m_s. This corresponds to points on the line $(x, p) = (x, (m_s + \delta m_s)x)$. These points are mapped by the Jacobian into a line of slope

$$(m_s + \delta m_s)' \;\; = \;\; \frac{J_{21} + J_{22}(m_s + \delta m_s)}{J_{11} + J_{12}(m_s + \delta m_s)}. \tag{9.34}$$

According to (9.33) we expect the result to be of the form

$$(m_s + \delta m_s)' \;\; = \;\; m_s + \lambda \delta m_s + \mathcal{O}(\delta m_s^2) \tag{9.35}$$

we therefore expand the denominator to the first order in δm_s

$$(m_s + \delta m_s)' \;\; \simeq \;\; \frac{(J_{21} + J_{22} m_s)(1 + \frac{J_{22}\delta m_s}{J_{21} + J_{22}m_s})(1 - \frac{J_{12}\delta m_s}{J_{11} + J_{12}m_s})}{J_{11} + J_{12}m_s}$$
$$= \;\; \frac{J_{21} + J_{22}m_s}{J_{11} + J_{12}m_s}\left(1 + \left(\frac{J_{22}}{J_{21} + J_{22}m_s} - \frac{J_{12}}{J_{11} + J_{12}m_s}\right)\delta m_s\right)$$

But since m_s was an invariant of the map this simply gives

$$(m_s + \delta m_s)' = m_s + \frac{J_{22} - J_{12}m_s}{J_{11} + J_{12}m_s}\delta m_s \tag{9.36}$$

Putting in the entities from the Jacobian we get

$$(m_s + \delta m_s)' = m_s + \Lambda^2 \delta m_s \tag{9.37}$$

that is $\lambda_s = \Lambda^2$ for the stable direction. For the unstable direction everything is similar and we get $\lambda_u = \Lambda^{-2}$.

The trace integration in 2 dimensions

To get the trace of the new evolution operator $\mathcal{L}$ we have to do the integral

$$\text{Tr}\mathcal{L} = \int dq dp d\mathbf{M}\mathcal{L}(q, p, \mathbf{M}, t|q, p, \mathbf{M}, 0) \tag{9.38}$$

with the kernel

$$e^{i\pi\nu + \int_0^t d\tau \frac{iL}{\hbar} + \frac{1}{2}\text{Tr}\left\{\frac{\partial^2 H}{\partial p \partial q} + \frac{\partial^2 H}{\partial p \partial p}\mathbf{M}\right\}} \delta(q - q^t(q, p))\delta(p - p^t(q, p))\delta(\mathbf{M} - \mathbf{M}^t(q, p, \mathbf{M})), \tag{9.39}$$

where $q^t(q, p)$, $p^t(q, p)$ and $\mathbf{M}^t(q, p, \mathbf{M})$ denote the evolution of q, p and $\mathbf{M}$ from the initial coordinates $q, p = \nabla S_0(q)$ and $\mathbf{M} = \partial_i \partial_j S_0(q)$ during the time t, and ν is the Maslov index. this integral is exactly of the type (9.16.) For a 2-dimensional flow we saw that the stabilities of the $\mathbf{M}$ flow could be found in terms of the stabilities of the periodic orbits. So what is left is to evaluate the integral of the trace. Assuming the Hamiltonian to be of the form $H(q, p) = p^2/2m + V(q)$, we are left with the integral

$$\exp\{\frac{1}{2}\int_0^t d\tau \text{Tr}\mathbf{M}(\tau)\} = (\frac{V(q^t)}{V(q_0)})^{1/2}. \tag{9.40}$$

Now the volume ratio in (9.40) is in configuration space but is determined by the initial $\mathbf{M}$ matrix since this gives the variations in initial momenta of the δq's spanning the initial configuration space volume element. This means that the initial $\mathbf{M}$ matrix decides if we are on the stable or the unstable manifold. Therefore the volume ratio is quite simple to determine since it is simply Λ or Λ^{-1} if we are on the unstable respectively stable manifold.

In higher dimensions we are in general on some mixed stability manifold L spanned by N phase space vectors $\mathbf{e}_i$. To determine the volume ratio we select N infinitesimal vectors $\delta\mathbf{q}_1, \delta\mathbf{q}_2 \ldots \delta\mathbf{q}_N$ spanning a small parallelepiped around the periodic point in configuration space. The volume of this is $\det(\delta\mathbf{q}_1 \delta\mathbf{q}_2 \ldots \delta\mathbf{q}_N)$. We then evolve these according to the Jacobian and evaluate the volume of the projection of the image on configuration space. By choosing $\delta\mathbf{q}_i = \pi_q(\mathbf{e}_i)$ the projection of the $\mathbf{e}_i$ vector on the q-space, we can easily calculate the image of

the N $\delta\mathbf{x}_i = (\delta\mathbf{q}_i, \delta\mathbf{p}_i) = \delta\mathbf{e}_i$ vectors. The volume of the evolved parallelepiped in configuration space is then given by $\det(\Lambda_1 \pi_q \mathbf{e}_1, \Lambda_2 \pi_q \mathbf{e}_2 \ldots \Lambda_N \pi_q \mathbf{e}_N)$. Since multiplication of a column of a matrix by a factor Λ changes the determinant of the matrix with the same factor we get the volume ratio as the product of the stabilities of the manifold

$$\frac{V(q^t)}{V(q_0)} \quad = \quad \prod_{i=1}^{N} \Lambda_i \tag{9.41}$$

We now have everything we need to do the integral in 2-dimensions. The unstable and the stable manifold through the periodic orbit yields in the $\mathbf{M}$ integration respectively $|\Lambda_p|^{1/2}/(1 - \Lambda_p^{-2})$ and $|\Lambda_p|^{-1/2}/(1 - \Lambda_p^2)$. Putting this into (9.28) yields

$$\begin{aligned}
\Delta_{p,r} \quad &= \quad \frac{|\Lambda_p^r|^{1/2}}{|1 - \Lambda_p^{-2r}|} + \frac{|\Lambda_p^r|^{-1/2}}{|1 - \Lambda_p^{2r}|} \\
&= \quad \frac{|\Lambda_p^r|^{1/2}}{1 - \Lambda_p^{-2r}} + \frac{|\Lambda_p^r|^{-5/2}}{1 - \Lambda_p^{-2r}}
\end{aligned} \tag{9.42}$$

which is the formula obtained in [15] for $\beta = 1/2$.

Higher dimensions

As we saw above we know how to do the trace integral in any number of dimensions, and we know what the periodic solutions of $\mathbf{M}$ are. The only thing we need now is to generalize the scheme in the above section (9.1.1). To see how it works let us consider the following simple example in 3-dimensions. Here the phase space is 6-dimensional but a Poincaré section and reduction to the energy shell reduces the problem to a 4-dimensional map. Let us further assume that the Jacobian in these coordinates is diagonal with diagonal elements: $\Lambda_1, \Lambda_2, \Lambda_1^{-1}, \Lambda_2^{-1}$. Then $\mathbf{M}_0 = \mathbf{0}$ is a periodic solution since this corresponds to a swarm of points lying in the $\mathbf{q}$-plane with zero momentum:

$$L \quad = \quad \{(q_1, q_2, p_1, p_2)|p_1 = p_2 = 0\}$$

We then make a small variation $\delta\mathbf{M}$ of the curvature matrix and select two vectors that spans the manifold corresponding to $\delta\mathbf{M}$. As an example we might choose:

$$v_1 = \begin{pmatrix} 1 \\ 0 \\ \delta m_{11} \\ \delta m_{21} \end{pmatrix} , \ v_2 = \begin{pmatrix} 0 \\ 1 \\ \delta m_{12} \\ \delta m_{22} \end{pmatrix}$$

The image under the Jacobian of these two vectors is given by

$$\mathrm{span}\{ \begin{pmatrix} \Lambda_1 \\ 0 \\ \delta m_{11}\Lambda_1^{-1} \\ \delta m_{21}\Lambda_2^{-1} \end{pmatrix} , \begin{pmatrix} 0 \\ \Lambda_2 \\ \delta m_{12}\Lambda_1^{-1} \\ \delta m_{22}\Lambda_2^{-1} \end{pmatrix} \}$$

from which we get the evolved curvature matrix by "division" $\mathbf{M}' = \delta \mathbf{p}'/\delta \mathbf{x}'$

$$\delta m'_{11} = \frac{\delta m_{11}}{\Lambda_1^2} \quad \delta m'_{12} = \frac{\delta m_{12}}{\Lambda_1 \Lambda_2}$$

$$\delta m'_{21} = \frac{\delta m_{21}}{\Lambda_1 \Lambda_2} \quad \delta m'_{22} = \frac{\delta m_{22}}{\Lambda_2^2}$$

From this we can directly get the stabilities of the periodic $\mathbf{M}$ solution corresponding to this choice of initial curvature. One should of course take care that the bonds on $\mathbf{M}$ require this to be symmetric and we should also remember to take other $\mathbf{M}$ solutions into account in the final result. The last point is not so straight forward in this example because all the other Lagrangian planes will be caustics since they have zero variation in one of the q-directions (in two dimensions this would correspond to that the invariant subspaces was the x and y axis. The x-axis is of course well described as a function of x whereas the y-axis is not given as $y = m \cdot x$!).

The general N-dimensional case

The idea of the above 2-dimensional example is good and we should try to make use of the eigenvectors of the flow. The main strategy is straight forward: we make a variation of the curvature matrix giving us a variated Lagrangian manifold. This we express in the basis of eigenvectors of the Jacobian, and then evolve it for one period by use of the cycle stabilities. Then we go back to the original curvature space and read off the eigenvalues in terms of the cycle stabilities.

This program is simple but require that we account for some details about how the δM_{ij}'s are related to the vectors spanning the variated Lagrangian manifold (these vectors are of course not eigenvectors anylonger).

To simplify the notation we start with a few definitions. Suppose we have a Lagrangian manifold: $L = \text{span}\{\mathbf{e}_1, \mathbf{e}_2, \dots \mathbf{e}_N\}$ which also can be spanned by the curvature matrix $\mathbf{M}$. This we can express by introducing the usual orthonormal basis of unit vectors in *configuration* space $\mathbf{1}_i = (0, \dots, 1, \dots, 0)$ where the '1' is on the i'th place of the only N entities. Then we also have

$$L = \text{span}\{ \begin{pmatrix} \mathbf{1}_i \\ \mathbf{M}\mathbf{1}_i \end{pmatrix} \}_{i=1}^{N}$$

which also in short can be written

$$L = \text{span}\{ \begin{pmatrix} \mathbf{1} \\ \mathbf{M}\mathbf{1} \end{pmatrix} \}$$

For the variated lagrangian manifold we use the notation

$$\delta L = \text{span}\{\begin{pmatrix} \mathbf{1} \\ (\mathbf{M} + \delta\mathbf{M})\mathbf{1} \end{pmatrix}\}$$

This we can also expand as before in terms of the eigenvectors but then we just have to add a small displacement vector to each of the eigenvectors to get the correct variated manifold. These displacement vectors can in turn be expanded by all the vectors we did not use to expand the original L. This reads:

$$\delta L = \text{span}\{\mathbf{e}_i + \sum_{j=N+1}^{2N} \delta\tilde{M}_{ij}\mathbf{e}_j\}_{i=1}^{N}.$$

We can also define

$$
\begin{aligned}
\delta\tilde{\mathbf{m}}_i &\equiv \sum_{j=N+1}^{2N} \delta\tilde{M}_{ij}\mathbf{e}_j \\
&\equiv \delta\tilde{\mathbf{M}}\mathbf{E}
\end{aligned}
\tag{9.43}
$$

where $\mathbf{E}$ is the matrix consisting of the last N eigenvectors which does not lie in the original manifold:

$$\mathbf{E} = (\mathbf{e}_{N+1}, \mathbf{e}_{N+2}, \ldots, \mathbf{e}_{2N}). \tag{9.44}$$

Analogously we finaly define

$$\delta\mathbf{m}_i = \begin{pmatrix} \delta m_{1i} \\ \delta m_{2i} \\ \vdots \\ \delta m_{Ni} \end{pmatrix}$$

whereas

$$\delta\mathbf{M} = \begin{pmatrix} \delta m_{11} & \ldots & \delta m_{1N} \\ \vdots & & \vdots \\ \delta m_{N1} & \ldots & \delta m_{NN} \end{pmatrix}.$$

which ends our initial definitions. The geometrical interpretation of the defined vectors is indicated on figure 9.2.

Since we can interpret $\delta\mathbf{M}$ and $\delta\tilde{\mathbf{M}}$ as vectors themselves in $\mathbf{R}^{N^2}$, there exist an invertible matrix $\mathbf{P}$ such that

$$\vec{\delta\tilde{\mathbf{M}}} = \mathbf{P}\vec{\delta\mathbf{M}} \tag{9.45}$$

and

$$\vec{\delta\mathbf{M}} = \mathbf{P}^{-1}\vec{\delta\tilde{\mathbf{M}}}. \tag{9.46}$$

where the entities of the matrices are now written as single column of length N^2. This simply corresponds to a rescaling and rotation of the matrices and
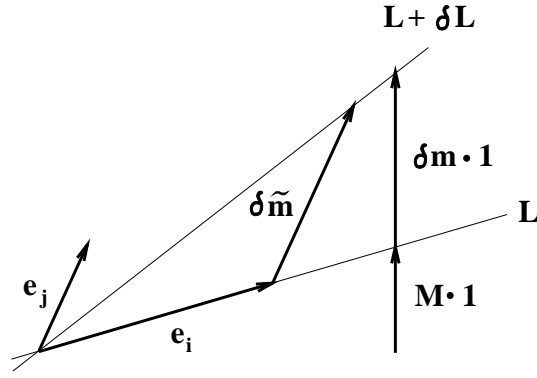
Figure 9.2: The geometrical significance of the introduced vectors. The $\delta\tilde{\mathbf{m}}_i$ vectors connects the original Lagrangian manifold L to the variated manifold along the directions not used to span L. The $\delta\mathbf{m}_i$ vectors on the contrary connects L to $L + \delta L$ in vertical direction.

is therefore obviously a welldefined transformation. We note that the map $\mathbf{P}$ only gives a valid relation between $\delta\mathbf{M}$ and $\delta\tilde{\mathbf{M}}$ around vectors of the form

$$\delta\mathbf{e}_i + \sum_{j=N+1}^{2N} \delta\tilde{M}_{ij}\delta\mathbf{e}_j \tag{9.47}$$

Now we evolve the variated Lagrangian manifold by applying the Jacobian on the $\mathbf{e}_i + \delta\tilde{\mathbf{m}}_i$ vectors

$$\mathbf{J}(\mathbf{e}_i + \sum_{j=N+1}^{2N} \delta\tilde{M}_{ij}\mathbf{e}_j) = \Lambda_i\mathbf{e}_i + \sum_{j=N+1}^{2N} \delta\tilde{M}_{ij}\Lambda_j\mathbf{e}_j$$
$$\tag{9.48}$$

This image we can not immideately map back to the δM_{ij}'s because this map was only defined in the neighbourhood of of the $\mathbf{e}_i$ vectors. The evolved manifold can however also be described by

$$
\begin{aligned}
L + \delta L' &= \text{span}\{\Lambda_i\mathbf{e}_i + \sum_{j=N+1}^{2N} \delta\tilde{M}_{ij}\Lambda_j\mathbf{e}_j\}_{i=1}^N \\
&= \text{span}\{\mathbf{e}_i + \sum_{j=N+1}^{2N} \delta\tilde{M}_{ij}\frac{\Lambda_j}{\Lambda_i}\mathbf{e}_j\}_{i=1}^N
\end{aligned}
\tag{9.49}
$$

where the latter is a description of the same manifold in a form that can be mapped directly back to the δM_{ij} description by $\mathbf{P}$. We then have that the evolved $\delta\tilde{M}_{ij}$ is given in diagonal form by

$$\delta\tilde{M}'_{ij} = \frac{\Lambda_j}{\Lambda_i}\delta\tilde{M}_{ij} \tag{9.50}$$

or

$$\vec{\delta\tilde{\mathbf{M}}}' = \left[\frac{\Lambda_j}{\Lambda_i}\right] \vec{\delta\tilde{\mathbf{M}}}$$

$$(9.51)$$

where we have introduced the vector form of the matrices $\vec{\delta\tilde{\mathbf{M}}} = (\delta M_{11}, \ldots, \delta M_{1N}, \ldots, \delta M_{NN})$, and where $[\Lambda_j/\Lambda_i]$ is a diagonal matrix, having the eigenvalues of the original manifold in the denominator. This implies

$$\begin{aligned}\vec{\delta\mathbf{M}}' &= \mathbf{P}^{-1}\vec{\delta\tilde{\mathbf{M}}}' \\ &= \mathbf{P}^{-1}\left[\frac{\Lambda_j}{\Lambda_i}\right]\mathbf{P}\vec{\delta\mathbf{M}}\end{aligned}$$

$$(9.52)$$

where we now got rid of the tilded coordinates by mapping back with $\mathbf{P}$. The eigenvalues of the $\vec{\delta\mathbf{M}}$ map is given by the zeros of the determinant

$$\begin{aligned}\det(\mathbf{P}^{-1}\left[\frac{\Lambda_j}{\Lambda_i}\right]\mathbf{P} - \lambda\mathbf{1}) &= \det(\left[\frac{\Lambda_j}{\Lambda_i}\right] - \lambda\mathbf{1}) \\ &= \prod_{i=1}^{N}\prod_{j=N+1}^{2N}(\frac{\Lambda_j}{\Lambda_i} - \lambda) \\ &= 0.\end{aligned}$$

$$(9.53)$$

This gives the N^2 eigenvalues of the $\vec{\delta\mathbf{M}}$ map

$$\lambda_{ij} = \frac{\Lambda_j}{\Lambda_i}$$

$$(9.54)$$

where the indices run like $i = 1, \ldots, N$ representing the first N eigenvectors used to span the original manifold, and $j = N + 1, \ldots, 2N$ denotes the remaining N eigenvectors. We now must recall that the $\mathbf{M}$ integration takes place over the space of *symmetric* matrices, since the curvature matrix $\mathbf{M}$ is the second derivative of the action and therefore is symmetric. We therefore also only can allow for symmetric variations of the solution. That $\delta\mathbf{M}$ is symmetric implies that we only have the $N(N + 1)/2$ symmetric eigenvectors $\delta\mathbf{M} = \delta_{i,j} + \delta_{j,i}$, where $i = 1, \ldots, N$ and $j = i, \ldots N$ with the stabilities

$$\lambda_i = \frac{\Lambda_{i+N}}{\Lambda_j}, \quad i = 1, \ldots, N \quad j = j, \ldots, N$$

$$(9.55)$$

We can now write down the general result of the $\mathbf{M}$ integration

$$\begin{aligned}\Delta_{p,r} &= \int d\mathbf{M}e^{\int_0^t d\tau\frac{1}{2}\mathrm{Tr}(H_{pq}+H_{pp}\mathbf{M})}\delta(\mathbf{M} - \mathbf{M}^t(\mathbf{M})) \\ &= \sum_{l=1}^{2^N}\prod_{i_l=1}^{N}|\Lambda_{i_l}|^{r/2}\prod_{j=i_l}^{N}|1 - \Lambda_{i_l+N}^r\Lambda_{i_l}^r|^{-1},\end{aligned}$$

$$(9.56)$$

where l labels the periodic $\mathbf{M}$ solutions.

In the simple 2-dimensional case the above formula would reduce to

$$
\begin{aligned}
\Delta_{p,r} &= \int d\mathbf{M} e^{\int_0^t d\tau \frac{1}{2}\mathrm{Tr}\mathbf{M}} \delta(\mathbf{M} - \mathbf{M}^t(\mathbf{M})) \\
&= \sum_{l=1}^{2} \prod_{i_l=1}^{1} |\Lambda_{i_l}^{r/2}| \prod_{j=1}^{1} |1 - \Lambda_{i_l+N}^{r}/\Lambda_{i_l}^{r}|^{-1} \\
&= \frac{|\Lambda_p^r|^{1/2}}{|1 - \Lambda_p^{-2r}|} + \frac{|\Lambda_p^r|^{-1/2}}{|1 - \Lambda_p^{2r}|} \\
&= \frac{|\Lambda_p^r|^{1/2}}{1 - \Lambda_p^{-2r}} + \frac{|\Lambda_p^r|^{-5/2}}{1 - \Lambda_p^{-2r}}
\end{aligned}
\tag{9.57}
$$

which is the previously obtained result.

Example: solution of the usual second order equation

To see how the formula (5.62) works let us try first to solve a usual second order equation. To be specific we can try

$$
-x^2 + x + 2 = 0
$$

that has the roots $x_1 = 2$ and $x_2 = -1$. First we should get the equation on the form (5.44) which implies $B = -1, C = -2$ and for instance $A = 1$ and $D = 0$ since we are more free to choose the two latter constants. $\mathbf{J}$ then looks like

$$
\mathbf{J} = \begin{bmatrix} 1 & -1 \\ -2 & 0 \end{bmatrix}
$$

To diagonalize $\mathbf{J}$ we have to solve the characteristic second order equation

$$
y^2 - y - 2 = 0
$$

which yields $y = 2, y = -1$. It is obvious that we have now solved the original equation already, but in the N-dimensional case we would at this point have solved an equation

$$
a_0 + a_1 y + \ldots + a_{2N} y^{2N} = 0
$$

in stead of dealing with $N \times N$ matrices! The eigenvectors are easily found to be

$$
v_1 = \begin{bmatrix} 1 \\ -1 \end{bmatrix} , \text{ and } v_2 = \begin{bmatrix} 1 \\ 2 \end{bmatrix}
$$

so that the matrix that diagonalizes $\mathbf{J}$ is given by the inverse

$$\mathbf{T}_1^{-1} = \begin{bmatrix} 1 & 1 \\ -1 & 2 \end{bmatrix} \ , \ \text{or} \ \mathbf{T}_2^{-1} = \begin{bmatrix} 1 & 1 \\ 2 & -1 \end{bmatrix}$$

since we are allowed to permute the columns. The linear fixpoint equation (5.58) now yields

$$\tilde{m} = 1 \cdot \tilde{m} \cdot 2^{-1} \ , \ \text{or} \ \tilde{m} = 2 \cdot \tilde{m} \cdot 1^{-1}$$

which both has the solution $\tilde{m} = 0$. This finaly gives us the solutions

$$m = -T_{pp}^{-1} T_{pq}$$

which yields respectively $m = -1$ and $m = 2$.

Example: solution of a second order matrix equation

Here we try with a bit more complicated 2-dimensional example. Let the matrices be given by

$$\mathbf{A} = \begin{bmatrix} 5 & 0 \\ 0 & 2 \end{bmatrix}, \mathbf{B} = \begin{bmatrix} 0 & 2 \\ 0 & -2 \end{bmatrix}$$

and

$$\mathbf{C} = \begin{bmatrix} 0 & -1 \\ 0 & 1 \end{bmatrix}, \mathbf{D} = \begin{bmatrix} 1 & -4 \\ 1 & 6 \end{bmatrix}$$

This gives

$$\mathbf{J} = \begin{bmatrix} 5 & 0 & 0 & 2 \\ 0 & 2 & 0 & -2 \\ 0 & -1 & 1 & -4 \\ 0 & 1 & 1 & 6 \end{bmatrix}$$

which turns out to be diagonalized by

$$\mathbf{T}_1 = \begin{bmatrix} 0 & 0 & 1 & 1 \\ 0 & 1 & 1 & 2 \\ 0 & 1 & 1 & 3 \\ 1 & 1 & 1 & 4 \end{bmatrix}$$

where the rows can be permuted arbitrarily. Since the two lower rows of $\mathbf{T}$ determines the solution there will be $K_{4,2} = 6$ different solutions of the form

$$\tilde{\mathbf{M}} = -\mathbf{T}_{pp}^{-1}\mathbf{T}_{pq}$$

We note here that permutations within the rows does not change the $\mathbf{M}$ solution since

$$
\begin{aligned}
-(\mathbf{PT}_{pp})^{-1}\mathbf{PT}_{pq} &= -\mathbf{T}_{pp}^{-1}\mathbf{P}^{-1}\mathbf{PT}_{pq} \\
&= \tilde{\mathbf{M}}
\end{aligned}
\tag{9.58}
$$

For $\mathbf{T}_1$ the solution is

$$\mathbf{M}_1 = -\begin{bmatrix} 1 & 3 \\ 1 & 4 \end{bmatrix}^{-1}\begin{bmatrix} 0 & 1 \\ 1 & 1 \end{bmatrix} = \begin{bmatrix} 3 & -1 \\ -1 & 0 \end{bmatrix}$$

The remaining solutions are

$$\mathbf{M}_2 = \begin{bmatrix} 1 & -1 \\ -1/2 & 0 \end{bmatrix}, \mathbf{M}_3 = \begin{bmatrix} 1/3 & 1/3 \\ -1/3 & -1/3 \end{bmatrix}$$

$$\mathbf{M}_4 = \begin{bmatrix} 0 & -1 \\ 0 & 0 \end{bmatrix}, \mathbf{M}_5 = \begin{bmatrix} 0 & 1/2 \\ 0 & -1/2 \end{bmatrix}$$

and finaly

$$\mathbf{M}_6 = \begin{bmatrix} 0 & 1 \\ 0 & -1 \end{bmatrix}$$

That all these are in fact solutions can easily be verified by direct substitution into (5.44).

Example: The periodic M solutions generated by a symplectic Jacobian

As a demonstration of the considerations about symplectic matrices we shall in this example diagonalize a symplectic 4 by 4 Jacobian by a symplectic rotation. This leads us to $2^2 = 4$ symmetric $\mathbf{M}$ solutions using the results obtained in section (5.3.1).

Let $\mathbf{J}$ be the Jacobian

$$\mathbf{J} = \begin{bmatrix} -13 & -11 & -8 & -2 \\ -49 & -263/6 & -76/3 & -41/3 \\ 60 & 52 & 33 & 14 \\ 87 & 155/2 & 46 & 23 \end{bmatrix}$$

The symplectic matrix $\mathbf{T}$ given by

$$
\mathbf{T} = \left[\begin{array}{cccc} -8 & -6 & -4 & -2 \\ 6 & 6 & 3 & 2 \\ 1 & 3/2 & 0 & 1 \\ 3 & 4 & 1 & 2 \end{array} \right]
$$

diagonalizes $\mathbf{J}$ and we have

$$
\mathbf{T}\mathbf{J}\mathbf{T}^{-1} = \left[\begin{array}{cccc} 2 & 0 & 0 & 0 \\ 0 & -3 & 0 & 0 \\ 0 & 0 & 1/2 & 0 \\ 0 & 0 & 0 & -1/3 \end{array} \right]
$$

where we note that the eigenvalues enters in the right sequence according to
(5.70) in order for the diagonalized Jacobian to be symplectic. Using eq. (5.62)
we get the solutions

$$
\mathbf{M}_1 = - \left[\begin{array}{cc} 1 & 1 \\ 1 & 3/2 \end{array} \right]
$$

for the identity permutation $\tau(1234) = 1234$,

$$
\mathbf{M}_2 = -\frac{1}{3} \left[\begin{array}{cc} 5 & 2 \\ 2 & 5 \end{array} \right]
$$

with the permutation $\tau(1234) = 3214$,

$$
\mathbf{M}_3 = - \left[\begin{array}{cc} 4/3 & 1 \\ 1 & 3/2 \end{array} \right]
$$

with $\tau(1234) = 1432$, and finaly

$$
\mathbf{M}_4 = - \left[\begin{array}{cc} 2 & 0 \\ 0 & 3 \end{array} \right]
$$

with $\tau(1234) = 3412$.

So this is an example where $\mathbf{J}$ can be diagonalized by symplectic rotations
in four different ways each leading to different $\mathbf{M}$ solutions of the fixpoint equa-
tions.

Example: The Hamilton Jacobi equation near a periodic orbit

As another application of our solution to the fixpoint equation of the rational fraction transformation of the curvature matrix, we can create the solution to the Hamilton Jacobi equation in the neighbourghood of a periodic orbit going through (x_0, p_0). In that case we simply have

$$S(\mathbf{x}) \quad = \quad S(\mathbf{x}_0) + \mathbf{p}_0(\mathbf{x} - \mathbf{x}_0) + (\mathbf{x} - \mathbf{x}_0)^{tr}\mathbf{M}(\mathbf{x} - \mathbf{x}_0) + \mathcal{O}(\|\mathbf{x} - \mathbf{x}_0\|^3) \tag{9.59}$$

As we shall see in section 7.1 this can be used to speed up the calculation of $\hbar$ corrections to the Gutzwiller-Voros zeta function.

9.2 Derivations and examples of chapter 6

The geometrical contribution to the semiclassical propagator

The expression for the geometrical part reads

$$G_{\text{geo}}(k\vec{r}, k\vec{r}') \quad = \quad -\frac{i}{8} \int_{-\infty+i\epsilon}^{+\infty+i\epsilon} d\nu \, e^{i\nu\theta} \left(H_\nu^{(1)}(kr')H_\nu^{(2)}(kr) - H_\nu^{(1)}(kr')\frac{H_\nu^{(2)}(ka)}{H_\nu^{(1)}(ka)}H_\nu^{(1)}(kr) \right)$$

We first discuss the saddle point approximation of the first term. The saddle-point condition here is

$$\theta + \arccos\frac{\nu_{S1}}{kr} - \arccos\frac{\nu_{S1}}{kr'} = 0 \tag{9.60}$$

The geometrical interpretation of this is that the two points $\vec{r}$ and $\vec{r}'$ should be on the same side on the line joining $\vec{r}'$ with $\vec{r}$ as measured from the point of closest approach to the center of the disk (see fig. 9.3). If $\vec{r}'$ and $\vec{r}$ are on
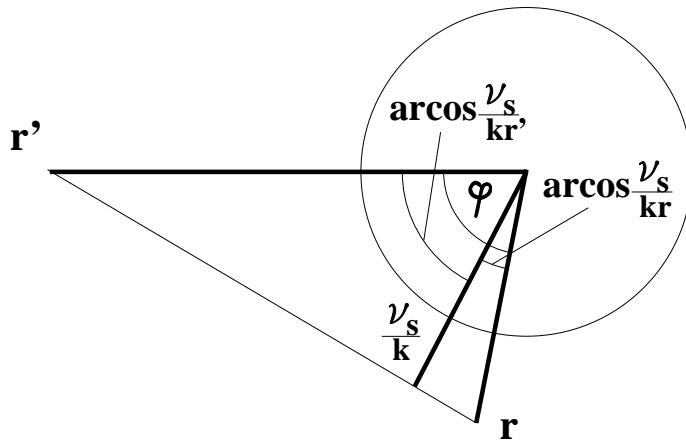
Figure 9.3: the line joining $\vec{r}'$ with $\vec{r}$. The point of closest approach to the center of the disk is indicated.

opposite sides with respect to this point the first summand in (9.60) wil have

a vanishing contribution in the semiclassical limit. So in case there is a real saddle the contribution of the first summand in (6.33) reads

$$
\begin{aligned}
-\frac{i}{8} \int_{-\infty+i\epsilon}^{+\infty+i\epsilon} d\nu \, e^{i\nu\theta} H_\nu^{(1)}(kr') H_\nu^{(2)}(kr) \quad \sim & \quad -\frac{i}{8}\frac{2}{\pi} \frac{e^{i\sqrt{k^2 r'^2 - \nu_{S1}^2} - i\sqrt{k^2 r^2 - \nu_{S1}^2}}}{(k^2 r'^2 - \nu_{S1}^2)^{\frac{1}{4}}(k^2 r^2 - \nu_{S1}^2)^{\frac{1}{4}}} \times \\
& \times \int d\tilde{\nu}\, e^{-i\frac{1}{2}(\tilde{\nu}-\nu_{S1})^2 \left(\frac{1}{\sqrt{k^2 r^2 - \nu_{S1}^2}} - \frac{1}{\sqrt{k^2 r'^2 - \nu_{S1}^2}}\right)} \\
\sim & \quad -\frac{i}{4}\sqrt{\frac{2}{\pi}}\frac{e^{iL_{\text{direct1}} - i\pi/4}}{\sqrt{kL_{\text{direct1}}}} \qquad (9.61)
\end{aligned}
$$

where $L_{\text{direct1}} = \sqrt{(kr')^2 - \nu_{S1}^2} - \sqrt{(kr)^2 - \nu_{S1}^2} = |\vec{r}' - \vec{r}|$ is the geometrical distance between $\vec{r}'$ and $\vec{r}$. Note that the result (9.61) is exactly what we get if we insert the semiclassical Debye approximation is the expression (6.21) for the free propagator, as it also should in the semiclassical limit $kr \gg 1$.

The evaluation of the second summand in (9.60) is slightly more tedious because it involves the ratio of the two Hankel functions $H_\nu^{(2)}(ka)/H_\nu^{(1)}(ka)$. For the first summand we deformed the integration path in order to pick up a saddlepoint at the real ν axis if it existed, and otherwise we received a vansihing contribution which we then neglected. In the evaluation of the second summand we shall now see that we are guarantied the existence of a real saddle $\nu_R < ka$ and in addition a saddle $\nu_{S2} > ka$ if the saddle in the first summand was nonexisting. In order to use this the path is deformed so that starting from the left-upper asymptotic region in the ν plane it goes via the saddle $\nu_R < ka$ on the real ν axis to the first zero of the Hankel function $H_\nu^{(2)}(ka)$ in the lower complex ν plane. Secondly, from there the path passes to the right asymptotic region which lies (depending on the existence of the other saddle ν_{S2} on the real axis) in the upper or lower part of the ν plane. We first discuss the contribution from the first saddle $\nu_R < ka$ after the Debye asymptotic condition has been inserted for *all* Hankel functions appearing in the second geometrical summand in (9.60). The saddle is determined from the condition

$$
\theta + 2\arccos\frac{\nu_R}{ka} - \arccos\frac{\nu_R}{kr'} - \arccos\frac{\nu_R}{kr} = 0 \qquad (9.62)
$$

which is guaranteed to exist and to be real-valued when $\vec{r}$ lies in the light region of $\vec{r}'$ and when $r' > r > a$. The existence of the saddle becomes obvious when we note the geometrical significance of the saddle point condition. We see that this corresponds to the geometrical reflection off the disk of the ray from $\vec{r}$ to $\vec{r}'$ see fig(9.4). The semiclassical result for the second geometrical summand in (9.60) therefore reads

$$
+\frac{i}{4}\sqrt{\frac{2}{\pi}}\frac{e^{ikL_{\text{refl}} - i\pi/4}}{\sqrt{kR_{\text{eff}}}} \qquad (9.63)
$$

where where

$$
\begin{aligned}
L_{\text{refl}} &= d' + d \qquad\qquad\qquad\qquad\qquad\qquad (9.64) \\
R_{\text{eff}} &= d' + d + \frac{2dd'}{\sqrt{a^2 - b^2}}
\end{aligned}
$$
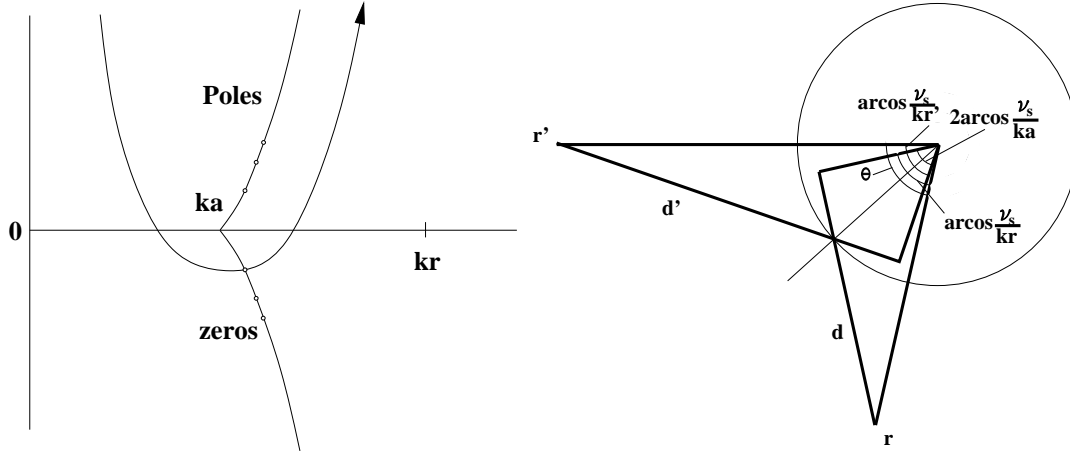
Figure 9.4: The reflection condition leads to the saddle point $\nu_R < ka$.

$$= d' + d + \frac{2dd'}{a\cos\varphi} \tag{9.65}$$

with

$$
\begin{aligned}
d' &\equiv \sqrt{r'^2 - b^2} - \sqrt{a^2 - b^2} \\
d &\equiv \sqrt{r^2 - b^2} - \sqrt{a^2 - b^2} \\
b &\equiv a|\sin\varphi| \;,
\end{aligned}
$$

where φ is the angle of incidence measured with repect to the normal at the point of reflection.

For $\nu > ka$ there might exist yet another saddle if the condition

$$\theta - \arccos\frac{\nu_{S2}}{kr'} - \arccos\frac{\nu_{S2}}{kr} = 0 \tag{9.66}$$

can be met for a real ν_{S2}. In the limit $\nu \gg ka$ the ratio of the two a-dependent Hankel function becomes $H_\nu^{(2)}(ka)/H_\nu^{(1)}(ka) \approx -1$. and the remaining evaluation of the integral with respect to the saddle ν_{S2} follows completely the one presented for the geometrical saddle ν_{S1} with the result

$$-\frac{i}{4}\sqrt{\frac{2}{\pi}}\frac{e^{iL_{\text{direct2}} - i\pi/4}}{\sqrt{kL_{\text{direct2}}}} \tag{9.67}$$

where $L_{\text{direct2}} = \sqrt{(kr')^2 - \nu_{S2}^2} + \sqrt{(kr)^2 - \nu_{S2}^2}$ is the distance $|\vec{r}' - \vec{r}|$ of the direct geometrical path between $\vec{r}'$ and $\vec{r}$ in this situation. The only difference to the above discussed case of the first geometrical summand in (6.33) is that here $\vec{r}$ and $\vec{r}'$ lie on opposite sides on the line connecting these points with respect to the line's point of closest approach to the origin. This case and the case of the first summand therefore exclude each other and we get no double counting: either the direct geometrical semiclassical propagator comes from the first summand in (6.33) or from the second saddle of the second summand, but not from both. Finally as we assumed $r' > r$ there is only the special situation

left where $\vec{r}$ coincides with the point of closest approach to the origin of the line joining $\vec{r}'$ are and $\vec{r}$. Since this is just a single point which depends on the choice of the origin of the coordinate system and which can be approached from both sides ($\vec{r}$ on the same or opposite side as $\vec{r}'$) with the same result, we do not have to deal further with this problem.

The stability-cumulant expansion relation for the 2-disk system

The stability reads

$$\Lambda \;=\; \frac{R - a + \sqrt{R^2 - 2Ra}}{a} \tag{9.68}$$

The identity that should be prooven is

$$\frac{1}{2}\sqrt{\frac{a}{2R}}\left(1 + \frac{1}{\sqrt{1 - 2a/R}}\right) \;=\; \frac{1}{\sqrt{\Lambda}(1 - \Lambda^{-2})}$$
$$\equiv\; S \tag{9.69}$$

We first note that

$$S \;=\; \frac{1}{2}\left(\frac{1}{\sqrt{\Lambda} + \frac{1}{\Lambda}} + \frac{1}{\sqrt{\Lambda} - \frac{1}{\Lambda}}\right) \tag{9.70}$$

and therefore calculate

$$\frac{1}{\sqrt{\Lambda} + \frac{1}{\Lambda}} \;=\; \frac{R + \sqrt{R^2 - 2aR}}{\sqrt{a(R - a + \sqrt{R^2 - 2aR})}} \tag{9.71}$$

and

$$\frac{1}{\sqrt{\Lambda} - \frac{1}{\Lambda}} \;=\; \frac{R - 2a + \sqrt{R^2 - 2aR}}{\sqrt{a(R - a + \sqrt{R^2 - 2aR})}} \tag{9.72}$$

and the sum S is therefore reduced to

$$S \;=\; \frac{\sqrt{a(R - a + \sqrt{R^2 - 2aR})}(R - a + \sqrt{R^2 - 2aR}}{2(R^2 - 2aR + (R - a)\sqrt{R^2 - 2aR}} \tag{9.73}$$

pulling out hte square root we get

$$S \;=\; \frac{1}{2}\frac{\sqrt{a(R - a + \sqrt{R^2 - 2aR}}(R - a + \sqrt{R^2 - 2aR})}{\sqrt{R^2 - 2aR}(\sqrt{R^2 - 2aR} + R - a)}$$
$$=\; \frac{1}{2}\sqrt{\frac{a(R - a + \sqrt{R^2 - 2aR})}{R^2 - 2aR}} \tag{9.74}$$

Now we are in a position where we can easily check if the two expressions coincides. This would imply

$$\sqrt{\frac{R - a + \sqrt{R^2 - 2aR}}{R^2 - 2aR}} \;=\; \frac{1}{\sqrt{2R}}\left(1 + \frac{1}{\sqrt{1 - 2a/R}}\right) \tag{9.75}$$

By squaring both sides we obtain

$$\frac{2R(R - a + \sqrt{R^2 - 2aR})}{R^2 - 2aR} \quad = \quad 1 + \frac{1}{1 - 2a/R} + \frac{2}{\sqrt{1 - 2a/R}} \qquad (9.76)$$

or

$$\frac{R^2 - Ra + R\sqrt{R^2 - 2aR}}{R^2 - 2aR} \quad = \quad \frac{R^2 - Ra + R\sqrt{R^2 - 2aR}}{R^2 - 2aR} \qquad (9.77)$$

which proves the identity since both sides were positive from the beginning.

9.3 A program that calculates $C_l^{p(1)}$

In this section we present the FORTRAN code that calculaties the first order $\hbar$ correction in the case of two-dimensional billard systems. In this version the program finds the correction contribution associated with a single periodic orbit, in the full 3-disk domain. The program is easily generalized to arbitrary 2-dimensinal billard systems, by specifying the length segments (Li) and the bouncing angles (angles) of the periodic orbit, together with the expansion coefficients of the billard wall (C2,C3 and C4) at the bouncing points. The program first solves locally the Hamilton Jacobi equation in terms of the expansion coefficients $S_y(t), S_{y^2}(t), S_{y^3}(t), S_{y^4}(t)$. These solutions are then used to drive the amplitude equation (7.31) which is then finaly used to calcuate the correction term by means of the integral (7.128),(7.135).

```fortran
program hbarcorrection
implicit none
integer Npmax,Norbit        !Max number of flight segments,
                                  !number of orbits.
parameter(Npmax=40,Norbit=1)
* Note all the arrays can only handle Npmax orbit segments!!

real*8 Li(Norbit,Npmax)     ! length(orbit,segment)
real*8 angles(Norbit,Npmax)! bounceangle(orbit,teta_i)

integer i,j,iteration,Np    !counting dummies, iteration =
                                  !numbers of iterations of the P.O.
                                  !N_p =
                                  !topological length of orbit.

real*8 teta,A,B,C,D,E,l     !Current bouncing angle, integration
                                  !constants and index of
                                  !the wave funciton.
```

```
real*8 C2,C3,C4               !Expansion coefficients of the
                                   !circle.


real*8 Syy,Syyy,Syyyy         !Discontinuous evolution variables
real*8 A0,Ay,Ayy,Ayplus       !of phase and amplitude.
real*8 Sy2minus(Npmax),Sy3minus(Npmax),Sy4minus(Npmax)
real*8 Sy2plus(Npmax),Sy3plus(Npmax),Sy4plus(Npmax)


real*8 A0array(Npmax)
real*8 Ayarray(Npmax)         !Arrays for the amplitude coefficients.


real*8 Aarray(Npmax)          !Arrays for the integration
real*8 Barray(Npmax)          !constants.
real*8 Carray(Npmax),Darray(Npmax),Earray(Npmax),Int


* Arrays for the value of the phase coefficients just before and
* after a bounce:
real*8 Sy2minus(Npmax),Sy3minus(Npmax),Sy4minus(Npmax)
real*8 Sy2plus(Npmax),Sy3plus(Npmax),Sy4plus(Npmax)


real*8 t,t0,t0array(Npmax) !Time variables, array for t0 constants.
  real*8 lambda,pi             !Stability of the orbit and pi.
parameter(pi = 3.141592653589793238462643383327950d0 )


* Internal functions:
real*8 Sy2,Sy3,Sy4            !Continuous time evolution functions
        real*8 Afct,Ayfct,Ayyfct   !of phase and amplitude
real*8 Ayplusfct              !Function that gives Ay right after bounce.
real*8 IntegralDt,Int         !The integral and its accumulated
                                   !value.


* External functions:
real*8 SmxyyypSpxyyy,SmxxyymSpxxyy,SmyyymSpyyy
real*8 SmxyymSpxyy,SmxyypSpxyy,SmyymSpyy,SmyypSpyy
*Above functions gives: Sm(inus)... (p(lus)/m(inus)) Sp(lus)....


real*8 segn                   !gives the sign: segn(l) = (-1)^l.



* The evolution functions:

Sy2(t,t0) = 1.0d0/(t + t0)
  Sy3(A,t,t0) = A/((t + t0)**3.0d0)
Sy4(A,B,t,t0) = B/(t + t0)**4.0d0 - 3.0d0/(t + t0)**3.0d0
     &                     + 3.0d0*A*A/(t + t0)**5.0d0
```

```
Afct(E,t0,t,l) = E*dexp((l+0.5d0)*dlog( t0/(t + t0)))
Ayfct(A,C,E,t0,t,l) = (E/dexp((l+1.5d0)*dlog(t + t0)))
     &    *(C + (l+1.d0)*(l+1.d0)*(A/2.0d0)*(t0**(l+0.5d0)))/(t+t0))
Ayyfct(A,B,C,D,E,t0,t,l) = (E/dexp((l+2.5d0)*dlog(t + t0)))
     &    *(D
     &    + ( ((l+2.0d0)**2.0d0)*A*C/2.0d0
     &   +(l*l+3.d0*l+2.0d0)*(1.5d0+l)*(B/6.0d0)*(t0**(l+0.5d0)))
     &    /(t+t0)
     &    + ((l+2.0d0)*(l+1.0d0)*(0.5d0*(l+2.0d0)
     &    *(l+1.0d0)+l+1.5d0)
     &    *(A*A/4.0d0)*(t0**(l+0.5d0)))/((t + t0)**2.0d0) )


      Ayplusfct(A0,Ay,C2,teta,l) =  -segn(l)*(Ay -
     &                   C2*(dsin(teta)/dcos(teta)**2.0d0)*A0
     &    *(l+1.0d0)*(l+1.0d0) )


* The integral:
IntegralDt(A,B,C,D,t0,t,l) =
     &   ( (l+0.5d0)*(l+1.5d0)
     &    + D/(t0**(l+0.5d0)))*t/(t0*(t + t0))
     & +( ((l+2.d0)**2.d0)*(A*C/4.d0)/(t0**(l+0.5d0))+
     &    + (l+2.d0)*(l+1.d0)*(1.5d0+l)*B/12.0d0 )
     &    *(t*(t + 2.0d0*t0)/(t0*(t + t0))**2.0d0)
     &    +(l+2.d0)*(l+1.0d0)
     &    *((l*l+3.d0*l+2.0d0)*0.5d0+l+1.5d0)*(A*A/12.d0)
     &    *(1.0d0/t0**3.0d0 - 1.0d0/(t + t0)**3.0d0)


********************************************************************
* Main program:
********************************************************************
* initialisations :

5       continue
iteration = 0
write(*,*) 'l='
read(*,*) l

C2 = 1.0d0  !
C3 = 0.0d0  ! Constants for the circle
C4 = 3.0d0  !

t=0

enddo


* Orbit input: Np = number of flight segments,Li = length of flight
```

```
* segments, angles = bouncing angles.
******************************************************************
  open(unit = 13, file = 'orbit.segm', status = 'old')

  read(13,*) Np

  do i = 1, Np
  read(13,*) Li(1,i)
  read(13,*) angles(1,i)
  enddo
  Li(1,Np+1) = Li(1,1)          ! To ensure periodic
  angles(1,Np+1) = angles(1,1) ! boundary conditions
******************************************************************

Syy  =  5.0d0     ! First the phase
Syyy  = 1.0d0     ! coefficients are initialized
        Syyyy = -1.0d0    ! arbitrarily.


10      continue
*
*  Here is the orbit loop for solving the HJ equation around the P.O.
*
*First calculating the constants t0,A and B:

do j=1,Np

t=0.0d0

t0 = 1.0d0/Syy
A = Syyy*(t0**3.0d0)
B = (Syyyy + 3.0d0/t0**3.0d0
    &                   - 3.0d0*A*A/t0**5.0d0)*(t0**4.0d0)


        Aarray(j) = A
        Barray(j) = B
        t0array(j) = t0


* Then evolving the phase coefficients in continuous time:

t = Li(1,j)   !flight time = length of j'th orbit segment.

Syy = Sy2(t,t0)
Syyy = Sy3(A,t,t0)
Syyyy = Sy4(A,B,t,t0)
```

```
Sy2minus(j+1) = Syy     !
Sy3minus(j+1) = Syyy   !minus indicates the value
Sy4minus(j+1) = Syyyy  !just before next bounce.


* Then the discontinuous jumps at the bouncing points:

teta = angles(1,j+1)    !teta = the current bouncing angle.

Syyyy = Syyyy
      &       - 4.0d0*dsin(teta)/dcos(teta)
      &                      *SmxyyypSpxyyy(Syyy,Syy,C2,C3,teta)
      &      + 6.0d0*(dsin(teta)/dcos(teta))**2.0d0
      &                      *SmxxyymSpxxyy(Syy,C2,teta)
      &      + 6.0d0*dsin(teta)/dcos(teta)**2.0d0*C2
      &                      *SmyyymSpyyy(Syyy,Syy,C2,C3,teta)
      &     + 12.0d0*(1.0d0/(2.0d0*dcos(teta)**1.0d0)
      &        - dsin(teta)**2.0d0/dcos(teta)**3.0d0)*C2
      &                      *SmxyypSpxyy(Syy,C2,teta)
      &     +3.0d0*dsin(teta)**2.0d0/dcos(teta)**4.0d0*C2**2.0d0
      &                      *SmyymSpyy(Syy,C2,teta)
      &     -4.0d0*dsin(teta)/dcos(teta)**3.0d0*C3
      &                      *SmyypSpyy(Syy,C2,teta)
      &      + 2.0d0*C4/dcos(teta)**3.0d0


        Syyy = -Syyy + 2.0d0*C3/dcos(teta)**2.0d0
      &        - 3.0d0*dsin(teta)/dcos(teta)**2.0d0*C2
      &                             *SmyypSpyy(Syy,C2,teta)
      &        + 3.0d0*dsin(teta)/dcos(teta)
      &                             *SmxyymSpxyy(Syy,C2,teta)

Syy = Syy + 2.0d0*C2/dcos(teta)

Sy2plus(j+1) = Syy
Sy3plus(j+1) = Syyy
Sy4plus(j+1) = Syyyy


enddo
* End of orbit loop for the HJ equation. Then to ensure periodicity:

        Sy2plus(1) = Sy2plus(Np+1)
        Sy3plus(1) = Sy3plus(Np+1)
        Sy4plus(1) = Sy4plus(Np+1)
!to be able to read Sy(1) = Sy(Np+1)
Sy2minus(1) = Sy2minus(Np+1)
Sy3minus(1) = Sy3minus(Np+1)
Sy4minus(1) = Sy4minus(Np+1)
```

```
iteration = iteration + 1
if(iteration.ge. 25) then
goto 100     ! At least in the 3-disk case it turns
else                    ! out that 25 iterations is even more than
goto 10      ! sufficient.
endif

*This ends the solution of the HJ equation.

100     continue

* Now for the evolution of the amplitudes:


        iteration = 0
        A0 = 1.0d0                    ! A0 is set to 1, by normalization conditions.
        Ay = 3.0d0                    ! Ay and Ayy are initialized arbitrarily.
        Ayy = 5.0d0


110     continue

* start of orbit loop:
do j = 1,Np

A0array(j) = A0

t0 = t0array(j)
        A = Aarray(j)
        B = Barray(j)

        teta = angles(1,j+1)    !teta = the current bouncing angle.
t = Li(1,j)               !t = current flight time = length of curent
!orbit segment.

* First the calculation of the integration constants.
        E = A0
        C =(t0**(1+1.5d0))*Ay/E-(A/2.0d0)
    &     *(t0**(1-0.5d0))*((1+1.0d0)**2.0d0)
        D = dexp((1+2.5d0)*dlog(t0))*Ayy/E
    &     -((1+2.0d0)**2.d0)*A*C/(2.d0*t0)
    &     -B*(1+2.d0)*(1+1.d0)*(1/3.d0+0.5d0)*(t0**(1-0.5d0))/2.0d0
    &     - (((1+2.d0)*(1+1.d0))**2.d0)/8.d0
    &        +(1+2.d0)*(1+1.d0)*(1+1.5d0)/4.d0 )
```

```
      &      *A*A*dexp((1-1.5d0)*dlog(t0) )


Earray(j) = E
Carray(j) = C
Darray(j) = D



* then the continous evoln. of the amplitudes:


         A0 = Afct(E,t0,t,l)
         Ay = Ayfct(A,C,E,t0,t,l)
Ayarray(j+1) = Ay
         Ayy = Ayyfct(A,B,C,D,E,t0,t,l)


* then finaly the jumps for the amplitudes:



Ayplus = Ayplusfct(A0,Ay,C2,teta,l)

Ayy = segn(l)*Ayy + dtan(teta)*
      &                ((segn(l)*Sy2minus(j+1)*Ay + Sy2plus(j+1)*Ayplus)
      &              *(l+2.d0)*(l+1.5d0)
      &                      + segn(l)*(Sy3minus(j+1) + Sy3plus(j+1))*A0
      &           *(l+2.0d0)*(l+1.0d0)*(l+1.0d0)/2.0d0)
      &              + dtan(teta)**2.0d0*A0
      &       *(l+1.0d0)*(l+2.0d0)*(l+0.5d0)*(l+1.5d0)/2.0d0
      &       *segn(l)*(Sy2minus(j+1)**2.0d0 - Sy2plus(j+1)**2.0d0 )
      &        + C2*dsin(teta)/dcos(teta)**2.0d0*(segn(l)*Ay - Ayplus)
      &       *(l+2.0d0)/2.0d0
      &             - C2/dcos(teta)*0.5d0*A0
      &             *segn(l)*(Sy2minus(j+1) + Sy2plus(j+1) )
      &             *(l+2.0d0)*(l+1.0d0)*(l+0.5d0)
      &       +segn(l)*2.0d0*l*(l+1.0d0)*(l+2.0d0)*A0
      &        *(C2*C2*l*dtan(teta)**2.d0/4.0d0 -
      &        C3*dtan(teta)/6.0d0)/dcos(teta)**2.0d0
      &    +l*(l+2.d0)*(l+1.0d0)*(l+0.5d0)*A0*C2*segn(l)*Sy2minus(j+1)
      &        *dtan(teta)**2.d0/dcos(teta)
      &        + segn(l)*l*(l+2.d0)*C2*Ay*dtan(teta)/dcos(teta)


Ay = Ayplus

         A0 = segn(l)*A0              ! just for completenes


enddo
*End of the individual orbit loop
*For periodicity we redefine:
```

```
        A0array(Np+1) = A0
Ayarray(1) = Ayarray(Np+1)


*And after running through the orbit we renormalize the A coeffs.:

  Ayy = Ayy/A0
  Ay = Ay/A0
  A0 = A0/A0


*(Lambda is just the stability of the orbit included to check the
*validity of final result)
  lambda = 1.0d0/(dabs(A0)**(1.d0/(0.5d0+1)))

  write(*,*) A0,Ay,Ayy !we check the convergence visualy.

        iteration = iteration + 1
        if(iteration.ge. 25) then
                goto 200                !Also for the amplitude
        else    !25 iterations seems to be
                goto 110     !ok in the 3-disk system.
        endif

200     continue

* Now we should have everything to do the integration to find a(1)

Int = 0.0d0
do j = 1, Np
t=Li(1,j)
teta = angles(1,j)
A0 = A0array(j+1)
        t0 = t0array(j)
        A = Aarray(j)
              B = Barray(j)
C = Carray(j)
D = Darray(j)
E = Earray(j)
write(*,*) A,B,C,D,E,t0
Int = Int + IntegralDt(A,B,C,D,t0,t,1)
enddo

write(*,*) 'C(1) = ',Int/2.0d0
        write(*,*) 'lambda ',lambda        !To be checked with correct stability
close(13)  !to ensure convergence has set in.
goto 5
end
```

```
***********************************************************
* The bouncing functions:
***********************************************************
real*8 function SmyypSpyy(Syy,C2,teta)
implicit none
real*8 Syy,C2,teta

SmyypSpyy = 2.0d0*(Syy + C2/dcos(teta))

return
end
***********************************************************
real*8 function SmyymSpyy(Syy,C2,teta)
        implicit none
        real*8 Syy,C2,teta

        Syy=Syy
SmyymSpyy = -2.0d0*C2/dcos(teta)

        return
        end
***********************************************************
real*8 function SmxyymSpxyy(Syy,C2,teta)
        implicit none
        real*8 Syy,C2,teta

SmxyymSpxyy = -Syy**2.0d0
     &             + ( Syy + 2.0d0*C2/dcos(teta))**2.0d0

        return
        end
***********************************************************
real*8 function SmxyypSpxyy(Syy,C2,teta)
implicit none
        real*8 Syy,C2,teta

 SmxyypSpxyy = -Syy**2.0d0
     &             - ( Syy + 2.0d0*C2/dcos(teta))**2.0d0

        return
        end
***********************************************************
        real*8 function SmyyymSpyyy(Syyy,Syy,C2,C3,teta)
        implicit none
        real*8 Syyy,Syy,C2,C3,teta,Spyyy
```

```
SmyyymSpyyy = Syyy - Spyyy(Syyy,Syy,C2,C3,teta)


return
end
**********************************************************
        real*8 function SmxxyymSpxxyy(Syy,C2,teta)
        implicit none
        real*8 Syy,C2,teta



SmxxyymSpxxyy = 2.0d0*(Syy**3.0d0
     &                        - ( Syy + 2.0d0*C2/dcos(teta))**3.0d0)


return
end
**********************************************************
real*8 function SmxyyypSpxyyy(Syyy,Syy,C2,C3,teta)
        implicit none
        real*8 Syyy,Syy,C2,C3,teta,Spyyy


SmxyyypSpxyyy = -3.0d0*(Syy*Syyy + (Syy + 2.0d0*C2/dcos(teta))*
     &                               Spyyy(Syyy,Syy,C2,C3,teta))


return
end
**********************************************************
        real*8 function Spyyy(Syyy,Syy,C2,C3,teta)
implicit none
real*8 Syyy,Syy,C2,C3,teta,SmyypSpyy,SmxyymSpxyy


        Spyyy = -Syyy + 2.0d0*C3/dcos(teta)**2.0d0
     &          - 3.0d0*dsin(teta)/dcos(teta)**2.0d0
     &                            *C2*SmyypSpyy(Syy,C2,teta)
     &          + 3.0d0*dsin(teta)/dcos(teta)*SmxyymSpxyy(Syy,C2,teta)


        return
end
**********************************************************
real*8 function segn(l)
implicit none


real*8 l,pi
parameter(pi = 3.141592653589793238462643383827950d0 )


        segn = dsin(pi/2.0d0 + l*pi)
return
```

```
end
```

****